

Dissertation zur Erlangung des Doktorgrades
der Fakultät für Chemie und Pharmazie
der Ludwig-Maximilians-Universität München

**Synthesis and Characterization
of Oxygen-rich Materials
and
Investigations on the Toxicity
of Energetic Materials**

Cornelia Claudia Unger
aus Erding, Deutschland

2020

Erklärung

Diese Dissertation wurde im Sinne von § 7 der Promotionsordnung vom 28. November 2011 von Herrn Prof. Dr. Thomas M. Klapötke betreut.

Eidesstattliche Versicherung

Diese Dissertation wurde eigenständig und ohne unerlaubte Hilfe erarbeitet.

München, den 6. August 2020

Cornelia Claudia Unger

Dissertation eingereicht am	18. August 2020
1. Gutachter:	Prof. Dr. Thomas M. Klapötke
2. Gutachter:	Prof. Dr. Konstatin Karaghiosoff
Mündliche Prüfung am	28. September 2020

Meiner geliebten Familie

*und im Gedenken
an meine Tante
Otilie Wiedemann*

** 07.12.1957*

† 12.06.2016

Danksagung

Mein Dank gilt zuallererst meinem Doktorvater Herrn Prof. Dr. Thomas M. Klapötke als Teil seines Arbeitskreises interessante Themenstellungen bearbeiten zu können. Auch möchte ich mich für die finanzielle Unterstützung und das uneingeschränkte Vertrauen, sowie die Förderungen der forscherschen Freiheiten danken.

Herrn Prof. Dr. Konstantin „Conny“ Karaghiosoff danke ich für die freundliche Übernahme des Zweitgutachtens dieser Dissertation, seiner ansteckenden Faszination für die Kristallographie und seinem unermüdlichen Optimismus.

Der Prüfungskommission, bestehend aus Herrn Prof. Dr. Thomas M. Klapötke, Herrn Prof. Dr. Konstantin Karaghiosoff, Herrn Prof. Dr. Robert Schmucker, Herrn Prof. Dr. Sebastian Eibl, Herrn Prof. Dr. Hans-Christian Böttcher und Herrn Prof. Dr. Ingo-Peter Lorenz, danke ich für ihre Zeit und der Bereitschaft zur Bildung ebendieser, insbesondere unter diesen Umständen.

Ebenfalls möchte ich Herrn Dr. Burkhard Krumm für das problemlose Messen von zum Teil empfindlichen NMR Proben und NMR Kernen abseits von ^1H , ^{13}C und ^{14}N danken. Ebenso bin ich für die akribische Korrektur von Manuskripten und Vorträgen dankbar.

Herrn Dr. Jörg Stierstorfer, der mich immer wieder durch den ein oder anderen Ratschlag motiviert hat und stets eine offene Tür für fachliche Fragen hat, gebührt ebenso besonderer Dank. Auch seine teambildenden Maßnahmen im Arbeitskreis, sei es z. B. das Literaturseminar oder beim Campusturnier, sollen erwähnt werden.

Nicht minder möchte ich Frau Irene Scheckenbach, für ihr Organisationstalent und ihre Unterstützung bei allen bürokratischen Angelegenheiten, sowie für die netten und unterhaltsamen Gespräche/Emailverläufe danken.

Es sind einige Wegbegleiter, denen ich an dieser Stelle danken möchte. Zunächst ist Dr. Regina Scharf für die Einarbeitung in das Thema der Oxidatoren und energetischen Materialien zu nennen, sowie im weiteren Verlauf Dr. Quirin Axthammer, Dr. Carolin Pflüger und Dr. Thomas Reith. Letzterem und insbesondere Dr. Teresa („Resi“) Küblböck ist für kreativen Input, hervorragender Musikauswahl und den ebenso wichtigen Schokopausen zu danken. Der Post-Pardubice Gruppe um Dr. Johann Glück, Dr. Ivan Gospodinov, Dr. Marc Bölter, Dr. Marcel Holler, Dr. Teresa Küblböck, Anne Friedrichs und Maximilian Wurzenberger gilt mein Dank

nicht nur den vielen weltanschaulichen Diskussionen, sondern auch dem freundschaftlichen Rückhalt. Dem gesamten Arbeitskreis möchte ich für die offene und harmonische Atmosphäre danken und möchte auf diesem Wege der „neuen Generation“ viel Erfolg wünschen.

Auch möchte ich mich für die Korrekturen dieser Arbeit und die damit investierten Stunden bei Dr. Ivan Gospodinov, Dr. Teresa Küblböck und David Añón bedanken. Eure konstruktive Kritik wird sehr geschätzt.

Stefan Huber danke ich für die erfrischenden Messungen der Sensitivitäten und dafür, dass er immer mit einer helfenden Hand bei Seite steht.

Bei meinen Praktikanten Florian Freund, Christian Riedelsheimer, Moritz Kofen, David Helmiger und Robin Hess bedanke ich mich für ihr Engagement, welches einen wichtigen Anteil an dieser Arbeit hat.

Außerhalb der Uni gibt es einige liebe Menschen, welchen in den letzten Jahren durch Zuspruch und Rückhalt auf der einen, und Ablenkung auf der anderen Seite mein Dank gilt: Clara, Gabriele, Theresa, Katharina, Anna, Walter + Katrin und weitere – nicht namentlich genannte, dennoch nicht minder wichtige – Freunde aus dem Taufkirchner und Münchner Umfeld, dem WIWEB, sowie der Hausgemeinschaft 93a.

Abschließend möchte ich mich bei meiner gesamten Familie bedanken. Dabei allen voran bei meinen Eltern Adelheid und Helmut, deren Unterstützung und Liebe dies erst ermöglicht hat, sowie bei meinem Bruder Günther. Vielen Dank!

Table of Contents

I	General Introduction	1
1	Classification of High-Energy Dense Materials	1
2	Rocket Propellants	3
3	High-Energy Dense Oxidizers	5
4	Toxicity Measurements	8
5	Objectives	9
6	References	11
II	Results and Discussion	15
1	Michael Addition of Trinitromethane	17
1.1	Abstract	18
1.2	Introduction	18
1.3	Results and Discussion	19
1.3.1	Synthesis	19
1.3.2	Multinuclear NMR Spectroscopy	21
1.3.3	Vibrational Spectroscopy	21
1.3.4	Single Crystal Structure Analysis	22
1.3.5	Thermal Stabilities and Energetic Properties	26
1.4	Conclusion	30
1.5	Experimental Section	30
1.5.1	General Information	30
1.5.2	X-ray Crystallography	31
1.5.3	Computational Details	31
1.5.4	Synthesis	32
1.6	References	39
2	Trinitropropylammonium Salts	43
2.1	Abstract	44
2.2	Introduction	44
2.3	Results and Discussion	45
2.3.1	Synthesis	45
2.3.2	NMR Spectroscopy	45
2.3.3	Single Crystal Structure Analysis	46

2.3.4	Thermal Stabilities and Energetic Properties	46
2.4	Experimental Section.....	48
2.5	References	50
3	Trinitroethyl Esters Based on Divalent Acids.....	51
3.1	Abstract.....	52
3.2	Introduction	52
3.3	Results and Discussion	53
3.3.1	Synthesis.....	53
3.3.2	NMR Spectroscopy.....	54
3.3.3	Single-Crystal Structure Analysis	54
3.3.4	Physical and Energetic Properties	56
3.3.5	Thermal Decomposition Characteristics and Kinetics	57
3.4	Conclusion.....	61
3.5	Experimental Details	61
3.6	References	64
4	Azoles with Trinitroalkyl Substitution	69
4.1	Abstract.....	70
4.2	Introduction	70
4.3	Results and Discussion	71
4.3.1	Synthesis.....	71
4.3.2	NMR Spectroscopy.....	72
4.3.3	Single Crystal Structure Analysis.....	72
4.3.4	Thermal Stabilities and Energetic Properties	74
4.4	Conclusion.....	74
4.5	Experimental Section.....	75
4.5.1	General Information	75
4.5.2	Synthesis.....	75
4.6	References	78
5	Urazine Derivatives.....	81
5.1	Abstract.....	82
5.2	Introduction	82
5.3	Results and Discussion	83
5.3.1	Synthesis.....	83
5.3.2	NMR Spectroscopy.....	85
5.3.3	Crystal Structures	85
5.3.4	Physical and Energetic Properties	90

5.4	Conclusion	94
5.5	Experimental Section	94
5.6	References	100
6	Salts of Pentaerythritol Tetranitrocarbamate.....	103
6.1	Abstract	104
6.2	Introduction.....	104
6.3	Results and Discussion.....	105
6.3.1	Synthesis	105
6.3.2	NMR and Vibrational Spectroscopy.....	107
6.3.3	Single-Crystal Structure Analysis.....	107
6.3.4	Physical and Energetic Properties.....	108
6.3.5	Toxicity Assessment	111
6.4	Conclusions.....	111
6.5	Experimental Section	112
6.5.1	General.....	112
6.5.2	Synthesis	113
6.6	References.....	115
7	Aquatic Toxicity Measurements.....	119
7.1	Abstract	120
7.2	Introduction.....	120
7.3	Experimental Section	122
7.3.1	Test Compounds	122
7.3.2	Measurement.....	122
7.4	Results and Discussion.....	123
7.5	Conclusion	133
7.6	References.....	134
8	Comparative Toxicological Study.....	141
8.1	Abstract	142
8.2	Introduction.....	142
8.3	Materials and Methods.....	143
8.3.1	Test Compounds	143
8.3.2	Microtox Assay	144
8.3.3	Experimental Ames test	144
8.3.4	QSAR Ames test.....	144
8.4	Results and Discussion.....	145
8.5	Conclusion	149

8.6	References	149
III	Summary and Conclusion	152
IV	Appendix	161
A1	Supporting Information to Michael Addition of Trinitromethane.....	161
A2	Supporting Information to Trinitropropylammonium Salts	170
A3	Supporting Information to Trinitroethyl esters Based on Divalent Acids.....	176
A4	Supporting Information to Azoles with Trinitroethyl Substitution	188
A5	Supporting Information to Urazine Derivatives	195
A6	Supporting Information to Salts of Pentaerythritol Tetranitrocarbamate	209
A7	Supporting Information to Aquatic Toxicity Measurements.....	216
A8	Credits.....	220

I General Introduction

1 Classification of High-Energy Dense Materials

An energetic material, in general is defined as a compound or mixture of substances which contains both, the fuel and the oxidizer and reacts readily with the release of energy and gas.^[1] Apart from that, an explosive is in a metastable state, owning the potential of a fast chemical reaction, whereby a large amount of heat and pressure is released. For this rapid chemical reaction under the influence of an external stimuli, such as impact, friction, spark, shock, flame or heating, no additional reaction partners are required. Along with propellants and pyrotechnics, explosives form the main categories of energetic materials, which can be classified as shown in Figure I1.1.^[1-2]

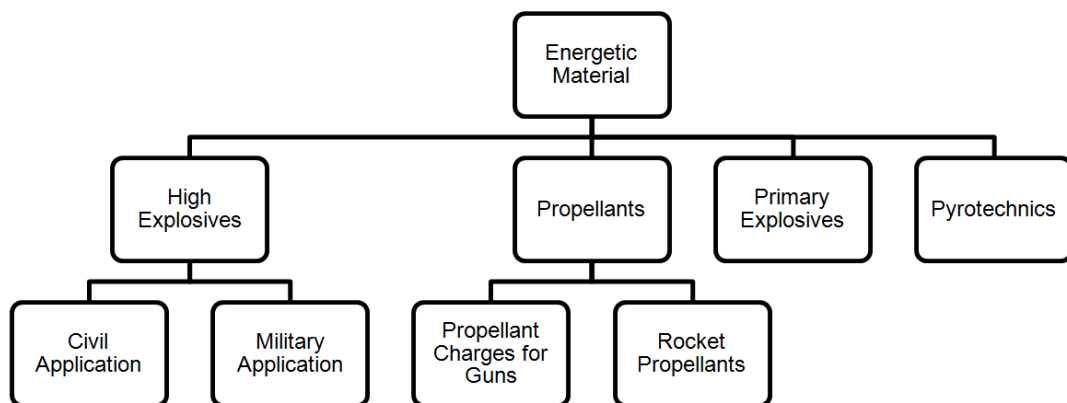


Figure I1.1 Classification of energetic materials.^[1]

Primary explosives, as the first class of explosives, were widely used from 1864 on by Alfred Nobel, when he initiated nitroglycerine by mercury fulminate.^[3] In the further development lead(II) styphnate (LS) and lead(II) azide (LA) were applied as primary explosives. Due to the high toxicity of Pb^{2+} , research efforts focus on replacing these heavy-metal containing explosives. Under current investigation are for example the copper salt DBX-1 and the potassium salt of dinitraminobistetrazole (K_2DNABT) (Figure I1.2) The predominant application remained the initiation of a main charge such as propellants or secondary explosives in detonators. Since the initiation of primary explosives leads to a fast deflagration to detonation transition (DDT) a supersonic shock wave is generated. This shockwave is used as an initiator, being the impact sensitivity usually less than 4 J and the friction sensitivity less than 10 N, moreover, the detonation velocity ranges between 3500 and 5500 $m\ s^{-1}$. The characteristics of primary explosives are a subtle balance of being initiated reliably, but not too sensitive to be exceedingly dangerous to handle.^[1, 4]

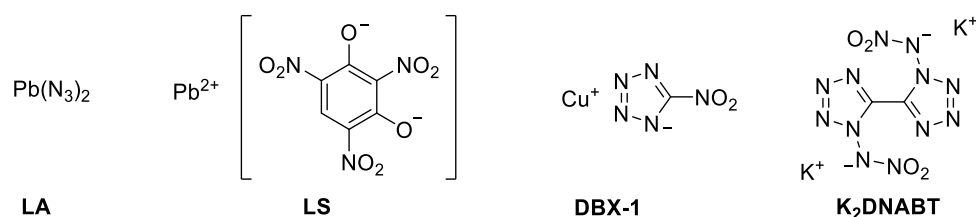


Figure 11.2 Molecular structures of the primary explosives LA, LS, DBX-1 and K₂DNABT.

For the second class, the **secondary explosives** or high explosives (HE) once again a historical milestone is based on Alfred Nobel. In 1867 Nobel patented “Guhr Dynamite”, whereby he mixed nitroglycerine (75%) with an absorbent clay called “Kieselguhr” (25%). Dynamite got popular in the civil sector; however, it was never properly applied in the military field. In the particular case of 2,4,6-trinitrotoluene (TNT), it was widely used in the first and second World War. Similarly, 1,3,5-trinitro-1,3,5-triazinane (hexogen or RDX) and 1,3,5,7-tetranitro-1,3,5,7-tetrazoctane (octogen or HMX) conquered the secondary explosives market for military use during the second World War.^[1] Although RDX even nowadays is the reference for new developed secondary explosives, there are other modern compounds such as the booster explosive pentaerythritol tetranitrate (PETN), the relatively new 2,2-dinitroethene-1,1-diamine (FOX-7) and the tetrazole based dihydroxylammonium 5,5'-bistetrazole-1,1'-diolate (TKX-50)^[5] (Figure 11.3).

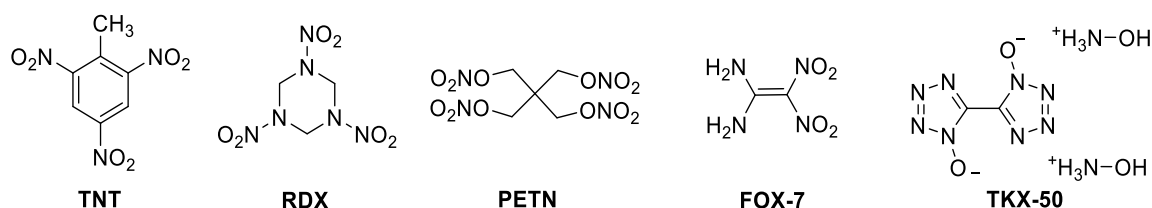


Figure 11.3 Molecular structures of typical secondary explosives. TNT, RDX, PETN, FOX-7 and TKX-50.

A typical secondary explosive possesses a detonation velocity of 6500–9000 m s⁻¹. The sensitivities shall be higher than 4 J (impact) and 50 N (friction), in order to be initiated by a stronger stimulus like the shock wave generated by a primary explosive. Research efforts are driven towards increased energetic performance parameters, lower sensitivities as well as lower environmental impact.

Pyrotechnics took their name from the ancient Greek word *pyr* (“fire”) and *tekhnikos* (“made by art”). The desired artistic effect is either heat, light, sound, gas or smoke or a combination of these, based on non-detonative self-sustaining exothermic reactions. The speed of reaction is slower compared to the reaction speed of explosives. Another distinguishing feature between explosives like TNT or RDX and traditional pyrotechnics is, that explosives often combine fuel and oxidizer in one molecule and pyrotechnics are more likely mixtures of different substances. One approach in pyrotechnics research is to replace the rather toxic barium or strontium salts as

light emitters with more environmentally benign alternatives. One example are lithium salts with elemental lithium as alternative red-light emitter.^[1, 6]

Propellants have a history which goes back much farther. Black powder should be considered the first described propellant. In general propellants are distinguished into gun and rocket propellants, whereby both rely on the large amounts of hot gases formed during the combustion as driving force. Nitrocellulose (NC), nitroglycerin (NG) and nitroguanidine (NQ) entered the market at the end of the 19th century and are still ingredients in triple-based gun propellants. Moreover, they serve as main ingredients in double- (NC + NG) and single-based (NC) propellants. The trend in R+D is focusing on overcoming erosion problems of the gun barrel, e. g. with triaminoguanidinium azotetrazolate (TAGzT) mixtures, as they possess lower combustion temperatures. However, propellant charge powders burn considerably faster with pressures up to 4000 bar in the combustion chamber, compared to 70 bar in the combustion chamber of rocket propellants.

2 Rocket Propellants

In 1923 Hermann Oberth published theoretical and technical foundations for the first space rockets, nevertheless it was not taken serious at that time.^[7] More than 30 years later in 1957 *Sputnik 1* became the first artificial satellite.^[8] It was launched by a R-7 rocket, which was fueled by kerosene and liquid oxygen (LOX).

Modern rocket propellants are divided into solid and liquid propellants. The latter can be further subdivided into mono- and bipropellants. Hydrazine is an example of a monopropellant. It is an endothermic liquid, which decomposes exothermically without the presence of an external oxidizing agent. Hydrazine and its derivatives, such as monomethylhydrazine, have been also used in bipropellants. For bipropellant systems, oxidizer and fuel are separately transported in two storage tanks and are only injected into the combustion chamber when the motor is fired. They can be distinguished even further according to their storability and their ignition behavior (Figure I2.1).^[1]

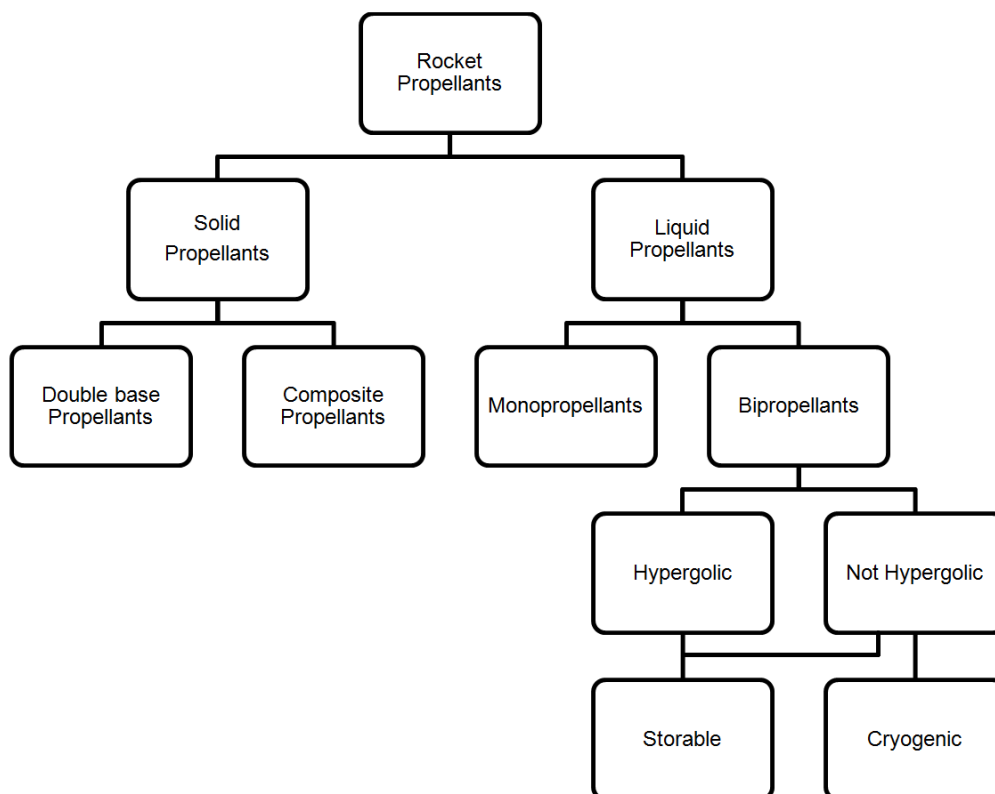


Figure 12.1 Classification of various propellants.^[1]

Solid rocket propellants are either homogeneous double-base or heterogeneous composite propellants. Similar to gun propellants, double-base rocket propellants mainly consist of nitrocellulose and nitroglycerin. Heterogeneous propellants are based on a crystalline oxidizer and metal-containing fuel in a polymer binder agent. Further additives such as burn rate modifiers, plasticizers and stabilizers can be introduced. The most common oxidizer, ammonium perchlorate (AP), provides the oxygen for the combustion of the fuel and the binder. Addition of aluminum increases the density of the fuel which releases high amounts of heat when burned. Under current investigation for enhancing this fuel is to lower the grain size of aluminum or to introduce AlH_3 as alternative fuel, however, both come along with a higher air sensitivity. The structure and mechanical properties of the final propellant are determined by the polymeric binder, *e. g.* polybutadiene acrylonitrile (PBAN) or hydroxy-terminated polybutadiene (HTPB). The binder itself can act as a fuel as it mainly contains carbon and hydrogen. Energetic binders even improve the performance but suffer from lower mechanical stability. Newer developments on that field are for example poly(glycidyl)nitrate (poly-GLYN), glycidylazide polymer (GAP) or poly(3,3-bis-azidomethyl-oxetane) (poly-BAMO).^[1]

3 High-Energy Dense Oxidizers

Ammonium perchlorate (AP) is used since the 1940s and remained the most important high energy dense oxidizer (HEDO) for solid rocket composite propellants for decades. Even the new p120 rocket booster for Ariane 6 and Vega E and C are based on AP.^[9] The advantages are manifold. It is reliable to use; the industrial production starts from commercially available and cheap starting materials and it is simple and scalable; furthermore, the performance of the AP is excellent. Unfortunately, it has a negative effect on the environment due to the products formed during the combustion, as well as due to the substance itself. The perchlorate anion competes with iodine for the uptake into the thyroid gland at the sodium/iodide symporter.^[10] This consequently affects the thyroid hormone synthesis, which is critical for the development of vertebrates, including unborn children.^[11] Moreover, uncommon pigmentation of amphibian embryos was observed in correlation with perchlorate contaminated water as well as a delayed metamorphosis.^[12] Due to the high solubility, chemical stability and persistence it can be widely distributed throughout ground water systems.^[11b] This especially is associated with the release of ammonium perchlorate by defense contractors, military operations, and aerospace programs.^[13]



Figure I3.1 Launch of the Atlantis space shuttle, NASA's fourth space rated space shuttle.

In 2020 the United States Environmental Protection Agency (EPA) released fact sheets to address perchlorate in drinking water, which also state that the occurrence has decreased over time. Besides, the European Union established the REACH regulation (Registration, Evaluation, Authorization and Restriction of Chemicals), which considers the potential impact of a chemical substance on human health and the environment. Chemicals, which are manufactured or imported in a specific amount, or are already known to have a certain hazardous potential, need to be registered. In this context, ammonium perchlorate is under assessment as endocrine disruptor.^[14] During the combustion of common composite solid rocket propellants massive amounts of

gaseous products such as CO, CO₂, H₂, H₂O, Al₂O₃ and HCl are exhausted.^[1] Thereby, HCl is the reason for acid rain formation and the main reason for ozone layer depletion as well.^[15] In order to develop a sustainable chlorine-free alternative, research programs have been launched in the past and remain a challenging task until today. Currently ammonium nitrate (AN) and ammonium dinitramide (ADN) are discussed as the most promising AP replacements. Even though, both salts have their own drawbacks, *e. g.* on the one hand pure AN is hygroscopic and shows phase transitions in the purposed temperature ranges. ADN on the other hand has a decomposition point of about 133 °C without further treatment and suffers from compatibility problems with HTPB.^[16] However, projects which are based on combining the cost-efficient AN with the high-performing ADN, seem to achieve comparable performance data to AP.^[9a]

One of the most important characteristics of propellant compositions, and particularly HEDOs, is the specific impulse, which is the change in the impulse per unit of the propellant. The specific impulse expresses the effective velocity of the combustion gases when leaving the nozzle. A nozzle is designed to modify the flow of fluids and gases. In the case of rocket propellants its design is used to increase the velocity of the flow of the enormous amounts of hot gases in the combustion chamber. The generated thrust then accelerates the spacecraft.^[1]

$$I_{sp} = \frac{\bar{F} \cdot t_b}{m} \quad (1)$$

In equation (1) the nominator describes the impulse (classically: mass × velocity or force × time) as the average thrust \bar{F} multiplied by the combustion time t_b . Subject to (1) the unit is m s⁻¹; is the specific impulse based on the gravitation of earth ($g = 9.81 \text{ m s}^{-2}$) the unit is seconds (s), which is the case throughout this thesis. Classical values for the I_{sp} of solid rocket boosters are approximately 250 s, whereas double-base propellants should achieve around 450 s. Chemically it is important, that the specific impulse is proportional to the square root of the temperature in the combustion chamber (T_c) divided by the molecular mass of the combustion products (M):

$$I_{sp} \propto \sqrt{\frac{T_c}{M}} \quad (2)$$

With regards to a practical application, the maximum payload of a rocket or missile can be doubled by increasing the specific impulse by 20 s.

In order to replace AP in solid rocket compositions, further requirements have to be taken into account, which are as follows:^[1, 17]

- high density, best close to 2 g cm^{-3} or even superior
- high oxygen balance, close to AP ($\Omega_{\text{CO}} = 34\%$) or even superior
- high thermal stability, at least a melting point of $150 \text{ }^\circ\text{C}$
- lower sensitivity compared to PETN ($\text{IS} > 4 \text{ J}$, $\text{FS} > 80 \text{ N}$)
- low vapor pressure
- convenient synthesis with minimum number of synthetic steps
- compatibility with fuel and binder
- high enthalpy of formation
- long term stable and storable.

Unlike some other requirements, the oxygen balance Ω can be determined, prior to practical experiments. It represents the relative amount of oxygen provided or needed during the combustion of a material without external sources of oxygen. The oxygen balance is calculated with the following equation for compounds with the empirical formula $\text{C}_a\text{H}_b\text{N}_c\text{O}_d$ and M is the molecular weight of the compound assuming the formation of CO .^[1]

$$\Omega_{\text{CO}} = \frac{[d - a - (\frac{b}{2})] \times 1600}{M} \quad (3)$$

To get to the oxygen balance assuming the formation of carbon dioxide (Ω_{CO_2}) the number of carbons needs to be multiplied by two in equation 3.

In the recent years several functional groups for HEDOs were investigated, ranging from excellent performing but very toxic fluorodinitro moiety, to trinitroalkyl compounds, which mainly possess great performance data but low thermal stability, as well as organic nitrates, which are often easily accessed from the corresponding alcohol but can suffer from long-term stability issues.^[18] Three of the current synthesized and most promising candidates are depicted in Figure I3.2.^[19] Even though first attempts concerning their activation energy and therefore their stability were made, there is still a long way to a practical application, starting from compatibility considerations *e. g.* with a possible binder.^[20]

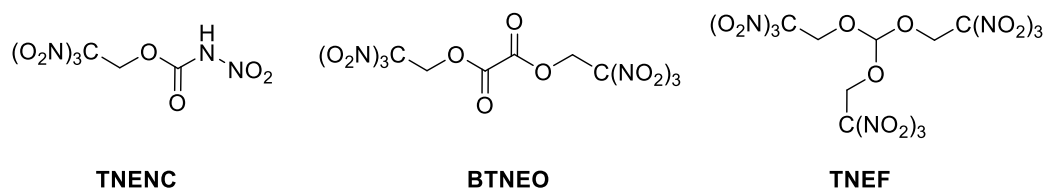


Figure I3.2 Molecular structures of potential HEDOs: 2,2,2-trinitroethyl *N*-nitrocarbamate (TNENC), bis(2,2,2-trinitroethyl) oxalate (BTNEO) and tris(2,2,2-trinitroethyl) orthoformate (TNEF).^[19, 20]

Altogether, ammonium perchlorate remains the most important applied oxidizer for composite propellants. Ammonium nitrate as well as ammonium dinitramide currently are the most promising alternatives, but they have not been used on a large scale yet. Therefore, establishing a new oxidizer remains a challenging task.

4 Toxicity Measurements

When talking about toxicity, one of the first things that comes to one's mind is Paracelsus, who is “the father” of toxicology. He lived in the 15th century and is credited with having said: “All things are poisonous, and nothing is without poison; only the dose makes a thing not poisonous.” This definition of a poison or a toxin remains quite up to date for substances, such as carcinogens, mutagens, teratogens and harmful pollutants.^[21] Furthermore, along with the dose, the toxic effect can vary from one organism to another as well as the exposure time, just to name a few parameters. Rosenbaum *et. al.* stated that to assess the toxicological effect of a chemical emitted into the environment a cause-effect chain is implied, which links emissions to impacts through three steps, the environmental fate, exposure and effects (Figure I4.1).^[22]

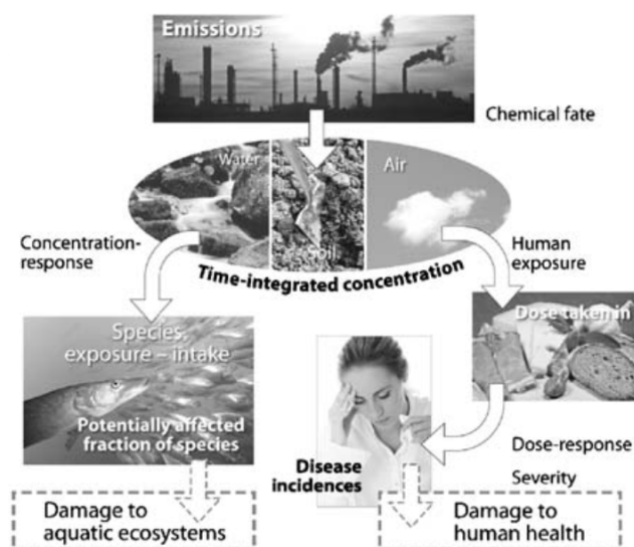


Figure I4.1 Proposed framework for comparative toxicity assessment.^[22]

To get a first impression on the aquatic toxicity of a certain substance, short-term tests based on *Aliivibrio fischeri* or *Daphnia magna* can be applied. For labeling compounds as "environmentally hazardous substances (aquatic environment)" according to the Globally Harmonized System of Classification, Labeling and Packaging of Chemicals (GHS) tests based on fish (96 h), crustacea (48 h), algae or other aquatic plants (min. 72 h) need to be applied. One of the first OECD accepted tests in the course of the chemical assessment of REACH is the AMES test. It is a relatively fast test to show the mutagenic potential of a certain compound and therefore may act as a carcinogen. Negative results received from the AMES test, are also mentioned in the GHS for the germ cell mutagenicity.^[23]

5 Objectives

The objective of this thesis is to synthesize and investigate unknown environmentally benign molecules, which contain a high amount of oxygen. This potentially high energy dense oxidizers are designed to be a possible ammonium perchlorate replacement in composite propellants. The investigated compounds should meet several requirements, such as excellent energetic performance parameters, as well as stable physical and chemical properties and a facile synthesis if possible. Different energetic moieties were implemented to develop molecules with a high oxygen content.

Even though, trinitroalkyl compounds tend to have low thermal stabilities, some general concepts of this work are based on this unit, because the trinitromethyl moiety possess a high oxygen balance and a high density through its intra- and intermolecular interactions. Nevertheless, the recent most promising HEDOs are aliphatic hydrocarbons equipped with this unit. It is possible to start with a trinitromethyl containing carbon backbone or add this moiety at the very end. The latter attempt is preferred, in case a synthesis should be performed on a larger scale.

Whenever it is possible and reasonable, salt formation is ought to be considered. Salts provide opportunities towards increasing the density and therefore the performance, due to the formation of hydrogen bonds on the one hand. On the other hand, sensitive ions can be exchanged with less sensitive or oxygen-richer ions. In this case considerable ions are:

- hydroxylammonium cation (NH_3OH^+ ; ✓ high performance; ✗ not that thermally stable)
- perchlorate anion (ClO_4^- ; ✓ thermally stable, high performance; ✗ not suitable as ammonium perchlorate replacement),
- periodate anion (IO_4^- ; ✓ high density; ✗ average performance),
- nitrate anion (NO_3^- ; ✓ cheap and easy to access; ✗ hygroscopic and average performance)

- dinitramide anion ($[\text{N}(\text{NO}_2)_2]^-$); ✓ high performance and oxygen content; ✗ higher price and low thermal stability).

Another attempt for using anionic polynitro-compounds is based on nitrocarbammates. Just like organic nitrates, nitrocarbammates are derived from alcohols, they form a class of energetic materials, tending to have lower sensitivities, higher thermal stabilities and just slightly lower performance as shown by the pentaerythritol derivatives pentaerythritol tetranitrate (PETN) and pentaerythritol tetranitrocarbamate (PETNC).

Another strategy towards oxygen-rich CHNO compounds is based on the formation of oxygen and nitrogen-rich heterocycles. They tend to go along with high densities, thermal stabilities and heats of formation, but stable naturally oxygen-rich heterocycles are barely found.

According the toxicity measurements of several energetic materials, the results of the luminescent bacteria inhibition test showed some toxicity trends of certain (energetic) functionalities. Moreover, three very promising compounds were tested towards their mutagenic potential in the experimental AMES test and the results were compared to *in silicio* obtained values.

6 References

- [1] T. M. Klapötke, *Chemistry of High-Energy Materials*, 5th ed., De Gruyter, Berlin, **2019**.
- [2] J. P. Agrawal, *High Energy Materials Propellants, Explosives and Pyrotechnics*, 1st ed., Wiley-VCH, Weinheim (Germany), **2010**.
- [3] J. Akhavan, *The Chemistry of Explosives*, 2nd ed., Royal Soc. of Chemistry, Cambridge, **2004**.
- [4] a) D. Fischer, T. M. Klapötke, J. Stierstorfer, Potassium 1,1'-Dinitramino-5,5'-Bistetrazolate: A Primary Explosive with Fast Detonation and High Initiation Power, *Angew. Chem. Int. Ed.* **2014**, *53*, 8172–8175; b) J. W. Fronabarger, M. D. Williams, W. B. Sanborn, J. G. Bragg, D. A. Parrish, M. Bichay, DBX-1 – a Lead Free Replacement for Lead Azide, *Propellants, Explos., Pyrotech.* **2011**, *36*, 541–550.
- [5] a) N. V. Latypov, J. Bergman, A. Langlet, U. Wellmar, U. Bemm, Synthesis and Reactions of 1,1-Diamino-2,2-Dinitroethylene, *Tetrahedron* **1998**, *54*, 11525–11536; b) N. Fischer, D. Fischer, T. M. Klapötke, D. G. Piercey, J. Stierstorfer, Pushing the Limits of Energetic Materials - the Synthesis and Characterization of Dihydroxylammonium 5,5'-Bistetrazole-1,1'-Diolate, *J. Mater. Chem.* **2012**, *22*, 20418–20422.
- [6] J. Glück, T. M. Klapötke, M. Rusan, J. J. Sabatini, J. Stierstorfer, A Strontium- and Chlorine-Free Pyrotechnic Illuminant of High Color Purity, *Angew. Chem. Int. Ed.* **2017**, *56*, 16507–16509.
- [7] H. Oberth, *Wege Zur Raumschiffahrt*, De Gruyter, Berlin (Germany), **1929**.
- [8] H. A. Neal, T. Smith, J. McCormick, *Beyond Sputnik : U. S. Science Policy in the Twenty-First Century*, University of Michigan Press, Ann Arbor (United States), **2008**.
- [9] a) N. Wingborg, M. Skarstind, M. Sjöblom, A. Lindborg, M. Brantlind, J. Johansson, S. Ek, M. Liljedahl, J. Kjellberg, in *7th European Conference for Aeronautics and Space Sciences (EUCASS)*, EUCASS, Milan, **2017**; b) A. Davenas, *Solid Rocket Propulsion Technology*, Pergamon Press, Oxford (UK), **1993**; c) P120c Static Fire Test, <https://blogs.esa.int/ariane6/2018/07/25/p120c-static-fire-test/> (June 03, 2020)
- [10] a) A. Srinivasan, T. Viraraghavan, Perchlorate: Health Effects and Technologies for Its Removal from Water Resources, *Int. J. Environ. Res. Public Health* **2009**, *6*, 1418–1442; b) J. Wolff, Perchlorate and the Thyroid Gland, *Pharmacol. Rev.* **1998**, *50*, 89–105; c) C. Portulano, M. Paroder-Belenitsky, N. Carrasco, The Na⁺/I⁻ Symporter (NIS): Mechanism and Medical Impact, *Endocr. Rev.* **2014**, *35*, 106–149.
- [11] a) E. D. McLanahan, J. L. Campbell, Jr., D. C. Ferguson, B. Harmon, J. M. Hedge, K. M. Crofton, D. R. Mattie, L. Braverman, D. A. Keys, M. Mumtaz, J. W. Fisher, Low-Dose Effects of

Ammonium Perchlorate on the Hypothalamic-Pituitary-Thyroid Axis of Adult Male Rats Pretreated with PCB126, *Toxicol. Sci.* **2007**, *97*, 308–317; b) EPA, *Health Risk Reduction and Cost Analysis of the Proposed Perchlorate National Primary Drinking Water Regulation*, **2019**.

[12] The Effects of Ammonium Perchlorate on Reproduction and Development of Amphibians, <https://apps.dtic.mil/dtic/tr/fulltext/u2/a495519.pdf> (June 04, 2020)

[13] a) E. T. Urbansky, Perchlorate as an Environmental Contaminant, *Environ. Sci. and Pollut. Res.* **2002**, *9*, 187–192; b) C. W. Trumpolt, M. Crain, G. D. Cullison, S. J. P. Flanagan, L. Siegel, S. Lathrop, Perchlorate: Sources, Uses, and Occurrences in the Environment, *Remediation* **2005**, *16*, 65–89.

[14] a) Ammonium Perchlorate, Substance Infocard, <https://echa.europa.eu/de/substance-information/-/substanceinfo/100.029.305> (May 18, 2020); b) Reductions of Perchlorate in Drinking Water, https://www.epa.gov/sites/production/files/2020-05/documents/perchlorate_reductions_5.14.20.pdf (July 27, 2020)

[15] N. Kubota, *Propellants and Explosives*, Wiley-VCH, Weinheim (Germany), **2002**.

[16] a) A. Larsson, N. Wingborg, *Green Propellants Based on Ammonium Dinitramide (ADN)*, INTECH Open Access Publisher, Rijeka (Croatia), **2011**; b) C. Oommen, S. R. Jain, Ammonium Nitrate: A Promising Rocket Propellant Oxidizer, *J. Haz. Mater.* **1999**, *67*, 253–281; c) S. Löbbbecke, H. H. Krause, A. Pfeil, Thermal Analysis of Ammonium Dinitramide Decomposition, *Propellants, Explos., Pyrotech.* **1997**, *22*, 184–188.

[17] NATO, *Manual of Data Requirements and Tests for the Qualification of Explosive Materials for Military Use*, **2003**.

[18] a) T. M. Klapötke, B. Krumm, S. F. Rest, M. Reynders, R. Scharf, (2-Fluoro-2,2-Dinitroethyl)-2,2,2-Trinitroethylnitramine: A Possible High-Energy Dense Oxidizer, *Eur. J. Inorg. Chem.* **2013**, 5871–5878; b) Q. J. Axthammer, B. Krumm, T. M. Klapötke, R. Scharf, A Study of the 3,3,3-Trinitropropyl Unit as a Potential Energetic Building Block, *Chem. – Eur. J.* **2015**, *21*, 16229–16239; c) T. M. Klapötke, B. Krumm, T. Reith, Polynitrocarbmates Derived from Nitromethane, *Z. Anorg. Allg. Chem.* **2017**, *643*, 1474–1481.

[19] a) Q. J. Axthammer, T. M. Klapötke, B. Krumm, R. Moll, S. F. Rest, The Energetic Nitrocarbmate $O_2NN(H)CO[OCH_2C(NO_2)_3]$ Derived from Phosgene, *Z. Anorg. Allg. Chem.* **2014**, *640*, 76–83; b) T. M. Klapötke, B. Krumm, R. Moll, S. F. Rest, Chno Based Molecules Containing 2,2,2-Trinitroethoxy Moieties as Possible High Energy Dense Oxidizers, *Z. Anorg. Allg. Chem.* **2011**, *637*, 2103–2110; c) T. M. Klapötke, B. Krumm, R. Scharf, Oxalyl Chloride and Hydrazide Based Energetic Polynitro Derivatives, *Eur. J. Inorg. Chem.* **2016**, 3086–3093.

[20] a) M. Abd-Elghany, A. Elbeih, T. M. Klapötke, Thermo-Analytical Study of 2,2,2-Trinitroethyl-Formate as a New Oxidizer and Its Propellant Based on a Gap Matrix in

Comparison with Ammonium Dinitramide, *J. Anal. App. Pyrolysis* **2018**, *133*, 30–38; b) M. Abd-Elghany, A. Elbeih, M. Klapötke Thomas, Thermal Behavior and Decomposition Kinetics of Bis(2,2,2-Trinitroethyl)-Oxalate as a High Energy Dense Oxidizer and Its Mixtures with Nitrocellulose, *Propellants, Explos. Pyrotech.* **2017**, *42*, 1373–1381; c) M. Abd-Elghany, A. Elbeih, M. Klapötke Thomas, B. Krumm, Higher Performance and Safer Handling: Formulation Based on 2,2,2-Trinitroethyl Formate and Nitrocellulose, *ChemPlusChem* **2018**, *83*, 128–131.

[21] H.-W. Vohr, *Toxikologie*, John Wiley & Sons, Hoboken (United States), **2012**.

[22] R. K. Rosenbaum, T. M. Bachmann, L. S. Gold, M. A. J. Huijbregts, O. Jolliet, R. Juraske, A. Koehler, H. F. Larsen, M. MacLeod, M. Margni, T. E. McKone, J. Payet, M. Schuhmacher, D. van de Meent, M. Z. Hauschild, Usetox—the Unep-Setac Toxicity Model: Recommended Characterisation Factors for Human Toxicity and Freshwater Ecotoxicity in Life Cycle Impact Assessment, *Int. J. of Life Cycle Assess.* **2008**, *13*, 532.

[23] UN, *Globally Harmonized System of Classification and Labelling of Chemicals (GHS)*, **2019**.

II Results and Discussion

1 Michael Addition of Trinitromethane

2 Trinitropropyl Ammonium Salts

3 Trinitroethyl Esters Based on Divalent Acids

4 Azoles with Trinitroalkyl Substitution

5 Urazine Derivatives

6 Salts of Pentaerythritol Tetranitrocarbamate

7 Aquatic Toxicity Measurements

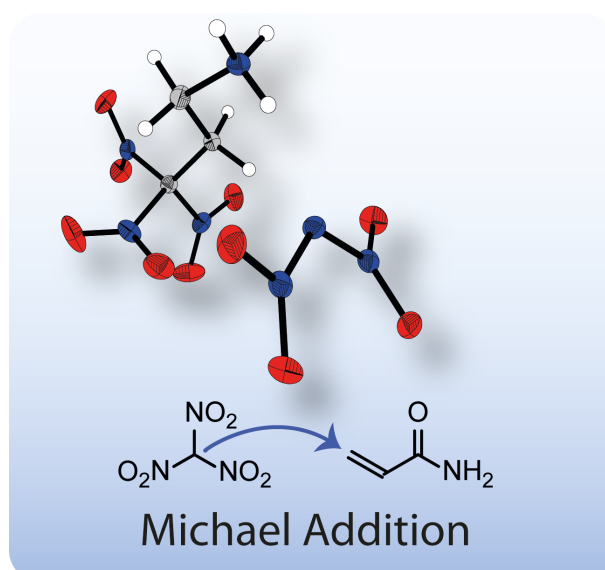
8 Comparative Toxicological Study

1 Michael Addition of Trinitromethane

Convenient Synthesis of Energetic Polynitro Materials including $(\text{NO}_2)_3\text{CCH}_2\text{CH}_2\text{NH}_3$ -salts via Michael Addition of Trinitromethane

Q. J. Axthammer, T. M. Klapötke, B. Krumm, R. Scharf and C. C. Unger

Dalton Trans. **2016**, 45, 18909–18920.



1.1 Abstract

The nucleophilic Michael addition of nitroform with acrylamide creates a variety of energetic products. Several interesting compounds with a trinitromethyl group were synthesized, among them salts containing the trinitropropylammonium cation $[(\text{NO}_2)_3\text{CCH}_2\text{CH}_2\text{NH}_3]\text{X}$. Owing to their positive oxygen balance, the suitability of these compounds as potential high-energy dense oxidizers (HEDOs) in energetic formulations was investigated and discussed. Furthermore, numerous important and reactive compounds for the continuing synthesis of molecules with a high oxygen balance are presented. All compounds were fully characterized, including multinuclear NMR spectroscopy, vibrational analysis (IR, Raman), elemental analysis as well as single crystal X-ray diffraction. Thermal stabilities were studied using differential scanning calorimetry and sensitivity data against friction, impact and electrostatic discharge were collected. The energies of formation were calculated using Gaussian 09 and energetic properties, like the specific impulse and detonation velocity, were predicted with the EXPLO5 (V6.02) computer code.

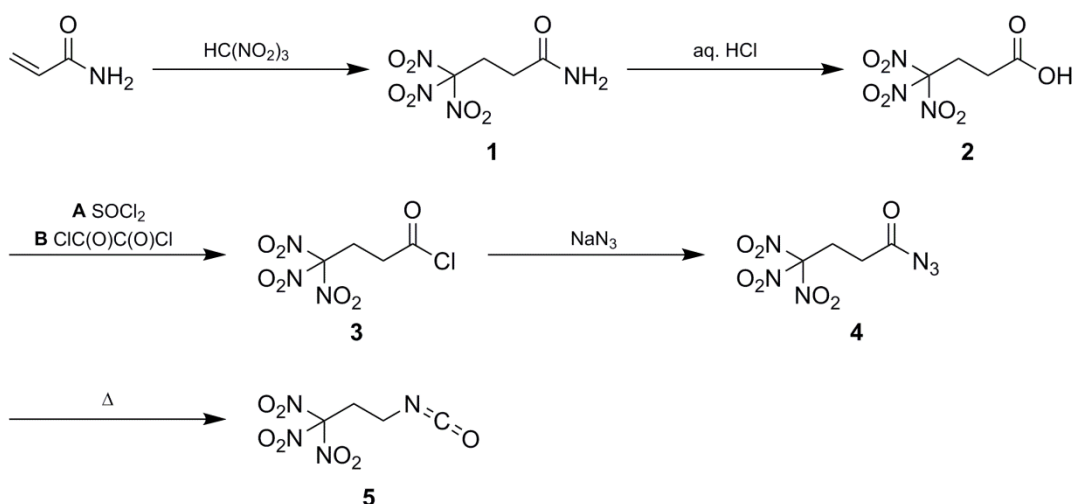
1.2 Introduction

The trinitromethane (nitroform) unit is an important building block in the chemistry of high-energy materials, especially in the field of high-energy dense oxidizers (HEDOs).^[1] This trinitromethane unit can easily be introduced by a nucleophilic addition on electron deficient α,β -unsaturated starting materials. The so-called Michael addition is one of the most important carbon-carbon bond forming reactions in synthetic organic chemistry. Michael donors are substrates with acidic protons which therefore are capable of forming carbanions. This includes anions from nitroform, fluorodinitromethane, primary nitroalkanes, and secondary nitroalkanes.^[2] The electron deficient alkene in this nucleophilic addition is called the Michael acceptor and includes a wide range of α,β -unsaturated ketones, aldehydes, carboxylic acids, esters, amides and cyanides.^[3] One such example is reported in the nucleophilic addition of some polynitroalkanes to acrolein oxime.^[4] In this contribution nitroform and the readily available acrylamide are used to build several new oxygen-rich molecules as well as energetic salts containing the $(\text{NO}_2)_3\text{CCH}_2\text{CH}_2\text{NH}_3$ -cation.

1.3 Results and Discussion

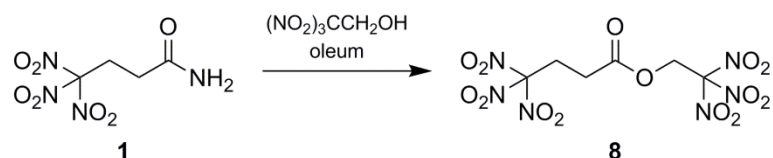
1.3.1 Synthesis

Earlier investigations showed, that with tetranitromethane and various acrylamides, mostly mixtures of 3-nitroisoxazoles and Michael addition products were formed.^[5] However the reaction of acrylamide with nitroform resulted exclusively in the formation of the Michael addition product 4,4,4-trinitrobutanamide (**1**). A similar synthesis of **1** has been reported earlier.^[6a, 7] However, in the herein presented advanced synthesis **1** was obtained without the use of further chemicals, as mentioned in literature procedures from readily available chemicals (Scheme 1.1).^[6a, 7] A further advantage is the faster conversion without heating as well as increased yields from 64% to 97%. Due to the almost full conversion of acrylamide pure **1** without further purification was obtained.



Scheme 1.1 Synthesis of 1,1,1-trinitropropan-3-isocyanate (**5**) starting from acrylamide and trinitromethane.

The acid 4,4,4-trinitrobutanoic acid (**2**) was prepared by hydrolysis of the amide **1** in aqueous concentrated hydrochloric acid. The crude material was recrystallized from chloroform to obtain a pure product in 80% yield. Due to their straightforward synthesis with high yields compounds **1** and **2** are excellent starting materials for various compounds containing the trinitromethyl moiety.^[8] The acid **2** was converted to the corresponding carbonyl chloride by refluxing in excess thionyl chloride (Method A). The reaction time should be longer than 20 hours to ensure complete conversion to the acid chloride and to prevent the formation of the acid anhydride.^[9] 4,4,4-Trinitrobutanoyl chloride (**3**) was isolated in 88% yield. A more convenient synthesis for the carbonyl chloride **3** is the conversion of acid **2** with a stoichiometric amount of oxalyl chloride and DMF as catalyst (Method B). Compound **3** was obtained in 96% yield while the reaction time was reduced to 4 h.



Scheme 1.4 Esterification of the amide **1** to form 2,2,2-trinitroethyl-4,4,4-trinitrobutanoate (**8**).

An oxygen rich molecule was also prepared by the esterification of the amide **1** with the alcohol 2,2,2-trinitroethanol. The reaction was performed in oleum as strong dehydrating agent.^[13] After recrystallization from water/methanol the ester 2,2,2-trinitroethyl-4,4,4-trinitrobutanoate (**8**) was obtained as pure colorless solid (Scheme 1.4).

1.3.2 Multinuclear NMR Spectroscopy

All compounds were thoroughly characterized by ^1H , ^{13}C and ^{14}N NMR spectroscopy. In the ^1H NMR spectra the two neighboring CH_2 groups are within the range of 3.90 to 2.52 ppm. The methylene unit next to the trinitromethyl moiety is mostly shifted to higher field compared to the CH_2 groups next to a nitrogen or oxygen atom. The vicinal coupling constants of the hydrogen atoms in the ethylene group are not equal due to the rotation around the C–C bond, which causes a AA'XX' spin system.^[14] The resonances of the CH_2 moiety of the trinitroethyl group is observed at lower field (4.96 ppm (**7**) and 5.20 ppm (**8**)) compared to the trinitropropyl group.

In the ^{13}C NMR spectra the carbon resonances of the two CH_2 groups of the trinitropropyl part are very variable and are found in the range of 40.5 to 27.6 ppm. The carbon resonances of the trinitromethyl moieties are observed as broadened signals. Those of the trinitropropyl unit are located at around 128 ppm whereas the resonances of the trinitroethyl unit of compounds **7** and **8** are slightly upfield shifted to approximately 126 ppm.

In the ^{14}N NMR spectra the resonances for the nitro groups of the trinitromethyl moieties are all quite sharp and found in the range of –13 to –31 ppm. For the ammonium moieties of the salts **6a–e** resonances are observed around –355 ppm.

1.3.3 Vibrational Spectroscopy

All compounds were also characterized by IR and Raman spectroscopy. The most characteristic frequencies in the compounds are the carbonyl and nitro groups. The characteristic $\nu(\text{C}=\text{O})$ stretching vibration is located in a large range from 1785 to 1676 cm^{-1} . Noticeable is the shift of the carbonyl stretching vibrations to higher wave numbers in molecules which are connected to electron-withdrawing moieties. The maximum is the acid chloride **3** where the $\nu(\text{C}=\text{O})$ is located at 1785 cm^{-1} , while for the two amides **1** and **7** signals at 1695 and 1676 cm^{-1} are observed. For the trinitromethyl units both the asymmetric $\nu_{\text{as}}(\text{NO}_2)$ in the range of 1604–1582 cm^{-1} and the symmetric stretching vibrations $\nu_{\text{s}}(\text{NO}_2)$ at 1303–1288 cm^{-1} are observed. The

antisymmetric stretching vibration of the azide moiety of compound **4** is found as characteristic strong signal at 2148 cm^{-1} .

1.3.4 Single Crystal Structure Analysis

Single crystals suitable for X-ray diffraction measurements were obtained by crystallization at ambient temperature from water (**1**, **2**, **6a**, **6b**, and **6d**), from neat material (**4**) or from chloroform (**8**). A full list of the crystallographic refinement parameters and structure data can be found in Appendix A1.

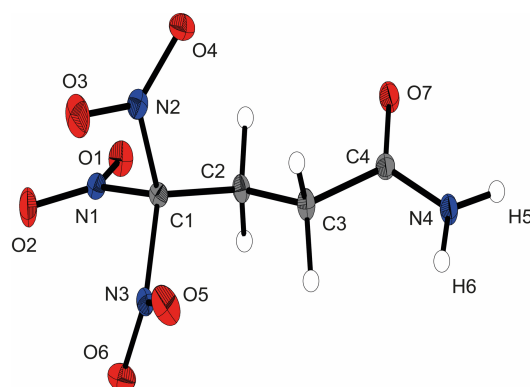


Figure 1.1 X-ray molecular structure of 4,4,4-trinitrobutanamide (**1**). Selected atom distances (Å) and angles (deg.): C1–C2 1.502(2), C1–N1 1.540(2), C1–N2 1.538(2), C1–N3 1.521(1), C2–C3 1.524(2), C3–C4 1.522(2), C4–N4 1.332(2), C4–O7 1.237(1), N1–O1 1.211(1), N4–H5 0.89(2), N4–H6 0.87(1), C2–C1–N2 114.15(9), C2–C1–N1 112.09(9), C2–C1–N3 110.49(9), H6–N4–C4–C3 $-178(1)$, H5–N4–C4–O7 $-177(1)$, N4–C4–C3–C2 $-157.3(1)$, C3–C2–C1–N1 $-175.87(9)$.

The amide **1** crystallizes in the triclinic space group $P\bar{1}$ with one molecule as asymmetric unit. The density is 1.835 g cm^{-3} and the molecular structure is shown in Figure 1.1. The geometry of the structure has some very typical characteristics of trinitromethyl compounds.^[1b,c, 8] The C–N bond lengths in the trinitromethyl moiety are in the range of 1.54 Å , which is significantly longer than a regular C–N bond (1.47 Å) and results from steric repulsion of the proportionally large nitro groups.^[1c] As expected, the amide unit is nearly planar and shows a shortened C–N bond.

The acid **2** crystallizes in the monoclinic space group $P2_1/n$ and is shown in Figure 1.2. The quite low density of 1.720 g cm^{-3} can be explained by the strong hydrogen bonds which are formed between two carbonyl moieties with a donor acceptor distance of 2.632 Å (O8–H8 \cdots O7) and a donor acceptor angle of 176.5° (O8–H8 \cdots O7).^[15] In this structure another characteristic structure feature, the propeller-like arrangement of the trinitromethyl group can be observed. The three nitro groups are organized around the carbon in a propeller-like geometry to optimize the non-bonded N \cdots O intramolecular attractions (N2 \cdots O2, O5 \cdots N1, N3 \cdots O4). This results in an intramolecular interaction between the partial positive charged nitrogen and the negative charged oxygen in the nitro group. These N \cdots O attractions are found with distances in the range of

2.55 Å, which are much shorter than the sum of the van der Waals radii of nitrogen and oxygen (3.07 Å).^[1c, 16]

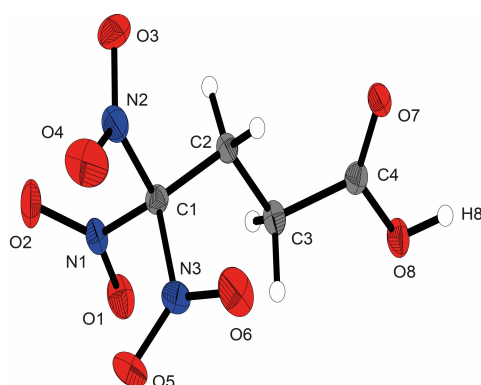


Figure 1.2 X-ray molecular structure of 4,4,4-trinitrobutanoic acid (**2**). Selected atom distances (Å) and angles (deg.): C1–N1 1.523(2), C2–C3 1.528(2), C3–C4 1.509(2), C3–H3 0.99(2), C4–O7 1.218(2), C4–O8 1.311(2), N1–O1 1.216(1), O8–H5 0.86(2), C2–C1–N1 115.2(1), H5–O8–C4–C3 –175(1), O8–C4–C3–C2 179.0(1), C4–C3–C2–C1 –158.4(1), C3–C2–C1–N2 178.3(1), N2–O2 2.557(2), O5–N1 2.571(1), N3–O4 2.550(2).

The carbonyl azide **4** crystallizes in the triclinic space group $P\bar{1}$ with one molecule as an asymmetric unit and shows the propeller-like geometry of the trinitromethyl group. The molecular structure is shown in Figure 1.3. The azide, the carbonyl and the carbon backbone inclusively, shows a nearly planar arrangement which is shown by the torsion angle of 1.2(2)° (N5–N4–C4–O7). Typical for carbonyl azides is the slight bending of the azide moiety with an angle of 174.2°. The N4–N5 and N5–N6 bond lengths (1.273(3) and 1.121(3) Å, respectively) are comparable with those in other carbonyl azides.^[17]

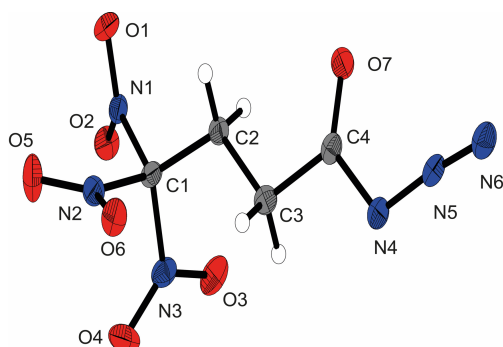


Figure 1.3 X-ray molecular structure of 4,4,4-trinitrobutanoyl azide (**4**). Selected atom distances (Å) and angles (deg.): C1–C2 1.512(2), C1–N1 1.532(2), C2–C3 1.528(3), C3–C4 1.503(2), C4–N4 1.409(2), C4–O7 1.205(2), N4–N5 1.273(2), N5–N6 1.112(2), C2–C1–N3 114.4(1), C4–N4–N5 111.5(1), N4–N5–N6 174.2(2), N6–N5–N4–C4 –176(1), N5–N4–C4–O7 1.2(2), N4–C4–C3–C2 –175.0(1), C4–C3–C2–C1 178.0(1), O2–N2 2.573(2), N1–O5 2.577(2), O4–N3 2.541(1).

The chloride salt **6a** crystallizes as a monohydrate in the triclinic space group $P\bar{1}$ and a density of 1.733 g cm⁻³. The asymmetric unit is shown in Figure 1.4. The conformation of the C1, C2, C3 and N4 atoms is almost perfectly staggered. The extended structure involves secondary

interactions in terms of classical intermolecular N–H···O hydrogen bonds and unusual so-called non-classical hydrogen bonds of the type C–H···O. The majority are classified as quite strong.^[15]

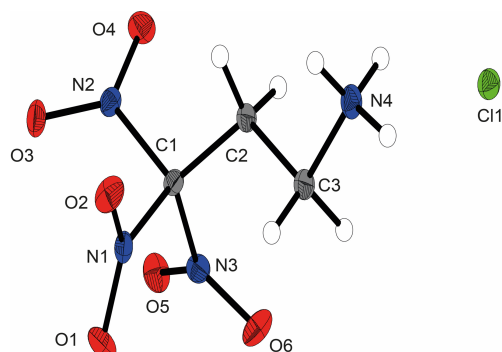


Figure 1.4 X-ray molecular structure of 3,3,3-trinitropropyl-1-ammonium chloride (**6a**). Selected atom distances (Å) and angles (deg.): C1–C2 1.507(2), C1–N1 1.522(2), C2–C3 1.533(2), C3–N4 1.491(2), N1–O1 1.217(1), N4–H6 0.89(2), N4–H7 0.88(2), N4–H8 0.88(2), C2–C1–N3 114.5(1), C3–N4–H7 111(1), C3–N4–H8 107(1), C3–N4–H6 109(1), H7–N4–C3–C2 –178(1), N4–C3–C2–C1 –160.1(1), O5–N2 2.582(2), O1–N3 2.555(2), N1–O3 2.545(2).

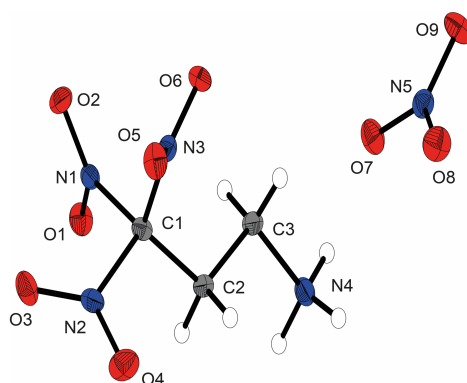


Figure 1.5 X-ray molecular structure of 3,3,3-trinitropropyl-1-ammonium nitrate (**6b**). Selected atom distances (Å) and angles (deg.): C1–C2 1.512(2), C1–N1 1.529(2), C2–C3 1.526(2), C3–N4 1.492(2), N1–O1 1.223(2), N5–O7 1.269(2), N5–O8 1.233(2), N5–O9 1.266(2), N4–C3–C2–C1 –173.7(1), C3–C2–C1–N2 175.8(1), H6–N4–C3–C2 170(1), O8–N5–O7–O9 179.7(3), O5–N2 2.581(2), O2–N3 2.587(2), N1–O3 2.530(2).

The nitrate salt **6b** crystallizes in the orthorhombic space group $P2_12_12_1$ with a density of 1.804 g cm^{-3} . The asymmetric unit consists of one anion and cation and is illustrated in Figure 1.5. The protonated form of the 3,3,3-trinitropropan-1-amine shows the same structure characteristics as the hydrochloric salt **6a**.

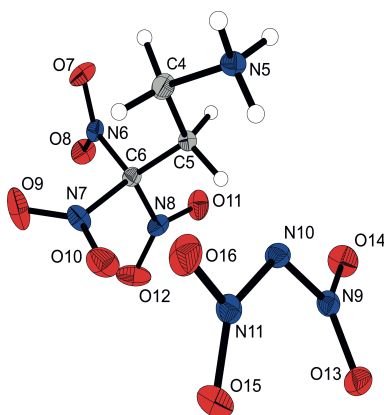


Figure 1.6 X-ray molecular structure of 3,3,3-trinitropropyl-1-ammonium dinitramide (**6d**). Selected atom distances (Å) and angles (deg.): O7–N6 1.216(2), O8–N6 1.209(2), N5–C4 1.484(2), N6–C6 1.529(3), N7–C6 1.523(2), N8–C6 1.528(2), C4–C5 1.530(2), C5–C6 1.505(2), O13–N9 1.220(2), O14–N9 1.239(2), O15–N11 1.233(2), O16–N11 1.243(2), N9–N10 1.380(2), N10–N11 1.357(2), O13–N9–N10 124.2(1), O14–N9–N10 111.7(1), N9–N10–N11 115.4(1), O15–N11–N10 124.7(1), O16–N11–N10 112.8(1), O13–N9–N10–N11 –20.8(2).

The molecular structure of the dinitramide salt **6d** is shown in Figure 1.6. Compound **6d** crystallizes in the monoclinic space group $P-1$ with two anions and two cations as asymmetric unit and a density of 1.872 g cm^{-3} . The 3,3,3-trinitropropyl-1-ammonium cation shows similar structural features as the ionic structures discussed before. The nitro groups of the dinitramide moiety are slightly twisted out of plane with torsion angles about 20° . The N–N bond lengths with an average distance of 1.37 Å are also slightly shorter than common N–N single bonds.

The ester **8** crystallizes in the monoclinic space group $P2_1/n$ with four formula units per unit cell. The asymmetric unit consists of one molecule and is displayed in Figure 1.7. The average of the N–O and C–NO₂ bond lengths of the trinitromethyl units are all in the same range of 1.21 Å in N–O and 1.52 Å in C–NO₂ whereas no distinction between the ethyl and propyl moiety is visible. Also, both trinitromethyl groups show independently the propeller-like orientation of the nitro groups. Also, the carbon-carbon bonds are virtually identical within a range of 1.50 to 1.52 Å . Although no classical hydrogen bonds are found in the crystal structure a high density is 1.869 g cm^{-3} was observed. However, non-classical hydrogen bonds of the type C–H \cdots O are found, whereas the majority is classified as quite strong.^[15]

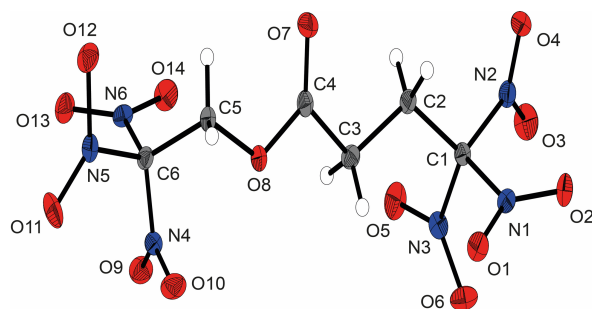


Figure 1.7 X-ray molecular structure of 2,2,2-trinitroethyl-4,4,4-trinitrobutanoate (**8**). Selected atom distances (Å) and angles (deg.): C1–C2 1.515(2), C1–N1 1.528(2), C2–C3 1.514(2), C3–C4 1.497(2), C4–O7 1.200(2), C4–O8 1.363(2), C5–C6 1.520(2), C5–O8 1.424(2), C6–N4 1.525(2), N1–O1 1.222(1), N4–O9 1.213(2), N2–C1–C2–C3 161.5(1), C1–C2–C3–C4 169.4(1), C3–C4–O8–C5 –175.6(1), C4–O8–C5–C6 131.7(1), O8–C5–C6–N5 160.2(1), N3–O3 2.558(2), O6–N1 2.567(2), N2–O2 2.534(1), N4–O11 2.608(2), N5–O13 2.583(2), O9–N6 2.557(1).

1.3.5 Thermal Stabilities and Energetic Properties

Compounds **1**, **2**, **6a–e**, **7**, and **8** were stable when exposed to air and moisture. The azide **4** has to be handled very carefully, owing to its high sensitivity towards heat. Reactions of the isocyanate **5** must be carried out with exclusion of moisture. Furthermore, it should be stored frozen and is not longtime stable, due to rapid polymerization. The thermal stabilities of all compounds were investigated by performing various DSC measurements with a heating rate of $5\text{ }^{\circ}\text{C min}^{-1}$. The temperatures at which melting and decomposition occurred are shown in Table 1.1 together with other physical properties. A remarkably high decomposition point of $178\text{ }^{\circ}\text{C}$ was observed for compound **6a**, likely owing to its stability to form strong hydrogen bonds through the salt structure. Moreover, compounds **7** and **8** (both $155\text{ }^{\circ}\text{C}$) showed satisfying decomposition points for applications as high-energy dense oxidizers based on CHNO compounds. The sensitivities of compounds **2–8** towards impact, friction, and electrostatic discharge were experimentally determined according to the NATO Standardization Agreements,^[18] the results are displayed in Table 1.1. All compounds, with exception of the azide **4**, the dinitramide salt **6d**, and the 5,5'-azobistetrazolate salt **6e** showed moderate impact and friction sensitivities.^[19] For the amide **1** as well as the nitrate salt **6b** impact sensitivities of 6 J are found, which are in the range of the well-known explosive Hexogen (RDX).

Predictions of the detonation and combustion parameters by using the EXPLO5 V6.02^[20] code have been performed based on the heats of formations which were obtained from *ab initio* calculations. The energetic parameters were calculated with the room temperature densities, which were measured experimentally by gas pycnometer. The resulting heats of detonation Q_v , detonation temperatures T_{ex} , detonation pressures p , and detonation velocities V_{det} for compounds **1**, **2**, **4**, and **6–8** are shown in Table 1.2. The dinitramide salt **6d** has the highest detonation parameters with a detonation velocity V_{det} of 9282 m s^{-1} and a detonation pressure of 372 kbar and exceeds the high military explosive RDX (8838 m s^{-1}) by far.^[20]

The specific impulses I_{sp} of compounds **1**, **2**, **4**, and **6–8** were calculated for the neat compounds, for compositions with different amounts of aluminum as fuel, and additional with binder and are also listed in Table 1.2. These impulses were compared with the calculated impulses of ammonium perchlorate (AP) in an analogous composition. The chosen mixture with AP as an oxidizer provided a specific impulse of 261 s. All compounds show good properties, especially when calculated without binder. The value for the specific impulse of the 5,5'-azobistetrazolate salt **6e** exceeds all others; for the neat compound it is calculated to 271 s, with an admixture of 10% aluminum as fuel 282 s could be achieved (Table 1.2). For the nitrate and dinitramide salts **6b** and **6d** remarkable high specific impulses of 278 s were reached in compositions containing 85% oxidizer and 15% fuel. In composites containing oxidizer, fuel and binder the specific impulses decrease slightly. The best specific impulse is obtained for the dinitramide salt **6d** with a calculated value of 275 s in a composite propellant consisting of 15% aluminum and 14% binder. However, also the specific impulses of the nitrate and perchlorate salts **6b** and **6c** with values of 270 (**6b**) and 272 s (**6c**) exceed the specific impulse of the standard optimized mixture of AP (261 s).

Table 1.1 Physical properties of the compounds **1**, **2**, **4**, **6a–e**, **7**, and **8** in comparison to AP.

	1	2	4	6a	6b	6c	6d	6e	7	8	AP
Formula	C ₄ H ₆ N ₄ O ₇	C ₄ H ₅ N ₃ O ₈	C ₄ H ₄ N ₆ O ₇	C ₃ H ₇ N ₄ O ₆ Cl	C ₃ H ₇ N ₅ O ₉	C ₃ H ₇ N ₄ O ₁₀ Cl	C ₃ H ₇ N ₇ O ₁₀	C ₈ H ₁₄ N ₁₈ O ₁₂	C ₆ H ₆ N ₆ O ₁₄	C ₆ H ₇ N ₇ O ₁₃	NH ₄ ClO ₄
MW [g mol ⁻¹]	222.11	223.10	248.11	230.56	257.12	294.56	301.13	554.31	385.16	386.14	117.49
Density RT [a]	1.78	1.67	1.71	1.76	1.77	1.97	1.84	1.67	1.83	1.84	1.95
T _m [°C] ^[b]	93	55	22	161	135	-	-	-	92	150	-
T _{dec} [°C] ^[c]	120	176	85	178	138	164	112	120	155	155	240
IS [J] ^[d]	6	40	2	20	6	2.5	2	2	30	10	15
FS [N] ^[e]	360	324	144	>360	120	16	30	54	240	240	>360
ESD [J] ^[f]	0.50	0.30	0.10	0.40	0.20	0.08	0.40	0.60	0.10	0.20	>1.50
N [%] ^[g]	25.2	18.8	33.9	24.3	27.2	19.0	32.6	54.6	21.8	25.5	11.9
O [%] ^[h]	50.4	57.4	45.1	41.6	56.0	54.3	53.1	26.7	58.0	54.0	54.5
N + O [%] ^[i]	75.6	76.2	79.0	65.9	83.2	73.3	85.7	81.3	79.8	79.5	66.4
Ω _{CO} [%] ^[j]	0.0	+10.1	+6.5	0.0	+15.6	+21.7	+18.6	-11.1	+20.7	+14.5	+34.6
Ω _{CO₂} [%] ^[j]	-28.1	-17.9	-19.4	-2.4	-3.1	+5.4	+2.7	-33.4	-4.1	-10.4	+34.6
ΔH _f ^o [kJ mol ⁻¹] ^[k]	-326	-506	54	-96	-169	-119	32	972	-466	-330	-296
ΔU _f ^o [kJ kg ⁻¹] ^[l]	-1374	-2178	301	-318	-554	-312	205	1851	-1124	-770	-2433

[a] Densities at RT measured by gas pycnometer. [b] Onset melting T_m and [c] onset decomposition point T_{dec} from DSC measurement carried out at a heating rate of 5 °C min⁻¹. [d] Impact sensitivity. [e] Friction sensitivity. [f] Sensitivity toward electrostatic discharge. [g] Nitrogen content. [h] Oxygen content. [i] Sum of nitrogen and oxygen content. [j] Oxygen balance assuming the formation of CO and the formation of [j] CO₂ at the combustion. [k] Enthalpy and [l] energy of formation calculated by the CBS-4M method using Gaussian 09.

Table 1.2 Calculated detonation and combustion parameters of compound **1**, **2**, **4**, **6a–e**, **7**, and **8** (using EXPLO5 V6.02)^[20a] in comparison to AP.

	1	2	4	6a	6b	6c	6d	6e	7	8	AP
Formula	C ₄ H ₆ N ₄ O ₇	C ₄ H ₅ N ₃ O ₈	C ₄ H ₄ N ₆ O ₇	C ₃ H ₇ N ₄ O ₆ Cl	C ₃ H ₇ N ₅ O ₉	C ₃ H ₇ N ₄ O ₁₀ Cl	C ₃ H ₇ N ₇ O ₁₀	C ₈ H ₁₄ N ₁₈ O ₁₂	C ₆ H ₆ N ₆ O ₁₄	C ₆ H ₇ N ₇ O ₁₃	NH ₄ ClO ₄
Q_v [kJ kg ⁻¹] ^[a]	-4956	-4786	-5607	-5281	-6697	-6250	-6671	-6212	-6121	-5820	-1422
T_{ex} [K] ^[b]	3383	3505	4071	3793	4319	4309	4382	4141	4277	4009	1735
V_0 [L kg ⁻¹] ^[c]	733	731	759	744	821	787	828	814	719	718	885
P_{CJ} [kbar] ^[d]	292	246	291	282	335	390	372	299	324	335	158
V_{det} [m s ⁻¹] ^[e]	8187	7624	8259	8019	8913	9096	9282	8541	8616	8628	6368
I_{sp} [s] ^[f]	238	241	261	255	274	265	274	271	258	262	157
I_{sp} [s] (5% Al) ^[g]	248	248	266	261	276	268	276	278	261	264	198
I_{sp} [s] (10% Al) ^[g]	256	253	269	267	277	270	277	282	262	266	224
I_{sp} [s] (15% Al) ^[g]	261	256	270	269	278	270	278	276	263	267	235
I_{sp} [s] (20% Al) ^[g]	262	258	265	267	276	270	277	270	263	267	244
I_{sp} [s] (25% Al) ^[g]	251	256	252	265	275	269	276	258	262	264	247
I_{sp} [s] (5% Al, 14% binder) ^[h]	216	215	237	230	258	264	266	249	242	239	250
I_{sp} [s] (10% Al, 14% binder) ^[h]	232	229	248	243	264	269	272	256	251	248	257
I_{sp} [s] (15% Al, 14% binder) ^[h]	244	241	247	247	270	272	275	254	255	253	261

[a] Heat of detonation. [b] Detonation temperature. [c] Volume of gaseous products. [d] Detonation pressure. [e] Detonation velocity calculated by using the EXPLO5 (Version 6.02) program package.^[20a] [f] Specific impulse of the neat compound using the EXPLO5 (Version 6.02) program package (70.0 bar chamber pressure, initial temperature 3700 K, ambient pressure 1.0 bar, equilibrium expansion conditions).^[20a] [g] Specific impulse for compositions with different amounts of aluminum using the EXPLO5 (Version 6.02) program package (70.0 bar chamber pressure, initial temperature 3700 K, ambient pressure 1.0 bar, equilibrium expansion conditions).^[20a] [h] Specific impulse for compositions with different amounts of oxidizer/compound and aluminum, and 14% binder (6% polybutadiene acrylic acid, 6% polybutadiene acrylonitrile and 2% bisphenol A ether) using the EXPLO5 (Version 6.02) program package (70.0 bar chamber pressure, initial temperature 3700 K, ambient pressure 1.0 bar, equilibrium expansion conditions).^[20a]

1.4 Conclusion

Based on the Michael addition of nitroform with acrylamide several energetic polynitro compounds with a positive oxygen balance were synthesized. Although several synthesis steps are needed for most compounds presented herein, only common commercially available chemicals are used and syntheses proceed in high yields. All of the compounds were comprehensively characterized. Several salts containing the 3,3,3-trinitropropylammonium cation were investigated in terms of their energetic properties. Excellent detonation parameters were found for the dinitramide salt **6d** with a detonation velocity of 9282 m s^{-1} and a detonation pressure of 372 kbar. These values are significantly higher than those of TNT, RDX, and PETN.^[21] With respect to an application as high-energy dense oxidizer in composite solid rocket propellants, the best value was obtained for the 5,5'-bisazotetrazolate salt **6e**; in a mixture comprised of 85% oxidizer and 15% fuel a calculated specific impulse of 282 s was reached. In composites consisting of oxidizer, fuel and binder best values were obtained for the nitrate salt **6b** (270 s), the perchlorate salt **6c** (272 s) and the dinitramide salt **6d** (275 s). All of these exceed the specific impulse of AP in a similar composition (261 s). However, the perchlorate salt **6c**, the dinitramide salt **6d**, and the 5,5'-bisazotetrazolate salt **6e** show low thermal stabilities and/or high sensitivities to external stimuli and therefore likely will be less considered for practical use.

1.5 Experimental Section

1.5.1 General Information

Chemicals were used as supplied (Sigma-Aldrich, Fluka, Acros Organics). Raman spectra were recorded in a glass tube with a Bruker MultiRAM FT-Raman spectrometer with Nd:YAG laser excitation up to 1000 mW (at 1064 nm) in the range between 400 and 4000 cm^{-1} . Infrared spectra were measured with a Perkin-Elmer Spectrum BX-FTIR spectrometer equipped with a Smiths DuraSamplIR II ATR device. All spectra were recorded at ambient ($20 \text{ }^\circ\text{C}$) temperature. NMR spectra were recorded with a JEOL Eclipse 400 instrument and Bruker AV400 and chemical shifts were determined with respect to external standards Me_4Si (^1H , 399.8 MHz; ^{13}C , 100.5 MHz), MeNO_2 (^{14}N , 28.9 MHz; ^{15}N 40.6 MHz), and 1.0 M aqueous NaCl (^{35}Cl , 39.2 MHz). Mass spectrometric data were obtained with a JEOL MStation JMS 700 spectrometer (DCI+, DEI+). Analysis of C/H/N were performed with an Elemental Vario EL Analyzer. Melting and decomposition points were measured with a Perkin-Elmer Pyris6 DSC and an OZM Research DTA 552-Ex with a heating rate of $5 \text{ }^\circ\text{C min}^{-1}$ in a temperature range of 15 to $400 \text{ }^\circ\text{C}$ and checked by a Büchi Melting Point B-540 apparatus (not corrected).

1.5.2 X-ray Crystallography

The low-temperature single-crystal X-ray diffraction of compounds **1**, **2**, **4**, **6a**, **6b**, **6d**, and **8** were performed on an Oxford XCalibur3 diffractometer equipped with a Spellman generator (voltage 50 kV, current 40 mA) and a KappaCCD detector operating with MoK α radiation ($\lambda = 0.7107 \text{ \AA}$). Data collection was performed using the CRYCALIS CCD software.^[22] The data reduction was carried out using the CRYCALIS RED software.^[23] The solution of the structure was performed by direct methods (SIR97)^[24] and refined by full-matrix least-squares on F^2 (SHELXL)^[25] implemented in the WINGX software package^[26] and finally checked with the PLATON software.^[27] All non-hydrogen atoms were refined anisotropically. The hydrogen atom positions were located in a difference Fourier map. ORTEP plots are shown with thermal ellipsoids at the 50% probability level. Crystallographic data (excluding structure factors) for the structures reported in this paper have been deposited at the Cambridge Crystallographic Data Centre 1506284–1506290 (**1**, **2**, **4**, **6a**, **6b**, **6d**, and **8**) Additional crystallographic data and structure refinement parameters are listed in the Appendix A1.

1.5.3 Computational Details

All *ab initio* calculations were carried out using the program package Gaussian 09 (Rev. A.03)^[28] and visualized by GaussView 5.08.^[29] The initial geometries of the structures were taken from the corresponding experimentally determined crystal structures. Structure optimizations and frequency analyses were performed with Becke's B3 three parameter hybrid functional using the LYP correlation functional (B3LYP). For C, H, N and O a correlation consistent polarized double- ξ basis set was used (cc-pVDZ). The structures were optimized with symmetry constraints and the energy is corrected with the zero point vibrational energy.^[30] The enthalpies (H) and free energies (G) were calculated using the complete basis set (CBS) method in order to obtain accurate values. The CBS models use the known asymptotic convergence of pair natural orbital expressions to extrapolate from calculations using a finite basis set to the estimated complete basis set limit. CBS-4 starts with a HF/3-21G(d) geometry optimization, which is the initial guess for the following SCF calculation as a base energy and a final MP2/6-31+G calculation with a CBS extrapolation to correct the energy in second order. The used CBS-4M method additionally implements a MP4(SDQ)/6-31+(d,p) calculation to approximate higher order contributions and also includes some additional empirical corrections.^[31] The enthalpies of the gas-phase species were estimated according to the atomization energy method.^[32] The liquid (solid) state energies of formation (ΔH_f°) were estimated by subtracting the gas-phase enthalpies with the corresponding enthalpy of vaporization (sublimation) obtained by Trouton's rule.^[33] All calculations affecting the detonation parameters were carried out using the program package EXPLO5 V6.02 (EOS BKWG-S).^[20] The detonation parameters were calculated at the Chapman–Jouguet (CJ) point

with the aid of the steady-state detonation model using a modified Becker–Kistiakowski–Wilson equation of state for modeling the system. The CJ point is found from the Hugoniot curve of the system by its first derivative. The specific impulses I_{sp} were also calculated with the program package EXPLO5 V6.02 program, assuming an isobaric combustion of a composition of an oxidizer, aluminum as fuel, 6% polybutadiene acrylic acid, 6% polybutadiene acrylonitrile as binder and 2% bisphenol A as epoxy curing agent^[20a]. A chamber pressure of 70.0 bar, an initial temperature of 3300 K and an ambient pressure of 1.0 bar with equilibrium expansion conditions were estimated for the calculations.

1.5.4 Synthesis

CAUTION! All prepared compounds are energetic materials with sensitivity toward heat, impact, and friction. No hazards occurred during the preparation and manipulation. However, additional proper protective precautions (face shield, leather coat, earthed equipment and shoes, Kevlar® gloves, and ear plugs) should be used when undertaking work with these compounds.

4,4,4-Trinitrobutanamide (1)

An aqueous solution of nitroform (30%, 22.6 g, 45 mmol) was cooled in an ice-bath and acrylamide (3.2 g, 45 mmol) was added. The mixture was stirred 10 minutes at this temperature and 5 h at ambient temperature. The formed precipitate was filtered off and washed several times with cold ethanol and diethyl ether. After drying on air pure 4,4,4-trinitrobutanamide (**1**) was obtained as colorless solid in 97% yield.

DSC (5 °C min⁻¹): 93 °C (mp.), 120 °C (dec.). **IR** (ATR): $\nu = 3475$ (m), 3368 (w), 3310 (w), 3192 (w), 3010 (w), 2948 (w), 2360 (w), 2340 (w), 1695 (m), 1595 (s), 1567 (vs), 1418 (m), 1364 (w), 1344 (m), 1311 (m), 1299 (m), 1288 (s), 1217 (w), 1155 (w), 1116 (w), 878 (w), 856 (w), 816 (m), 798 (s), 776 (w), 747 (w), 637 (w) cm⁻¹. **Raman** (500 mW): $\nu = 3009$ (41), 2969 (24), 2938 (78), 1679 (17), 1615 (29), 1599 (43), 1575 (11), 1433 (16), 1417 (43), 1367 (43), 1348 (26), 1307 (31), 1125 (24), 1066 (13), 1055 (14), 967 (13), 904 (12), 881 (43), 858 (60), 811 (20), 546 (18), 441 (71), 390 (100), 364 (73), 312 (69), 274 (17), 208 (66) cm⁻¹. **¹H NMR** ([D₆]DMSO) $\delta = 7.48$ (s, 1H, NH₂), 7.09 (s, 1H, NH₂), 3.59 (m, 2H, CH₂C(NO₂)₃), 2.52 (m, 2H, OCC₂H₂) ppm. **¹³C NMR** ([D₆]DMSO) $\delta = 170.7$ (CO), 131.7 (C(NO₂)₃), 29.1 (CH₂), 29.0 (CH₂) ppm. **¹⁴N NMR** ([D₆]DMSO) $\delta = -28$ (C(NO₂)₃) ppm. **MS** (DEI+) m/e : 223.2 [(M+H)⁺]. **Elemental analysis** C₄H₆N₄O₇ (222.11): calc. C 21.63, H 2.72, N 25.22%; found C 21.65, H 2.65, N 25.05%. IS: 6 J (grain size 250–500 μm). FS: 360 N (grain size 250–500 μm). ESD: >0.5 J (grain size 250–500 μm).

4,4,4-Trinitrobutanoic acid (2)

4,4,4-trinitrobutanamide (**1**) (2.0 g, 9.0 mmol) was added to concentrated hydrochloric acid (37%, 8 mL) and refluxed for 4 hours. The oily layer which formed solidified after standing overnight at 4 °C. The solid was filtered off and recrystallized from chloroform. After drying in the desiccator 4,4,4-trinitrobutanoic acid (**2**) was obtained as pure colorless product in 70% yield.

DSC (5 °C min⁻¹): 55 °C (mp.), 167 °C (dec.). **IR** (ATR): $\nu = 3006$ (w), 2958 (w), 2880 (w), 2730 (w), 2651 (w), 2527 (w), 1709 (s), 1587 (vs), 1440 (m), 1425 (m), 1312 (s), 1297 (s), 1237 (s), 1153 (m), 1070 (m), 928 (m), 906 (m), 816 (s), 798 (vs), 665 (m). cm⁻¹. **Raman** (500 mW): $\nu = 3006$ (8), 2987 (11), 2956 (89), 1652 (10), 1605 (33), 1454 (9), 1418 (46), 1380 (25), 1359 (22), 1312 (31), 1226 (8), 1154 (13), 1071 (21), 982 (21), 908 (42), 857 (101), 802 (8), 655 (11), 628 (9), 546 (7), 484 (11), 412 (56), 402 (58), 377 (91), 313 (35), 275 (9) cm⁻¹. **¹H NMR** ([D₆]acetone) $\delta = 3.71$ (m, 2H, CH₂C(NO₂)₃), 2.89 (m, 2H, OCCH₂) ppm. **¹³C NMR** ([D₆]acetone) $\delta = 170.4$ (CO), 126.3 (C(NO₂)₃), 29.2 (CH₂), 27.6 (CH₂) ppm. **¹⁴N NMR** ([D₆]acetone) $\delta = -29$ (C(NO₂)₃) ppm. **MS** (DCI+) *m/e*: 224.1 [(M+H)⁺]. **Elemental analysis** C₄H₅N₃O₈ (223.10): calc. C 21.53, H 2.26, N 18.83%; found C 21.39, H 2.24, N 18.70%. IS: 40 J (grain size 250–500 μm). friction tester: 324 N (grain size 250–500 μm). ESD: >0.5 J (grain size 250–500 μm).

4,4,4-Trinitrobutanoyl chloride (3)

Method A:

A mixture of 4,4,4-trinitrobutanoic acid (**2**) (6.7 g, 30.0 mmol) and thionyl chloride (16.7 mL, 200 mol) was stirred at room temperature for one hour. After this the reaction mixture was refluxed for 24 hours under exclusion of moisture. The excess of thionyl chloride was removed and the remaining oil was distilled (bp. 65 °C, 0.7 mbar) yielding 4,4,4-trinitrobutanoyl chloride as colorless pure product (88%).

Method B:

Oxalyl chloride (326 mg, 2.6 mmol) and a catalytical amount of DMF were added to a suspension of 4,4,4-trinitrobutanoic acid (**2**) (500 mg, 2.2 mmol) in chloroform (10 mL). The reaction mixture was stirred under exclusion of moisture at ambient temperature for 40 min and was refluxed for 3 h. The solvent was removed under reduced pressure yielding 4,4,4-trinitrobutanoyl chloride (**3**) in 96% yield as pure colorless oil.

IR (ATR): $\nu = 2997$ (w), 2957 (w), 2892 (w), 1785 (s), 1585 (vs), 1425 (m), 1411 (w), 1356 (w), 1294 (s), 1216 (w), 1153 (w), 1062 (w), 996 (m), 943 (s), 857 (m), 799 (s), 780 (s), 693 (m) cm⁻¹. **Raman** (400 mW): $\nu = 2950$ (51), 1792 (16), 1608 (25), 1414 (24), 1381 (22), 1358 (35), 1304 (30), 1224 (11), 1155 (15), 1065 (26), 998 (13), 948 (15), 905 (17), 858 (102), 784 (21), 694 (19), 635 (17), 532 (20), 456 (58), 396 (44), 374 (65), 275 (50), 233 (31) cm⁻¹. **¹H NMR** (CDCl₃)

$\delta = 3.38$ (m, 4H, OCCH_2 , $\text{CH}_2\text{C}(\text{NO}_2)_3$) ppm. ^{13}C NMR (CDCl_3) $\delta = 171.1$ (CO), 127.9 ($\text{C}(\text{NO}_2)_3$), 40.5 (OCCH_2), 29.4 ($\text{CH}_2(\text{NO}_2)_3$) ppm. ^{14}N NMR (CDCl_3) $\delta = -31$ ($\text{C}(\text{NO}_2)_3$) ppm. MS (DEI+) m/e : 206.1 [$(\text{M}-\text{Cl})^+$]. **Elemental analysis** $\text{C}_4\text{H}_4\text{N}_3\text{O}_7\text{Cl}$ (241.54): calc. C 19.89, H 1.67, N 17.40%; found C 19.75, H 1.68, N, 17.80%.

4,4,4-Trinitrobutanoyl azide (**4**)

To a solution of sodium azide (0.31 g, 4.8 mmol) in water (2 mL) a solution of 4,4,4-trinitrobutanoyl chloride (**3**) (0.59 g, 2.4 mmol) in acetone (1 mL) was added slowly at 4 °C. After the addition the solution was stirred at 0 °C for two hours. The reaction mixture was extracted with chloroform (3 × 20 mL). The combined organic phases were washed with ice-water (20 mL), an ice-cold sodium bisulfate solution (5%, 20 mL), ice-water (2 × 20 mL) and brine (20 mL). The extracts were dried over magnesium sulfate and the organic solvent was removed at temperatures below 20 °C. The remaining oil solidified in the refrigerator over-night and 4,4,4-trinitrobutanoyl azide (**4**) was obtained as pure colorless solid in 66% yield.

DSC (5 °C min^{-1}): 22 °C (mp.), 85 °C (dec.). **IR** (ATR): $\nu = 3000$ (w), 2956 (w), 2893 (w), 2148 (s), 1711 (s), 1585 (vs), 1427 (m), 1359 (m), 1296 (s), 1153 (vs), 1098 (s), 1047 (s), 967 (w), 908 (w), 855 (s), 800 (vs), 704 (m) cm^{-1} . **Raman** (500 mW): $\nu = 2947$ (71), 2156 (26), 2147 (26), 1716 (22), 1608 (26), 1419 (26), 1360 (36), 1305 (30), 1151 (9), 1101 (16), 1050 (14), 968 (12), 910 (31), 857 (101), 788 (10), 669 (26), 543 (9), 502 (29), 373 (69), 279 (39), 262 (36) cm^{-1} . ^1H NMR (CDCl_3) $\delta = 3.38$ (m, 2H, $\text{CH}_2\text{C}(\text{NO}_2)_3$), 2.78 (m, 2H, OCCH_2) ppm. ^{13}C NMR (CDCl_3) $\delta = 176.2$ (CO), 128.6 ($\text{C}(\text{NO}_2)_3$), 30.6 (CH_2), 29.3 (CH_2) ppm. ^{14}N NMR (CDCl_3) $\delta = -30$ ($\text{C}(\text{NO}_2)_3$), -136 (N_β), -147 (N_γ) ppm. **Elemental analysis** $\text{C}_4\text{H}_4\text{N}_6\text{O}_7$ (248.11): calc. C 19.36, H 1.62, N 33.87%; found C 19.89, H 1.65, N 33.54%. IS: 2 J (grain size 250–500 μm). FS: 144 N (grain size 250–500 μm). ESD 0.3 J (grain size 250–500 μm).

1,1,1-Trinitropropan-3-isocyanate (**5**)

To a solution of sodium azide (0.31 g, 4.8 mmol) in water (2 mL) a solution of 4,4,4-trinitrobutanoyl chloride (**3**) (0.59 g, 2.4 mmol) in acetone (1 mL) was added slowly at 4 °C. After the addition the solution was stirred at 0 °C for two hours. The reaction mixture was extracted with chloroform (3 × 20 mL). The combined organic phases were washed with ice-water (20 mL), an ice-cold sodium bisulfate solution (5%, 20 mL), ice-water (2 × 20 mL) and brine (20 mL). The extracts were dried over magnesium sulfate. The solution was slowly heated up to 55 °C and kept at this temperature until no more nitrogen evolved (2 h). The organic solvent was removed to obtain 1,1,1-trinitropropan-3-isocyanate (**5**) as colorless liquid in 68% yield.

Raman (500 mW): $\nu = 2953$ (70), 2156 (13), 2147 (13), 1718 (11), 1610 (24), 1451 (18), 1421 (22), 1363 (37), 1304 (30), 1100 (10), 1051 (13), 914 (20), 887 (12), 856 (100), 811 (10), 535

(10), 502 (16), 460 (10), 375 (68), 305 (17), 279 (22), 254 (20) cm^{-1} . $^1\text{H NMR}$ (CDCl_3) δ = 3.90 (m, 2H, CH_2), 3.32 (m, 2H, CH_2) ppm. $^{13}\text{C NMR}$ (CDCl_3) δ = 127.4 ($\text{C}(\text{NO}_2)_3$), 123.6 (NCO), 37.4 (CH_2), 35.0 (CH_2) ppm. $^{14}\text{N NMR}$ (CDCl_3) δ = -31 ($\text{C}(\text{NO}_2)_3$), -360 (NCO) ppm. **Elemental analysis** $\text{C}_4\text{H}_4\text{N}_4\text{O}_7$ (220.10): calc. C 21.83, H 1.83, N 25.46%; found C 21.31, H 1.80, N 26.07%.

3,3,3-Trinitropropyl-1-ammonium chloride (6a)

1,1,1-Trinitropropan-3-isocyanate (**5**) (1.10 g, 5.0 mmol) was refluxed in hydrochloric acid (6 M, 10 mL) for five hours. The solution was concentrated to dryness and the colorless solid was washed with 1,2-dichloroethane. 3,3,3-Trinitropropyl-1-ammonium chloride (**6a**) was yielded as colorless solid in 90% yield.

DSC ($5\text{ }^\circ\text{C min}^{-1}$): 161 $^\circ\text{C}$ (mp.), 178 $^\circ\text{C}$ (dec.). **IR** (ATR): ν = 2974 (m), 2884 (m), 2660 (w), 2497 (w), 2305 (w), 1989 (w), 1588 (vs), 1501 (m), 1483 (m), 1458 (m), 1417 (w), 1365 (w), 1292 (s), 1160 (m), 1062 (w), 1032 (w), 995 (w), 931 (w), 911 (w), 855 (w), 846 (w), 836 (w), 796 (s), 768 (w), 734 (w) cm^{-1} . **Raman** (300 mW): ν = 3068 (11), 3022 (18), 2998 (40), 2976 (58), 2938 (68), 2913 (25), 2904 (24), 2878 (18), 2859 (44), 2804 (12), 2083 (7), 1610 (37), 1580 (8), 1548 (17), 1491 (10), 1478 (9), 1460 (17), 1423 (21), 1396 (7), 1367 (39), 1300 (33), 1168 (19), 1119 (6), 1065 (8), 1031 (9), 999 (15), 970 (9), 931 (8), 901 (16), 858 (100), 802 (8), 654 (6), 633 (7), 569 (9), 516 (6), 457 (9), 402 (50), 374 (56), 341 (29), 302 (7) cm^{-1} . $^1\text{H NMR}$ ($[\text{D}_6]\text{DMSO}$) δ = 8.63 (br, 3H, NH_3), 3.82 (m, 2H, CH_2), 3.19 (m, 2H, CH_2) ppm. $^{13}\text{C NMR}$ ($[\text{D}_6]\text{DMSO}$) δ = 128.8 ($\text{C}(\text{NO}_2)_3$), 33.4 (CH_2), 30.3 (CH_2) ppm. $^{14}\text{N NMR}$ ($[\text{D}_6]\text{DMSO}$) δ = -31 (NO_2), -356 (NH_3) ppm. **Elemental analysis** $\text{C}_3\text{H}_5\text{N}_4\text{O}_7$ (230.56): calc. C 15.63, H 3.06, N 24.30%; found C 16.09, H 3.06, N 24.30%. IS: 20 J (grain size 100–250 μm). FS: 360 N (grain size 100–250 μm). ESD >0.5 J (grain size 100–250 μm).

3,3,3-Trinitropropyl-1-ammonium nitrate (6b)

1,1,1-Trinitropropan-3-isocyanate (**5**) (1.10 g, 5.0 mmol) was refluxed in nitric acid (6 M, 10 mL) for five hours. The solution was concentrated to dryness to give a yellow powder. Recrystallization from ethyl acetate yielded 3,3,3-trinitropropyl-1-ammonium nitrate (**6b**) as colorless solid in 89% yield.

DSC ($5\text{ }^\circ\text{C min}^{-1}$): 135 $^\circ\text{C}$ (mp.), 138 $^\circ\text{C}$ (dec.). **IR** (ATR): ν = 3120 (m), 3070 (m), 3032 (m), 2977 (m), 2889 (m), 2840 (m), 2763 (w), 2716 (w), 2666 (w), 2588 (w), 2503 (w), 1604 (s), 1506 (w), 1479 (w), 1460 (m), 1425 (w), 1303 (m), 1040 (w), 996 (w), 972 (w), 934 (w), 875 (w), 850 (w), 806 (m), 799 (w), 766 (w), 735 (w), 680 (w) cm^{-1} . **Raman** (1000 mW): ν = 3037 (12), 2984 (47), 3948 (64), 2913 (12), 2859 (52), 2836 (5), 2817 (6), 2083 (11), 2028 (5), 1609 (25), 1465 (13), 1424 (22), 1373 (38), 1305 (27), 1186 (10), 1155 (9), 1035 (99), 1010 (10), 935 (7), 908

(15), 859 (102), 800 (7), 727 (9), 711 (6), 661 (5), 630 (8), 563 (9), 538 (7), 419 (41), 404 (44), 378 (50), 340 (24), 306 (10) cm^{-1} . $^1\text{H NMR}$ ($[\text{D}_6]$ DMSO) δ = 8.10 (br, 3H, NH_3), 3.71 (m, 2H, CH_2), 3.24 (m, 2H, CH_2) ppm. $^{13}\text{C NMR}$ ($[\text{D}_6]$ DMSO) δ = 128.8 ($\text{C}(\text{NO}_2)_3$), 33.5 (CH_2), 30.6 (CH_2) ppm. $^{14}\text{N NMR}$ ($[\text{D}_6]$ DMSO) δ = -4 (NO_3^-), -30 (NO_2), -359 (NH_3) ppm. **Elemental analysis** $\text{C}_3\text{H}_7\text{N}_5\text{O}_9$ (257.12): calc. C 14.01, H 2.74, N 27.24%; found C 13.89, H 2.76, N 27.01%. IS: 6 J (grain size 250–500 μm). FS: 120 N (grain size 250–500 μm). ESD 0.3 J (grain size 250–500 μm).

3,3,3-Trinitropropyl-1-ammonium perchlorate (6c)

To a solution of 3,3,3-trinitropropyl-1-ammonium chloride (**6a**) (196 mg, 0.9 mmol) in water (10 mL) was added at 0 °C under exclusion of light a solution of silver perchlorate monohydrate (190 mg, 0.9 mmol) in water (10 mL). The reaction mixture was stirred 1.5 h at 0 °C. The precipitated silver chloride was filtered off, washed with cold water and the filtrate was evaporated to dryness. 3,3,3-Trinitropropyl-1-ammonium perchlorate (**6c**) was obtained as colorless solid in 90% yield.

DSC (5 °C min^{-1}): 164 °C (dec.). **IR** (ATR): ν = 3259 (w), 3227 (w), 3168 (w), 2992 (w), 2888 (w), 2361 (w), 2333 (w), 1596 (s), 1513 (w), 1501 (w), 1478 (m), 1430 (w), 1368 (w), 1293 (m), 1152 (m), 1067 (vs), 980 (m), 941 (w), 893 (w), 855 (w), 798 (s), 749 (w), 667 (w) cm^{-1} . **Raman** (1000 mW): ν = 3258 (7), 3241 (6), 3214 (6), 3189 (5), 3143 (5), 3133 (6), 3119 (5), 3067 (4), 3028 (9), 2994 (17), 2960 (29), 2821 (6), 1863 (5), 1601 (39), 1467 (10), 1431 (18), 1370 (25), 1356 (15), 1343 (9), 1302 (21), 1162 (16), 1115 (8), 1078 (12), 1019 (17), 982 (14), 942 (101), 858 (88), 803 (10), 664 (5), 634 (5), 628 (25), 563 (13), 467 (25), 453 (22), 417 (38), 405 (38), 382 (49), 341 (32), 300 (8) cm^{-1} . $^1\text{H NMR}$ ($[\text{D}_6]$ DMSO) δ = 8.03 (br, 3H, NH_3), 3.70 (m, 2H, CH_2), 3.23 (m, 2H, CH_2) ppm. $^{13}\text{C NMR}$ ($[\text{D}_6]$ DMSO) δ = 128.8 ($\text{C}(\text{NO}_2)_3$), 33.5 (CH_2), 30.4 (CH_2) ppm. $^{14}\text{N NMR}$ ($[\text{D}_6]$ DMSO) δ = -31 (NO_2), -356 (NH_3) ppm. $^{35}\text{Cl NMR}$ ($[\text{D}_4]$ methanol) = -1011 (ClO_4^-) ppm. **Elemental analysis** $\text{C}_3\text{H}_7\text{N}_4\text{O}_6\text{Cl}$ (294.56): calc. C 12.23, H 2.40, N 19.02%; found C 12.25, H 2.57, N 18.44%. IS: 2.5 J (grain size <100 μm). FS: 16 N (grain size <100 μm). ESD 0.08 J (grain size <100 μm).

3,3,3-Trinitropropyl-1-ammonium dinitramide (6d)

To a solution of 3,3,3-trinitropropyl-1-ammonium chloride (**6a**) (350 mg, 1.5 mmol) in water (10 mL) was added at 0 °C under exclusion of light a solution of silver dinitramide (320 mg, 1.5 mmol) in water (10 mL). The reaction mixture was stirred 1.5 h at 0 °C. The precipitated silver chloride was filtered off, washed with cold water and the filtrate was evaporated to dryness. 3,3,3-Trinitropropyl-1-ammonium dinitramide (**6d**) was obtained as colorless solid in 96% yield.

DSC (5 °C min⁻¹): 112 °C (dec.). **IR** (ATR): ν = 3285 (w), 3047 (w), 2981 (m), 2947 (m), 2662 (w), 1989 (w), 1588 (vs), 1520 (m), 1502 (m), 1478 (w), 1448 (m), 1412 (w), 1365 (w), 1295 (m), 1231 (w), 1183 (s), 1160 (s), 1026 (s), 986 (w), 947 (w), 898 (w), 855 (w), 827 (w), 798 (s), 761 (m), 755 (m), 743 (w), 734 (w), 722 (w) cm⁻¹. **Raman** (1000 mW): ν = 3236 (5), 3228 (4), 3208 (4), 3046 (9), 2984 (24), 2948 (30), 2859 (20), 2818 (4), 1609 (19), 1522 (6), 1484 (7), 1469 (9), 1440 (12), 1419 (10), 1368 (40), 1334 (100), 1313 (30), 1300 (21), 1183 (13), 1162 (11), 1143 (22), 1053 (16), 1027 (21), 984 (17), 950 (10), 919 (6), 899 (10), 858 (88), 826 (75), 805 (6), 759 (14), 748 (10), 647 (6), 559 (11), 488 (23), 403 (39), 377 (52), 341 (45), 298 (16), 209 (7) cm⁻¹. **¹H NMR** ([D₄]methanol) δ = 8.31 (br, 3H, NH₃), 3.72 (m, 2H, CH₂), 3.43 (m, 2H, CH₂) ppm. **¹³C NMR** ([D₄]methanol) δ = 129.6 (C(NO₂)₃), 35.4 (CH₂), 32.3 (CH₂) ppm. **¹⁵N NMR** ([D₄]methanol) δ = -12.6 (N(NO₂)), -30.2 (NO₂), -352.0 (NH₃) ppm. **Elemental analysis** C₃H₇N₇O₁₀ (301.13): calc. C 11.97, H 2.34, N 32.56%; found C 12.00, H 2.41, N 31.27%. IS: 2 J (grain size <100 μ m). FS: 30 N (grain size <100 μ m). ESD 0.45 J (grain size <100 μ m).

Bis(3,3,3-Trinitropropyl-1-ammonium) 5,5'-azobistetrazolate (6e)

A solution of 3,3,3-trinitropropylammonium chloride (233 mg, 1.0 mmol) in water (10 mL) was added to a solution of potassium 5,5'-azobistetrazolate (123 mg, 0.5 mmol) in water (2 mL) at 0 °C. Immediately a yellow precipitate was formed. The reaction mixture was stirred 1 h at 0 °C. The precipitate was filtered off, washed with water and dried to yield 49% of bis(3,3,3-trinitropropyl-1-ammonium) 5,5'-azobistetrazolate (**6e**) as yellow solid.

DSC (5 °C min⁻¹): 120 °C (dec.). **IR** (ATR): ν = 2934 (w), 2757 (w), 2675 (w), 2623 (w), 2512 (w), 2084 (w), 1632 (w), 1603 (s), 1590 (s), 1517 (w), 1458 (w), 1424 (w), 1414 (w), 1394 (w), 1369 (w), 1312 (w), 1297 (w), 1185 (w), 1174 (m), 1148 (w), 1080 (w), 1051 (w), 1042 (w), 1010 (w), 903 (w), 856 (w), 806 (s), 796 (s), 774 (w), 756 (w), 738 (m), 667 (s) cm⁻¹. **Raman** (500 mW): ν = 2935 (2), 1484 (48), 1423 (4), 1390 (100), 1195 (2), 1086 (10), 1058 (40), 927 (8), 857 (3), 341 (2) cm⁻¹. **¹H NMR** ([D₄]methanol) δ = 3.76 (m, 2H, CH₂), 3.48 (m, 2H, CH₂) ppm. **¹³C NMR** ([D₄]methanol) δ = 171.9 (CN₄), 128.3 (C(NO₂)₃), 34.0 (CH₂), 31.1 (CH₂) ppm. **¹⁴N NMR** ([D₄]methanol) δ = -19 (CN₄), -30 (NO₂), -352 (NH₃) ppm. **Elemental analysis** C₈H₁₄N₁₈O₁₂ (554.31): calc. C 17.33, H 2.55, N 45.48%; found C 17.48, H 2.49, N 45.28%. IS: 2 J (grain size <100 μ m). FS: 54 N (grain size <100 μ m). ESD 0.6 J (grain size <100 μ m).

4,4,4-Trinitro-N-(2,2,2-trinitroethyl)butanamide (7)

To a saturated solution of barium hydroxide in water (10 mL) was added acrylamide (1.30 g, 18.2 mmol) and aqueous formaldehyde (37%, 1.50 g, 18.2 mmol) and stirred for 20 minutes. The solution was treated with solid carbon dioxide (5 g) and the precipitated barium carbonate was filtered off. To the filtrate was added aqueous nitroform solution (30%, 18.3 g, 36.4 mmol),

stirred for 20 minutes and refluxed for further 30 minutes. The reaction mixture was cooled in an ice-water bath and the formed precipitate was filtered off. The yellow powder was recrystallized two times from a mixture of methanol/water, to yield 3.93 g (10.2 mmol, 56%) of colorless pure product.

DSC (5 °C min⁻¹): 150 °C (mp.), 155 °C (dec.). **IR** (ATR): $\nu = 3304$ (w), 3071 (w), 3011 (w), 2960 (w), 2892 (w), 1676 (m), 1589 (vs), 1543 (s), 1418 (w), 1363 (w), 1299 (s), 1236 (w), 1217 (w), 1155 (w), 1115 (w), 1092 (w), 1050 (w), 935 (w), 854 (m), 803 (s). **Raman** (400 mW): $\nu = 3006$ (19), 2957 (39), 1677 (18), 1605 (29), 1421 (24), 1365 (28), 1337 (20), 1305 (36), 1117 (14), 1058 (13), 936 (15), 913 (13), 857 (102), 545 (18), 412 (46), 394 (47), 377 (68), 278 (29) cm⁻¹. **¹H NMR** (CD₃CN) $\delta = 7.21$ (s, 1H, NH), 4.96 (d, 2H, ³J = 6.8 Hz, CH₂NH), 3.47 (m, 2H, CH₂C(NO₂)₃), 2.70 (m, 2H, OCCH₂) ppm. **¹³C NMR** (CD₃CN) $\delta = 169.9$ (CO), 131.4 (C(NO₂)₃), 127.5 (NHCH₂C(NO₂)₃), 42.2 (NHCH₂), 28.8 (CH₂), 28.6 (CH₂) ppm. **¹⁴N NMR** (CD₃CN) $\delta = -29$ (C(NO₂)₃), -32 (NHCH₂C(NO₂)₃) ppm. **MS** (DCI+) *m/e*: 386.2 [(M+H)⁺]. **Elemental analysis** C₆H₇N₇O₁₃ (385.16): calc. C 18.71, H 1.83, N 25.46%; found C 18.83, H 1.81, N 25.49%. IS: 10 J (grain size <100 μm). FS: 240 N (grain size <100 μm). ESD 0.2 J (grain size 100 μm).

2,2,2-Trinitroethyl 4,4,4-trinitrobutanoate (8)

To a mixture of fuming sulfuric acid (30% SO₃, 4 mL) and concentrated sulfuric acid (8 mL) was added 4,4,4-trinitrobutanoic acid (**2**) (1.7 g, 7.8 mmol) in small portions with cooling to 4 °C and stirred till complete solution. 2,2,2-Trinitroethanol (1.53 g, 7.8 mmol) was dissolved in water (0.5 mL) and is added very carefully to the reaction mixture at 4 °C and stirred for further 12 hours at room temperature. The reaction was quenched with ice-water (5 mL) and the colorless precipitate was filtered off. The product was washed three times with water (20 mL) and dried to obtain 1.20 g (40%) of pure product.

DSC (5 °C min⁻¹): 92 °C (mp.), 155 °C (dec.). **IR** (ATR): $\nu = 3007$ (w), 2964 (w), 2895 (w), 1761 (s), 1582 (vs), 1441 (w), 1430 (m), 1419 (w), 1400 (w), 1379 (w), 1363 (w), 1299 (s), 1222 (w), 1169 (s), 1100 (w), 1086 (m), 1037 (w), 1015 (w), 913 (w), 873 (w), 855 (m), 799 (vs), 780 (m), 759 (w), 744 (w), 730 (w), 689 (w), 655 (w) cm⁻¹. **Raman** (500 mW): $\nu = 3009$ (12), 2987 (21), 2953 (49), 1762 (18), 1609 (36), 1442 (10), 1419 (27), 1401 (129), 1364 (38), 1302 (36), 1263 (10), 1154 (9), 1086 (18), 1038 (10), 1015 (13), 972 (8), 915 (21), 873 (13), 857 (105), 798 (11), 781 (9), 744 (6), 647 (11), 539 (17), 487 (11), 404 (70), 373 (95), 341 (13), 326 (12), 269 (28), 232 (21) cm⁻¹. **¹H NMR** (CDCl₃) $\delta = 5.44$ (s, 2H, OCH₂), 3.43 (m, 2H, CH₂C(NO₂)₃), 2.90 (m, 2H, OCCH₂) ppm. **¹³C NMR** (CDCl₃) $\delta = 167.4$ (CO), 128.2 (C(NO₂)₃), 122.5 (OCH₂C(NO₂)₃) 61.3 (OCCH₂), 29.3 (CH₂), 28.0 (CH₂) ppm. **¹⁴N NMR** (CDCl₃) $\delta = -31$ (C(NO₂)₃), -35 (C(NO₂)₃) ppm. **MS** (DCI+) *m/e*: 387.1 [(M+H)⁺]. **Elemental analysis**

(C₆H₆N₆O₁₄, 386.14): calc.: C 18.66, H 1.57, N 21.76%; found: C 18.92, H 1.59, N 21.46%. IS: 30 J (grain size <100 µm). FS: 240 N (grain size <100 µm). ESD 0.1 J (grain size 100 µm).

1.6 References

- [1] a) T. M. Klapötke, *Chemistry of High-Energy Materials*, 2nd ed., de Gruyter, Berlin, **2012**; b) Q. J. Axthammer, B. Krumm, T. M. Klapötke, *J. Org. Chem.* **2015**, *80*, 6329–6335; c) Q. J. Axthammer, T. M. Klapötke, B. Krumm, R. Moll, S. F. Rest, *Z. Anorg. Allg. Chem.* **2014**, *640*, 76–83.
- [2] a) M. Göbel, T. M. Klapötke, P. Mayer, *Z. Anorg. Allg. Chem.* **2006**, *632*, 1043–1050; b) M. Göbel, T. M. Klapötke, *Adv. Funct. Mater.* **2009**, *19*, 347–365; c) M. Göbel, T. M. Klapötke, *Z. Anorg. Allg. Chem.* **2007**, *633*, 1006–1017.
- [3] J. P. Agrawal, *High Energy Materials*, Wiley-VCH, Weinheim, **2010**.
- [4] A. D. Nikolaeva, I. L. Tsentsiper, V. S. Perekhod'ko, *Izv. Vyssh. Uchebn. Zaved. Khim. Tekhnol.*, **1980**, *23*, 152–156.
- [5] a) Y. A. Volkova, E. B. Averina, Y. K. Grishin, P. Bruheim, T. S. Kuznetsova, N. S. Zefirov, *J. Org. Chem.*, **2010**, *75*, 3047–3052; b) Y. A. Volkova, O. A. Ivanova, E. M. Budynina, E. B. Averina, T. S. Kuznetsova, N. S. Zefirov, *Chem. Bull.*, **2008**, *57*, 2034–2035.
- [6] a) M. J. Kamlet, J. C. Dacons, J. C. Hoffsommer, *J. Org. Chem.* **1961**, *26*, 4881–4886; b) I. J. Schaffner **1962**, US3051743.
- [7] D. J. Glover, J. C. Dacons, D. V. Sickman, M. E. Hill, M. J. Kamlet **1964**, US3125606.
- [8] Q. J. Axthammer, B. Krumm, T. M. Klapötke, R. Scharf, *Chem. – Eur. J.* **2015**, *21*, 16229–16239.
- [9] M. H. Gold, M. B. Frankel, G. B. Linden, K. Klager, *J. Org. Chem.* **1962**, *27*, 334–336.
- [10] M. B. Frankel, *Tetrahedron* **1963**, *19*, 213–217.
- [11] M. B. Frankel **1961**, US2978509.
- [12] a) H. Feuer, U. E. Lynch-Hart, *J. Org. Chem.* **1961**, *26*, 391–394; b) H. Feuer, U. E. Lynch-Hart, *J. Org. Chem.* **1961**, *26*, 587–589; c) I. J. Schaffner **1962**, US3038009.
- [13] a) R. H. Saunders **1961**, US2996537; b) M. E. Hill **1966**, US3230247.
- [14] S. Bienz, L. Bigler, T. Fox, M. Hesse, H. Meier, B. Zeeh, *Spektroskopische Methoden in der Organischen Chemie*, 8th ed., Thieme, Stuttgart, **2014**.
- [15] T. Steiner, *Angew. Chem., Int. Ed.* **2002**, *41*, 48–76.

- [16] T. M. Klapötke, B. Krumm, R. Moll, S. F. Rest, Y. V. Vishnevskiy, C. Reuter, H.-G. Stammler, N. W. Mitzel, *Chem. – Eur. J.* **2014**, *20*, 12962–12973.
- [17] a) T. M. Klapötke, B. Krumm, R. Scharf, *Eur. J. Inorg. Chem.* **2016**, *2016*, 3086–3093; b) A. Wolter-Steingrube, B. E. C. Bugenhagen, C. Herrmann, J. Heck, *Eur. J. Inorg. Chem.* **2014**, *2014*, 4115–4122; c) A. Baumann, A. Erbacher, C. Evangelisti, T. M. Klapötke, B. Krumm, S. F. Rest, M. Reynders, V. Sproll, *Chem. – Eur. J.* **2013**, *19*, 15627–15638; d) G. C. Hsu, L. M. Singer, D. B. Cordes, M. Findlater, *Acta Crystallogr.* **2013**, *69E*, 1298; e) J. Lopic, A. Pezerovic, M. Cetina, S. Djakovic, V. Ropic, *J. Mol. Struct.* **2011**, *990*, 209–216; f) G. Laus, V. Kahlenberg, K. Wurst, S. Nerdinger, H. Schottenberger, *Z. Naturforsch.* **2011**, *66B*, 479–486; g) D. Siebler, C. Forster, T. Gasi, K. Heinze, *Organometallics* **2011**, *30*, 313–327; h) L. Parkanyi, G. Besenyi, *J. Mol. Struct.* **2004**, *691*, 97–106; i) F. M. Menger, J. Bian, V. A. Azov, *Angew. Chem., Int. Ed.* **2002**, *41*, 2581–2584; j) Y. Jiao, E. Valente, S. T. Garner, X. Wang, H. Yu, *Tetrahedron Lett.* **2002**, *43*, 5879–5881.
- [18] a) NATO, Standardization Agreement 4487 (STANAG 4487), Explosives, Friction Sensitivity Tests, **2002**; b) NATO, Standardization Agreement 4489 (STANAG 4489), Explosives, Impact Sensitivity Tests, **1999**.
- [19] Test methods according to the *UN Manual of Test and Criteria, Recommendations on the Transport of Dangerous Goods*, United Nations Publication, New York, Geneva, 4th revised ed., **2003**, Impact: Insensitive > 40 J, less sensitive \geq 35 J, sensitive \geq 4 J, very sensitive \leq 3 J; Friction: Insensitive > 360 N, less sensitive = 360 N, sensitive < 360 N > 80 N, very sensitive \leq 80 N, extremely sensitive \leq 10 N.
- [20] a) M. Sućeska, *EXPLO5 V.6.02*, Zagreb (Croatia), **2013**; b) M. Sućeska, *Propellants, Explos., Pyrotech.* **1991**, *16*, 197–202.
- [21] R. Meyer, J. Köhler, A. Homburg, *Explosives*, 7th ed., Wiley-VCH, Weinheim (Germany), **2015**.
- [22] Oxford Diffraction Ltd., *CrysAlis CCD*, Version 1.171.35. (release 16-05-2011 CrysAlis 171.Net), Abingdon, Oxford (U. K.), **2011**.
- [23] Oxford Diffraction Ltd., *CrysAlis RED*, Version 1.171.35.11 (release 16-05-2011 CrysAlis 171.NET), Abingdon, Oxford (U. K.), **2011**.
- [24] A. Altomare, M. C. Burla, M. Camalli, G. L. Casciarano, C. Giacovazzo, A. Guagliardi, A. G. G. Moliterni, G. Polidori, R. Spagna, *J. Appl. Crystallogr.* **1999**, *32*, 115–119.
- [25] a) G. M. Sheldrick, SHELX-97, Programs for Crystal Structure Determination, **1997**; b) G. M. Sheldrick, *Acta Crystallogr., Sect. A: Found. Crystallogr.* **2008**, *64*, 112–122.
- [26] L. Farrugia, *J. Appl. Crystallogr.* **1999**, *32*, 837–838.

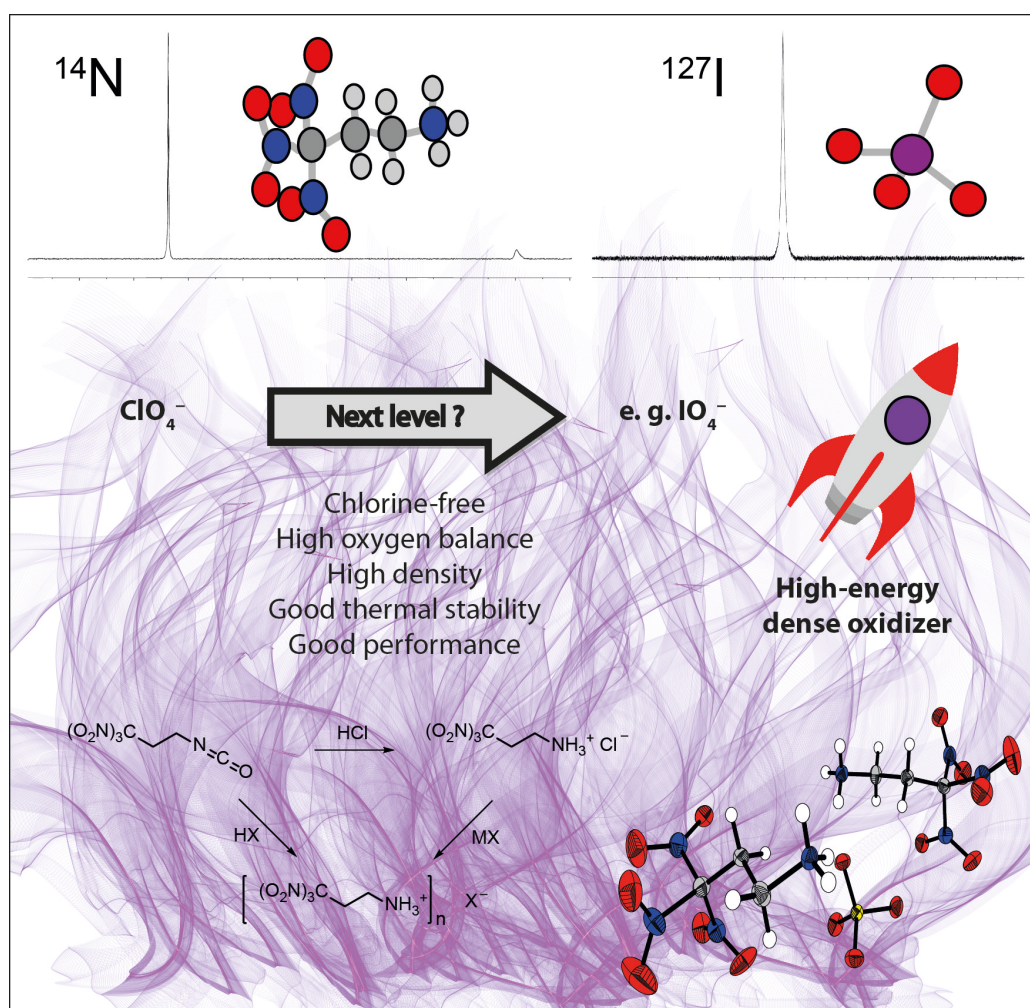
- [27] A. Spek, *Acta Crystallogr., Sect. D: Biol. Crystallogr.* **2009**, *65*, 148–155.
- [28] M. J. Frisch, G. W. Trucks, H. B. Schlegel, G. E. Scuseria, M. A. Robb, J. R. Cheeseman, V. B. G. Scalmani, B. Mennucci, G. A. Petersson, H. Nakatsuji, M. Caricato, X. Li, H. P. Hratchian, A. F. Izmaylov, J. Bloino, G. Zheng, J. L. Sonnenberg, M. Hada, M. Ehara, K. Toyota, R. Fukuda, J. Hasegawa, M. Ishida, T. Nakajima, Y. Honda, O. Kitao, H. Nakai, T. Vreven, J. J. A. Montgomery, J. E. Peralta, F. Ogliaro, M. Bearpark, J. J. Heyd, E. Brothers, K. N. Kudin, V. N. Staroverov, R. Kobayashi, J. Normand, K. Raghavachari, A. Rendell, J. C. Burant, S. S. Iyengar, J. Tomasi, M. Cossi, N. Rega, J. M. Millam, M. Klene, J. E. Knox, J. B. Cross, V. Bakken, C. Adamo, J. Jaramillo, R. Gomperts, R. E. Stratmann, O. Yazyev, A. J. Austin, R. Cammi, C. Pomelli, J. W. Ochterski, R. L. Martin, K. Morokuma, V. G. Zakrzewski, G. A. Voth, P. Salvador, J. J. Dannenberg, S. Dapprich, A. D. Daniels, Ö. Farkas, J. B. Foresman, J. V. Ortiz, J. Cioslowski, D. J. Fox, *Gaussian 09*, Rev. A.02 ed., Gaussian, Inc., Wallingford CT (US), **2009**.
- [29] R. D. Dennington, T. A. Keith, J. M. Millam, *GaussView*, Ver. 5.08 ed., Semichem, Inc., Wallingford CT, **2009**.
- [30] J. A. Montgomery, M. J. Frisch, J. W. Ochterski, G. A. Petersson, *J. Chem. Phys.* **2000**, *112*, 6532–6542.
- [31] J. W. Ochterski, G. A. Petersson, J. A. Montgomery, *J. Chem. Phys.* **1996**, *104*, 2598–2619.
- [32] E. F. C. Byrd, B. M. Rice, *J. Phys. Chem.* **2005**, *110*, 1005–1013.
- [33] a) F. Trouton, *Philos. Mag.* **1884**, *18*, 54–57; b) M. S. Westwell, M. S. Searle, D. J. Wales, D. H. Williams, *J. Am. Chem. Soc.* **1995**, *117*, 5013–5015.

2 Trinitropropylammonium Salts

Unusual Energetic Periodate, Sulfate and Amino-bistetrazolate Salts of the Trinitropropylammonium Cation

C. C. Unger, T. M. Klapötke, B. Krumm

Z. Anorg. Allg. Chem. **2020**, 646, 2–4. (Front cover)



2.1 Abstract

Starting from a nucleophilic Michael Addition of nitroform to acrylamide, three synthetic strategies towards 1,1,1-trinitropropyl-1-ammonium salts are described. Due to the high oxygen content and density of one periodate salt, its suitability as high-energy dense oxidizer in energetic formulations was predicted according to its specific impulse and detonation velocity. Furthermore, those properties were compared to the nitrogen-rich amino-bis(5-tetrazolate) salt. The parameters were calculated with the EXPLO5 (V6.03) computer code and compared to the common solid rocket propellant ammonium perchlorate (AP). Calculations towards the energies of formation were performed using Gaussian 09. Characterization including multinuclear NMR spectroscopy, vibrational analysis (IR, Raman) as well as elemental analysis and a single crystal X-ray diffraction study was performed. The thermal stability was studied using differential scanning calorimetry and the sensitivities against impact and friction were determined.

2.2 Introduction

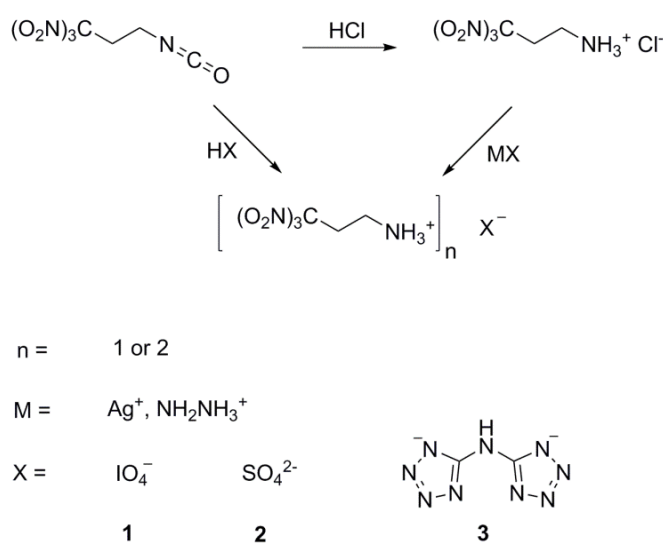
In the area of high-energy dense oxidizers (HEDOs), ammonium perchlorate (AP) still is one of the most popular oxidizers in composite propellants. While the ammonium cation acts as a reducing agent, the perchlorate anion is the important oxidizer during the combustion.^[1] The formed oxygen reacts with the aluminum and binder, which are present in the composite, and in consequence leads to a very high heat of combustion and high burning temperature.^[2] Nevertheless, toxic gases such as hydrogen chloride are also released, as well as the own toxicity of perchlorate anion, as it competes with iodine in the thyroid gland.^[3] An interesting building block for designing new perchlorate free HEDOs is the trinitromethyl unit, due to its high oxygen content. Whereas the more oxygen-rich but chemically less stable 2,2,2-trinitroethyl moiety has been studied exhaustively, the 3,3,3-trinitropropyl moiety gained more attention lately. Our initial study concerning the 3,3,3-trinitropropyl unit as promising energetic building block showed, that compounds carrying the propyl moiety, although not exhibiting higher thermal stabilities, in general were less sensitive, compared to the corresponding ethyl salts.^[4] Until now, no salts are known containing the 2,2,2-trinitroethyl-1-ammonium unit. However, with the 3,3,3-trinitropropyl-1-ammonium cation, it is possible to study salts containing this particular cation. The first exemplary salts showed excellent performance data, but increased sensitivities towards impact and friction. Furthermore, only the 3,3,3-trinitropropyl-1-ammonium perchlorate displayed a thermal stability up to 164 °C.^[5] In this contribution, we tested two oxygen-rich and one

nitrogen-rich counterions, namely the periodate, sulfate and amino-bis(5-tetrazolate) salts of the 3,3,3-trinitropropyl-1-ammonium moiety

2.3 Results and Discussion

2.3.1 Synthesis

The central precursors are the reactive isocyanate 1,1,1-trinitropropan-3-isocyanate and the 3,3,3-trinitropropyl-1-ammonium chloride, which are available by a route starting from a Michael Addition of nitroform with acrylamide.^[5]



Scheme 2.1. Synthesis of the 3,3,3-trinitropropyl-1-ammonium salts **1–3**.

Reaction of the isocyanate with periodic acid resulted in the corresponding periodate salt **1**, similar to the chloride (Scheme 2.1) and nitrate salts. The sulfate and amino-bis(5-tetrazolate) salts **2** and **3** were obtained via metathesis reactions of 3,3,3-trinitropropyl-1-ammonium chloride with the corresponding silver or hydrazinium salts.

2.3.2 NMR Spectroscopy

Identification and characterization is performed as usual with multinuclear NMR spectroscopy. Since the resonances in the ^1H , ^{13}C , and ^{14}N NMR spectra are as to be expected in the same ranges as already described salts with this cation, they are not discussed in detail. For the periodate salt **1** the ^{127}I NMR resonance was obtained at 4103 ppm, for the sulfate salt **2** the ^{33}S resonance at -1.5 ppm, both as relatively sharp singlets.

2.3.3 Single Crystal Structure Analysis

Low-temperature X-ray diffraction analysis was possible for the sulfate salt **2** after recrystallization from water. However, in the second 3,3,3-trinitropropyl-1-ammonium unit a disorder is observed and omitted in Figure 2.1. Due to the steric repulsion from the three relatively large nitro groups around one carbon atom, the C-N bond lengths in the trinitromethyl moiety are in the range 1.51–1.54 Å, which is longer than a regular C-N bond (1.47 Å).^[6] The structure shows also the typical propeller-like arrangement of the trinitromethyl moieties, which optimizes the non-bonded N···O attractions. These attractions are much shorter (2.55–2.56 Å) than the sum of the van der Waals radii of nitrogen and oxygen (3.07 Å).^[7]

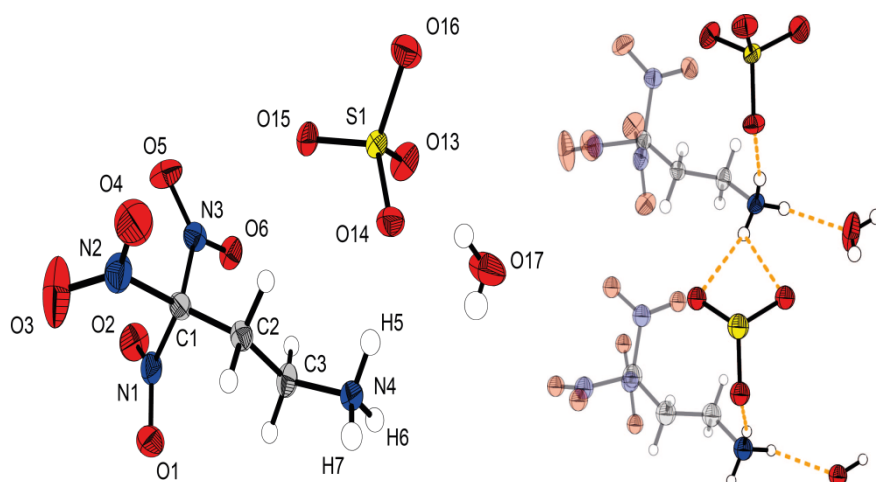


Figure 2.1 Crystal structure of bis(3,3,3-trinitropropyl-1-ammonium) sulfate (**2**). Selected distances [Å] and angles [°]: O2–N1 1.221(4), O3–N2 1.200(6), N3–C1 1.524(4), C1–C2 1.504(3), C2–C3 1.522(8), C1–N4 1.477(5), S1–O16 1.463(9), S1–O14 1.482(8), O1–N1–O2 127.3(9), C3–C2–C1 116.8(3), N3–C1–N2 106.4(8), O13–S1–O15 108.6(9), O14–S1–O16 107.9(8).

Strong hydrogen bonds (image at right in Figure 2.1) are observed between the hydrogen atoms of the ammonium moiety and the oxygen of the sulfate ion [DHA N4–H7···O14, bond angle DHA 166.9 °, d(D–A) = 2.73 Å, d(H–A) = 1.84 Å, DHA N4–H5···O15, bond angle DHA 153.2 °, d(D–A) = 3.11 Å, d(H–A) = 2.27 Å, DHA N4–H5···O13, bond angle DHA 122.0 °, d(D–A) = 2.90 Å, d(H–A) = 2.31 Å] as well as the hydrate water [DHA N4–H6···O17, bond angle DHA 146.6 °, d(D–A) = 2.84 Å, d(H–A) = 2.03 Å].

2.3.4 Thermal Stabilities and Energetic Properties

The periodate **1** was obtained hydrate-water free and has a relatively high oxygen content, in contrast to the amino-bis(5-tetrazolate) **3** which owns the nitrogen-rich amino-bis(tetrazole) moiety. Their energetic potential and physical properties were determined as outlined in Table 2.1 (the sulfate salt **2** is not considered here due to its water content, sensitivities see Appendix A2).

Table 2.1 Physical properties, calculated heat of formation and predicted detonation and combustion parameters of salts **1** and **3**, as well as ammonium perchlorate (AP).^[8]

	1	3	AP
Formula	C ₃ H ₇ N ₄ O ₁₀ I	C ₈ H ₁₅ N ₁₇ O ₁₂	NH ₄ ClO ₄
<i>FW</i> /g mol ⁻¹	386.01	541.32	117.49
<i>T_m</i> /°C ^[a]	105	—	—
<i>T_{dec}</i> /°C ^[b]	138	118	240
<i>IS</i> /J ^[c]	2	15	20
<i>FS</i> /N ^[d]	6	360	360
<i>ρ</i> /g cm ⁻³ ^[e]	2.12	1.66	1.95
<i>N</i> /% ^[f]	14.5	44.0	11.9
<i>O</i> /% ^[g]	41.5	35.5	54.5
<i>Ω_{CO2}</i> /% ^[h]	2.1*	-34.0	34.0
<i>ΔH_f[°]</i> /kJ mol ⁻¹ ^[i]	35	833	-296
<i>ΔU_f[°]</i> /kJ kg ⁻¹ ^[j]	63	1640	-2433
<i>Q_v</i> /kJ kg ⁻¹ ^[k]	-4902	-5924	-1421
<i>T_{ex}</i> /K ^[l]	4663	3953	1725
<i>V₀</i> /L kg ⁻¹ ^[m]	619	825	884
<i>p_{CJ}</i> /kbar ^[n]	258	293	183
<i>V_{det}</i> /m s ⁻¹ ^[o]	7074	8486	6810
<i>I_{sp}</i> /s ^[p]	225	267	155
<i>I_{sp}</i> /s (Al) ^[q]	240	275	233
<i>I_{sp}</i> /s (Al and 14% binder) ^[r]	236	239	256

[a] Onset melting and [b] onset decomposition point from DSC measurement, heating rate of 5 °C min⁻¹. [c] Impact sensitivity. [d] Friction sensitivity. [e] RT densities are measured by gas pycnometer [f] Nitrogen content. [g] Oxygen content. [h] Oxygen balance assuming the formation of CO₂ according to the Springall-Roberts-Rules (*as calculated by EXPLO5 (V6.03) computer code^[9]). [i] Enthalpy and [j] energy of formation calculated by the CBS-4M method using Gaussian 09.^[10][k] Heat of detonation, [l] detonation temperature. [m] volume of gaseous products, [n] detonation pressure and [o] detonation velocity calculated by using the EXPLO5 (V6.03) code.^[9] [p] Specific impulse for the neat compound, [q] for optimized compositions with aluminum and, [r] for three component compositions with oxidizer, aluminum and 14% binder (6% polybutadiene acrylic acid, 6% polybutadiene acrylonitrile and 2% bisphenol A ether) at 70.0 bar chamber pressure, isobaric combustion conditions (1 bar) and equilibrium to throat and frozen to exit (see Appendix A2).

Both salts **1** and **3** are stable for over a year under standard conditions, though **1** should be stored under the exclusion of light. Compared to the other already published 3,3,3-trinitropropylammonium salts, **3** showed most moderate impact and friction sensitivities. Furthermore, its room temperature density and thermal stability are most comparable to the 5,5'-azobistetrazolate salt (1.67 g cm⁻³, 120 °C).^[5] In contrast, the periodate salt **1** is the most sensitive salt so far, having the

highest decomposition temperature amongst the energetic, perchlorate-free 3,3,3-trinitropropyl-ammonium salts. In addition, due to the relatively heavy iodine atom, its density exceeds clearly 2.00 g cm^{-3} and also, that from all salts of this cation. The specific impulses I_{sp} of **1** and **3** were calculated for the neat compounds, for compositions with different amounts of aluminum as fuel, and additionally with binder. These impulses were compared with the calculated impulses of ammonium perchlorate (AP) as neat compound, as mixture with 15% aluminum, and as mixture with 15% aluminum and 14% binder. The amino-bis(5-tetrazolate) **3** has high specific impulses as neat compound and in mixtures with aluminum, but in composites containing oxidizer, fuel and binder the specific impulse decreases. The optimized composites of salts **1** and **3** are in appropriate ranges, but are neither superior to the former trinitropropyl-ammonium salts, nor to the optimized composites of ammonium perchlorate. Optimization plots can be found in Appendix A2.

2.4 Experimental Section

General experimental details are described in Appendix A2.

CAUTION! The 1,1,1-trinitropropyl-1-ammonium salts show increased sensitivities towards heat, impact and friction. No hazards occurred during the preparation and manipulation of those salts, but they should be handled with caution, especially the periodate salt. Protective equipment, such as leather jacket, face shield, ear protection, Kevlar® gloves, is strongly recommended.

3,3,3-Trinitropropyl-1-ammonium periodate (**1**)

Periodic acid (H_5IO_6 , 308 mg, 1.4 mmol) was dissolved in small amounts of water and immediately added to freshly prepared 1,1,1-trinitropropan-3-isocyanate (269 mg, 1.2 mmol). The reaction mixture was stirred at $50 \text{ }^\circ\text{C}$ for 5 hours under exclusion of light. The solvent was removed *in vacuo*, the resulting crude product was suspended in 1,2-dichloroethane and filtered. The periodate salt (**1**) was obtained as colorless solid in 53% yield (250 mg). $^1\text{H NMR}$ (D_2O): $\delta = 8.27$ (br, 3H, NH_3), 3.80 (m, 2H, CH_2), 3.56 (m, 2H, CH_2). $^{13}\text{C NMR}$ (D_2O): $\delta = 127.8$ ($\text{C}(\text{NO}_2)_3$), 34.0 (CH_2), 30.8 (CH_2). $^{14}\text{N NMR}$ (D_2O): $\delta = -32$ (NO_2) -351 (NH_3^+). $^{127}\text{I NMR}$ (D_2O): $\delta = 4103$ (IO_4^-) **EA**: $\text{C}_3\text{H}_7\text{N}_4\text{O}_{10}\text{I}$ (386.01): calc. C 9.33, H 1.83, N 14.51 %; found C 9.27, H 1.80, N 14.26 %. **IR** (ATR): $\tilde{\nu} = 3208$ (w), 3103 (w), 2972 (w), 2937 (w), 2361 (w), 2339 (w), 1586 (vs), 1495 (m), 1469 (m), 1431 (w), 1361 (w), 1314 (m), 1297 (m), 1158 (m), 1143 (m), 1015 (w), 994 (w), 906 (w), 844 (s), 832 (s), 797 (w), 739 (w) 680 (w) cm^{-1} . **Raman** (500 mW): $\tilde{\nu} = 3007$ (3), 2974 (6), 2939 (7), 1618 (4), 1601 (5), 1470 (2), 1432 (4), 1375 (5), 1298 (4), 1167 (2), 1016 (4), 907 (2), 858 (22), 852 (20), 841 (20), 792 (100), 625 (2), 567 (3), 424 (8), 400 (10), 384 (11), 361 (6),

341 (7), 325 (14), 313 (9), 269 (18) cm^{-1} . **Sensitivities (BAM):** impact: 2 J; friction: 9 N; (grain size: <100 μm) **DSC** (5 $^{\circ}\text{C min}^{-1}$): 105 $^{\circ}\text{C}$ (mp.), 138 $^{\circ}\text{C}$ (dec.).

Bis(3,3,3-trinitropropyl-1-ammonium) sulfate hydrate (2)

A solution of silver sulfate (156 mg, 0.5 mmol) in water (25 mL) was poured to a solution of 3,3,3-trinitropropyl-1-ammonium chloride (231 mg, 1.00 mmol) in water (10 mL). After stirring for 1 hour under exclusion of light, the filtrate was evaporated to dryness and a yellowish solid was obtained (210 mg, 86%). **$^1\text{H NMR}$** (D_2O): δ = 8.26 (br, 3H, NH_3), 3.76 (m, 2H, CH_2), 3.52 (m, 2H, CH_2). **$^{13}\text{C NMR}$** (D_2O): δ = 128.0 ($\text{C}(\text{NO}_2)_3$), 34.0 (CH_2), 30.9 (CH_2). **$^{14}\text{N NMR}$** (D_2O): δ = -26 (NO_2) -346 (NH_3^+). **$^{33}\text{S NMR}$** (D_2O): δ = -1.5 (SO_4^{2-}). **EA:** $\text{C}_6\text{H}_{14}\text{N}_8\text{O}_{16}\text{S} \cdot \text{H}_2\text{O}$ (504.29): calc. C 14.29, H 3.20, N 22.22, S 6.36 %; found C 14.05, H 3.57, N 21.34, S 6.69 %. **IR** (ATR): $\tilde{\nu}$ = 2987 (w), 2940 (w), 2883 (w), 2777 (w), 2695 (w), 2637 (w), 2526 (w), 2360 (w), 2339 (w), 1589 (vs), 1532 (m), 1473 (w), 1425 (w), 1369 (w), 1300 (m), 1197 (w), 1172 (w), 1154 (w), 1099 (s), 1052 (s), 971 (w), 856 (w), 801 (s), 756 (w) cm^{-1} . **Raman** (500 mW): $\tilde{\nu}$ = 3100 (4), 3041 (6), 2991 (24), 2948 (29), 2847 (4), 2808 (5), 2730 (4), 1613 (20), 1473 (12), 1427 (11), 1371 (32), 1337 (12), 1303 (25), 1187 (4), 1171 (7), 1158 (9), 1044 (9), 1030 (10), 1004 (10), 973 (67), 932 (4), 910 (12), 859 (102), 802 (7), 757 (4), 742 (4), 636 (9), 563 (10), 469 (7), 416 (39), 404 (44), 380 (40), 362 (27), 346 (30), 295 (12) cm^{-1} . **Sensitivities (BAM):** impact: 6 J, friction: 252 N (grain size: <100 μm). **DSC** (5 $^{\circ}\text{C min}^{-1}$): 120 $^{\circ}\text{C}$ (dec.).

Bis(3,3,3-trinitropropyl-1-ammonium) amino-bis(5-tetrazolate) (3)

Dihydrazinium amino-bis(5-tetrazolate) (109 mg, 0.5 mmol) was dissolved in H_2O (5 mL) and cooled to 0 $^{\circ}\text{C}$. A pre-cooled solution of 3,3,3-trinitropropyl-1-ammonium chloride (231 mg, 1.0 mmol) and water (1 mL) was added slowly. After 5 minutes an orange precipitate was formed, which was filtered and air dried. The amino-bis(5-tetrazolate) salt **3** was obtained as an orange powder in 31% yield (85 mg). **$^1\text{H NMR}$** (CD_3OD): δ = 8.63 (br, 3H, NH_3), 3.70 (m, 2H, CH_2), 3.41 (m, 2H, CH_2). **$^{13}\text{C NMR}$** (CD_3OD): δ = 157.5 (CN_4^-), 35.5 (CH_2), 32.7 (CH_2). **$^{14}\text{N NMR}$** (CD_3OD): δ = -30 (NO_2), -355 (NH_3^+). **EA:** $\text{C}_8\text{H}_{15}\text{N}_{17}\text{O}_{12}$ (541.31): calc. C 17.75, H 2.79, N 43.99 %; found C 17.66, H 2.97, N 42.05 %. **IR** (ATR): $\tilde{\nu}$ = 3213 (w), 3023 (w), 2982 (w), 2941 (w), 2874 (w), 2826 (w), 2510 (w), 2366 (w), 2136 (w), 1733 (w), 1717 (w), 1645 (m), 1586 (vs), 1540 (m), 1506 (s), 1464 (w), 1442 (w), 1421 (w), 1363 (m), 1322 (m), 1295 (m), 1230 (w), 1176 (m), 1154 (w), 1131 (w), 1109 (w) 1050 (m), 1032 (m), 1020 (m), 1006 (m), 909 (w), 854 (w) 797 (s), 736 (m), 693 (w) cm^{-1} . **Raman** (500 mW): $\tilde{\nu}$ = 3080 (9), 3039 (11), 2980 (40), 2946 (48), 2900 (13), 2832 (10), 2797 (9), 2103 (6), 1912 (6), 1712 (5), 1664 (10), 1631 (18), 1606 (43), 1581 (54), 1540 (18), 1511 (66), 1473 (16), 1464 (46), 1424 (26), 1366 (71), 1302 (37), 1226 (22), 1204 (5), 1178 (6), 1156 (7), 1148 (6), 1130 (17), 1122 (15), 1069 (68), 1034 (30), 1012

(19), 931 (8), 912 (9), 876 (10) 857 (100), 836 (4), 801 (9), 785 (8), 745 (8), 627 (7), 560 (8), 505 (5), 481 (5), 458 (7), 417 (40), 406 (50) cm^{-1} . **Sensitivities (BAM)**: impact: 15 J, friction: 360 N (grain size: <100 μm). **DSC** (5 $^{\circ}\text{C min}^{-1}$): 118 $^{\circ}\text{C}$ (dec.).

2.5 References

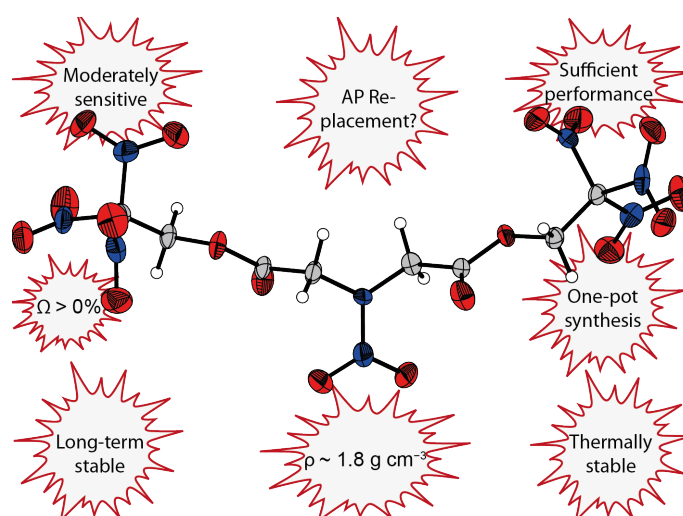
- [1] A. E. Simchen, *J. Appl. Chem.* **1963**, *13*, 369–374.
- [2] J. Akhavan, *The Chemistry of Explosives*, 2nd. ed., The Royal Society of Chemistry, Cambridge, **2004**
- [3] a) T. M. Klapötke, *Chemistry of High-Energy Materials*, 4th ed., De Gruyter, Berlin, **2017**; b) J. Wolff, *Pharmacol. Rev.* **1998**, *50*, 89–105.
- [4] Q. J. Axthammer, B. Krumm, T. M. Klapötke, R. Scharf, *Chem. – Eur. J.* **2015**, *21*, 16229–16239.
- [5] Q. J. Axthammer, T. M. Klapötke, B. Krumm, R. Scharf, C. C. Unger, *Dalton Trans.* **2016**, *45*, 18909–18920.
- [6] Q. J. Axthammer, T. M. Klapötke, B. Krumm, R. Moll, S. F. Rest, *Z. Anorg. Allg. Chem.* **2014**, *640*, 76–83.
- [7] A. Bondi, *J. Phys. Chem.* **1964**, *68*, 441–451.
- [8] T. M. Klapötke, *Energetic Materials Encyclopedia*, De Gruyter, Berlin / Boston, **2018**.
- [9] M. Sućeska, *EXPLO5 V6.03*, Zagreb (Croatia), **2015**.
- [10] M. J. Frisch, G. W. Trucks, H. B. Schlegel, G. E. Scuseria, M. A. Robb, J. R. Cheeseman, V. B. G. Scalmani, B. Mennucci, G. A. Petersson, H. Nakatsuji, M. Caricato, X. Li, H. P. Hratchian, A. F. Izmaylov, J. Bloino, G. Zheng, J. L. Sonnenberg, M. Hada, M. Ehara, K. Toyota, R. Fukuda, J. Hasegawa, M. Ishida, T. Nakajima, Y. Honda, O. Kitao, H. Nakai, T. Vreven, J. J. A. Montgomery, J. E. Peralta, F. Ogliaro, M. Bearpark, J. J. Heyd, E. Brothers, K. N. Kudin, V. N. Staroverov, R. Kobayashi, J. Normand, K. Raghavachari, A. Rendell, J. C. Burant, S. S. Iyengar, J. Tomasi, M. Cossi, N. Rega, J. M. Millam, M. Klene, J. E. Knox, J. B. Cross, V. Bakken, C. Adamo, J. Jaramillo, R. Gomperts, R. E. Stratmann, O. Yazyev, A. J. Austin, R. Cammi, C. Pomelli, J. W. Ochterski, R. L. Martin, K. Morokuma, V. G. Zakrzewski, G. A. Voth, P. Salvador, J. J. Dannenberg, S. Dapprich, A. D. Daniels, Ö. Farkas, J. B. Foresman, J. V. Ortiz, J. Cioslowski, D. J. Fox, *Gaussian 09*, Rev. A.02 ed., Gaussian, Inc., Wallingford CT (US), **2009**.

3 Trinitroethyl Esters Based on Divalent Acids

Oxygen-rich Bis(trinitroethyl esters): Suitable Oxidizers as Potential Ammonium Perchlorate Replacements

C. C. Unger, M. Holler, B. Krumm, and T. M. Klapötke

Energy Fuels 2020, in press.



3.1 Abstract

In the area of solid rocket propellants research efforts are ongoing to find suitable oxidizers as ammonium perchlorate (AP) replacement. On the one hand AP's performance data are excellent, on the other hand itself and its combustion products lead to health and environmental issues. Herein, nitramino diacetic acid bis(2,2,2-trinitroethyl ester) (NABTNE) is presented as a green AP-alternative and compared to the bis(trinitroethyl ester) of malonic acid (MaBTNE). Simple syntheses based on economic starting materials furnished both compounds, with NABTNE having a positive oxygen balance (according to CO), a density of 1.84 g cm^{-3} (@T = $-118 \text{ }^\circ\text{C}$) and a decomposition point of $180 \text{ }^\circ\text{C}$. The density of MaBTNE ($\delta = 1.81 \text{ g cm}^{-3}$ @T = $-147 \text{ }^\circ\text{C}$) and thermal stability ($T_{dec} = 157 \text{ }^\circ\text{C}$) are also advantageous. NABTNE as a moderately sensitive and the most promising derivative was shown to be of good stability towards long-term storage. Moreover, mixtures for a potential application in solid rocket formulations were calculated using EXPLO5 (V 6.03).

3.2 Introduction

Oxidizers are the main part (~70%) of solid rocket propellants apart from further components, such as a polymeric binder and a fuel, mostly aluminum. During their combustion plenty of hot gases are produced, which are used for the propulsion of rockets.¹ Due to the excellent performance and low cost, composite propellants still rely on ammonium perchlorate (AP). The drawbacks are based on the perchlorate anion, which leads to the release of large amounts of toxic gases during combustion. One of them is hydrogen chloride, causing the corrosion of the rocket launch sites and environmental problems.²⁻³ Another issue is groundwater pollution with the hormone active perchlorate anion.⁴⁻⁵ Therefore, halogen-free CHNO-based high energy dense oxidizers (HEDOs) are desirable.

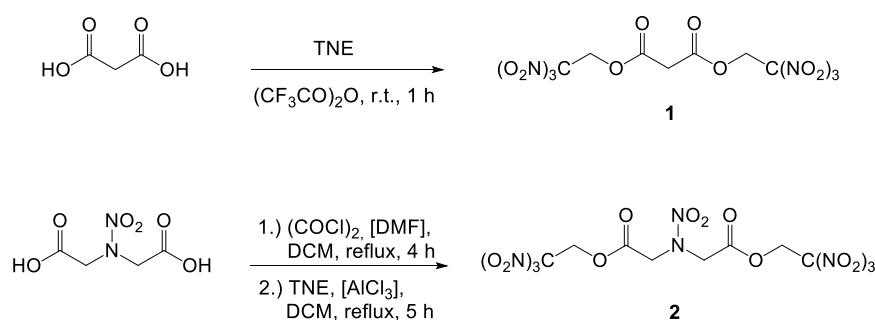
In the recent years several functional groups for HEDOs were investigated. For example, the excellent performing but very toxic fluorodinitromethyl moiety,⁶⁻⁷ trinitroalkyl compounds, where great performance data often goes along with low thermal stability,⁸⁻⁹ as well as organic nitrates, that are often easily accessed from the corresponding alcohol but can suffer from long-term stability issues.¹⁰⁻¹¹ Nitrocarbamates are also obtained from alcohols and form a more recently developed class of energetic materials, tending to have lower sensitivities, higher thermal stabilities and just slightly lower performance as shown by the pentaerythritol derivatives, the tetranitrate (PETN) and the tetranitrocarbamate (PETNC).¹²⁻¹³ Apart from aliphatic building blocks, oxadiazoles are a choice to combine a nitrogen- and oxygen-containing ring, which

possesses usually a high density, with various oxygen-containing moieties.¹⁴⁻¹⁷ Recently, highly nitrated pyrazoles and triazoles were also shown to be promising new materials.¹⁸⁻¹⁹ New oxidizers should fulfill the requirements of a high density ($\sim 2 \text{ g cm}^{-3}$), oxygen balance ($\Omega_{\text{CO}}/\Omega_{\text{CO}_2} > 0\%$), thermal stability ($T_{\text{melt}} > 150 \text{ }^\circ\text{C}$) and a comparable performance to AP (I_{sp} in mixtures $\sim 260 \text{ s}$). Furthermore, molecules with less synthetic steps,²⁰⁻²¹ which are compatible with the binder²² and long term stable, are desired.²³ Currently discussed alternatives are ammonium dinitramide (ADN), ammonium nitrate (AN), or hydrazinium nitroformate (HNF), because of being chlorine free and having promising properties.²⁴⁻²⁵ In this contribution, we report the synthesis of two easy accessible trinitroethyl esters and highlight their thoroughly analyzed physical and energetic parameters.

3.3 Results and Discussion

3.3.1 Synthesis

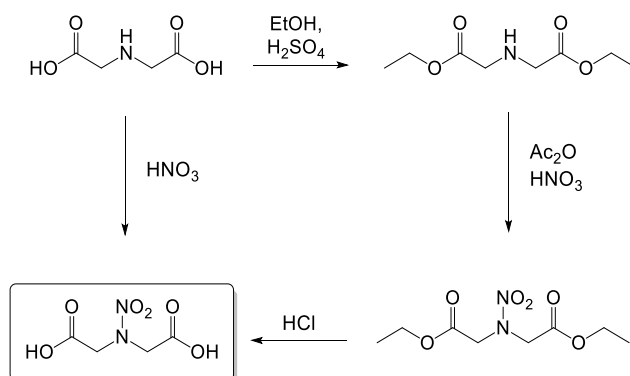
Both bis(trinitroethyl esters) can be synthesized in simple synthetic protocols starting from their corresponding acids, malonic acid and nitraminodiacetic acid (Scheme 3.1).



Scheme 3.1 Syntheses of MaBTNE (**1**) and NABTNE (**2**).

The commercially available malonic acid is reacted with trinitroethanol (TNE) and trifluoroacetic anhydride to form malonic acid bis(2,2,2-trinitroethyl ester) (**1**) (MaBTNE) in 43% yield after recrystallization from water/methanol (which is the most convenient synthesis among others).²⁶⁻²⁷ The esterification of nitraminodiacetic acid into nitraminodiacetic acid bis(2,2,2-trinitroethyl ester) (NABTNE (**2**)), normally is based on a two-step synthesis to the acid chloride, which is further reacted after work-up.²⁸⁻³⁰ In this case, it was possible to optimize the conditions toward an one-pot synthesis, whereby the energetic moiety is added latest, which is important for a safe scale-up. The starting material nitraminodiacetic acid was first synthesized in 1917, but was not considered further since then.³¹⁻³² Herein, it was obtained either by direct nitration of iminodiacetic acid using 100% HNO₃ in 22% yield. Another possible synthesis is based on the

nitration of the esterified iminodiacetic acid followed by acidic hydrolysis, with overall almost comparable yields (Scheme 3.2).



Scheme 3.2 Two possible synthetic pathways towards nitraminodiacetic acid.

3.3.2 NMR Spectroscopy

Both esters **1** and **2** were analyzed with multinuclear NMR spectroscopy in CD_3CN and additionally investigated in various solvents (see Appendix A3).

Singlets for the CH_2 hydrogen atoms in α -position to the carboxyl groups are found in the range 4.96–3.63 ppm in the ^1H NMR spectra and those of the ester functionality in the range 6.03–5.45 ppm. In the ^{13}C NMR spectra four resonances are found: in the region from 53.7 to 39.4 ppm respectively from 62.6 to 61.1 ppm (CH_2), in the region from 166.1 to 162.4 ppm (CO), and for $\text{C}(\text{NO}_2)_3$ at 124.5–122.7 ppm. In the ^{14}N NMR spectra, the resonances for the nitro groups are all in the narrow range of –37 to –30 ppm.

3.3.3 Single-Crystal Structure Analysis

Suitable crystals were obtained for nitraminodiacetic acid and the trinitroethyl ester NABTNE (**2**). Nitraminodiacetic acid crystallizes as colorless platelets in the orthorhombic space group $Pnma$ with a density of 1.776 g cm^{-3} at 123 K (Figure 3.1).

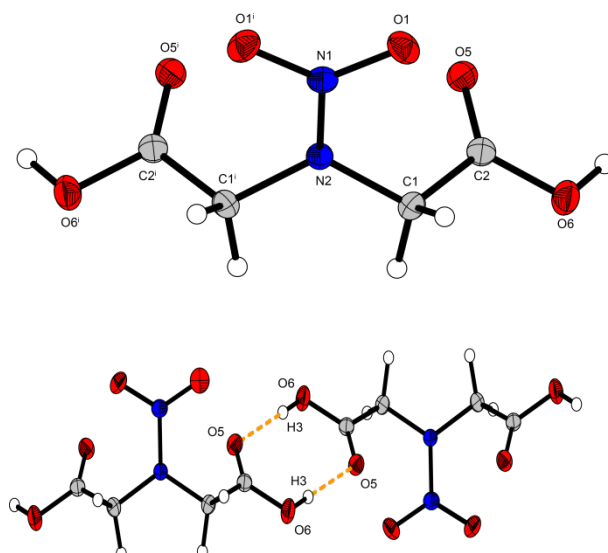


Figure 3.1 Thermal ellipsoid plot (50%) for the single-crystal X-ray structure of nitraminodiacetic acid (top) and dimers connected via hydrogen bonds of the carboxyl units (bottom). Selected bond lengths [Å]: N1–O1 1.2310(11), N1–N2 1.358(2), C1–N2 1.4508(15), C1–C2 1.508(2), C2–O5 1.2158(17), and C2–O6 1.3164(16). Symmetry code (i): $x, 1/2-y, z$.

In this molecule the only C–C single bond length is 1.51 Å, which is a bit shorter than classical sp^3 hybridized single bonds. Furthermore, the N1–N2 bond length are shorter (1.36 Å) compared to a common N–N bond length (~1.45 Å) due to the partial double bond character resulting from the nitramino group.³³ Relatively strong hydrogen bonds are observed between two carboxylic acid functionalities. Therefore, the donor acceptor angle is 172.47° (O6–H3⋯O5) and the donor acceptor distance is 2.71 Å (O6–H3⋯O5).

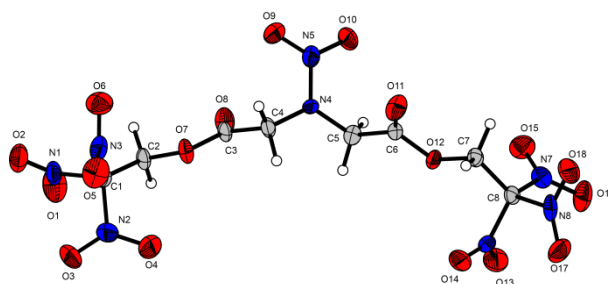


Figure 3.2 Thermal ellipsoid plot (50%) for the single-crystal X-ray structure of NABTNE. Selected bond lengths [Å]: N5–O10 1.234(6), N4–N5 1.363(7), C5–N4 1.444(7), C5–C6 1.510(7), C6–O11 1.180(6), C6–O12 1.357(7), C7–O12 1.416(6), C7–C8 1.512(8), N7–C8 1.511(8), and N7–O15 1.200(7).

Colorless needles of NABTNE, which crystallized in the triclinic space group $P\bar{1}$, were obtained from dichloromethane at ambient temperature (Figure 3.2). It contains four formula units in a cell and a density of 1.82 g cm⁻³ at 153 K. The bond lengths of the C–C (1.51 Å) and the N4–N5 (1.36 Å) bonds correspond very well with the values found in the crystal structure of the nitraminodiacetic acid. The trinitromethyl moiety is found to arrange in a propeller like motif,

which optimizes the non-bonded intramolecular attractions and electrostatic repulsion of two neighboring nitro groups., whereby intramolecular N \cdots O attractions (N1 \cdots O3, N2 \cdots O5, N3 \cdots O2; N6 \cdots O17, N7 \cdots O13, N8 \cdots O16) are found.³⁴ Furthermore, the distances of these are attractions are 2.54–2.61 Å, which is shorter than the sum of the van der Waals radii for nitrogen and oxygen (3.07 Å). Between the nitrogen of the trinitromethyl functionality N3 \cdots O7, as well as N6 \cdots O12, other relatively strong N \cdots O attractions are found with 2.69–2.72 Å. In addition, the distances of the N4 \cdots O8 and N4 \cdots O11 are 2.76 Å, shorter than their sum of the van der Waals radii. The extensive strong short attractive interactions might be one reason for the good thermal stability of NABTNE.

3.3.4 Physical and Energetic Properties

The physical and energetic properties of the compounds were determined and as both trinitroethyl esters MaBTNE (**1**) and NABTNE (**2**) are very attractive materials to be considered as potential oxidizers, compared to the common oxidizer for solid rocket propellants, AP (Table 3.1). The thermal stability measurements using DTA at a heating rate of 5 K min⁻¹ revealed decomposition points higher than 150 °C, which is the benchmark temperature for HEDOs. Melting prior to decomposition is observed for both compounds. Friction and impact sensitivities are especially important for the manipulation of energetic materials and were evaluated according to BAM standards, thereby the trinitroethyl esters are considered less sensitive compared to PETN (IS = 3–4 J, FS = 80 N). The good density values also result in high detonation velocities of 8263–8415 m s⁻¹, which are almost in the range for the secondary explosive PETN (pentaerythritol tetranitrate, $V_{\text{det}} = 8525 \text{ m s}^{-1}$).³⁵ One of the determining parameters for HEDOs is the specific impulse I_{sp} . It is used to evaluate the performance of the high energy dense oxidizer and furthermore the performance of the solid rocket propellant. A classical AP based mixture of AP/Al/HTPB of 68/18/14% leads to values of 259 s according to version 6.03 of EXPLO5. In the mixtures of both compounds with various common binders and varying amounts of aluminum, values of specific impulses similar as in the region of optimized mixtures for AP were obtained.

Table 3.1 Physical and energetic properties of MaBTNE and NABTNE compared to AP.

	MaBTNE	NABTNE	AP
Formula	C ₇ H ₆ N ₆ O ₁₆	C ₈ H ₈ N ₈ O ₁₈	NH ₄ ClO ₄
T_{melt} [°C] ^[a]	55	151	—
T_{dec} [°C] ^[b]	157	180	240
IS [J] ^[c]	5	6	20
FS [N] ^[d]	252	252	360
N [%] ^[e]	19.5	22.2	11.9
O [%] ^[f]	59.6	57.1	54.5
Ω_{CO} [%] ^[g]	22.3	19.1	34.0
Ω_{CO_2} [%] ^[h]	-3.7	-6.4	34.0
ρ [g cm ⁻³] ^[i]	1.76	1.78	1.95
ΔH_f° [kJ mol ⁻¹] ^[j]	-759	-691	-296
p_{CJ} [kbar] ^[k]	286	302	183
V_{det} [m s ⁻¹] ^[l]	8263	8415	6810
I_{sp} [s] ^[m]	240	246	155
I_{sp} [s] ^[m] (Al, 14% binder)	259	261	259

[a] Onset melting T_{melt} and [b] onset decomposition point T_{dec} from DTA measurement carried out at a heating rate of 5 °C min⁻¹. [c] Impact sensitivity. [d] Friction sensitivity. [e] Nitrogen content. [f] Oxygen content. [g] Oxygen balance assuming the formation of CO and [h] CO₂ [i] RT densities are recalculated from X-ray densities. [j] Enthalpy of formation calculated by the CBS-4M method. [k] Predicted detonation pressure and [l] detonation velocity using EXPLO5 (Version 6.03).³⁶ [m] Specific impulse of the neat compound using the EXPLO5 (Version 6.03) program package at 70.0 bar chamber pressure. [n] Specific impulse for compositions with oxidizer, aluminum, and 14% most promising binder (MaBTNE: 3,3,-bis(azidomethyl)oxetane [BAMO], 17.5% Al; NABTNE: BAMO, 16% Al; AP: Hydroxyl-terminated polybutadiene [HTPB]; 18% Al, for detailed plots, see Appendix A3)

3.3.5 Thermal Decomposition Characteristics and Kinetics

As all energetic materials, NABTNE is a potentially self-reactive substance which can undergo self-accelerated decomposition upon heating, releasing large amounts of heat and hot gasses and ultimately resulting in serious runaway reactions. To evaluate a possible production and application of NABTNE in larger scale, it is of great importance to study the thermal decomposition characteristics and kinetics. In addition to the synthesis and characterization, a series of TGA measurements at various heating rates was performed, providing a dataset to develop kinetic models. The models are based on different theoretical approaches as shown in ASTM 698, Friedman and Flynn–Wall–Ozawa.³⁷⁻³⁹

The ASTM kinetics approach relies on assuming first order reaction kinetics. Deriving the obtained TGA data and determining the peak temperature T_p for each heating rate, the method also assumes a constant extent of the reaction rate at T_p , which is independent of the heating rate.

Using a set of heating rates β and plotting $\ln(\beta)$ against $1/T_p$ results in a straight line, which slope is proportional to the activation energy.

A drawback of this method is to oversimplify complex, multi-stage decomposition processes by assuming first order kinetics as well as constancy of the activation energy.⁴⁰ Therefore, other “model-free” approaches can be employed. These assumptions utilize the dependence of activation energy E_a and preexponential factor A on reaction progress α by an isoconversional method, which can be described by equation (1):

$$\beta \frac{d\alpha}{dT} = A(\alpha) \exp\left(\frac{E_a(\alpha)}{RT}\right) f(\alpha) \quad (1)$$

The Ozawa-Flynn-Wall approach uses the integral dependence for solving equation (1):

$$g(\alpha) = \int_0^1 \frac{d\alpha}{f(\alpha)} = \frac{A(\alpha)}{\beta} \int_{T_0}^T \exp\left(-\frac{E(\alpha)}{RT}\right) dT \quad (2)$$

Using the approximation by Doyle⁴¹ and rearranging equation (2) gives equation (3):

$$\log(\beta) = \log\left(\frac{AE_a}{R}\right) - 2.315 - 0.4567 \frac{E_a}{RT} \quad (3)$$

When plotting $\log(\beta)$ against $1/T$ for different values of α , straight lines are obtained, which allow calculation of A and E_a . In contrast to Ozawa-Flynn-Wall, Friedman proposed differential methods for solving equation (1). Using the logarithm of the isothermal rate law gives equation (4), a plot of $\ln(d\alpha/dt)$ vs. $1/T$ for each α then allows to determine E_a and $A \cdot f(\alpha)$ from the slope and intercept:

$$\ln\left(\frac{d\alpha}{dt}\right) = \ln(A f(\alpha)) - \frac{E_a}{RT} \quad (4)$$

In order to obtain precise measurements for kinetic analysis, TGA measurements of NABTNE with sample masses between 2 and 3 mg using heating rates of 0.5, 1, 2, 4 and 8 K min⁻¹ and air as purge gas were performed (see Figure 3.3). All data analyses were carried out with the help of AKTS thermokinetics software, version 5.2.⁴² The TGA curves of NABTNE show good thermal stability with a sharp mass loss of approx. 70–80% shortly after onset of decomposition, which is continued by a slower, second process that leads to a final overall mass loss of $-82.95 \pm 1.6\%$. Integration of measurement data and further data analysis allowed the development of a model to

describe the kinetic behavior. In Figure 3.4, the measured reaction rates are plotted against the temperature for every heating rate (colored lines) together with simulated signals of the developed model (dashed lines). Very good correlation of simulation and measurement was achieved, reaching a correlation coefficient R of 0.99112. In Figure 3.5, the activation energies E_a determined according to Friedman, Flynn-Wall-Ozawa and ASTM E698 methods are shown. Due to the simplifications in the ASTM method, only one generalized activation energy of $152.11 \text{ kJ mol}^{-1}$ over the whole decomposition process was determined. Because of different mathematical approaches for solving the isoconversional equation (2), results for activation energy determination by Friedman and Flynn-Wall-Ozawa are slightly different. Analyzed with Friedman approach, the activation energy starts at a level of 196 kJ mol^{-1} ($\alpha = 0,5\%$) shows a peak maximum of 226 kJ mol^{-1} at $\alpha = 0,9\%$ followed by sharp drop to 170 kJ mol^{-1} . From $\alpha = 2$ to 84% , E_a decreases in linear fashion to a value of 96 kJ mol^{-1} . The final decomposition process is characterized by a drop in E_a to 68 kJ mol^{-1} at $\alpha = 89\%$, followed by somewhat irregular, stepwise increase to a final value of 141 kJ mol^{-1} . Using Ozawa-Flynn-Wall method the overall course of E_a vs. α is similar to the described behavior with the exception that values for E_a are higher, the difference becoming more prominent from $\alpha = 20\%$ to $\alpha = 80\%$ (see Table 3.2).

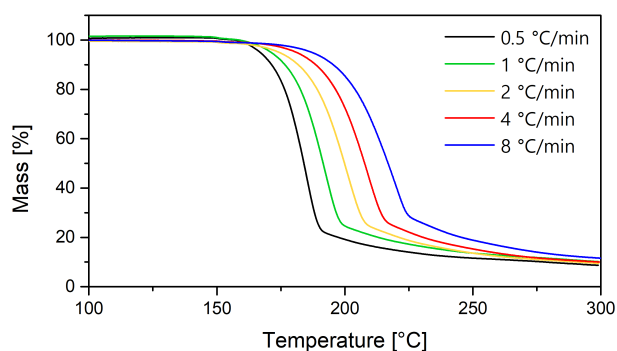


Figure 3.3 TGA plots of NABTNE at different heating rates.

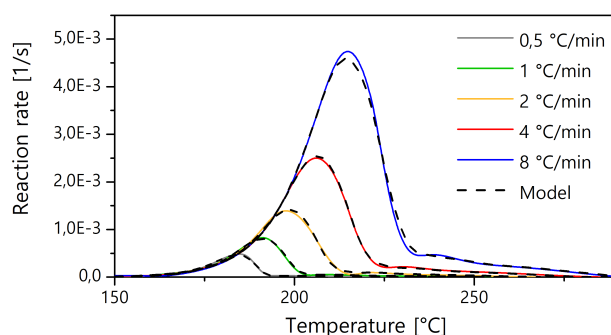


Figure 3.4 Reaction rates of NABTNE at various heating rates. Straight lines show measured data, dashed lines are simulations from the developed kinetic model.

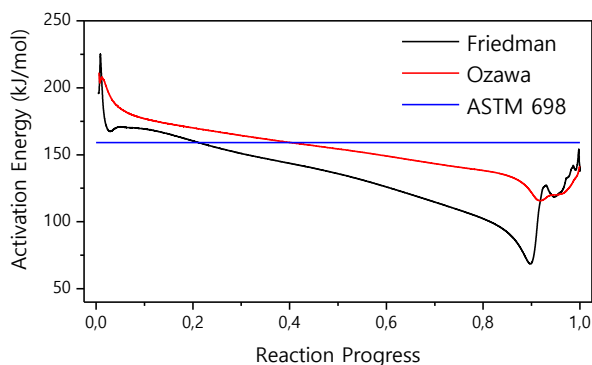


Figure 3.5 Activation energy of NABTNE decomposition determined with different methods.

Table 3.2 Activation energies at different states of the reaction progress.

	α [%]						
	0,5	1	10	30	50	70	95
E_a [kJ/mol] <i>Ozawa</i>	220.4	206.3	177.8	164.5	154.4	144.2	119.3
E_a [kJ/mol] <i>Friedman</i>	195.0	218.9	169.6	150.8	136.6	114.8	118.7

The established kinetic model based on differential isoconversional methods according to Friedman was used to simulate the long-term stability of NABTNE with the AKTS thermodynamics software package. Figure 3.6 shows simulated mass loss curves for various isothermal conditions (note the logarithmic scale of x-axis), Figure 3.7 is a detailed plot of the reaction progress up to $\alpha = 5\%$ to show early decomposition onset processes. It can be seen that NABTNE is highly stable at typical temperatures used in explosives and propellants: even constant storage at 80 °C (which is 9 °C higher than the maximum described in NATO Standardization agreements for ammunition⁴³) for 1000 days shows no significant decomposition reactions and even after a hypothetical 21.000 days, the conversion level would be 1%. Simulating high temperature stress levels of 140 °C, it would take 1.78 h until a conversion level 1% is reached.

The presented data ought to be supported by heat-flow measurements based on a series of DSC experiments at different heating rates. Autocatalytic and self-heating processes as well as extended evaluation of behavior at large-scale, quasi-adiabatic conditions should be taken into account (Appendix A3). Close examination of measurement results show that the main exothermic signal is accompanied by a preceding endothermic signal, rendering exact peak separation and overall data evaluation too inaccurate ($R < 0.96$). In order to develop firm and precise kinetic models based on heat flow experiments, extensive long-term measurements (e.g. by heat flow calorimetry at constant temperatures) are suggested. Nevertheless, the presented data

and simulation give reliable estimations of the thermal stability and long-term behavior of NABTNE.

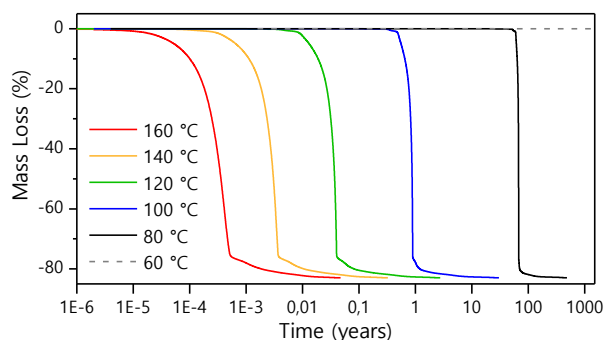


Figure 3.6 Simulation of NABTNE decomposition at different temperatures in isothermal conditions.

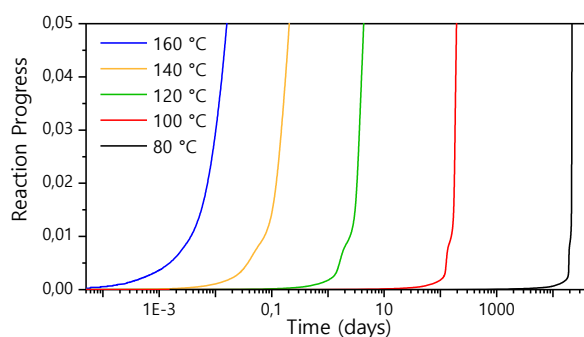


Figure 3.7 Simulation of reaction progress of NABTNE at different temperatures in isothermal conditions.

3.4 Conclusion

In this contribution two trinitroethyl esters were synthesized from commercially available starting materials in straightforward synthetic protocols. Thereby, the thorough examination revealed especially for NABTNE promising characteristics, such as oxygen balance of $\Omega_{CO} = 19.1\%$, melting point of $T_{melt} > 150\text{ °C}$ and comparable performance to AP (I_{sp} in optimized mixtures = 261 s). Moreover, activation energies were determined according to Friedman, Flynn-Wall-Ozawa and ASTM E698 methods based on a series of TGA measurements. According to the simulations with the AKTS thermodynamics software package concerning a long-term stability, initial and promising results were obtained for NABTNE as a stable energetic material.

3.5 Experimental Details

Caution! Both trinitroethyl esters are potentially energetic materials. Although no hazards occurred during synthesis and manipulation, appropriate personal protection equipment such as

face shield, ear protection, Kevlar® gloves, as well as a plastic spatula, should be used all the time.

Malonic acid bis(2,2,2-trinitroethyl ester) MaBTNE (1)

Malonic acid (165 mg, 1.58 mmol) was suspended in 3 mL trifluoroacetic anhydride and trinitroethanol was added (610 mg, 3.40 mmol). After 1.5 h at room temperature, the reaction mixture was poured on a cooled aqueous solution of K_2HPO_4 (10 mL, $c = 1$ M). The resulting ester was stirred at 0 °C until it solidified. After recrystallization from water/methanol MaBTNE (1) was obtained as colorless solid in 43% yield (292 mg).

DTA (5 °C min^{-1} , onset): 57 °C (mp.), 155 °C (dec.). **1H NMR** (CD_3CN , 399.8 MHz): $\delta = 5.60$ (s, 4H, CH_2), 3.68 (s, 2H, CH_2) ppm. **$^{13}C\{^1H\}$ NMR** (CD_3CN , 100.5 MHz): $\delta = 164.3$ (CO), 124.5 ($C(NO_2)_3$), 62.0 (CH_2), 40.6 (CH_2) ppm. **^{14}N NMR** (CD_3CN , 28.9 MHz): $\delta = -34$ (NO_2) ppm. **IR** (ATR, cm^{-1}): 3017 (w), 2974 (w), 2895 (w), 1795 (m), 1764 (m), 1582 (s), 1444 (w), 1410 (w), 1390 (m), 1330 (m), 1265 (m), 1297 (s), 1169 (m), 1125 (s), 1057 (m), 958 (w), 877 (w), 855 (m), 817 (m), 794 (m), 776 (s), 639 (m), 599 (m), 572 (w), 541 (m), 435 (w). **Raman** (1064 nm, 800 mW, cm^{-1}): 3005 (16), 2960 (39), 1798 (9), 1786 (15), 1767 (9), 1611 (32), 1445 (11), 1410 (12), 1391 (24), 1356 (38), 1305 (32), 1265 (11), 1171 (7), 1093 (6), 1051 (16), 1005 (7), 959 (9), 928 (13), 895 (7), 877 (8), 858 (101), 822 (5), 801 (7), 781 (6), 681 (4), 643 (8), 602 (4), 543 (16), 436 (15), 412 (39), 374 (66), 298 (9), 284 (13), 241 (4). **EA** ($C_7H_6N_6O_{16}$, 430.15 $g\ mol^{-1}$): C 19.55, H 1.41, N 19.54%; found: C 19.65, H 1.41, N 19.37%. **IS**: 5 J (grain size 100–500 μm), **FS**: 252 N (grain size 100–500 μm).

Nitraminodiacetic acid

Method A: Into fuming nitric acid (5 mL, >99.5%) iminodiacetic acid (500 mg, 3.76 mmol) was added in small portions at 0 °C. The mixture was slowly allowed to warm to room temperature and stirred at this temperature for 24 h. The solution was poured onto 75 mL of ice water and extracted with ethyl acetate (3 x 20 mL) and the combined organic phases were washed with water (25 mL) and brine (25 mL). After drying with magnesium sulfate, the solvent was removed under reduced pressure to get a colorless solid; 146 mg nitraminodiacetic acid was obtained in 22% yield without further purification.

Method B: Nitraminodiacetic acid diethyl ester was synthesized according to literature procedures.⁴⁴⁻⁴⁵ The ester (1.00 g, 4.27 mmol) was suspended in hydrochloric acid (37%, 25 mL) and afterwards refluxed for 6 h. After evaporating the solvent, nitraminodiacetic acid was obtained in quantitative yield as colorless solid.

DTA (5 °C min^{-1} , onset): 138 °C (mp.), 154 °C (dec.). **1H NMR** ($(CD_3)_2CO$, 399.8 MHz): $\delta = 4.70$ (CH_2) ppm. **$^{13}C\{^1H\}$ NMR** ($(CD_3)_2CO$, 100.5 MHz): $\delta = 168.4$ (CO), 53.7 (CH_2) ppm. **^{14}N**

NMR ($(\text{CD}_3)_2\text{CO}$, 28.9 MHz): $\delta = -30$ (NO_2) ppm. **IR** (ATR, cm^{-1}): 2967 (w), 1720 (s), 1561 (m), 1418 (m), 1401 (s), 1343 (m), 1304 (m), 1279 (m), 1212 (s), 1189 (s), 1136 (m), 1093 (m), 960 (m), 880 (m), 840 (m), 774 (s), 739 (m), 681 (w), 652 (m), 627 (s), 556 (w), 473 (w), 431 (w). **Raman** (1064 nm, 800 mW, cm^{-1}): 3007 (46), 2965 (65), 2912 (8), 1683 (13), 1568 (7), 1541 (5), 1464 (12), 1439 (8), 1396 (7), 1362 (26), 1329 (8), 1315 (25), 1288 (22), 1214 (9), 1127 (14), 976 (17), 927 (14), 883 (100), 770 (4), 681 (9), 655 (11), 631 (19), 555 (9), 451 (12), 403 (26), 353 (21), 338 (13); **EA** ($\text{C}_4\text{H}_6\text{N}_2\text{O}_6$, 178,10 g mol^{-1}): C 26.98, H 3.40, N 15.73%; found: C 26.95, H 3.41, N 15.51%. IS: >40 J (grain size 100–500 μm); FS: 360 N (grain size 100–500 μm).

Nitraminodiacetyl dichloride

Nitraminodiacetic acid (150 mg, 0.84 mmol) and oxalyl chloride (240 mg, 1.89 mmol) were added to 15 mL dichloromethane under exclusion of moisture. After addition of catalytic amounts of dimethyl formamide, the reaction mixture was stirred for 1 h at ambient temperature and was afterwards refluxed for 3 h under nitrogen atmosphere. After removing the solvent *in vacuo* 177 mg of reddish nitraminodiacetic acid chloride was obtained (98% yield).

^1H NMR (CDCl_3 , 399.8 MHz): $\delta = 4.94$ (s, 4H, CH_2) ppm **$^{13}\text{C}\{^1\text{H}\}$ NMR** (CDCl_3 , 100.5 MHz): $\delta = 168.4$ (CO), 60.5 (CH_2) ppm **^{14}N NMR** (CDCl_3 , 28.9 MHz): $\delta = -36$ (NO_2) ppm **IR** (ATR, cm^{-1}): 3566 (w), 2997 (w), 2954 (w), 1797 (s), 1785 (s), 1537 (m), 1429 (s), 1379 (s), 1351 (m), 1331 (m), 1309 (m), 1275 (s), 1183 (m), 1121 (m), 1005 (m), 974 (m), 950 (m), 928 (s), 779 (m), 764 (s), 631 (s), 479 (m), 458 (s).

Nitraminodiacetic acid bis(2,2,2-trinitroethyl ester) NABTNE (2)

Method A: 362 mg of nitraminodiacetic acid chloride (1.68 mmol) and 609 mg of 2,2,2-trinitroethanol were dissolved in dry dichloromethane (40 mL) and aluminum chloride (246 mg, 1.85 mmol) was added. The mixture was stirred for 1 h at ambient temperature and for 4 h at 40 °C under exclusion of moisture. After cooling to room temperature, hydrochloric acid (30 mL, 2 M) was added and a solid precipitated. The solid was collected using filtration and washed with ice-water, whereas the remaining solution was extracted with dichloromethane (2 x 30 mL) and washed with brine (30 mL). After removing the solvent under reduced pressure, the collected solid was combined with the filtrate and recrystallized twice from boiling dichloromethane. NABTNE (2) was obtained as colorless solid in 20% (174 mg) yield.

Method B: 303 mg of nitraminodiacetic acid (1.70 mmol) was suspended in 40 mL dry dichloromethane and 481 mg (3.79 mmol) of oxalyl chloride was added. After the addition of catalytic amounts of dimethyl formamide the reaction mixture was stirred for 30 minutes at room temperature and was refluxed for further 3 h. The resulting solution was cooled to room temperature and 619 mg (3.42 mmol) trinitroethanol and 253 mg (1.89 mmol) AlCl_3 were added

and further refluxed for 4 h. The mixture was kept continuously under nitrogen atmosphere. The work up was carried out as described in method A and resulted in 109 mg of NABTNE (13% yield).

$^1\text{H NMR}$ (CD_3CN , 399.8 MHz): δ = 5.64 (s, 4H, CH_2), 4.65 (s, 4H, CH_2) ppm. $^{13}\text{C}\{^1\text{H}\}$ NMR (CD_3CN , 100.5 MHz): δ = 165.6 (CO), 124.7 ($\text{C}(\text{NO}_2)_3$), 62.1 (CH_2), 53.7 (CH_2) ppm. $^{14}\text{N NMR}$ (CD_3CN , 28.9 MHz): δ = -34 (NO_2), -31 (NO_2) ppm. **IR** (ATR, cm^{-1}): 3005 (w), 1778 (m), 1590 (s), 1534 (m), 1437 (m), 1391 (m), 1290 (s), 1189 (s), 1163 (s), 1103 (w), 1048 (w), 1005 (w), 950 (m), 874 (m), 855 (m), 805 (m), 780 (s), 765 (s), 635 (m), 545 (s), 444 (w), 416 (w). **Raman** (1064 nm, 800 mW, cm^{-1}): 3013 (28), 2996 (39), 2968 (71), 2960 (60), 1781 (28), 1618 (41), 1601 (34), 1439 (22), 1393 (29), 1374 (52), 1352 (40), 1305 (52), 1293 (59), 1278 (24), 1196 (16), 1108 (16), 1088 (17), 1052 (28), 914 (31), 881 (77), 857 (82), 632 (15), 556 (15), 547 (23), 441 (14), 416 (65), 400 (48), 386 (38), 376 (100), 334 (14), 292 (22), 274 (16), 231 (17). **EA** ($\text{C}_8\text{H}_8\text{N}_8\text{O}_{18}$, 504.19 g mol^{-1}): C 19.06, H 1.60, N 22.22%; found: C 18.97, H 1.67, N 22.26%; IS: 6 J (grain size 500–1000 μm); FS: 252 N (grain size 500–1000 μm).

3.6 References

1. Akhavan, J., *The Chemistry of Explosives*. 2nd. ed., The Royal Society of Chemistry, Cambridge, 2004.
2. Dennis, C. W.; Sutton, P. Assessing Rocket Plume Damage to Launch Vehicles. In *Joint Propulsion Conference & Exhibit*, Tucson, Arizona, 2005; 1–10.
3. Schmalzer, P. A.; Boyle, S. R.; Hall, P.; Oddy, D. M.; Hensley, M. A.; Stolen, E. D.; Duncan, B. W. *Monitoring Direct Effects of Delta, Atlas, and Titan Launches from Cape Canaveral Air Station*; NASA/TM-1998-207912; 1998. <https://ntrs.nasa.gov/archive/nasa/casi.ntrs.nasa.gov/19980235583.pdf> (accessed 2020-07-05)
4. Hogue, C. Changing Course on Perchlorate. *Chem. Eng. News* **2011**, *89*, 6.
5. McLanahan, E. D.; Campbell, J. L., Jr.; Ferguson, D. C.; Harmon, B.; Hedge, J. M.; Crofton, K. M.; Mattie, D. R.; Braverman, L.; Keys, D. A.; Mumtaz, M.; Fisher, J. W. Low-dose Effects of Ammonium Perchlorate on the Hypothalamic-pituitary-thyroid Axis of Adult Male Rats Pretreated with PCB126. *Toxicol. Sci.* **2007**, *97*, 308–317.
6. Klapötke, T. M.; Krumm, B.; Rest, S. F.; Reynders, M.; Scharf, R. (2-Fluoro-2,2-dinitroethyl)-2,2,2-trinitroethylnitramine: A Possible High-Energy Dense Oxidizer. *Eur. J. Inorg. Chem.* **2013**, 5871–5878.

7. Fridman, A. L.; Kremleva, O. B.; Zalesov, V. S.; Platonova, Z. V.; Gabitov, F. A.; Rubinshtein, L. A.; Plaksina, A. N. Synthesis and Physiological Activity of Aliphatic Nitro Compounds. *Pharm. Chem. J.* **1977**, *11*, 64–67.
8. Axthammer, Q. J.; Krumm, B.; Klapötke, T. M.; Scharf, R. A Study of the 3,3,3-Trinitropropyl Unit as a Potential Energetic Building Block. *Chem. – Eur. J.* **2015**, *21*, 16229–16239.
9. Thottempudi, V.; Gao, H.; Shreeve, J. M. Trinitromethyl-Substituted 5-Nitro- or 3-Azo-1,2,4-triazoles: Synthesis, Characterization, and Energetic Properties. *J. Am. Chem. Soc.* **2011**, *133*, 6464–6471.
10. Klapötke, T. M.; Krumm, B.; Reith, T. Polyfunctional Energetic Nitrates Derived from Tris(hydroxymethyl)aminomethane (TRIS). *Eur. J. Org. Chem.* **2017**, 3666–3673.
11. de Klerk, W. P. C. Assessment of Stability of Propellants and Safe Lifetimes. *Propellants, Explos., Pyrotech.* **2015**, *40*, 388–393.
12. Axthammer, Q. J.; Klapötke, T. M.; Krumm, B.; Moll, R.; Rest, S. F. The Energetic Nitrocarbamate $O_2NN(H)CO[OCH_2C(NO_2)_3]$ Derived from Phosgene. *Z. Anorg. Allg. Chem.* **2014**, *640*, 76–83.
13. Axthammer, Q. J.; Krumm, B.; Klapötke, T. M. Pentaerythritol-Based Energetic Materials Related to PETN. *Eur. J. Org. Chem.* **2015**, 723–729.
14. Johnson, E. C.; Sabatini, J. J.; Chavez, D. E.; Sausa, R. C.; Byrd, E. F. C.; Wingard, L. A.; Guzmán, P. E. Bis(1,2,4-oxadiazole)bis(methylene) Dinitrate: A High-Energy Melt-Castable Explosive and Energetic Propellant Plasticizing Ingredient. *Org. Process Res. Dev.* **2018**, *22*, 736–740.
15. Yu, Q.; Yin, P.; Zhang, J.; He, C.; Imler, G. H.; Parrish, D. A.; Shreeve, J. M., Pushing the Limits of Oxygen Balance in 1,3,4-Oxadiazoles. *J. Am. Chem. Soc.* **2017**, *139*, 8816–8819.
16. Yu, Q.; Wang, Z.; Yang, H.; Wu, B.; Lin, Q.; Ju, X.; Lu, C.; Cheng, G. *N*-Trinitroethyl-substituted Azoxyfurazan: High Detonation Performance Energetic Materials. *RSC Adv.* **2015**, *5*, 27305–27312.
17. Kettner, M. A.; Karaghiosoff, K.; Klapötke, T. M.; Sućeska, M.; Wunder, S. 3,3'-Bi(1,2,4-oxadiazoles) Featuring the Fluorodinitromethyl and Trinitromethyl Groups. *Chem. – Eur. J.* **2014**, *20*, 7622–7631.
18. Kumar, D.; Imler, G. H.; Parrish, D. A.; Shreeve, J. M. 3,4,5-Trinitro-1-(nitromethyl)-1*H*-pyrazole (TNNMP): A Perchlorate Free High Energy Density Oxidizer with High Thermal Stability. *J. Mater. Chem. A* **2017**, *5*, 10437–10441.

19. Zhao, G.; Yin, P.; Kumar, D.; Imler, G. H.; Parrish, D. A.; Shreeve, J. M. Bis(3-nitro-1-(trinitromethyl)-1*H*-1,2,3-triazol-5-yl)methanone: An Applicable and Very Dense Green Oxidizer. *J. Am. Chem. Soc.* **2019**, *141*, 19581–19584.
20. Vo, T. T.; Parrish, D. A.; Shreeve, J. M. Tetranitroacetimidic Acid: A High Oxygen Oxidizer and Potential Replacement for Ammonium Perchlorate. *J. Am. Chem. Soc.* **2014**, *136*, 11934–11937.
21. Klapötke, T. M.; Krumm, B.; Scharf, R. Oxalyl Chloride and Hydrazone Based Energetic Polynitro Derivatives. *Eur. J. Inorg. Chem.* **2016**, 3086–3093.
22. Hall, J., *Advances in Spacecraft Technologies*. InTech, Rijeka, 2011.
23. Abd-Elghany, M.; Elbeih, A.; Klapötke, T. M. Thermo-analytical Study of 2,2,2-Trinitroethyl-formate As a New Oxidizer and Its Propellant Based on a GAP Matrix in Comparison with Ammonium Dinitramide. *J. Anal. App. Pyrolysis* **2018**, *133*, 30–38.
24. Agrawal, J. P., *High Energy Materials Propellants, Explosives and Pyrotechnics*. 1st ed., Wiley-VCH, Weinheim (Germany), 2010.
25. Klapötke, T. M., *Chemistry of High-Energy Materials*. 5th ed., De Gruyter, Berlin, 2019.
26. Cochoy, R. E.; McGuire, R. R. Improved Procedure for the Synthesis of Fluorodinitroethyl and Trinitroethyl Esters of Carboxylic Acids. *J. Org. Chem.* **1972**, *37*, 3041–3042.
27. Sheremetev, A. B.; Yudin, I. L.; Suponitsky, K. Y. Ionic Liquid-assisted Synthesis of Trinitroethyl Esters. *Mendeleev Commun.* **2006**, *16*, 264–266.
28. Frankel, M. B., Synthesis and Reactions of Trinitromethyl Compounds. *Tetrahedron* **1963**, *19*, 213–217.
29. Hill, M. E., Esterification Catalysis by Metal Halides. *J. Am. Chem. Soc.* **1953**, *75*, 3020–3021.
30. Frankel, M. B. Polynitro Esters. US 2,978,494 A, 1961.
31. Franchimont, A. P. N.; Dubsky, J. V., Contributions à la Connaissance de la Réaction des Iminodérivés Aliphatiques avec-l'acide Azotique Réel. *Recl. Trav. Chim. Pays-Bas Belg.* **1917**, *36*, 80–109.
32. Kadeřábek, V.; Nymsová, V.; Suchy, V., Thermal Analysis of Nitraminocarboxylic Acids and Their Sodium and Barium Salts. *J. Therm. Anal.* **1976**, *9*, 349–356.
33. Holleman, A. F.; Wiberg, E.; Wiberg, N. *Lehrbuch der anorganischen Chemie*. 102 ed., de Gruyter, Berlin, 2008.

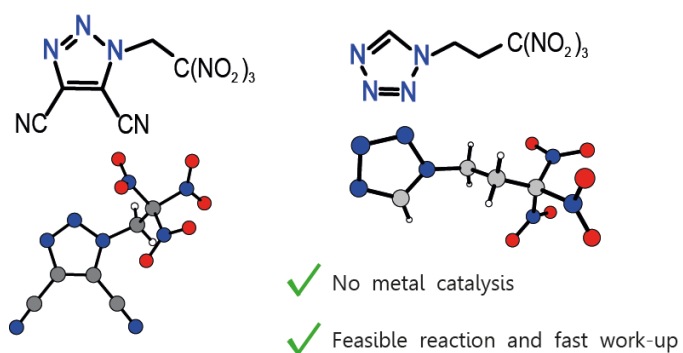
34. Axthammer, Q. J.; Klapötke, T. M.; Krumm, B.; Scharf, R.; Unger, C. C. Convenient Synthesis of Energetic Polynitro Materials Including (NO₂)₃CCH₂CH₂NH₃-salts *via* Michael Addition of Trinitromethane. *Dalton Trans.* **2016**, *45*, 18909–18920.
35. Klapötke, T. M. *Energetic Materials Encyclopedia*. De Gruyter, Berlin, 2018.
36. Sućeska, M., *EXPLO5 V6.03*. Zagreb (Croatia), 2015.
37. ASTM International. *Standard Test Method for Arrhenius Kinetic Constants for Thermally Unstable Materials*. ASTM E698-05; West Conshohocken, PA. 2005.
38. Friedman, H. L. Kinetics of Thermal Degradation of Char-forming Plastics From Thermogravimetry. Application to a Phenolic Plastic. *J. Polym. Sci., Part C: Polym Symp.* **1964**, *6*, 183–195.
39. Takeo, O. A New Method of Analyzing Thermogravimetric Data. *Bull. Chem. Soc. Jpn* **1965**, *38*, 1881–1886.
40. Stolarek, P.; Ledakowicz, S. Evaluation of the ASTM E 698 Method for Determination of Kinetic Parameters of Thermal Decomposition Processes. *Chem. Process Eng.* **2003**, *24*, 701–715.
41. Doyle, C. D. Series Approximations to the Equation of Thermogravimetric Data. *Nature* **1965**, *207*, 290–291.
42. Roduit, B.; Borgeat, C.; Berger, B.; Folly, P.; Alonso, B.; Aebischer, J. N.; Stoessel, F. Advanced Kinetic Tools for the Evaluation of Decomposition Reactions. *J. Therm. Anal. Calorim.* **2005**, *80*, 229–236.
43. NATO, *Manual of Data Requirements and Tests for the Qualification of Explosive Materials for Military Use*. **2003**.
44. Park, H. S.; Lin, Q.; Hamilton, A. D. Protein Surface Recognition by Synthetic Receptors: A Route to Novel Submicromolar Inhibitors for α -Chymotrypsin. *J. Am. Chem. Soc.* **1999**, *121*, 8–13.
45. Klapötke, T. M.; Krumm, B.; Reith, T.; Unger, C. C., Synthetic Routes to a Triazole and Tetrazole with Trinitroalkyl Substitution at Nitrogen. *J. Org. Chem.* **2018**, *83*, 10505–10509.

4 Azoles with Trinitroalkyl Substitution

Synthetic Routes to a Triazole and Tetrazole with Trinitroalkyl Substitution at Nitrogen

T. M. Klapötke, B. Krumm, T. Reith and C. C. Unger

J. Org. Chem. **2018**, *83*, 10505–10509.



4.1 Abstract

Two *N*-substituted trinitroalkyl azoles, one triazole and one tetrazole, were synthesized and isolated via efficient cyclization reactions. Both materials were thoroughly characterized, and their structures were confirmed by X-ray diffraction. The formation of the *N*-trinitroethyl substituted triazole proceeds unexpectedly via nitrosation of an *N*-substituted diaminomaleonitrile initially with HNO₃ and subsequently confirmed with HNO₂. The *N*-trinitropropyl substituted tetrazole was prepared via a standard cyclization route from trinitropropylammonium chloride with orthoformate and azide.

4.2 Introduction

The trinitromethyl group is an important building block in the research for new energetic materials with good availability of the sources nitroform or trinitroethanol.¹⁻³ In combination with already oxygen-rich energetic materials, many potent replacements for the common but harmful³ oxidizer ammonium perchlorate were investigated, such as trinitroethyl nitrocarbamate (**A**) and bis(trinitroethyl)oxalate (**B**).^{1, 4} In the ongoing research to replace the secondary explosive RDX, the combination of the trinitromethyl moiety with different azoles results in interesting compounds (Figure 4.1) (**C–F**).⁵⁻⁸ In general, either trinitroethanol was reacted with heterocyclic amines to incorporate the trinitromethyl unit^{8, 9} or the exhaustive nitration of activated methylene groups forms the trinitromethyl moiety e.g. in azolylacetic acids.^{6, 7, 10} However, only very sparse information exists about azoles with nitrogen substituted trinitroalkyl units.^{7, 10, 11} In those few examples, rather sensitive *N*-trinitromethyl triazoles were obtained either by exhaustive nitration mentioned above, or by nitration of dinitromethyl derivatives with nitronium tetrafluoroborate. The *N*-substitution with longer trinitroalkyl chains, such as trinitroethyl and trinitropropyl units, should provide better thermal and mechanical stability¹², but none have been described to the best of our knowledge. The low reactivity of deactivated aromatic azoles seems not sufficient enough to react with nitroform or trinitroethanol.¹³⁻¹⁵ At the same time, trinitromethyl containing starting materials tend to be chemically rather labile^{16, 17}, particularly against bases and high temperatures, which prevent many ring closing mechanisms of functional groups.¹⁸

4.3 Results and Discussion

4.3.1 Synthesis

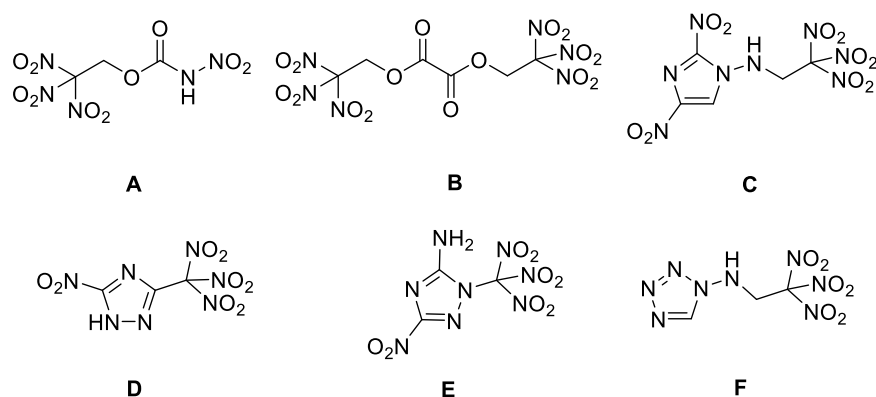
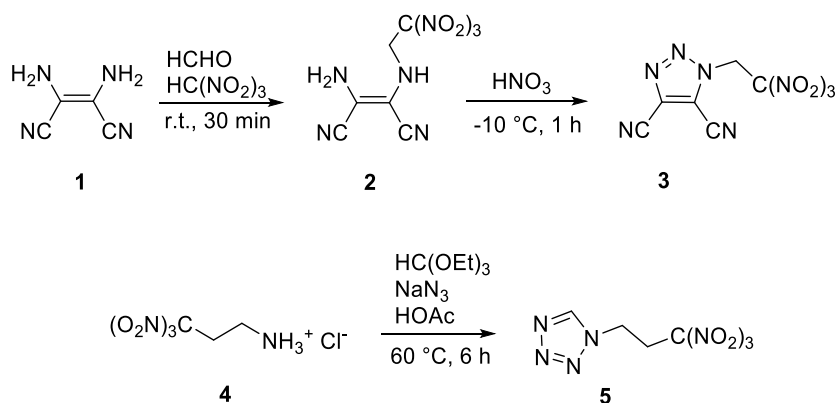


Figure 4.1 Oxygen-rich materials: trinitroethyl nitrocarbamate (**A**), bis(trinitroethyl)oxalate (**B**), 2,4-dinitro-*N*-(2,2,2-trinitroethyl)-1*H*-imidazol-1-amine (**C**), 5-nitro-3-trinitromethyl-1*H*-1,2,4-triazole (**D**), 3-nitro-1-trinitromethyl-1*H*-1,2,4-triazol-5-amine (**E**) and 1-(2,2,2-trinitroethylamino)tetrazole (**F**).

In this contribution, pathways to two polyazoles with *N*-substituted trinitroethyl and trinitropropyl moieties are reported and their properties examined. In both cases, a trinitromethyl containing precursor was selected to further cyclize to a triazole and a tetrazole (Scheme 4.1).



Scheme 4.1 Synthesis of 4,5-dicyano-1*N*-(trinitroethyl)-1,2,3-triazole (**3**) and 1*N*-trinitropropyl tetrazole (**5**) from the precursors diaminomaleonitrile (**1**) or trinitropropylammonium chloride (**4**).

Diaminomaleonitrile (**1**) was converted quantitatively into amino-(trinitroethylamino)maleonitrile (**2**) by reaction with formaldehyde and nitroform in aqueous solution. Without further purification, nitration was performed in white fuming nitric acid. Surprisingly, the originally intended nitration at the NH_2 -group of **2** was not observed, but a cyclized product, which was identified as 4,5-dicyano-1*N*-(trinitroethyl)-1,2,3-triazole (**3**), was isolated. The substituted maleonitrile **2** turns very sensitive upon thorough drying and may deflagrate spontaneously without external stimulation, which occurred once in our laboratory

during storage. The triazole **3** is still very sensitive towards impact (2 J) and moderately sensitive to friction (216 N), but is stable in air at room temperature for at least several months.

Primary amines undergo heterocyclization with triethyl orthoformate and sodium azide in acetic acid. This facile synthetic route yields *N*-substituted tetrazoles in good yields.¹⁹ Our precursor, 3,3,3-trinitropropyl amine as the HCl-salt (**4**),⁴ undergoes the cyclization reaction at 60 °C for 6 hours. Simple work-up procedures afforded 1*N*-trinitropropyl tetrazole (**5**) as an orange-colored solid.

4.3.2 NMR Spectroscopy

The substituted maleonitrile **2** starts to decompose quickly in several deuterated solvents. However, reasonable spectra were obtained from acetonitrile CD₃CN. The ¹H NMR spectrum shows three resonances at 5.1 ppm (br), 4.65 ppm (d) and 4.08 ppm (t). In the ¹³C{¹H} NMR spectra the expected six resonances are observed. The ¹⁴N NMR spectrum shows the signal for the nitro groups at -31 ppm. NMR spectroscopy of the triazole **3** in deuterated acetone reveals a singlet at 7.02 ppm in the ¹H NMR spectrum and six resonances in the range between 128.2 and 51.3 ppm in the ¹³C{¹H} NMR spectrum, including the typically broadened signal for the trinitromethyl carbon atom. The ¹⁴N NMR spectrum shows the resonance at -35 ppm for the nitro groups.

The tetrazole **5** shows the acidic tetrazole hydrogen resonance at 9.41 ppm and the methylene resonances at 5.00 and 4.20 ppm in the ¹H NMR spectrum. In the ¹³C{¹H} NMR spectrum the four carbon resonances are in the expected range between 144.4 ppm for the azole carbon atom and 32.3 ppm for the methylene group. In the ¹⁵N NMR spectrum the nitrogen atoms of the tetrazole ring and the trinitro moiety are detected at 12.4 (*N4*), -14.6 (*N2/N3*), -29.9 (*C(NO₂)₃*), -52 (*N3/N4*) and -147.5 ppm (*N1*).

4.3.3 Single Crystal Structure Analysis

Suitable single crystals for X-ray diffraction of triazole **3** were obtained from aqueous work up by evaporation at ambient temperature. The 4,5-dicyano-1*N*-(trinitroethyl)-1,2,3-triazole (**3**) crystallizes in the monoclinic space group *P2₁/n* with four molecules per unit cell and a density of 1.72 g cm⁻³ at 173 K (Figure 4.2).

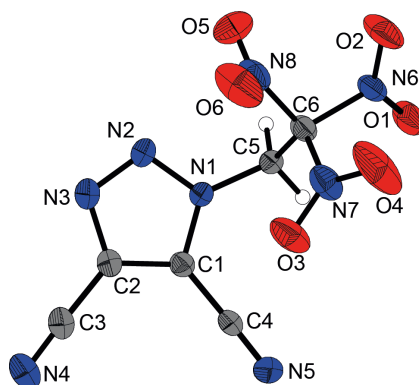


Figure 4.2 X-ray molecular structure of 4,5-dicyano-1*N*-(trinitroethyl)-1,2,3-triazole (**3**). Thermal ellipsoids represent the 50% probability level. Selected atom distances (Å) and angles (deg.): C1–C4 1.419 (3), C4–N5 1.135 (3), C1–C2 1.368 (3), C1–N1 1.337 (3), N1–N2 1.346 (2), N2–N3 1.304 (3), C2–N3 1.362 (3), N1–C5 1.460 (3); C2–C1–C4 130.9 (2), C1–C4–N5 179.2 (2), C1–C2–C3 128.0 (2), C2–C3–N4 178.1 (3), C1–N1–C5 129.6, N2–N1–C5 120.1, N1–C5–C6 114.0 (2); C1–N1–N2–N3 –0.4 (2), N1–N2–N3–C2 0.6 (2), N2–N3–C2–C1 –0.7 (2), N2–N3–C2–C3 –179.5 (2), N2–N1–C1–C4 178.9 (2), C5–N1–N2–N3 –177.4 (2).

In the solid state, the triazole ring forms an almost planar system with the two nitrile substituents (torsion angles along the triazole ring less than 1°, N2–N3–C2–C3 –179.5°). The trinitromethyl unit forms the typical propeller-type structure.²¹ The molecule contains no classical proton donor, therefore strong hydrogen bonds are absent. Some weak intermolecular hydrogen bonds can be found between the methylene group as proton donor and neighboring nitro oxygen atoms or nitrile nitrogen atoms as proton acceptors (C5–H2···O4, $d(\text{D–H}) = 0.94 \text{ \AA}$, $d(\text{H}\cdots\text{A}) = 2.49 \text{ \AA}$, $\angle(\text{D–H}\cdots\text{A}) = 141.0^\circ$).²¹

Suitable single crystals of tetrazole **5** were obtained from ethyl acetate at ambient temperature. The 1*N*-trinitropropyl tetrazole crystallizes as yellow platelets in the monoclinic space group $P2_1/c$ with four formula units per unit cell and a density of 1.75 g cm^{-3} at 143 K (Figure 4.3).

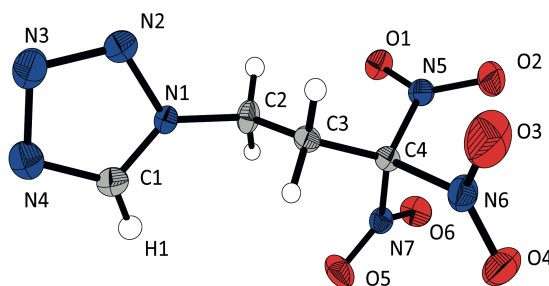


Figure 4.3 X-ray molecular structure of 1*N*-trinitropropyl tetrazole (**5**). Thermal ellipsoids represent the 50% probability level. Selected atom distances (Å) and angles (deg.): C2–C3 1.528 (3), C3–C4 1.499 (2), C1–N1 1.327 (3), C1–N4 1.308 (2), C4–N5 1.522 (3), C4–N6 1.535 (2), C4–N7 1.525 (3), N1–N2 1.343 (2), N2–N3 1.291 (2), N3–N4 1.358 (3), N5–O1 1.217 (2), N5–O2 1.214 (2), N6–O3 1.214 (2), N6–O4 1.213 (2), N7–O5 1.210 (3), N7–O6 1.219 (2), N1–C2–C3 108.23 (2), C2–C3–C4 117.34 (2), C3–C4–N5 116.06 (1), C4–N5–O1 115.06 (1), C2–N1–N2 121.14 (2), C2–N1–C1 130.94 (2), N1–C2–C3–C4 165.32 (2), C2–C3–C4–N6 –176.89 (2), N1–N2–N3–N4 –0.07 (2), N2–N3–N4–C1 –0.12 (2), C2–N1–C1–N4 –179.18 (2).

The aromatic tetrazole is almost planar as shown by the torsion angles N1–N2–N3–N4 -0.07° and N2–N3–N4–C1 -0.12° . As already mentioned for **3**, the structure of the **5** reveals the typical propeller-type structure of the trinitromethyl unit.²¹ Compared to common C–N bond lengths (1.47 Å),²² the C–N bonds in the trinitromethyl moiety are in the range of 1.53 Å, which is significantly longer. This may result from steric repulsion of the proportionally large nitro groups around the carbon atom C4.

4.3.4 Thermal Stabilities and Energetic Properties

DTA measurements of the heterocycles indicate a decomposition point of 132 °C for triazole **3** and of 125 °C for the tetrazole **5**, which additionally melts at 66 °C. Calculation²³⁻²⁵ of enthalpies on CBS-4M level led to heats of formation of $-1117 \text{ kJ mol}^{-1}$ (**3**) and 227 kJ mol^{-1} (**5**), which were further used for EXPLO5 calculations^{26, 27} to estimate the detonation parameters. The triazole **3** and the tetrazole **5** show detonation velocities (V_{Det}) of 4557 m s^{-1} and 8388 m s^{-1} , respectively. Furthermore, the detonation pressure (p_{CJ}) was determined ($p_{\text{CJ}} = 55 \text{ kbar}$ (**3**) and $p_{\text{CJ}} = 293 \text{ kbar}$ (**5**)). The energetic parameters of **5** are promising and almost in the range of PETN (pentaerythritol tetranitrate, $V_{\text{Det}} = 8405 \text{ m s}^{-1}$ and $p_{\text{CJ}} = 319 \text{ kbar}$), a commonly used secondary explosive. In addition, the specific impulse I_{sp} , a benchmark for composite propellants in rocket engines, was predicted for **5**. Neat **5** ($I_{\text{sp}} = 278 \text{ s}$) and mixtures with 15% aluminium and 14% binder ($I_{\text{sp}} = 252 \text{ s}$) are in an appropriate range. The nitrile units of the triazole **3** reduce the energetic parameters significantly with the tremendous high enthalpy of formation and the unfavorable influence on the oxygen balance. A further derivatization of **3** however could possibly give access to a variety of potential energetic materials.

Since the treatment of **2** with HNO₃ surprisingly yielded a triazole **3**, which could be due to nitrosation, control experiments were carried out by using nitrite in HCl and H₂SO₄. And indeed, with both systems the formation of the identical triazole **3** was observed, which is reported for other triazoles.²⁸ Therefore we conclude, that in the initial HNO₃ approach sufficient amounts of the nitrosonium cation NO⁺ prevail and react with the maleonitrile **2**. The formation of NO⁺ in white fuming HNO₃ can be explained by the presence of some nitrogen dioxide NO₂, which is known to disproportionate to nitrite and nitrate.²⁹ Subsequently, the unstable nitrous acid HNO₂ is the precursor for the nitrosonium cation after water elimination.

4.4 Conclusion

Two hitherto unknown azoles with *N*-substituted trinitroalkyl units have been synthesized in this study. The 4,5-dicyano-1*N*-(trinitroethyl)-1,2,3-triazole (**3**) was formed unexpectedly by nitrosation. The 1*N*-trinitropropyl tetrazole (**5**) was obtained by cyclization of trinitropropylammonium chloride with sodium azide and triethyl orthoformate, leading to the first

isolated *N*-substituted trinitroalkyl tetrazole. The energetic properties of **5** are in the range of PETN, a commonly used secondary explosive.

4.5 Experimental Section

4.5.1 General Information

All chemicals were used as received from the suppliers. Raman spectra were recorded with a Bruker MultRAM FT-Raman spectrometer using glass tubes or metal plates. A Nd:YAG laser excitation up to 1000 mW (at 1064 nm) in the range between 400 and 4000 cm^{-1} was used. The intensities are reported as percentages of the most intense peak and are given in parentheses. Infrared (IR) spectra were measured with an ATR device at ambient temperature (20 °C). Transmittance values are qualitatively described as “strong” (s), “medium” (m) and “weak” (w). The NMR spectra were recorded with a 400 MHz instrument and chemical shifts were determined relative to external Me_4Si (^1H , 399.8 MHz, ^{13}C , 100.5 MHz) and MeNO_2 (^{14}N , 28.9 MHz, ^{15}N , 40.6 MHz) at ambient temperature. The melting and decomposition points were measured with an OZM Research DTA 552-Ex with a heating rate of 5 °C min^{-1} in a temperature range of 20 to 400 °C. They were also checked with a Büchi Melting Point B-540 apparatus. Sensitivity data were determined using a BAM drophammer and friction tester. Single-crystal X-ray diffraction was performed with an Oxford XCalibur3 diffractometer equipped with a Spellman generator and a KappaCCD detector operating with $\text{Mo } K_\alpha$ radiation ($\lambda = 0.71073$) at low temperatures. The data collection was realized by using CRYALISPRO³⁰ software, structures were solved by direct methods (SIR-92 or SIR-97) implemented in the program package WINGX³¹ and finally checked using PLATON.³² All non-hydrogen atoms were refined anisotropically, hydrogen atom positions were located in a difference Fourier map.³³ Crystallographic data for the reported structures in this contribution have been deposited with the Cambridge Crystallographic Data Centre as supplementary publication numbers CCDC 1587493 (**3**) and CCDC 1822024 (**5**). The Cambridge Crystallographic Data Centre provides these data free of charge via www.ccdc.cam.ac.uk/data_request/cif.

4.5.2 Synthesis

CAUTION! These materials are energetic compounds with sensitivity to various stimuli, especially the maleonitrile **2** and the triazole **3** should be treated with caution. While no serious issues in the synthesis and handling of this material were encountered, proper protective measures (face shield, ear protection, body armor, Kevlar gloves and grounded equipment) as well as a plastic spatula, should be used all the time.

Amino-(trinitroethylamino)maleonitrile (2)

This compound deflagrated spontaneously without external stimuli when thoroughly dried. Therefore, it should be handled at least slightly moistened and with great caution!

Diaminomaleonitrile (**1**, 1.08 g, 10 mmol) was added to 40 ml of H₂O. To the slurry 8.31 g of an aqueous nitroform solution (40%, 22 mmol) and 1.8 ml of a formaldehyde solution (37% in water, 22 mmol) were added with stirring. Within 15 minutes the colour of the slurry turns from brown to orange and amino-(trinitroethylamino)maleonitrile (2.7 g, 99%) was obtained in high yield and purity by filtration and repeated washing with cold water. After hours to days exposed to air and humidity the substance will turn red and decompose slowly.

DTA (5 °C min⁻¹): 67 °C (onset dec.); **IR** (ATR, cm⁻¹): ν = 3362 (w), 3283 (w), 2200 (m), 2170 (m), 1589 (vs), 1488 (w), 1427 (m), 1378 (m), 1305 (s), 1266 (m), 1204 (m), 805 (m), 782 (m), 662 (w), 634 (w), 517 (w); **Raman** (1064 nm, 800 mW, cm⁻¹): 2957 (6), 2604 (4), 2264 (7), 2232 (48), 2200 (100), 2158 (5), 2137 (6), 2061 (4), 1625 (15), 1592 (46), 1380 (15), 1347 (9), 857 (20), 784 (6), 642 (6), 516 (5), 476 (6), 410 (5), 377 (14), 217 (7); **¹H NMR** (CD₃CN, ppm): δ = 5.1 (br, 2H), 4.65 (d, 2H, ³*J*(¹H,¹H) = 7.3 Hz), 4.08 (t, 1H, ³*J*(¹H,¹H) = 7.4 Hz); **¹³C{¹H} NMR** (CD₃CN, ppm): δ = 127 (br), 122.3, 116.1, 114.9, 102.9, 50.8; **¹⁴N NMR** (CD₃CN, ppm): δ = -31; **EA** (C₆H₅N₇O₆, 271.15 g mol⁻¹): calc.: C 26.58, H 1.86, N 36.16%; found: C 26.54, H 1.94, N 35.65%. Sensitivity tests unchecked due to extreme sensitivity in dry condition.

4,5-Dicyano-1N-(trinitroethyl)-1,2,3-triazole (3)

2-Amino-3-(2,2,2-trinitroethylamino) maleonitrile (**2**, 2.7 g, 10 mmol) was slowly added to 10 mL colorless fuming nitric acid at -10 °C with good stirring, accompanied by a heavy reaction. After one hour the red colored reaction mixture was poured on ice and 4,5-dicyano-1N-(trinitroethyl)-1,2,3-triazole (1.56 g, 55%) precipitated as colorless powder, which was obtained by filtration and washed several times with water.

DTA (5 °C min⁻¹): 132 °C (onset dec.); **IR** (ATR, cm⁻¹): ν = 3007 (w), 2963 (w), 2267 (w), 1626 (m), 1599 (vs), 1457 (m), 1427 (m), 1380 (w), 1332 (m), 1289 (s), 1255 (m), 1206 (w), 1138 (w), 1071 (w), 871 (m), 857 (w), 816 (m), 789 (s), 780 (s), 719 (w), 603 (w), 543 (s); **Raman** (1064 nm, 800 mW, cm⁻¹): 3008 (3), 2963 (8), 2265 (100), 1632 (3), 1554 (29), 1457 (3), 1333 (9), 1319 (3), 1256 (11), 1137 (5), 990 (4), 859 (14), 722 (4), 651 (5), 544 (4), 503 (9), 464 (4), 446 (5), 401 (5), 373 (9), 302 (8), 258 (4), 237 (4); **¹H NMR** (acetone-D₆, ppm): δ = 7.02 (s, 2H); **¹³C{¹H} NMR** (acetone-D₆, ppm): δ = 128.2, 123.3, 122.2, 109.4, 105.9, 51.3; **¹⁴N NMR** (acetone-D₆, ppm): δ = -35; **EA** (C₆H₂N₈O₆, 282.13 g mol⁻¹): calc.: C 25.54, H 0.71, N 39.72%; found: C 25.68, H 0.92, N 39.69%; **BAM drophammer**: 2 J (<100 μ m); **friction tester**: 216 N (<100 μ m).

Additional experiments with NaNO₂/HCl/H₂SO₄

2-Amino-3-(2,2,2-trinitroethylamino) maleonitrile (**2**, 268 mg, 1 mmol) was slowly added to a mixture of 2.5 mL water and 2.5 mL concentrated HCl or concentrated H₂SO₄ acid with good stirring and ice bath cooling. Sodium nitrite, NaNO₂ (70 mg, 1 mmol), was dissolved in 1 mL water and slowly added. After one hour at 0 °C the slightly orange colored reaction mixture was poured on ice and 4,5-dicyano-1*N*-(trinitroethyl)-1,2,3-triazole (**3**, 59 mg, 21% for HCl and 64 mg, 22% for H₂SO₄) precipitated as colorless powder, which was obtained by filtration and washed several times with water. Alternatively, the use of concentrated acids to form **3** did not improve the yields. The product was identified by NMR measurements and confirmed the previously obtained data with HNO₃.

1*N*-Trinitropropyl tetrazole (5)

3,3,3-Trinitropropyl-1-ammonium chloride (**4**, 118 mg, 0.51 mmol) and sodium azide (40 mg, 0.62 mmol) were suspended in triethyl orthoformate (0.5 mL, 3.0 mmol) and concentrated acetic acid (2 mL) was added. After heating up to 60 °C in an oil bath for 6 h, an orange precipitate was formed. The solvent was removed and the orange residue was dried under high vacuum. The residue was portioned between ethyl acetate (15 mL) and water (15 mL). The aqueous phase was extracted with ethyl acetate (2 × 15 mL) and the combined organic phases were washed with water (15 mL) and brine (15 mL). After drying with magnesium sulfate, the solvent was removed to obtain an orange oil. The oil was repeatedly treated with toluene and subsequently dried under high vacuum to obtain a red-orange crystalline solid (61.1 mg) in 48% yield.

DTA (5 °C min⁻¹): 66 °C (onset mp.), 125 °C (onset dec.); **IR** (ATR, cm⁻¹): ν = 3139 (w), 2985 (w), 2949 (w), 2132 (w), 1737 (w), 1681 (w), 1651 (w), 1591 (vs), 1482 (m), 1427 (w), 1371 (m), 1298 (s), 1242 (m), 1198 (m), 1171 (m), 1129 (m), 1103 (m), 1055 (m), 1014 (w), 963 (w), 856 (w), 801 (s), 707 (w), 649 (m), 546 (w), 475 (w), 475 (w), 416 (w); **Raman** (1064 nm, 800 mW, cm⁻¹): 3130 (35), 3045 (25), 2996 (82), 2948 (100), 2860 (12), 1616 (31), 1608 (28), 1592 (11), 1484 (15), 1409 (32), 1379 (44), 1352 (14), 1320 (26), 1306 (31), 1279 (37), 1259 (15), 1179 (23), 1136 (7), 1105 (16), 1063 (9), 1022 (33), 1006 (19), 967 (15), 907 (10), 855 (71), 774 (7), 677 (7), 647 (7), 622 (13), 521 (23), 467 (13), 410 (13), 396 (34), 378 (46), 311 (21), 269 (21), 223 (16), 212 (12); **¹H NMR** (DMSO-D₆, ppm): δ = 9.41 (s, 1H), 5.00 (t, 2H, ³*J*(¹H,¹H) = 6.9 Hz), 4.20 (t, 2H, ³*J*(¹H,¹H) = 6.9 Hz); **¹³C{¹H} NMR** (DMSO-D₆, ppm): δ = 144.4, 129.0, 41.5, 32.3; **¹⁵N NMR** (DMSO-D₆, ppm): δ = 12.4 (d, ²*J*(¹⁵N,¹H) = 2.9 Hz), -14.6, -29.9 (t, ³*J*(¹⁵N,¹H) = 2.9 Hz), -51.8, -147.5 (m); **EA** (C₄H₅N₇O₆, 247.13 g mol⁻¹): calc.: C 19.44, H 2.04, N 39.68%; found: C 21.09, H 2.21, N 38.26%. BAM drophammer: 25 J (500–1000 μ m); friction tester: 360 N (500–1000 μ m).

4.6 References

1. Klapötke, T. M.; Krumm, B.; Scharf, R. Oxalyl Chloride and Hydrazone Based Energetic Polynitro Derivatives. *Eur. J. Inorg. Chem.*, **2016**, 3086–3093.
2. Hill, M. E. Ortho Esters of 2,2,2-Trinitroethanol Useful as Explosives. US Patent 3.306.939, **1967**.
3. Klapötke, T. M. *Chemistry of High-Energy Materials, 4th ed.*, De Gruyter, Berlin, **2015**.
4. Axthammer, Q. J.; Klapötke, T. M.; Krumm, B.; Moll, R.; Rest, S. F. The Energetic Nitrocarbamate $O_2NN(H)CO[OCH_2C(NO_2)_3]$ Derived from Phosgene. *Z. Anorg. Allg. Chem.*, **2014**, *640*, 76–83.
5. Yin, P.; Zhang, Q.; Zhang, J.; Parrish, D. A.; Shreeve, J. M. *N*-Trinitroethylamino Functionalization of Nitroimidazoles: A New Strategy for High Performance Energetic Materials. *J. Mater. Chem. A*, **2013**, *1*, 7500–7510.
6. Thottempudi, V.; Shreeve, J. M. Synthesis and Promising Properties of a New Family of High-Density Energetic Salts of 5-Nitro-3-trinitromethyl-1*H*-1,2,4-triazole and 5,5'-Bis(trinitromethyl)-3,3'-azo-1*H*-1,2,4-triazole. *J. Am. Chem. Soc.*, **2011**, *133*, 19982–19992.
7. Kofman, T. P.; Kartseva G. Y.; Glazkova, E. Y. 5-Substituted 3-Nitro-1-trinitromethyl-1,2,4-triazoles. *Russ. J. Org. Chem.*, **2008**, *44*, 870–873.
8. Klapötke, T. M.; Piercey, D. G.; Stierstorfer, J. Amination of Energetic Anions: High-Performing Energetic Materials. *Dalton Trans.*, **2012**, *41*, 9451–9459.
9. Ovchinnikov, I. V.; Kulikov, A. S.; Epishina, M. A.; Makhova, N. N.; Tartakovsky, V. A. Synthesis of *N*-trinitroethyl Derivatives of Linear and Heterocyclic Nitrogen-Containing Compounds. *Russ. Chem. Bull.*, **2005**, *54*, 1346–1349.
10. Kofman, T. P.; Kartseva, G. Y.; Glazkova, E. Y.; Krasnov, K. N. Nitration of Triazolyl-Substituted Ketones. *Russ. J. Org. Chem.*, **2005**, *41*, 753–757.
11. Semenov, V. V.; Kanishev, M. I.; Shevelev, S. A.; Kiselyov, A. S. Thermal Ring-Opening Reaction of *N*-Polynitromethyl Tetrazoles: Facile Generation of Nitrilimines and their Reactivity. *Tetrahedron*, **2009**, *65*, 3441–3445.
12. Axthammer, Q. J.; Krumm, B.; Klapötke, T. M.; Scharf, R. A Study of the 3,3,3-Trinitropropyl Unit as a Potential Energetic Building Block. *Chem. Eur. J.*, **2015**, *21*, 16229–16239.
13. Kassimi, N. E.-B.; Doerksen, R. J.; Thakkar, A. J. Polarizabilities of Aromatic Five-Membered Rings: Azoles. *J. Phys. Chem.*, **1995**, *99*, 12790–12796.

14. Davies, D. T. *Aromatic Heterocyclic Chemistry*, Oxford University Press Inc., New York, **1992**.
15. Yu, Z.-H.; Xuan, Z.-Q.; Wang, T.-X.; Yu, H.-M. A Novel Energy Partition for Gaining New Insight into Aromaticity and Conjugation. *J. Phys. Chem. A*, **2000**, *104*, 1736–1747.
16. Feuer, H.; Kucera, T. Notes- Preparation of 2,2,2-Trinitroethanol. *J. Org. Chem.*, **1960**, *25*, 2069–2070.
17. Frankel, M. B. Synthesis and Reactions of Trinitromethyl Compounds. *Tetrahedron*, **1963**, *19*, 211–213.
18. Ramanathan, M.; Wang, Y.-H.; Liu, S.-T. One-Pot Reactions for Synthesis of 2,5-Substituted Tetrazoles from Aryldiazonium Salts and Amidines. *Org. Lett.*, **2015**, *17*, 5886–5889.
19. Gaponik, P. N.; Karavai, V. P.; Grigor'ev, Y. V. Synthesis of 1-Substituted Tetrazoles by Heterocyclization of Primary Amines, Orthoformic Ester, and Sodium Azide. *Chem. Heterocycl. Comd.*, **1985**, *21*, 1255–1258.
20. Axthammer, Q. J.; Klapötke, T. M.; Krumm, B.; Scharf, R.; Unger, C. C. Convenient Synthesis of Energetic Polynitro Materials Including (NO₂)₃CCH₂CH₂NH₃-Salts via Michael Addition of Trinitromethane. *Dalton Trans.*, **2016**, *45*, 18909–18920.
21. Steiner, T. The Hydrogen Bond in the Solid State. *Angew. Chem. Int. Ed.*, **2002**, *41*, 48–76.
22. Bondi, A. Van der Waals Volumes and Radii. *J. Phys. Chem.*, **1964**, *68*, 441–451.
23. Dennington, R. D.; Keith, T. A.; Millam, J. M. *GaussView*, v. 5.08, Semichem, Inc., Wallingford, **2009**.
24. Frisch, M. J.; Trucks, G. W.; Schlegel, H. B.; Scuseria, G. E.; Robb, M. A.; Cheeseman, J. R.; Scalmani, G.; Barone, V.; Mennucci, B.; Petersson, G. A.; Nakatsuji, H.; Caricato, M.; Li, X.; Hratchian, H. P.; Izmaylov, A. F.; Bloino, J.; Zheng, G.; Sonnenberg, J. L.; Hada, M.; Ehara, M.; Toyota, K.; Fukuda, R.; Hasegawa, J.; Ishida, M.; Nakajima, T.; Honda, Y.; Kitao, O.; Nakai, H.; Vreven, T.; Montgomery Jr., J. A.; Peralta, J. E.; Ogliaro, F.; Bearpark, M. J.; Heyd, J.; Brothers, E. N.; Kudin, K. N.; Staroverov, V. N.; Kobayashi, R.; Normand, J.; Raghavachari, K.; Rendell, A. P.; Burant, J. C.; Iyengar, S. S.; Tomasi, J.; Cossi, M.; Rega, N.; Millam, N. J.; Klene, M.; Knox, J. E.; Cross, J. B.; Bakken, V.; Adamo, C.; Jaramillo, J.; Gomperts, R.; Stratmann, R. E.; Yazyev, O.; Austin, A. J.; Cammi, R.; Pomelli, C.; Ochterski, J. W.; Martin, R. L.; Morokuma, K.; Zakrzewski, V. G.; Voth, G. A.; Salvador, P.; Dannenberg, J. J.; Dapprich, S.; Daniels, A. D.; Farkas, Ö.; Foresman, J. B.; Ortiz, J. V.; Cioslowski, J.; Fox, D. J. *Gaussian 09*, Gaussian, Inc.: Wallingford, **2009**.

25. Montgomery, J. A.; Frisch, M. J.; Ochterski, J. W.; Petersson, G. A. A Complete Basis Set Model Chemistry. VII. Use of the Minimum Population Method. *J. Chem. Phys.*, **2000**, *112*, 6532–6542.
26. Sućeska, M. Calculation of the Detonation Properties of CHNO Explosives. *Propellants, Explos., Pyrotech.*, **1991**, *16*, 197–202.
27. Sućeska, M. *Explo5 program*, 6.03 ed., Zagreb, **2015**.
28. Al-Azmi, A.; George, P.; El-Dusouqui, O. M. E. Novel 2*H*-1,2,3-Triazole Sodium Complex from *N*-[2-amino-1,2-dicyanovinyl]alkanamides. *Heterocycles*, **2007**, *71*, 2183–2201.
29. On Earth and Life Studies Division *Acute Exposure Guideline Levels for Selected Airborne Chemicals: Volume 14*, National Academies Press (US), Washington (DC), **2013**.
29. CrysAlisPro; Version 1.171.35.11 (release 16.05.2011 CrysAlis171.net), Agilent Technologies: **2011**.
30. Farrugia, L. J. WinGX Suite for Small-Molecule Single-Crystal Crystallography. *J. Appl. Crystallogr.* **1999**, *32*, 837.
31. Spek, A. L. *Platon, A Multipurpose Crystallographic Tool*: Utrecht University, Utrecht (NL) **1997**.
32. Brandenburg, K.; Diamond, 3.2k ed.; Crystal Impact GbR: Berlin, **2014**.

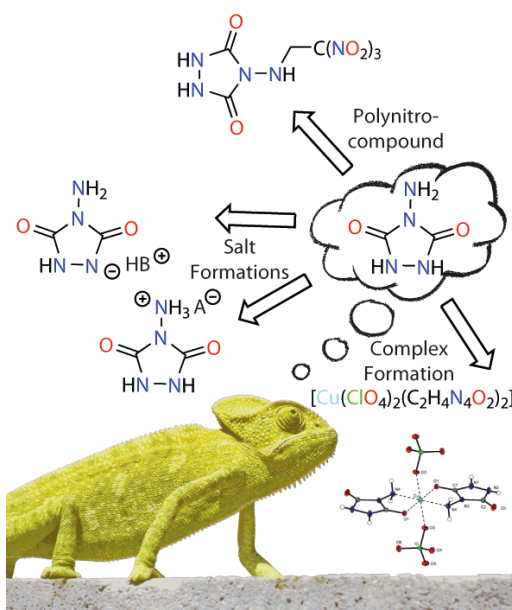
5 Urazine Derivatives

Urazine - a Long Established Heterocycle and Energetic Chameleon

T. M. Klapötke, B. Krumm, C. Riedelsheimer, J. Stierstorfer, C. C. Unger and

M. H. H. Wurzenberger

Eur. J. Org. Chem. **2020**, 4916–4924.



5.1 Abstract

Urazine is an easily accessible heterocycle from low-cost starting materials. In this contribution a colorful palette of reactions is presented: anionic and cationic salt formation, complexation to a transition metal and condensation with trinitroethanol. The structures of the resulting compounds were analyzed using X-ray diffraction studies, furthermore, the materials were thoroughly characterized using NMR spectroscopy, vibrational analysis, as well as elemental analysis. Depending on the field of application further investigations as energetic materials were carried out, including hot plate and hot needle, small-scale shock reactivity test (SSRT), laser initiation tests and the estimation of the performance parameters using EXPLO5 V6.03 and Gaussian 09.

5.2 Introduction

Urazoles (1,2,4-triazolidin-3,5-diones) are five-membered heterocycles with three nitrogen atoms. A wide variety of aliphatic and aromatic substituents at position 4 leads to various properties and applications. The examples shown in Figure 5.1 are mostly used for the production of herbicides, antifungal compounds and polymeric materials.^[1]

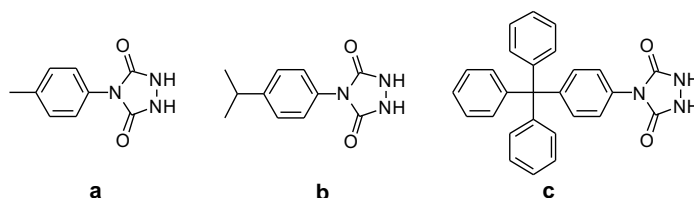


Figure 5.1 Urazole derivatives: (a) 4-p-toluene-, (b) 4-p-cumene-, (c) 4-(p-tritylphenyl)-1,2,4-triazolidin-3,5-dione.^[2]

Urazine (4-amino-1,2,4-triazolidine-3,5-dione or 4-amino-urazole) is based on urazole and is amino substituted at position 4 (Figure 5.2). This molecule is formed by the acid-catalyzed reaction of carbohydrazide.^[3]

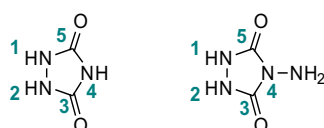


Figure 5.2 Urazole (left) and urazine (right).

Due to the relatively high nitrogen and oxygen content ($N+O = 75.8\%$) on one hand, and low carbon content on the other hand, urazine can be used as a potential building block for energetic

materials. Even though its first synthesis dates back to Curtius and Heidenreich in 1895, this molecule remained mostly unnoticed in the energetic materials community.^[4] This is quite remarkable, because urazole (1,2,4-triazolidin-3,5-dione) and some of its metal salts, were patented as ingredients in gas generating compositions for air-bags in 1995.^[5] Very recently some reports of urazine in energetic MOFs^[6] and theoretical methods to evaluate metal complexes appeared.^[7]

Urazine is a weak monoprotic acid and their sodium and silver salts have been reported.^[3] At lower pH values, the molecule can be incorporated as a neutral ligand in 3d transition metal complexes, in which one of the carbonyl groups and the exocyclic amine group act as coordination sites.^[8] This synthetic concept allows the syntheses of neutral or cationic complexes with the simultaneous integration of oxidizing anions such as perchlorate, chlorate or nitrate, leading to the formation of energetic coordination compounds (ECC). The main advantage of the ECC concept is based on the three different building blocks (metal cation, anion and endothermic ligands), which makes it possible to adjust the properties of the desired product by changing one of the components. In recent years several reports set the stage for future applications of ECC.^[9]

In order to further increase the oxygen content of several compounds, such as the heterocycle urazine, one option would be the incorporation of the 2,2,2-trinitroethyl moiety. This unit is usually synthesized via Mannich condensation of amine, formaldehyde and trinitromethane (nitroform). Many compounds, mainly high energy dense oxidizers (HEDO) with this moiety have been prepared and characterized in the recent past (Figure 5.3). However, the trinitroethyl group is rather sensitive towards bases and strong nucleophiles^[10] and decomposes into their precursors.^[11]

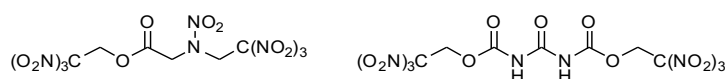


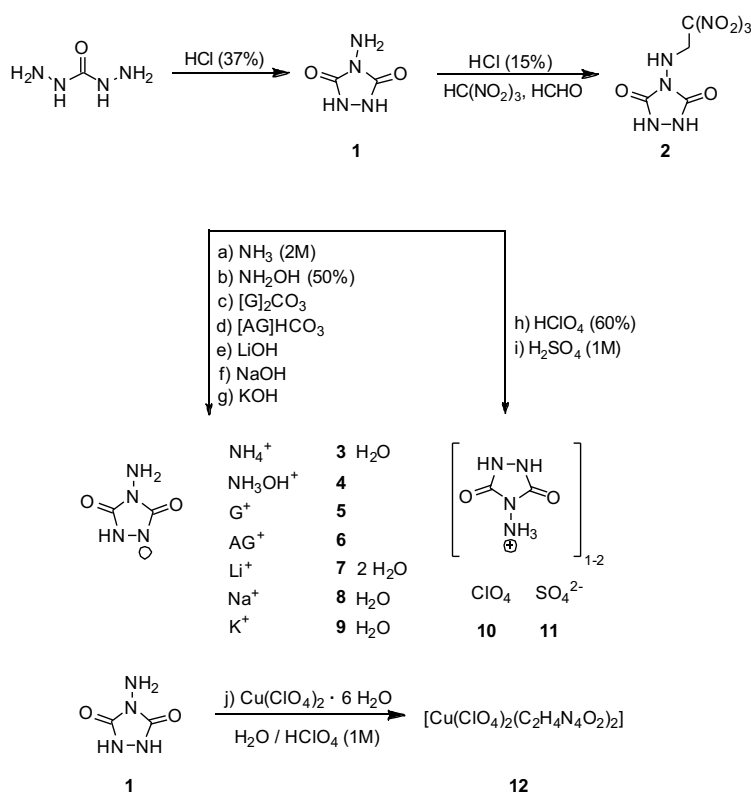
Figure 5.3 Examples for HEDOs with the 2,2,2-trinitroethyl group: 2,2,2-trinitroethyl 2-[nitro-(2,2,2-trinitroethyl)amino] acetate^[12] (left) and bis(2,2,2-trinitroethyl)carbonyl-N,N-dicarbamate (right).^[13]

5.3 Results and Discussion

5.3.1 Synthesis

Starting from carbodihydrazide in concentrated hydrochloric acid, 4-aminourazole (**1**) was prepared as described in the literature in a one-pot synthetic protocol according to Scheme 5.1.^[3] This procedure goes back to 1953 and contained outdated methods, which were adjusted to current techniques by using a round-bottom flask and reflux condenser (instead beaker on a heating plate). Hydrazinium chloride was formed as a by-product, which was dissolved in water,

whereas **1** was separated to obtain a pure colorless solid in 64% yield without further recrystallization from hydrochloric acid.



Scheme 5.1 Synthetic overview towards urazine based materials **1–12**.

The formation of 4-[(2,2,2-trinitroethyl)amino]-urazole (**2**) was achieved by the acid-catalyzed reaction of **1** with an aqueous solution of nitroform (30%) and formaldehyde (37%). Stirring at ambient temperature overnight resulted in **2** as a colorless solid, which could be isolated in 62% yield after filtration.

Due to the ability of urazine to act as a weak monoprotic acid, the salt conversion was performed with different bases, by dissolving **1** in a minimal amount of water and adding the base under constant stirring, which was continued at ambient temperature for 30 min to 1 h to obtain the dissolved salts **3–9**.

The exocyclic amine group on the other hand can act as a base to form salts. Adding sulfuric acid or perchloric acid to a mixture of **1** in a minimal amount of water and heating up the mixture to 50 °C, the perchlorate (**10**) and sulfate (**11**) salts were obtained.

When reacting copper(II) perchlorate hexahydrate with urazine in slightly acidic (1M HClO₄) aqueous media the complex [$\text{Cu}(\text{ClO}_4)_2(\text{C}_2\text{H}_4\text{N}_4\text{O}_2)_2$] (**12**) was obtained.

5.3.2 NMR Spectroscopy

The compounds **1–11** were characterized by ^1H , ^{13}C and additionally by ^{14}N NMR spectroscopy for **2**. The resonances for the cyclic hydrogen atoms (*NH*) at 9.83 ppm (**1**), 9.96 ppm (**10**) and 9.99 ppm (**11**) in the ^1H NMR spectra are not visible for salts **3–9** due to fast proton exchange. Those for the exocyclic amine group of **1** and **3–9** are in the narrow range of 4.03–4.80 ppm, which is shifted towards lower field for ammonium moiety of **10** and **11** ($\delta = 6.62$ –7.08 ppm). An additional singlet for the CH_2 group of **2** is detected at 5.04 ppm in the ^1H NMR spectrum.

In the ^{13}C NMR spectra the resonances for the carbonyl groups are, as expected, in the range of 153.4–161.3 ppm. The carbon resonance of the CH_2 group of the trinitroethyl moiety is located at 53.7 ppm and the broadened resonance for $\text{C}(\text{NO}_2)_3$ at 128.7 ppm. For salts **5** and **6**, the carbon signal of the cation is found at 158.4 ppm for guanidinium (**5**) and 155.4 ppm for aminoguanidinium (**6**). In the ^{14}N NMR spectrum the nitrogen resonance of the trinitromethyl moiety of **2** is found at -29 ppm.

5.3.3 Crystal Structures

Except for salts **5** and **11**, all compounds were investigated by single-crystal X-ray diffraction. Suitable single-crystals of compound **2** were obtained from acetone (Figure 5.4). It crystallizes in the orthorhombic space group *Pbca* with a density of 1.839 g cm^{-3} at 115 K. In the solid state the urazine ring forms an almost planar system with the two carbonyl oxygen atoms and the hydrogen atoms at N1 and N2. For the trinitromethyl unit the typical propeller-type structure is observed.

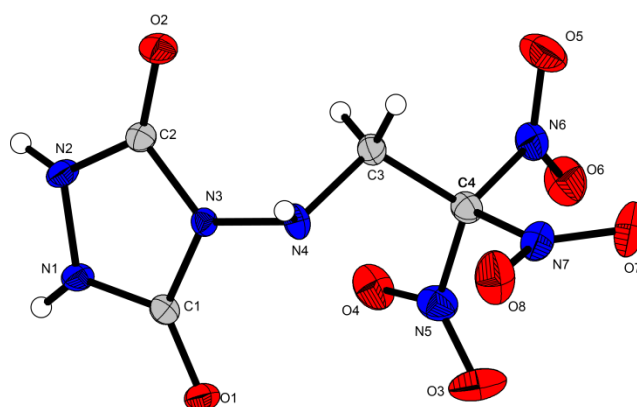


Figure 5.4 Molecular structure of **2** determined by X-ray diffraction. Selected distances [pm] and angles [°]: N1–N2 138.7(2), N1–C1 133.2(2), C1–O1 123.6(2), N3–N4 139.1(2), C3–C4 152.8(3), C4–N6 151.7(3), O6–N6 121.8(2), N2–N1–C1 110.4(2), N1–C1–N3 104.4(2), N1–C1–O1 128.4(2), N1–C1–O1 110.4(2), C1–N1–N2–C2 1.0(2), C1–N3–C2–N2 1.0(2), N4–N3–C2–N2 179.4(2), N2–N1–C1–O1 179.3(2).

Single crystals of ammonium urazinate (**3**) were obtained from water at ambient temperature. The salt crystallizes as a monohydrate as colorless platelets with the triclinic space group *P*–1

including two formula units per unit cell and a density of 1.45 g cm^{-3} at 117 K. The asymmetric unit with selected bond lengths and angles is shown in Figure 5.5.

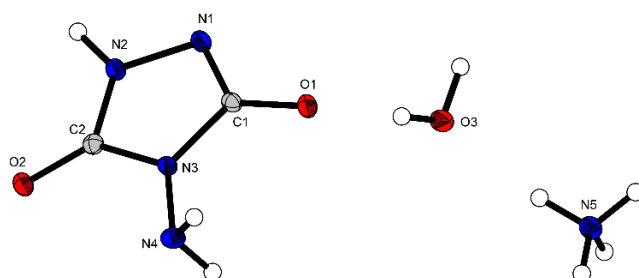


Figure 5.5 Molecular structure of ammonium salt **3** · H₂O determined by X-ray diffraction. Selected distances [pm] and angles [°]: N1–N2 141.1(2), N1–C1 131.5(2), C1–O1 127.5(2), C2–N3 137.8(2), N3–N4 139.5(1), N2–N1–C1 104.8(9), C1–N3–C2 109.3(9), N1–C1–O1 127.7(1), C2–N3–N4 123.7(9), N1–C1–N3–C2 0.2(1), N2–N1–C1–N3 $-1.5(1)$, N2–N1–C1–O1 178.8(1), N1–C1–N3–N4 $-176.4(1)$.

Compared to common C–N (147 pm) and C=N bond (122 pm) lengths the C–N bonds of the five-membered ring are in the range of 132–140 pm, which is in between. The C–O bond length on the other hand is 128 pm, which is longer as a common carbonyl double bond (~ 120 pm).^[14] This is a result from tautomerism between O2–C2–N2–H, respectively O1–C1–N1–H in the case of a proton shift between N2 and N1. The N1–N2 bond length (141 pm) as well as the N3–N4 bond length (140 pm) tend to be shorter than common N–N bond length (~ 145 pm).^[14] The five-membered ring is nearly planar as shown by the torsion angles N1–C1–N3–C2 0.20° and N2–N1–C1–N3 -1.45° .

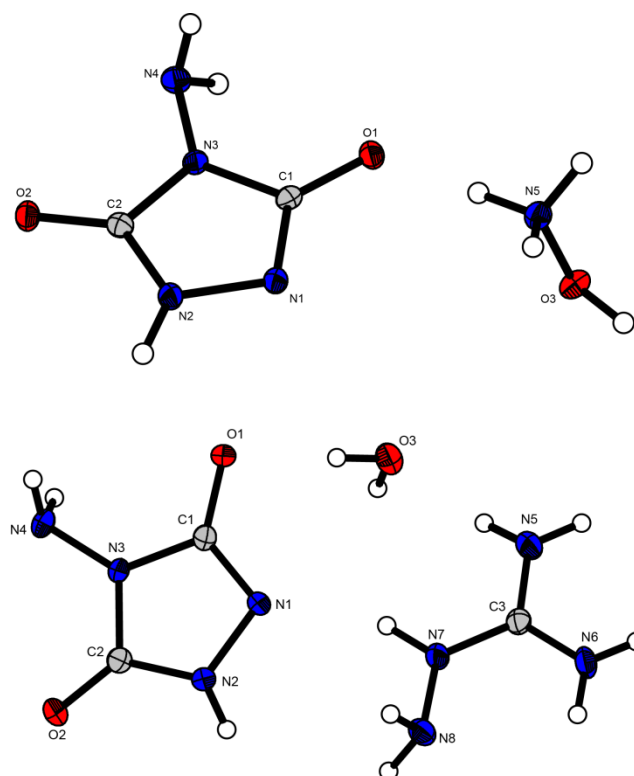


Figure 5.6 Molecular structures of hydroxylammonium salt **4** and aminoguanidinium salt **6**·H₂O determined by X-ray diffraction. Selected distances [pm] and angles [°] of **4**: N1–N2 141.2(2), N1–C1 132.5(2), C1–O1 127.2(2), C2–N3 138.6(2), N3–N4 140.3(2), N2–N1–C1 105.2(1), C1–N3–C2 109.4(1), N1–C1–O1 127.4(1), C2–N3–N4 122.9(1), N1–C1–N3–C2 0.3(2), N2–N1–C1–N3 –0.1(1), N2–N1–C1–O1 179.8(1), N1–C1–N3–N4 –175.9(1). Selected distances [pm] and angles [°] of **6**·H₂O: N1–N2 141.7(2), N1–C1 131.9(2), C1–O1 127.5(2), C2–N3 136.9(2), N3–N4 140.2(2), N2–N1–C1 104.5(1), C1–N3–C2 109.3(1), N1–C1–O1 128.0(2), C2–N3–N4 122.9(1), N1–C1–N3–C2 –1.0(2), N2–N1–C1–N3 –1.2(2), N2–N1–C1–O1 179.0(2), N1–C1–N3–N4 –174.8(2).

Salts **4** and **6**·H₂O both crystallize in the triclinic space group *P*–1 from water, even though the aminoguanidinium salt crystallizes as monohydrate and **4** free from hydrate water (Figure 5.6). For the C–N (132 pm–140 pm) and C–O bond lengths (125 pm–128 pm) the same trends as for salt **3**·H₂O are observed. Relatively strong hydrogen bonds are observed between the cation and the anion of **4** by the hydroxy group of the hydroxylammonium ion as donor and the deprotonated cyclic amine as proton acceptor (O3–H3···N1, *d*(D–H) = 93 pm, *d*(H···A) = 169 pm, \angle (D–H···A) = 168.4°).^[15] Comparable hydrogen bonds of salt **6**·H₂O are more likely to be considered moderately strong (N7–H8···N1, *d*(D–H) = 93 pm, *d*(H···A) = 199 pm, \angle (D–H···A) = 158.3°). In addition to the hydrate water this might also result in the lower density of **6**·H₂O (δ = 1.579 g cm^{–3}) at 110 K compared to the density of **4** (δ = 1.796 g cm^{–3}) at 127 K.

Single crystals of the lithium salt **7** were obtained from water by evaporating the solvent at ambient temperature. The dihydrate crystallizes as colorless prisms in the triclinic space group *P*–1 with two formula units per unit cell as shown in Figure 5.7.

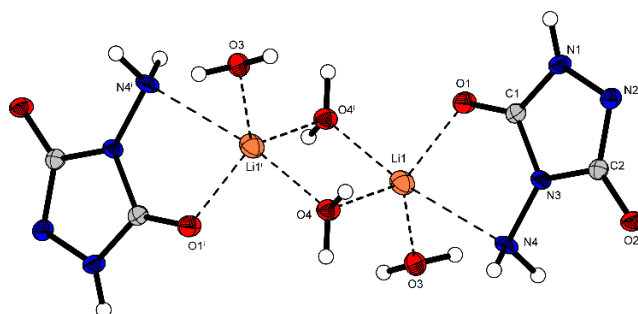


Figure 5.7 Molecular structure of lithium salt $7 \cdot 2 \text{H}_2\text{O}$ determined by X-ray diffraction. Selected distances [pm] and angles [°]: N1–N2 141.7(2), N1–C1 133.5(2), C1–O1 124.2(2), N3–N4 139.9(2), N2–N1–C1 112.0(2), N1–C1–N3 104.6(1), N1–C1–O1 129.1(2), C1–N1–N2–C2 2.9(2), C1–N3–C2–N2 $-0.7(2)$, N4–N3–C2–N2 $-176.2(2)$, N2–N1–C1–O1 178.6(2). Symmetry code: i) $1-x, 1-y, 2-z$.

Figure 5.7 illustrates the planarity of the urazinate anion, as also shown by the torsion angles C1–N1–N2–C2 2.86° and C1–N3–C2–N2 -0.70° . Furthermore, the exocyclic amino group (N4–N3–C2–N2 -176.24°) and the carbonyl functionality (N2–N1–C1–O1 178.62°) do not point out of plane. In addition, the lone pairs of the amino group and carbonyl functionality form a network with the lithium cation, which also includes both molecules of hydrate waters. The distances range from $d(\text{O1} \cdots \text{Li1}) = 194 \text{ pm}$, $d(\text{O4} \cdots \text{Li1}) = 199 \text{ pm}$, $d(\text{O3} \cdots \text{Li1}) = 198 \text{ pm}$ to $d(\text{N4} \cdots \text{Li1}) = 262 \text{ pm}$. The sodium salt crystallizes as colorless blocks in the triclinic space group $P\bar{1}$ from water and a density of 1.934 g cm^{-3} at 123 K. The asymmetric unit contains one hydrate water and is depicted in Figure 5.8. In contrast to $7 \cdot 2 \text{H}_2\text{O}$ the distances between the metal and the atoms carrying a lone pair are longer. Thereby, $d(\text{O3} \cdots \text{Na1})$ is the shortest contact (235 pm).

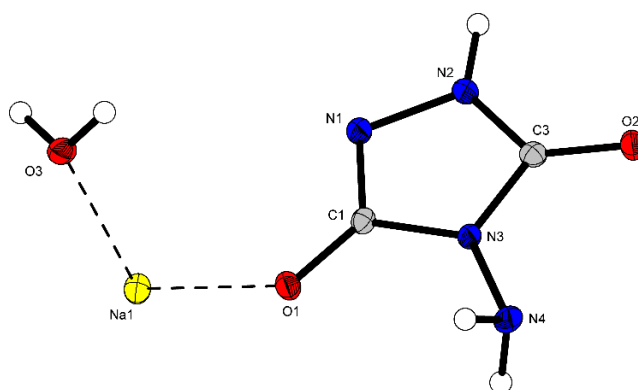


Figure 5.8 Molecular structure of sodium salt $8 \cdot \text{H}_2\text{O}$ determined by X-ray diffraction. Selected distances [pm] and angles [°]: N1–N2 141.0(2), N1–C1 132.7(2), C1–O1 126.7(2), N3–N4 139.8(2), N2–N1–C1 105.3(1), N1–C1–N3 108.3(1), N1–C1–O1 128.7(1), C1–N1–N2–C2 $-0.8(1)$, N2–C2–N3–C1 $-0.4(1)$, N4–N3–C2–N2 $-178.1(1)$, N2–N1–C1–O1 $-179.2(1)$.

The sodium salt $8 \cdot \text{H}_2\text{O}$ forms a layer-like structure which is comparable to the structure of the potassium salt $9 \cdot \text{H}_2\text{O}$ (Figure 5.9). The potassium salt was obtained as colorless blocks from water and contains one hydrate water as well. It also crystallizes in the triclinic space group $P\bar{1}$ and has a density of 2.003 g cm^{-3} at 122 K.

Bond distances and angles are in the same ranges as for salts **3** · H₂O, **4** and the hydrates of **6**–**9**. The layer is oriented along the *b* axis and is stabilized by several inter- and intramolecular hydrogen bridges within. The potassium cations and hydrate waters are acting as linkers, through which two urazine anions are connected with very comparable distances ($d(\text{O}2 \cdots \text{K}1) = 278$, $d(\text{O}3 \cdots \text{K}1) = 278$, $d(\text{O}2' \cdots \text{K}1) = 283$ pm)

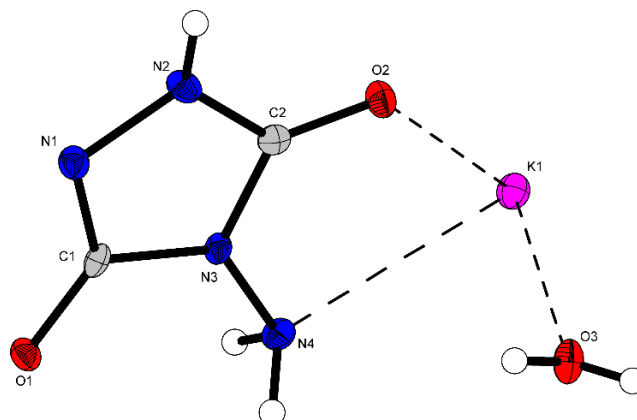


Figure 5.9 Molecular structure of potassium salt **9** · H₂O determined by X-ray diffraction. Selected distances [pm] and angles [°]: N1–N2 142.3(3), N1–C1 131.8(3), C1–O1 127.3(3), N3–N4 140.1(3), N2–N1–C1 104.6(2), N1–C1–N3 109.4(2), N1–C1–O1 127.9(2), C1–N1–N2–C2 2.7(6), C1–N3–C2–N2 –2.8(3), N4–N3–C2–N2 179.9(2), N2–N1–C1–O1 179.6(2).

The perchlorate salt **10** crystallizes in the orthorhombic space group *Pbca* and a density of 2.146 g cm^{–3} at 200 K (Figure 5.10).

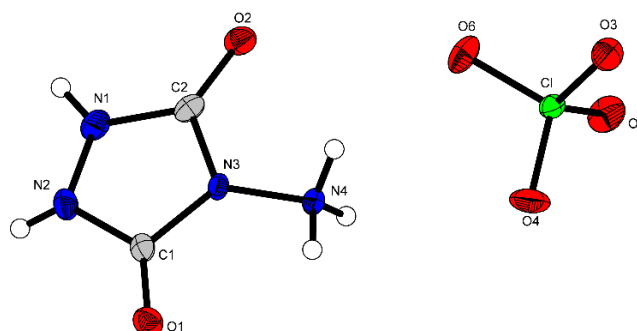


Figure 5.10 Molecular structure of perchlorate salt **10** determined by X-ray diffraction. Selected distances [pm] and angles [°]: N1–N2 138.8(2), N1–C2 133.9(2), C1–O1 122.0(2), C2–N3 138.7(2), N3–N4 140.4(2), N1–N2–C1 109.9(2), C1–N3–C2 112.9(1), N2–C1–O1 130.5(2), C2–N3–N4 123.5(2), C1–N3–C2–N1 –4.2(2), N2–N1–C2–N3 7.0(2), N1–N2–C1–O1 –176.1(2), N4–N3–C2–N1 177.8(4).

This is the only crystal structure where the urazine unit is protonated (at the N4 nitrogen atom), though the bond lengths and angles are just varying slightly. According to the bond lengths, N1–N2 and N3–N4 should be affected most, but the highest difference is between the bond length of salt **9** · H₂O and salt **10** for N1–N2 with 3.5 pm. Angles $\angle(\text{N}1\text{--N}2\text{--C}1) = 109.9^\circ$ and $\angle(\text{N}2\text{--N}1\text{--C}2) = 110.2^\circ$ are more obtuse angled than typical for sp^3 hybridized nitrogen atoms

(107°). Upon deprotonation at N1, which leads to a second lone pair, the angles in the crystal structure of salts **3** · H₂O, **4** and the hydrates of **6–9** become contracted to 104.5–105.3°.

The copper complex **12**, consisting of copper(II) perchlorate and neutral urazine, was obtained as green rods directly from the mother liquor. It crystallizes in the monoclinic space group *P*2₁/*n* with two formula units per unit cell and a calculated density of 2.369 g cm⁻³ at 293 K. The complex monomer is built up of one copper(II) cation octahedrally coordinated by two monodentate perchlorate anions and two chelating urazine ligands (Figure 5.11). The equatorial positions are occupied by the heterocyclic ligands, each binding with the amino and one of the carbonyl groups. A typical Jahn-Teller-distortion along the axial O3–Cu–O3ⁱ axis, built up by the two perchlorato ligands, can be observed. Due to the chelating effect and the distortion, the coordination sphere deviates from a perfect octahedron.

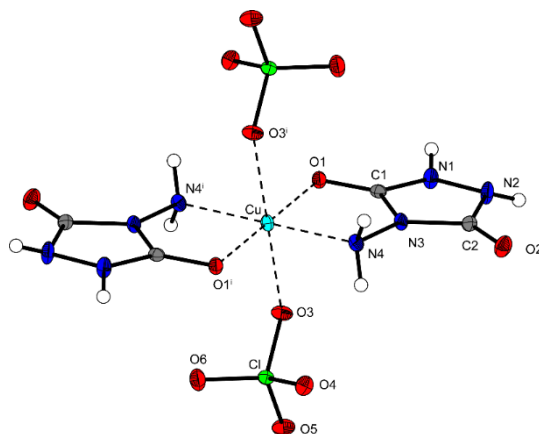


Figure 5.11 Molecular structure of [Cu(ClO₄)₂(C₂H₄N₄O₂)₂] (**12**) determined by X-ray diffraction. Selected distances [pm] and angles [°]: Cu–O1 201.1(1), Cu–O3 230.1(1), Cu–N4 203.9(2), O1–Cu–O3 81.3(5), O1–Cu–O1ⁱ 180.0, O1–Cu–N4 85.6(6), O1–Cu–N4ⁱ 94.4(6), O3–Cu–N4 88.2(5). Symmetry code: i) 1–*x*, –*y*, 1–*z*.

5.3.4 Physical and Energetic Properties

The physical and energetic properties were determined and are listed for all water-free substances in Table 1. DTA measurements revealed a high thermal stability for urazine (**1**), which melts at 278 °C, prior to an exothermic peak. A comparably high stability is observed for the trinitroethyl containing **2**, which decomposes at 152 °C without prior melting. According to DTA and TG measurements, the ammonium (**3**) and hydroxylammonium salt (**4**) show a mass loss indicating that ammonia and hydroxylamine are leaving the salts, whereby urazine itself remains. As shown from the TG measurements, the mass loss of **3** starts at 111 °C and at a temperature of 270 °C 77% of the original mass remains, which perfectly fits to the mass of **3** without water and ammonia. The hydrate water of **3** cannot be removed under ambient pressure, therefore its physical and energetic properties are not discussed in Table 5.1. For the hydroxylammonium salt **4** a beginning mass loss is observed at 130 °C. At the temperature of 168 °C, the molecule lost 22%

of its overall mass, which corresponds well to the loss of the hydroxylamine. Based on the DTA curve, further evidence for the loss of the base from the cation is found as melting and decomposition points of both salts, that are comparable to urazine. The aminoguanidinium salt (**6**) is obtained as hydrate water, which dehydrates at around 65 °C according to TG measurements (for DTA and TG plots see SI). The hydrate water can be removed residue-free under high vacuum; therefore, analytics refer to water-free **6**, and the room temperature density was obtained by a gas pycnometer. As also observed for the guanidinium salt (**5**), the aminoguanidinium salt shows an endothermic peak, which immediately leads to decomposition. As the onset of melting is 177 °C (**5**) and 159 °C (**6**), the thermal stability is in the range of **2**. However, salts **4–6** are underbalanced according to the oxygen content, but are not sensitive at all. In contrast 4-[(2,2,2-trinitroethyl)amino]-urazole (**2**) burns with a smokeless flame and practically residue free, due to an almost balanced amount of oxygen. The alkali salts **7–9** lose water before decomposing in a temperature range of 352–359 °C, this even exceeds the thermal stability of copper complex **12** ($T_{\text{dec}} = 214$ °C). The urazinium salts decompose at temperatures of 181°C (**10**) and 201°C (**11**) according to DTA measurements. Moreover, the perchlorate salt **10** burns with deflagration and is very sensitive. Compound **2** and complex **12** are considered as very sensitive as well. In order to evaluate the utility of new energetic materials, their performance characteristics are usually calculated by computer codes (details see SI). These energetic parameters are listed in Table 1 together with the parameters for the classical secondary explosive RDX (cyclotrimethylenetrinitramine) and common solid rocket propellant AP (ammonium perchlorate).

Table 5.1 Physical and energetic properties of **2** and salts **4**, **5**, **6**, **10**, and complex **12** compared to RDX and AP.

	RDX	2	4	5	6	10	12	AP
Formula	C ₃ H ₆ N ₆ O ₆	C ₄ H ₅ N ₇ O ₈	C ₃ H ₅ N ₅ O ₃	C ₃ H ₉ N ₇ O ₂	C ₃ H ₁₀ N ₈ O ₂	C ₂ H ₅ N ₄ O ₆ Cl	C ₄ H ₈ Cl ₂ CuN ₈ O ₁₂	NH ₄ ClO ₄
T_{dec} [°C] ^[a]	208	152	138	177	159	194	214	240
IS [J] ^[b]	7.5	3	>40	>40	>40	3	<1	20
FS [N] ^[c]	120	288	>360	>360	>360	28	2	360
N [%] ^[d]	37.8	35.1	47.0	56.0	58.9	25.9	22.7	11.9
O [%] ^[e]	43.2	45.9	32.2	18.3	16.8	44.3	38.8	54.5
Ω_{CO} [%] ^[f]	0	8.6	-26.8	-50.2	-50.5	14.8	—	34.0
Ω_{CO_2} [%] ^[g]	-21.6	-14.3	-48.3	-77.7	-75.7	0	—	34.0
ρ [g cm ⁻³] ^[h]	1.79	1.79	1.75	1.56 (pyc.)	1.62 (pyc.)	2.12	2.37	1.95
ΔH_f° [kJ mol ⁻¹] ^[i]	87	-201	-135	-210	-101	10	—	-67
EXPLO5 V6.03								
Q_v [kJ kg ⁻¹] ^[j]	-5807	-4884	-3740	-1710	-2218	-6181	—	-1422
T_{ex} [K] ^[k]	3800	3540	2511	1536	1750	4183	—	1735
V_0 [L kg ⁻¹] ^[l]	793	751	926	899	914	785	—	885
P_{CJ} [kbar] ^[m]	340	303	283	221	248	459	—	158
V_{det} [m s ⁻¹] ^[n]	8852	8454	8779	8177	8583	9799	—	6368
I_{sp} [s] ^[o]	265	245	198	156	168	252	—	155
I_{sp} [s] ^[p] (15% Al)	273	257	242	205	210	262	—	233
I_{sp} [s] ^[q] (15% Al, 14% binder)	242	228	221	198	204	244	—	256

[a] Onset decomposition point T_{dec} from DTA measurement carried out at a heating rate of 5 °C min⁻¹. [b] Impact sensitivity. [c] Friction sensitivity. [d] Nitrogen content. [e] Oxygen content. [f] Oxygen balance assuming the formation of CO and [g] CO₂ [h] RT densities are recalculated from X-ray densities if not otherwise noted. [i] Enthalpy and of formation calculated by the CBS-4M method. [j] Predicted heat of combustion, [k] detonation temperature, [l] volume of gaseous products [m] detonation pressure and [n] detonation velocity using EXPLO5 (Version 6.03). [o] Specific impulse of the neat compound using the EXPLO5 (Version 6.03) program package at 70.0 bar chamber pressure. [p] Specific impulse for compositions with 85% oxidizer/compound and 15% aluminum. [q] Specific impulse for compositions with 71% oxidizer/compound, 15% aluminum, and 14% binder (6% polybutadiene acrylic acid, 6% polybutadiene acrylonitrile, and 2% bisphenol A ether).

The energetic parameters of **2** and **10** are in promising ranges and exceed PETN (pentaerythritol tetranitrate, $V_{\text{Det}} = 8405 \text{ m s}^{-1}$ and $P_{\text{CJ}} = 319 \text{ kbar}$).^[16] The perchlorate salt **10** is even superior to RDX, however, it contains the undesirable perchlorate anion. Moreover, the hydroxylammonium salt **4** exceeds the detonation velocity of RDX as well and shows low sensitivities. Nevertheless, according to the specific impulse only neat **2** and **10** are superior to AP, in mixtures with aluminum and a binder they drop to values for the secondary explosive

RDX. Therefore, the trinitroethyl derivative **2** is an acceptable energetic material but should not be considered for a possible application as HEDO.

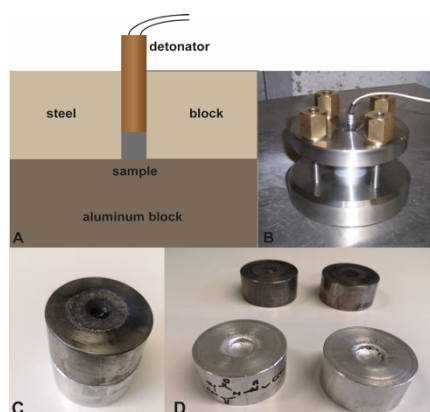


Figure 5.12 Small-scale shock reactivity test of **2**. Schematic drawing (A), photograph of test set-up (B), aluminum and steel block (C), dented aluminum block after initiation with a commercial detonator (D).

A standard test procedure to determine the output of a potential secondary explosive is the small-scale shock reactivity test (SSRT). As illustrated in Figure 5.12; a detonator is assembled in a steel block placed on an aluminum block of specified hardness and thickness. Between both blocks is the energetic material. The depth of the dent produced in the aluminum block after firing the detonator is used as a measure of the strength of the HEDM. It can be compared to common energetic materials such as RDX and hexanitrostilbene (HNS) or 2,6-bis(picrylamino)-3,5-dinitropyridine (PYX).^[17] The results of **2** show promising values (Table 5.2)

Table 5.2 Results of the SSRT of **2** compared to literature values of RDX, HNS and PYX.

	2	RDX	HNS	PYX
m_E [mg] ^[a]	495	504	469	474
m_{SiO_2} [mg] ^[b]	661	589	672	637

[a] Mass of explosive: $m_E = V_s \rho$ 0.95; [b] Mass of SiO₂.

The incorporation of urazine as a neutral ligand in the copper perchlorate **12** is drastically increasing the sensitivities (<1 J and 2 N). To get an insight into the compound's deflagration to detonation transition (DDT) and its energetic performance, hot-plate and hot-needle tests were performed. Complex **12** shows in both tests strong deflagrations (Figures A5.15 and A5.16), which suggests it to a potential primary explosive. A compound's capability to be initiated by a low-energy laser impulse allows its use in alternative, potentially safer initiation devices with very short reaction times. Therefore, a 45 W InGaAs laser diode working in the single-pulsed mode was used to test the laser ignitability of **12**. The irradiation with a pulse length of 1 ms and a current of 7 A resulting in a total energy of 1.7 mJ revealed a very strong detonation (Figure

5.13). Therefore, this copper perchlorate complex **12** could be considered as potential laser-ignitable primary explosive.



Figure 5.13 Moment of detonation during the positive laser initiation test of complex **12**.

5.4 Conclusion

Urazine represents a useful starting material for new energetic materials, such as a trinitroethyl containing derivative as well as several new salts and complexes. The amphoteric character of the heterocycle urazine is just one aspect for the wide variety of salt formations. Nonetheless, the alkaline salts decompose in temperature ranges of 352–359 °C, whereby the ammonia **3** and hydroxylammonium **4** salt lose the base at 162 °C (**3**) and 138 °C (**4**). As a consequence, strong acids and bases are needed to form temperature-stable salts. Most of the new compounds were characterized thoroughly using NMR, XRD, vibrational spectroscopy, as well as elemental analysis, which led to nine new crystal structures. Furthermore, some of the hydrate water-free new compounds were calculated according to their energetic parameters. At least the neutral trinitroethyl substituted derivative **2** ($V_{\text{Det}} = 8455 \text{ m s}^{-1}$) and the hydroxyl ammonium salt **4** ($V_{\text{Det}} = 8779 \text{ m s}^{-1}$), as well as the aminoguanidinium salt **6** ($V_{\text{Det}} = 8583 \text{ m s}^{-1}$) and the perchlorate salt **10** ($V_{\text{Det}} = 9799 \text{ m s}^{-1}$) show values above PETN ($V_{\text{Det}} = 8405 \text{ m s}^{-1}$). In the case of the easily accessible **2** this was also confirmed by a small-scale shock reactivity test. The copper complex **12** was tested according to its potential for a fast DDT; a deflagration was observed from the hot plate and needle test, as well as positive result for the laser ignition experiments.

5.5 Experimental Section

All chemicals were used as supplied. For general information of used devices, X-ray crystallography, DTA, TG and IR plots as well as calculation of the energetic performance data see Appendix A5.

CAUTION! These materials are energetic compounds with sensitivity to various stimuli, especially the trinitroethyl derivative **2**, the perchlorate salt **10** and the copper complex **12** should be treated with great caution. While no serious issues in the synthesis and handling of this

material were encountered, proper measures (face shield, ear protection, body armor, Kevlar® gloves and grounded equipment) as well as a plastic spatula, should be used all the time.

Urazine (1):

Urazine (1) was synthesized based on literature procedures.^[3] Instead of a beaker on heating plate a round-bottom flask in an oil-bath and reflux condenser were used. However, the pure compound was obtained without recrystallization in 64% yield.

¹H NMR (400 MHz, [D₆]DMSO): δ = 9.84 (s, 2H, NH), 4.76 (s, 2H, NH₂), ppm. **¹³C NMR** (101 MHz, [D₆]DMSO): δ = 155.1 (CO) ppm. **EA**: C₂H₄N₄O₂ (116.03): calc. C 20.69, H 3.47, N 48.27 %; found C 20.72, H 3.39, N 48.13 %. **IR** (ATR): $\tilde{\nu}$ = 3222 (s), 3023 (s), 2236 (w), 1674 (vs), 1611 (vs), 1520 (vs), 1468 (w), 1423 (m), 1252 (s), 1108 (m), 1078 (w), 1034 (m), 977 (w), 797 (m), 731 (w), 711 (w), 556 (s), 524 (s), 506 (s), 478 (m), 467 (m), 442 (m), 428 (m), 419 (m) cm⁻¹. **Raman** (1000 mW): $\tilde{\nu}$ = 3275 (13), 3250 (15), 3229 (15), 3191 (10), 3181 (9), 3147 (9), 1725 (36), 1642 (15), 1519 (9), 1267 (11), 1027 (100), 972 (26), 788 (97), 770 (15), 721 (11), 677 (9), 646 (23), 611 (12), 363 (9), 313 (10) cm⁻¹. **DTA** (5 °C min⁻¹) onset: 278 °C (mp.), 283 °C (exothermic).

4-[(2,2,2-Trinitroethyl)amino]-urazole (2):

Urazine (1) (0.56 g, 4.8 mmol) was dissolved in a minimal amount of hydrochloric acid (15%) and nitroform (30%, 2.66 g, 5.29 mmol) and a formaldehyde solution (37%, 0.43 g, 5.3 mmol) were added. The reaction mixture was stirred at ambient temperature overnight and the formed precipitate was filtered, washed with water and dried. 4-[(2,2,2-Trinitroethyl)amino]-urazole (2) (0.83 g) was obtained as a white solid in 62% yield.

¹H NMR (400 MHz, (CD₃)₂CO): δ = 5.04 (s, 2H, CH₂), ppm. **¹³C NMR** (101 MHz, (CD₃)₂CO): δ = 155.0 (CO), 128.7 (C(NO₂)₃), 53.7 (CH₂) ppm. **¹⁴N NMR** [29 MHz (CD₃)₂CO]: δ = -30 (NO₂) ppm. **EA**: C₄H₅N₇O₈ (279.02): calc. C 17.21, H 1.81, N 35.13 %; found C 17.38, H 2.01, N 35.29 %. **IR** (ATR): $\tilde{\nu}$ = 3311 (m), 3087 (m), 3038 (m), 2956 (m), 1695 (vs), 1585 (vs), 1490 (m), 1449 (m), 1382 (m), 1347 (m), 1301 (m), 1237 (m), 1189 (m), 1104 (m), 1078 (w), 1040 (w), 1011 (w), 902 (w), 857 (w), 807 (m), 784 (m), 757 (m), 732 (m), 713 (m), 611 (m), 526 (m), 505 (m), 465 (w), 425 (w), 408 (w) cm⁻¹. **Raman** (1000 mW): $\tilde{\nu}$ = 3011 (13), 2968 (23), 1609 (21), 1597 (20), 1417 (14), 1383 (22), 1348 (37), 1307 (35), 1270 (20), 904 (13), 858 (101), 810 (34), 789 (19), 769 (38), 660 (14), 409 (63), 375 (66), 345 (19), 275 (17), 210 (13) cm⁻¹. **DTA** (5 °C min⁻¹) onset: 152 °C (exothermic). **Sensitivities (BAM)**: impact 3 J; friction 288 N (grain size 500–1000 μ m).

Various amounts of 4-aminourazole (**1**) (1.0–1.5 mmol) were suspended in a minimal amount of water. To this mixture equimolar amounts of base or acid (ammonia [2M], guanidinium carbonate, aminoguanidinium bicarbonate, lithium hydroxide, sodium hydroxide, potassium hydroxide, perchloric acid [60%], and sulfuric acid [1M]) was added carefully. The resulting solution was first stirred for 60 min at ambient temperature (additionally 1 h at 50 °C for aminoguanidine, perchlorate and sulfate). The water was slowly evaporated at ambient pressure and the urazinate, respectively the urazinium salts were obtained in 93% (**3** · H₂O), 97% (**4**), quant. (**5**), quant. (**6** · H₂O), quant. (**7** · 2 H₂O), 78% (**8** · H₂O), 92% (**9** · H₂O), 91% (**10**), 94% (**11**) yield.

Ammonium urazinate hydrate (**3** · H₂O):

¹H NMR (400 MHz, [D₆]DMSO): δ = 4.69 (s, 2H, NH₂) ppm. ¹³C NMR (101 MHz, [D₆]DMSO): δ = 155.0 (CO) ppm. ¹⁴N NMR (29 MHz, [D₆]DMSO): δ = -372 (NH₄) ppm. EA: C₂H₉N₅O₃ (151.13): calc. C 15.90, H 6.00, N 46.34 %; found C 16.56, H 5.34, N 46.38 %. IR (ATR): $\tilde{\nu}$ = 3333 (m), 3091 (s), 3035 (s), 2732 (m), 1668 (vs), 1598 (vs), 1574 (vs), 1488 (m), 1455 (m), 1415 (m), 1340 (m), 1300 (m), 1243 (m), 1189 (m), 1169 (m), 1130 (m), 1101 (m), 1078 (w), 1051 (w), 955 (m), 789 (s), 731 (s), 712 (m), 647 (s), 599 (s), 525 (m), 505 (w), 461 (w), 441 (w) cm⁻¹. Raman (1000 mW): $\tilde{\nu}$ = 3334 (5), 3265 (5), 3102 (4), 3053 (3), 1725 (4), 1620 (11), 1585 (4), 1447 (5), 1303 (20), 1251 (18), 1130 (5), 1076 (5), 964 (13), 805 (53), 792 (100), 633 (37), 409 (11), 329 (19), 265 (4) cm⁻¹. DTA (5 °C min⁻¹) onset: 119 °C (endothermic; -H₂O), 162 °C (endothermic; -NH₃), 273 (endothermic), 283 °C (exothermic). Sensitivities (BAM): impact >40 J; friction >360 N (grain size >1000 μm).

Hydroxylammonium urazinate (**4**):

¹H NMR (400 MHz, [D₆]DMSO): δ = 7.6 (br, 4H, NH₃OH⁺), 4.80 (s, 2H, NH₂) ppm. ¹³C NMR (101 MHz, [D₆]DMSO): δ = 155.0 (CO) ppm. EA: C₂H₇N₅O₃ (149.11): calc. C 16.11, H 4.73, N 46.97 %; found C 16.35, H 4.65, N 47.13 %. IR (ATR): $\tilde{\nu}$ = 3331 (w), 3276 (w), 2991 (m), 2868 (m), 2795 (m), 2724 (m), 1740 (w), 1672 (s), 1623 (s), 1459 (s), 1368 (m), 1241 (m), 1198 (m), 1124 (w), 1098 (w), 955 (m), 807 (m), 791 (s), 749 (s), 666 (s), 632 (s), 600 (s), 447 (w) cm⁻¹. Raman (1000 mW): $\tilde{\nu}$ = 3206 (3), 1725 (4), 1623 (9), 1447 (5), 1316 (6), 1299 (13), 1269 (15), 1240 (4), 1099 (3), 1007 (47), 986 (9), 814 (15), 799 (100), 789 (38), 646 (6), 632 (21), 410 (6), 346 (10), 275 (5), 226 (4) cm⁻¹. DTA (5 °C min⁻¹) onset: 138 °C (endothermic; -NH₂OH), 269 (endothermic), 279 °C (exothermic). Sensitivities (BAM): impact >40 J; friction >360 N (grain size 100–500 μm).

Guanidinium urazinate (5):

¹H NMR (400 MHz, [D₆]DMSO): δ = 7.6 (br, 6H, NH₂), 4.35 (s, 2H, NH₂) ppm. **¹³C NMR** (101 MHz, [D₆]DMSO): δ = 158.4 (C(NH₂)₃) 155.4 (CO) ppm. **EA**: C₃H₉N₇O₂ (175.15): calc. C 20.57, H 5.18, N 55.98 %; found C 20.69, H 4.43, N 55.79 %. **IR** (ATR): $\tilde{\nu}$ = 3382 (m), 3329 (m), 3097 (m), 2843 (m), 2175 (w), 2030 (w), 2005 (w), 1862 (w), 1712 (m), 1658 (vs), 1597 (vs), 1574 (vs), 1447 (m), 1417 (m), 1295 (m), 1261 (m), 1213 (m), 1191 (m), 1135 (m), 1098 (w), 1061 (w), 1018 (m), 980 (m), 790 (m), 731 (m), 715 (m), 653 (m), 609 (s), 552 (s), 529 (m), 505 (m), 467 (m), 425 (w), 406 (w) cm⁻¹. **Raman** (1000 mW): $\tilde{\nu}$ = 3336 (4), 3242 (6), 3227 (7), 3227 (7), 3190 (8), 1656 (5), 1579 (5), 1465 (4), 1432 (5), 1282 (29), 1135 (7), 1008 (100), 805 (37), 791 (55), 672 (6), 637 (21), 559 (16), 532 (8), 389 (10), 320 (8), 239 (3) cm⁻¹. **DTA** (5 °C min⁻¹) onset: 177 °C (endothermic), 194 °C (exothermic). **Sensitivities (BAM)**: impact >40 J; friction >360 N (grain size 500–1000 μ m).

Aminoguanidinium urazinate (6):

¹H NMR (400 MHz, [D₆]DMSO): δ = 7.9 (br, 7H, NH, NH₂), 4.30 (s, 2H, NH₂) ppm. **¹³C NMR** (101 MHz, [D₆]DMSO): δ = 159.2 (C(NH₂)₂(NHNH₂)), 155.4 (CO) ppm. **EA**: C₃H₁₀N₈O₂ (190.17): calc. C 18.95, H 5.30, N 58.96 %; found C 18.84, H 5.14, N 58.96 %. **IR** (ATR): $\tilde{\nu}$ = 3380 (m), 3328 (m), 3250 (m), 3089 (s), 2845 (m), 1713 (m), 1657 (vs), 1601 (vs), 1463 (m), 1323 (m), 1296 (m), 1262 (m), 1213 (m), 1135 (w), 1096 (w), 1065 (w), 1019 (m), 981 (m), 789 (m), 733 (m), 718 (m), 654 (m), 604 (vs), 549 (vs), 531 (vs), 505 (m), 406 (w) cm⁻¹. **Raman** (1000 mW): $\tilde{\nu}$ = 3328 (6), 3307 (11), 3217 (11), 3184 (16), 3175 (14), 3136 (7), 3075 (7), 1639 (10), 1616 (12), 1295 (38), 1140 (9), 1089 (14), 1070 (43), 994 (15), 806 (101), 787 (98), 645 (33), 535 (24), 372 (13), 350 (6), 325 (25), 240 (5) cm⁻¹. **DTA** (5 °C min⁻¹) onset: 159 °C (endothermic), 178 °C (exothermic). **Sensitivities (BAM)**: impact >40 J; friction >360 N (grain size 100–500 μ m).

Lithium urazinate dihydrate (7 · 2 H₂O):

¹H NMR (400 MHz, [D₆]DMSO) δ = 4.48 (s, 2H, NH₂) ppm. **¹³C NMR** (101 MHz, [D₆]DMSO): δ = 155.1 (CO) ppm. **EA**: C₂H₃LiN₄O₂·2H₂O (158.06): calc. C 15.20, H 4.46, N 35.45 %; found C 15.43, H 4.26, N 35.64 %. **IR** (ATR): $\tilde{\nu}$ = 3321 (m), 3093 (m), 2842 (m), 1710 (m), 1605 (s), 1476 (s), 1324 (m), 1293 (m), 1138 (w), 1080 (m), 978 (m), 805 (s), 748 (s), 631 (s), 438 (m), 421 (w) cm⁻¹. **Raman** (1000 mW): $\tilde{\nu}$ = 3322 (10), 3208 (21), 3168 (12), 3156 (10), 3122 (9), 3108 (9), 3050 (7), 3010 (6), 2846 (5), 2836 (4), 1639 (26), 1592 (6), 1527 (4), 1445 (12), 1328 (15), 1296 (63), 1272 (30), 1138 (15), 1086 (7), 981 (19), 812 (100), 796 (87), 738 (6), 681 (14), 632 (330), 577 (4), 540 (3), 514 (3), 448 (9), 407 (14), 339 (37), 274 (3), 245 (4) cm⁻¹.

DTA ($5\text{ }^{\circ}\text{C min}^{-1}$) onset: $94\text{ }^{\circ}\text{C}$ (endothermic; $-2\text{ H}_2\text{O}$), $352\text{ }^{\circ}\text{C}$ (exothermic). **Sensitivities (BAM)**: impact $>40\text{ J}$; friction $>360\text{ N}$ (grain size $500\text{--}1000\text{ }\mu\text{m}$).

Sodium urazinate hydrate ($8 \cdot \text{H}_2\text{O}$):

$^1\text{H NMR}$ (400 MHz, $[\text{D}_6]\text{DMSO}$) $\delta = 4.03$ (s, 2H, NH_2) ppm. **$^{13}\text{C NMR}$** (101 MHz, $[\text{D}_6]\text{DMSO}$): $\delta = 155.1$ (CO) ppm. **EA**: $\text{C}_2\text{H}_3\text{N}_4\text{NaO}_2 \cdot \text{H}_2\text{O}$ (156.03): calc. C 15.39, H 3.23, N 35.90 %; found C 15.38, H 2.94, N 35.63 %. **IR**: $\tilde{\nu} = 3419$ (m), 3315 (m), 3178 (m), 3033 (m), 2847 (m), 1669 (s), 1631 (s), 1609 (s), 1479 (m), 1428 (m), 1336 (m), 1304 (m), 1143 (w), 1077 (m), 983 (m), 801 (s), 753 (m), 725 (m), 675 (m), 633 (s), 492 (s), 407 (m) cm^{-1} . **Raman** (1000 mW): $\tilde{\nu} = 3316$ (4), 3189 (8), 2847 (2), 1623 (13), 1607 (9), 1432 (5), 1339 (8), 1300 (32), 1265 (18), 1141 (4), 1075 (4), 995 (13), 808 (100), 798 (86), 645 (15), 509 (3), 403 (10), 387 (5), 355 (11), 268 (3), 218 (12) cm^{-1} . **DTA**: ($5\text{ }^{\circ}\text{C min}^{-1}$) onset: $154\text{ }^{\circ}\text{C}$ (endothermic; $-\text{H}_2\text{O}$), $358\text{ }^{\circ}\text{C}$ (exothermic). **Sensitivities (BAM)**: impact $>40\text{ J}$; friction $>360\text{ N}$ (grain size $500\text{--}1000\text{ }\mu\text{m}$).

Potassium urazinate hydrate ($9 \cdot \text{H}_2\text{O}$):

$^1\text{H NMR}$ (400 MHz, $[\text{D}_6]\text{DMSO}$) $\delta = 4.72$ (s, 2H, NH_2) ppm. **$^{13}\text{C NMR}$** (101 MHz, $[\text{D}_6]\text{DMSO}$): $\delta = 155.0$ (CO) ppm. **EA**: $\text{C}_2\text{H}_3\text{KN}_4\text{O}_2 \cdot \text{H}_2\text{O}$ (172.00): calc. C 13.95, H 2.93, N 32.54 %; found C 14.36, H 2.94, N 33.64 %. **IR**: $\tilde{\nu} = 3407$ (m), 3332 (m), 3240 (m), 3084 (m), 2843 (m), 2163 (w), 2096 (w), 2022 (w), 1993 (w), 1971 (w), 1700 (s), 1610 (s), 1465 (s), 1320 (m), 1299 (m), 1250 (w), 1133 (w), 1073 (m), 966 (m), 802 (s), 736 (s), 702 (m), 632 (s), 532 (m) cm^{-1} . **Raman** (1000 mW): $\tilde{\nu} = 3333$ (9), 3245 (10), 3169 (4), 3096 (6), 2851 (3), 1694 (5), 1621 (23), 1593 (8), 1434 (8), 1323 (20), 1303 (39), 1247 (33), 1132 (5), 1072 (5), 975 (14), 808 (100), 791 (76), 745 (12), 656 (7), 632 (56), 404 (23), 338 (33), 211 (5) cm^{-1} . **DTA**: ($5\text{ }^{\circ}\text{C min}^{-1}$) onset: $126\text{ }^{\circ}\text{C}$ (endothermic; $-\text{H}_2\text{O}$), 220 (endothermic), $359\text{ }^{\circ}\text{C}$ (exothermic). **Sensitivities (BAM)**: impact $>40\text{ J}$; friction $>360\text{ N}$ (grain size $500\text{--}1000\text{ }\mu\text{m}$).

Urazinium perchlorate (10):

$^1\text{H NMR}$ (400 MHz, $[\text{D}_6]\text{DMSO}$): $\delta = 10.0$ (br, 2H, NH), 7.1 (br, 3H, NH_3) ppm. **$^{13}\text{C NMR}$** (101 MHz, $[\text{D}_6]\text{DMSO}$): $\delta = 154.4$ (CO) ppm. **EA**: $\text{C}_2\text{H}_5\text{ClN}_4\text{O}_6$ (215.99): calc. C 11.09, H 2.33, N 25.87 %; found C 10.75, H 2.35, N 25.10 %. **IR** (ATR): $\tilde{\nu} = 3331$ (m), 3279 (w), 3113 (m), 2991 (m), 2882 (m), 2792 (m), 2731 (m), 1740 (m), 1666 (s), 1627 (s), 1576 (m), 1486 (m), 1463 (m), 1419 (m), 1371 (m), 1270 (w), 1242 (m), 1192 (w), 1124 (m), 1079 (w), 1061 (w), 1016 (w), 953 (m), 787 (s), 740 (s), 660 (s), 596 (s) 532 (m), 506 (m), 473 (m), 425 (w) cm^{-1} . **Raman** (1000 mW): $\tilde{\nu} = 3263$ (2), 1769 (5), 1726 (4), 1573 (6), 1470 (7), 1357 (5), 1279 (17), 1128 (5), 1095 (4), 1023 (3), 936 (101), 793 (56), 638 (30), 627 (14), 473 (19), 458 (14), 371 (6), 301 (4)

cm^{-1} . **DTA** ($5\text{ }^{\circ}\text{C min}^{-1}$) onset: $181\text{ }^{\circ}\text{C}$ (exothermic). **Sensitivities (BAM)**: impact 3 J; friction 28 N (grain size 500–1000 μm).

Bis(urazinium) sulfate (11):

$^1\text{H NMR}$ (400 MHz, $[\text{D}_6]\text{DMSO}$): $\delta = 10.0$ (br, 2H, NH), 6.6 (br, 3H, NH_3) ppm. $^{13}\text{C NMR}$ (101 MHz, $[\text{D}_6]\text{DMSO}$): $\delta = 154.8$ (CO) ppm. **EA**: $\text{C}_4\text{H}_{10}\text{N}_8\text{O}_8\text{S}$ (330.23): calc. C 14.55, H 3.05, N 33.93, S 9.71 %; found C 14.29, H 3.04, N 33.82; S 9.75 %. **IR** (ATR): $\tilde{\nu} = 3336$ (w), 3211 (m), 2865 (m), 2697 (m), 2570 (m), 1769 (m), 1679 (s), 1618 (m), 1548 (s), 1478 (m), 1416 (w), 1336 (m), 1267 (m), 1192 (m), 1137 (s), 1041 (s), 1019 (s), 890 (s), 820 (w), 774 (s), 735 (s), 640 (w), 592 (s), 577 (s), 442 (w), 419 cm^{-1} . **Raman** (800 mW): $\tilde{\nu} = 3332$ (6), 3200 (6), 3112 (6), 1799 (6), 1761 (11), 1730 (15), 1633 (8), 1603 (6), 1588 (6), 1479 (7), 1459 (6), 1418 (5), 1376 (5), 1322 (9), 1277 (13), 1269 (12), 1238 (8), 1156 (6), 1102 (5), 1052 (26), 1026 (6), 971 (6), 901 (15), 789 (100), 722 (9), 675 (7), 647 (22), 612 (10), 434 (11), 422 (10), 392 (8), 314 (10) cm^{-1} . **DTA** ($5\text{ }^{\circ}\text{C min}^{-1}$) onset: $156\text{ }^{\circ}\text{C}$ (endothermic), $201\text{ }^{\circ}\text{C}$ (exothermic).

Copper(II) bis(urazine) perchlorate $[\text{Cu}(\text{ClO}_4)_2(\text{C}_2\text{H}_4\text{N}_4\text{O}_2)_2]$ (12):

Urazine (0.62 g, 5.4 mmol) was dissolved in 10.7 mL of 1M perchloric acid (10.7 mmol) at $80\text{ }^{\circ}\text{C}$ and 5 mL of aqueous copper(II) perchlorate solution (10.7 mmol) was added under stirring. The resulting deep-green solution was left for crystallization at $50\text{ }^{\circ}\text{C}$. After 3 days the copper complex **12** was obtained as green rods in 24% yield (0.31 g).

EA: $\text{C}_4\text{H}_8\text{Cl}_2\text{CuN}_8\text{O}_{12}$ (494.60): calc. C 9.71, H 1.63, N 22.66, Cl 14.33 %; found C 9.45, H 1.45, N 22.68, Cl 14.68 %. **IR** (ATR): $\tilde{\nu} = 3308$ (m), 3252 (m), 3218 (m), 3166 (m), 3075 (m), 1763 (s), 1676 (vs), 1606 (s), 1508 (m), 1425 (w), 1282 (w), 1168 (s), 1103 (s), 1090 (vs), 1007 (vs), 925 (s), 811 (m), 782 (s), 743 (s), 712 (m), 667 (m), 640 (m), 614 (vs), 614 (vs), 575 (s), 488 (s), 474 (s), 461 (m), 426 (m) cm^{-1} . **DTA** ($5\text{ }^{\circ}\text{C min}^{-1}$) onset: $214\text{ }^{\circ}\text{C}$ (exothermic). **Sensitivities (BAM)**: impact <1 J; friction 2 N (grain size 100–500 μm).

Deposition numbers 2000061 (**2**), 1992639 (**3**), 1992643 (**4**), 1992641 (**6**) 1992642 (**7**), 1992644 (**8**), 1992640 (**9**), 1992645 (**10**) and 1993031 (**12**) contain the supplementary crystallographic data for this paper. These data are provided free of charge by the joint Cambridge Crystallographic Data Centre and Fachinformationszentrum Karlsruhe Access Structures service <http://www.ccdc.cam.ac.uk/structures>.

5.6 References

- [1] a) S. Mallakpour, Z. Rafiee, *Synlett*. **2007**, 8, 1255–1256; b) R. Simlot, R. A. Izydore, O. T. Wong, A. H. Hall, *J. Pharm. Sci.* **1994**, 83, 367–371; c) K. De Bruycker, S. Billiet, H. A. Houck, S. Chattopadhyay, J. M. Winne, F. E. Du Prez, *Chem. Rev.* **2016**, 116, 3919–3974.
- [2] A. Ghorbani-Choghamarani, M. Nikoorazm, G. Azadi, *Chin. Chem. Lett.* **2014**, 25, 451–454.
- [3] L. F. Audrieth, E. B. Mohr, E. Davis, W. R. jr. Tomlinson, in *Inorg. Synth.*, McGraw-Hill Book Company, New York City, **1953**, pp. 29–32.
- [4] T. Curtius, K. Heidenreich, *J. Prakt. Chem.* **1895**, 52, 454–489.
- [5] T. Yoshida, Y. Shimizu, K. Hara, S. Chijwa, J. Onishi (Otsuka Kagaku Kabushiki Kaish), US005827996A, **1998**.
- [6] Q. Wang, S. Wang, X. Feng, L. Wu, G. Zhang, M. Zhou, B. Wang, L. Yang, *ACS Appl. Mater. Interfaces* **2017**, 9, 37542–37547.
- [7] G. Yan, Q. Wu, Q. Hu, M. Li, Z. Zhang, W. Zhu, *J. Mol. Model.* **2019**, 25, 340.
- [8] a) F. Bigoli, M. Lanfranchi, M. A. Pellinghelli, *J. Crystallogr. Spectrosc. Res.* **1989**, 19, 357–367; b) D. A. Gianolio, M. Lanfranchi, F. Lusardi, L. Marchio, M. A. Pellinghelli, *Inorg. Chim. Acta* **2000**, 309, 91–102.
- [9] a) Q. Zhang, J. M. Shreeve, *Angew. Chem.* **2014**, 126, 2574–2576; Q. Zhang, J. M. Shreeve, *Angew. Chem. Int. Ed.* **2014**, 53, 2540–2542; b) T. W. Myers, J. A. Bjorgaard, K. E. Brown, D. E. Chavez, S. K. Hanson, R. J. Scharff, S. Tretiak, J. M. Veauthier, *J. Am. Chem. Soc.* **2016**, 138, 4685–4692; c) N. Szimhardt, M. H. H. Wurzenberger, A. Beringer, L. J. Daumann, J. Stierstorfer, *J. Mater. Chem. A* **2017**, 5, 23753–23765.
- [10] W. H. Gilligan, S. L. Stafford, *Synthesis* **1979**, 600–602.
- [11] H. Feuer, T. Kucera, *J. Org. Chem.* **1960**, 25, 2069–2070.
- [12] A. Baumann, A. Erbacher, C. Evangelisti, T. M. Klapötke, B. Krumm, S. F. Rest, M. Reynders, V. Sproll, *Chem. – Eur. J.* **2013**, 19, 15627–15638.
- [13] T. M. Klapötke, B. Krumm, S. F. Rest, M. Suceska, *Z. Anorg. Allg. Chem.* **2014**, 640, 84–92.
- [14] a) A. F. Holleman, E. Wiberg, N. Wiberg, *Lehrbuch der Anorganischen Chemie*, 102nd ed., de Gruyter, Berlin, **2008**, b) F. H. Allen, O. Kennard, D. G. Watson, *J. Chem. Soc., Perkin Trans. 2*, **1987**, S1–S19.
- [15] T. Steiner, *Angew. Chem.* **2002**, 114, 50–80; T. Steiner, *Angew. Chem., Int. Ed.* **2002**, 41, 48–76.

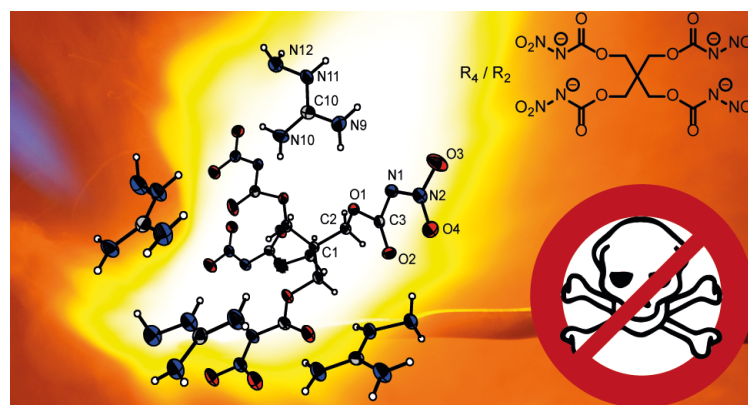
- [16] T. M. Klapötke, *Energetic Materials Encyclopedia*, De Gruyter, Berlin, **2018**.
- [17] a) T. M. Klapötke, T. G. Witkowski, *ChemPlusChem* **2016**, *81*, 357–360; b) T. M. Klapötke, *Chemistry of High-Energy Materials*, 5th ed., De Gruyter, Berlin, **2019**.

6 Salts of Pentaerythritol Tetranitrocarbamate

Energetic Metal and Nitrogen-rich Salts of the PETN Analogue Pentaerythritol Tetranitrocarbamate (PETNC)

T. M. Klapötke, B. Krumm, and C. C. Unger

Inorg. Chem. **2019**, *58*, 2881–2887.



6.1 Abstract

The tetravalent pentaerythritol tetranitrocarbamate (PETNC) is deprotonated by nitrogen-rich, alkaline, alkaline earth metal as well as silver bases to form the corresponding salts. Thorough analysis and characterization by multinuclear NMR, vibrational spectroscopy, elemental analysis, thermoanalytical techniques and single crystal X-ray diffraction was performed. Furthermore, the energies of formation for the nitrogen rich salts were calculated utilizing the GAUSSIAN program package. The detonation performances were calculated with the Explo5 (V6.03) computer code, as well as the sensitivities toward impact and friction were determined, and compared to the neutral PETNC and pentaerythritol tetranitrate (PETN). Ecotoxicological studies of the ammonium and guanidinium salt using *Vibrio fischeri* bacteria complete this study.

6.2 Introduction

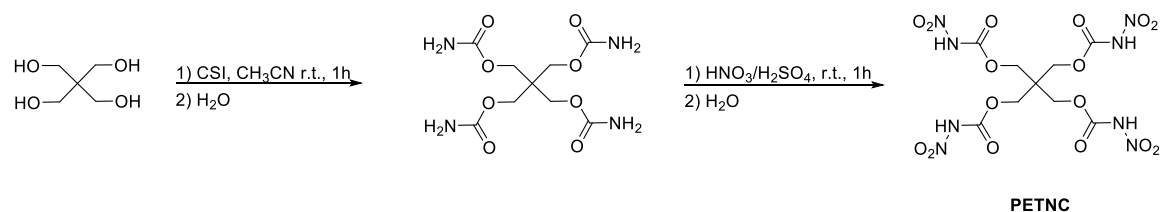
Pentaerythritol is a commercially available tetravalent alcohol with a neopentane backbone. It is a common source for energetic materials, such as pentaerythritol tetranitrate (PETN, Nitropenta),¹ which is used in detonators and, along with RDX, is the main ingredient in SEMTEX.² More recently, silicon-based pentaerythritol derivatives [Si(CH₂N₃)₄ and Si(CH₂ONO₂)₄] were synthesized, but are too sensitive for practical application.³ The less sensitive sila-nitrocarbamate derivative of PETN was also very recently investigated in our group, however its performance data are not favorable.⁴ Nitrocarbamates in general gained more attention in the field of energetic materials chemistry.⁵⁻⁹ Due to their resonance effects, which lead to a reduction in the electrophilicity of the carbonyl group, they are relatively stable towards acid hydrolysis.¹⁰ The high stability allows the nitration of carbamates using rough reaction conditions, like fuming nitric acid and concentrated sulfuric acid. Also, salt formation is possible, taking into account the increase of the acidity of the amino-hydrogen next to the electron withdrawing nitro group. Pentaerythritol tetranitrocarbamate (PETNC) combines the easy availability of pentaerythritol and the valuable properties of nitrocarbamates.¹¹ After our reports on trinitroethyl nitrocarbamates (TNENC),⁷⁻⁸ others were very quick to prepare the first organic salts of TNENC and examined their properties, however with low thermal stability.¹²⁻¹³ Up to now, PETNC and its ammonium salt were investigated, whereby PETNC shows better thermal stability, better sensitivity values and comparable density to PETN. The ammonium salt is even less sensitive than PETNC, however its density is lower. Concerning the energetic parameters, such as the calculated detonation velocity and experimental small-scale reactivity test, PETN is the superior compound. Though, PETNC was investigated with underwater explosion tests and showed

acceptable performance values.¹⁴ In this work new nitrogen-rich salts, as well as selected metal salts of PETNC are presented. These salts allow the determination of the aquatic toxicity of the PETNC anion. Further, some alkali and alkaline earth metal salts may serve as potential flame colorants.

6.3 Results and Discussion

6.3.1 Synthesis

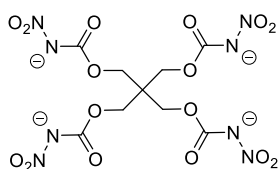
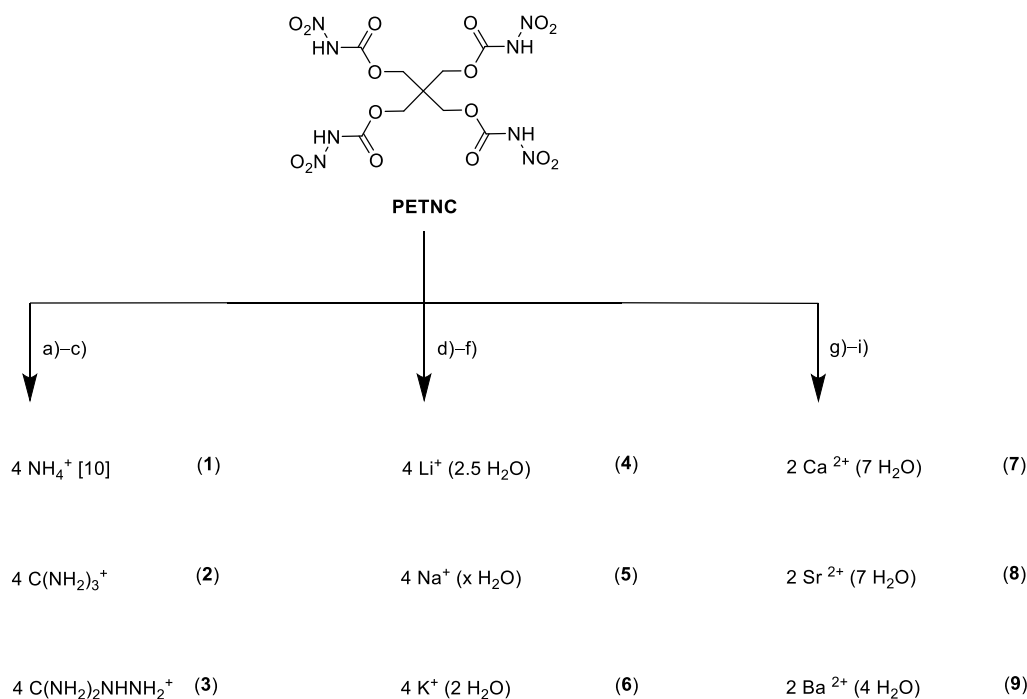
The previously described synthesis of primary carbamates based on two steps, starting from a reaction of the respective alcohol with toxic phosgene to the chloroformate and subsequent treatment with ammonia.¹⁵ A more convenient route is using the reactive chlorosulfonyl isocyanate (CSI) in a one-step synthesis, followed by feasible aqueous work-up.¹⁶ CSI was discovered in Germany in 1956, nowadays it is a commercially available reagent giving easier access to the corresponding carbamate.¹⁷⁻¹⁸ Using CSI, pentaerythritol tetracarbamate was synthesized in high yield and purity, and subsequently nitrated to pentaerythritol tetranitrocarbamate (PETNC) with mixed acid as outlined in Scheme 6.1.



Scheme 6.1 Synthesis of pentaerythritol tetranitrocarbamate (PETNC) starting from pentaerythritol.

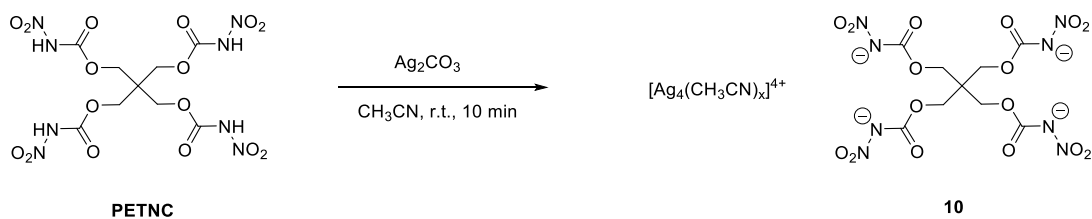
PETNC has four acidic nitramine hydrogen atoms, which can easily be deprotonated. Analogously to the tetraammonium salt,¹¹ nitrogen-rich, alkaline and alkaline earth metal and silver salts were obtained by the reaction of the free bases with PETNC in aqueous solution (Scheme 6.2). However, attempts to prepare hydrazinium or hydroxylammonium salts failed.

Salts of Pentaerythritol Tetranitrocarbamate



Scheme 6.2 Synthesis of various salts of PETNC. Bases used: a) ammonia, b) guanidinium carbonate, c) aminoguanidinium bicarbonate, hydroxides of d) lithium, e) sodium, f) potassium, g) calcium, h) strontium and i) barium.

The salt formation proceeds conveniently in aqueous solution at ambient temperature (except the guanidinium salt **2** had to be heated to reflux) and colorless solids are obtained in 63% up to quantitative yields. The metal salts form hydrates; their water content was calculated from the elemental analysis values, except for the sodium salt **5** (extremely hygroscopic and viscous). In addition, the water content was confirmed in most cases using thermal gravimetric analysis (TGA, Figure 6.2). Due to the general low solubility of silver salts in water, the silver salt **10** was synthesized with acetonitrile as solvent. Ag⁺ is known to form a stable diacetonitrile cationic complex [Ag(CH₃CN)₂]⁺. However, it was not possible to determine the exact solvate content, therefore denoted accordingly as shown in Scheme 6.3.¹⁹⁻²⁰



Scheme 6.3 Synthesis of the silver salt of PETNC (**10**)

6.3.2 NMR and Vibrational Spectroscopy

In the NMR spectra some trends are observed. In the ^1H NMR spectra the resonances of the CH_2 groups of the tetranitrocarbamates are found at 3.81–3.91 ppm and therefore shifted upfield compared to PETNC ($\delta = 4.15$ ppm) due to deprotonation.¹¹ This is consistent with the CH_2 -signal of the ammonium salt which is shifted to 3.88 ppm. Comparable tendencies are observed in the ^{13}C NMR spectra. The resonance of the carbonyl carbon atom in neutral PETNC is located at 148.9 ppm and the resonances for the salts are found at lower field between 158.8–160.5 ppm. The ^{13}C NMR resonances of the neopentane skeleton remain unaffected upon deprotonation of PETNC. The resonances of the cations guanidinium and aminoguanidinium are detected at 158.0 ppm (**2**) and 158.9 ppm (**3**). In the ^{14}N NMR spectra the resonances for the nitro groups of salts **2–8** can be detected as broadened signals between -2 and -13 ppm. The resonances for the nitrile solvate of **10** are found at $\delta = 2.07$ ppm in the ^1H NMR, at $\delta = 118.1$ ppm in the $^{13}\text{C}\{^1\text{H}\}$ NMR and at -134.9 ppm in the ^{14}N NMR spectra. The resonance of the silver-acetonitrile cation was detected at 255 ppm in the ^{109}Ag NMR spectrum with DMSO- D_6 as solvent. A comparison with a previous ^{109}Ag NMR study of solvate-free silver nitroformate solutions in various solvents revealed, that the shift of 255 ppm is in between those of 181 (DMSO) and 430 (acetonitrile) of $\text{Ag}[\text{C}(\text{NO}_2)_3]$.²¹ This deviation can be explained by solvate exchange between Ag^+ -acetonitrile and the DMSO solvent.

In the vibrational spectra (IR and Raman, Appendix A6), the characteristic strong carbonyl stretching vibrations are located in the range $\tilde{\nu} = 1688\text{--}1651\text{ cm}^{-1}$, which are in range of the NH_4^+ salt.¹¹ For the metal salts no N-H vibrations can be found in Raman spectra in the range $\tilde{\nu} = 3450\text{--}3200\text{ cm}^{-1}$, due to deprotonation. Because of the predominant hydrate water which overlaps this particular region, no statement can be made throughout the IR spectra. The N-H stretching vibrations for hydrate-free guanidinium salt **2** and aminoguanidinium salt **3** are located at $\tilde{\nu} = 3415\text{--}3208\text{ cm}^{-1}$.

6.3.3 Single-Crystal Structure Analysis

Single crystals suitable for X-ray diffraction measurements were obtained for the aminoguanidinium salt **3** by recrystallization from water. The molecular structure of **3** is shown in

Figure 6.1, which crystallizes as a colorless block in the triclinic space group $P\bar{1}$ with two molecules per unit cell and a density of 1.65 g cm^{-3} at 123 K.

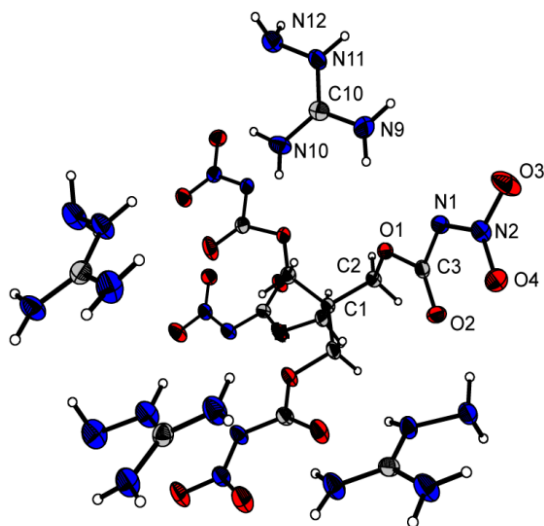


Figure 6.1 Crystal structure of tetrakis-aminoguanidinium pentaerythritol tetranitrocarbamate **3**. Selected distances [\AA] and angles [$^\circ$]: C3–N1 1.370(2), C3–O1 1.215(2), C3–O2 1.366(2), C2–C1 1.536(2), C2–O1 1.438(2), C2–H7 0.98(2), C2–H8 0.96(2), N1–N2 1.344(2), N2–O3 1.243(2), N2–O4 1.238(2), N2–C3–O2 132.1(1), N2–C3–O1 105.0(1), O2–C3–O1 122.8(1), C1–C2–O1 113.5(1), N1–N2–O3 114.1(1), N1–N2–O4 124.9(1), O3–N2–O4 120.9(1), C3–N1–N2 117.4(1), C3–O1–C2 118.1(1).

The structure of **3** is similar to the ammonium salt.¹¹ The nitro groups are rotated out of plane of the nitrocarbamates moiety, as demonstrated by the torsion angle O3–N2–O1–C3 (-12.5°). For the nitramine moiety the N1–N2 bond length is 1.344 \AA , which is shorter than the neutral compound (1.379 \AA) and more comparable to the N1–N2 bond length of the NH_4^+ salt (1.332 \AA).¹¹ For PETNC this indicates a substantial double-bond character, achieved by delocalization of the nitrogen lone pair of N1, which is more substantial for the salts.

6.3.4 Physical and Energetic Properties

The physical and energetic properties of the salts **2–9** were determined and are summarized in Table 6.1 and Table 6.2. PETNC and **1** were recalculated using Version 6.03 of Explo5.²² Concerning the energetic properties of the non-metal salts **1–3**, the aminoguanidinium salt **3** is in the range of TNT in terms of detonation velocity ($V_{\text{det}} = 6950 \text{ m s}^{-1}$).² Nevertheless, PETN and PETNC are still superior in terms of these properties

Table 6.1 Physical and energetic properties of salts **1–3** compared to PETNC and PETN.

	1^{II}	2	3	PETNC	PETN
Formula	C ₉ H ₂₄ N ₁₂ O ₁₆	C ₁₃ H ₃₂ N ₂₀ O ₁₆	C ₁₃ H ₃₆ N ₂₄ O ₁₆	C ₉ H ₁₂ N ₈ O ₁₆	C ₅ H ₈ N ₄ O ₁₂
M [g mol ⁻¹]	556.36	724.52	784.58	488.24	316.14
T_{dec} [°C] ^[a]	136	180	149	196	165
IS [J] ^[b]	>40	>40	>40	8	3
FS [N] ^[c]	>360	>360	>360	360	60
ESD [J] ^[d]	>1.0	>1.5	>1.5	0.75	0.50
ρ [g cm ⁻³] ^[e]	1.64	1.49 (pyc.)	1.62	1.76	1.78
N [%] ^[f]	30.2	38.7	42.9	23.0	17.7
O [%] ^[g]	46.1	34.6	54.5	3.3	60.7
Ω_{CO} [%] ^[h]	-14.4	-28.7	-30.6	3.3	15.2
Ω_{CO_2} [%] ^[i]	-40.3	-57.4	-57.1	-26.2	-10.1
ΔH_f° [kJ mol ⁻¹] ^[j]	-2378	-2306	-1882	-1311	-561
EXPLO5 V6.03					
$-\Delta_{\text{Ex}}U^\circ$ [kJ kg ⁻¹] ^[k]	1996	1735	2219	3826	5980
P_{CJ} [kbar] ^[k]	174	134	181	242	319
V_{det} [m s ⁻¹] ^[k]	7028	6336	7307	7686	8405
V_o [L kg ⁻¹] ^[k]	856	866	890	718	743

[a] Onset decomposition point T_{dec} from DSC measurement carried out at a heating rate of 5 °C min⁻¹. [b] Impact sensitivity. [c] Friction sensitivity. [d] Sensitivity towards electrostatic discharge. [e] RT densities are recalculated from X-ray densities or measured by gas pycnometer (pyc.). [f] Nitrogen content. [g] Oxygen content. [h] Oxygen balance assuming the formation of CO and [i] CO₂. [j] Enthalpy and of formation calculated by the CBS-4M method using Gaussian 09.²³ [k] Predicted heat of combustion, detonation pressure, detonation velocity, and volume of gaseous products calculated by using the EXPLO5 (Version 6.03) program package.²²

With decomposition temperatures of 136 °C (**1**), 180 °C (**2**), 149 °C (**3**), 186 °C (**4**), 156 °C (**5**), 177 °C (**6**) 161 °C (**7**), 152 °C (**8**), and 176 °C (**9**), the salts **2**, **4**, **6**, **7** and **9** show an appropriate thermal stability. The thermally most stable salt was the lithium salt **4** with a decomposition temperature of 186 °C. The neutral PETNC is still the thermally most stable compound. The sensitivities toward impact and friction were determined with a BAM Drophammer²⁴ and a BAM Friction Tester.²⁵ The salts were then classified according the UN recommendations on the transport of dangerous goods,²⁶ therefore **1–3** are considered as insensitive and **7–9** as less sensitive. Only the lithium (**4**) and potassium (**6**) salts show impact sensitivities in the range of sensitive compounds (20 and 7 J)

Table 6.2 Physical properties of salts 4–9.

	4	5	6	7	8	9
Formula	$\text{Li}_4\text{C}_9\text{H}_8\text{N}_8\text{O}_{16} \cdot 2.5 \text{H}_2\text{O}$	$\text{Na}_4\text{C}_9\text{H}_8\text{N}_8\text{O}_{16} \cdot x \text{H}_2\text{O}$	$\text{K}_4\text{C}_9\text{H}_8\text{N}_8\text{O}_{16} \cdot 2 \text{H}_2\text{O}$	$\text{Ca}_2\text{C}_9\text{H}_8\text{N}_8\text{O}_{16} \cdot 7 \text{H}_2\text{O}$	$\text{Sr}_2\text{C}_9\text{H}_8\text{N}_8\text{O}_{16} \cdot 7 \text{H}_2\text{O}$	$\text{Ba}_2\text{C}_9\text{H}_8\text{N}_8\text{O}_{16} \cdot 4 \text{H}_2\text{O}$
M [g mol^{-1}] ^[a]	557.0	—*	676.6	690.5	785.6	830.9
T_{dec} [$^{\circ}\text{C}$] ^[b]	186	156	177	161	152	176
IS [J] ^[c]	20	—*	7	40	40	35
FS [N] ^[d]	360	—*	360	360	360	360

[a] Onset decomposition point T_{dec} from DSC measurement carried out at a heating rate of $5^{\circ}\text{C min}^{-1}$. [b] Impact sensitivity. [c] Friction sensitivity. [d] Sensitivity towards electrostatic discharge. [*] The values of the sodium salt **5** were not determined, because of its high hygroscopicity.

When comparing the room temperature densities of the synthesized salts, **1** ($\rho = 1.62 \text{ g cm}^{-3}$) and **3** ($\rho = 1.64 \text{ g cm}^{-3}$) show acceptable values, however only the density of PETNC ($\rho = 1.76 \text{ g cm}^{-3}$) is in the range of PETN ($\rho = 1.78 \text{ g cm}^{-3}$).¹¹

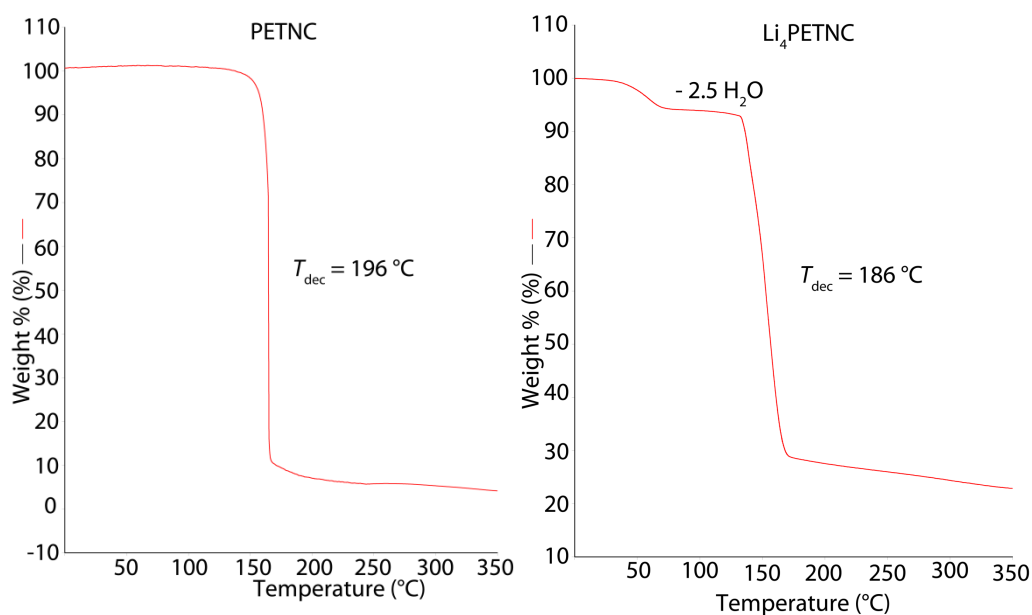


Figure 6.2 TGA measurements of PETNC (left) and the tetralithium salt **4** (right) at a heating rate of $5^{\circ}\text{C min}^{-1}$

TGA measurements of salts **4–9** at a heating rate of $5^{\circ}\text{C min}^{-1}$ revealed a starting weight loss in a temperature range of $103\text{--}108^{\circ}\text{C}$, which was not observed in the TGA measurement of PETNC (Figure 6.2). This leaving hydrate water is consistent with the hydrate water calculated from elemental analysis.

Additionally, the flame colors of the alkaline and alkaline earth salts were tested with a small-scale set-up in a Bunsen burner flame, as these salts are known to show visible flame colors and could be useful in terms of pyrotechnical applications. Thereby, the PETNC salts **4–8** combusted

with a visible flame color as expected (see Appendix A6), except the low soluble barium salt **9**. Further efforts are conducted to establish the potential use in pyrotechnical formulations.

6.3.5 Toxicity Assessment

In order to determine the ecotoxicological impact of water-insoluble PETNC, the EC_{50} (effective concentration) values of the ammonium **1** and guanidinium **2** salts were measured. EC_{50} refers to the concentration of a toxicant which induces a response of 50% after a specific exposure time. The herein used method based on bioluminescent *Vibrio fischeri* NRRL-B-11177 marine bacteria strains, whose luminescent is inhibited when exposed to a toxicant. Therefore, the EC_{50} is defined as the concentration level where the bioluminescence is halfway decreased. All measurements started with the determination of the bioluminescence of untreated reactivated bacteria. After exposure time of 15 and 30 minutes the bioluminescence was determined. The resulting effective concentration leads to a classification of the compounds as non-toxic ($> 1.00 \text{ g L}^{-1}$), toxic ($0.10\text{--}1.00 \text{ g L}^{-1}$) and very toxic ($< 0.10 \text{ g L}^{-1}$).²⁷ Our own previous results on RDX,²⁸ proved that the half maximum effective concentrations of RDX [EC_{50} (30 min) = 0.24 g L^{-1}] is in the range of toxic compounds [lit.: EC_{50} (30 min) = 0.27 g L^{-1}].²⁹ The ammonium salt **1** did not lead to an inhibition of the bioluminescence up to 10% after 15 and 30 minutes using a solution with $c = 2.02 \text{ g L}^{-1}$. The guanidinium salt **2** was measured in higher concentrations and revealed an EC_{50} value of 2.86 g L^{-1} at 15 minutes and of 1.42 g L^{-1} at 30 minutes. Therefore, the PETNC anion can be considered as nontoxic according to *Vibrio fischeri*.

6.4 Conclusions

New nitrogen-rich, alkaline, alkaline earth metal and silver salts of PETNC were synthesized and thoroughly characterized by various analytical methods. The thermal stability of the guanidinium salt **2** is in a promising range ($180 \text{ }^\circ\text{C}$) and the detonation velocity of the aminoguanidinium salt **3** is almost in the range of PETNC. All salts are of remarkably low sensitivity against impact, friction and electrostatic discharge. The burning behavior of the metal salts **4–8** show a combustion with a visible flame color, as to be expected for alkali and alkaline earth metal salts. Nevertheless, more efforts are necessary to find a practical application for salts **4–8** in pyrotechnic formulations based on their visible flame color. The tested ammonium and guanidinium salt are considered nontoxic according to *Vibrio fischeri*. Further tests should show if PETNC could have a potential application as non-toxic and stable safe-handling PETN alternative.

6.5 Experimental Section

6.5.1 General

Solvents, deuterated solvents of NMR experiments and all further chemicals were used as received from the suppliers, without further purification. NMR spectra were recorded with a Bruker 400 or Bruker 400 TR at ambient temperature. The chemical shifts were determined with respect to external standards, Me₄Si (¹H 399.8 MHz; ¹³C 100.5 MHz), MeNO₂ (¹⁴N 28.9 MHz) and AgNO₃ (¹⁰⁹Ag 18.6 MHz).

Infrared spectra were measured with a PerkinElmer Spectrum BX-FTIR spectrometer equipped with a Smiths DuraSamplIR ATR device. Raman spectra were recorded in a glass tube with a Bruker MultiRAM FT-Raman spectrometer with ND:YAG laser with excitation up to 1000 mW at 1064 nm in the range 4000–400 cm⁻¹. All spectra were recorded at ambient temperature.

Analyses of C/H/N contents were performed with an Elementar vario EL or Elementar vario micro cube. Melting and decomposition points were measured with a Linseis DSC-PT10 apparatus with a heating rate of 5 °C min⁻¹ in a temperature range 25–400 °C and partly by thermal gravimetric analysis (TGA) with a PerkinElmer TGA4000.

The sensitivities towards impact and friction were determined with a BAM drophammer²⁴ and a BAM friction tester.²⁵ The sensitivity towards electrostatic discharge was determined with an electric spark tester from OZM.

The toxicity assessments were carried out as described by the provider using a LUMI-Stox 300 spectrometer, obtained by HACH LANGE GmbH. According to DIN/EN/ISO 11348, a ten-point dilution series was prepared (without G1 level) with a known weight of the salts and a 2% NaCl stock solution.²⁹

Single crystal X-ray diffraction studies were performed on an Oxford Diffraction Xcalibur3 diffractometer with a generator (voltage 50kV, current 40 mA) and a KappaCCD area detector operating with Mo-*K*_α radiation ($\lambda = 0.7107 \text{ \AA}$). The solution of the structure was performed by direct methods using SIR97³⁰⁻³¹ and refined by full-matrix least-squares on F^2 (SHELXL)³²⁻³³ implemented in the WINGX software package³⁴ and finally checked with the PLATON software.³⁵ All non-hydrogen atoms were refined anisotropically. The hydrogen atom positions were located on a difference Fourier map. DIAMOND plots are shown with thermal ellipsoids at the 50% probability level.

The theoretical calculations were carried out by using the program package GAUSSIAN 09²³ and were visualized by GAUSSVIEW 5.08.³⁶ Structural optimizations and frequency analyzed were performed at the B3LYP level of theory (Becke's BE three parameter hybrid functional using the LYP correlation functional). For C, H, N, and O, a correlation-consistent polarized double-zeta

basis set cc-pVDZ was used. The enthalpies (H) and free energies (G) were calculated on the CBS-4M level of theory (complete basis set). CBS-4M starts with a HF/3-21G(d) geometry optimization, an initial guess for the following SCF calculation as base energy. This finishes with a final MP2/6-31+G calculation with a CBS extrapolation to correct the energy in second order. For an approximation of higher order contributions, implementations of MP4(SDQ)/6-31+(d,p) and additional empirical corrections are required. The enthalpies of the gas-phase species were estimated according to the atomization energy method.³⁷ The gas-phase enthalpies of formation were converted into the solid-state values using the lattice energy equation provided by Jenkins.³⁸⁻⁴¹ All calculations affecting the detonation parameters were based on condensed phase enthalpies of formation and carried out by using the program package EXPLO5 V6.03.²²

6.5.2 Synthesis

Caution! Pentaerythritol tetranitrocarbamate (PETNC) and potentially the metal salts are considered as sensitive materials and therefore should be handled with caution during synthesis or manipulation, and additional protective equipment (leather jacket, face shield, ear protection, Kevlar gloves) is strongly recommended.

General Procedure for the Salt Preparation (2–9)

Various amounts of PETNC (0.5–1 mmol) in 5–10 mL water are stirred and to this suspension equimolar amounts of the base (guanidinium carbonate; aminoguanidinium bicarbonate; hydroxides of lithium, sodium, potassium, calcium, strontium and barium) was added at ambient temperature. The resulting mixture is further stirred for 1–2 hours (additionally 1 hour at 100 °C for guanidinium carbonate) or 12 hours (Ca, Sr, Ba). In the case of Ca/Sr/Ba the precipitate is filtered and dried. In all other cases, the water is removed in vacuo and the PETNC salts isolated (**2** 83%, **3** 100%, **4** 65%, **5** 100%, **6** 93%, **7** 82%, **8** 63%, **9** 79%).

Tetrakis(guanidinium) PETNC (**2**)

¹H NMR ([D₆]DMSO): δ = 7.08 (s, 24H, NH₂), 3.84 (s, 8H, CH₂) ppm. ¹³C NMR ([D₆]DMSO): δ = 159.4 (CO), 158.0 (C(NH₂)₂), 63.5 (CH₂), 41.3 (C) ppm. ¹⁴N NMR ([D₆]DMSO): δ = -7 (NO₂) ppm. EA: C₁₃H₃₂N₂₀O₁₆ (724.52): calc. C 21.55, H 4.45, N 38.66 %; found C 21.56, H 4.35, N 38.57 %. IS: 40 J (grain size <100 μ m). FS: 360 N (grain size <100 μ m). ESD: 1.50 J (grain size <100 μ m). DSC (5 °C min⁻¹): 180 °C (dec.).

Tetrakis(aminoguanidinium) PETNC (**3**)

¹H NMR ([D₆]DMSO): δ = 8.60 (br, 4H, NHNH₂), 7.14 (br, 16H, C(NH₂)₂), 4.68 (s, 8H, NHNH₂), 3.84 (s, 8H, CH₂) ppm. ¹³C NMR ([D₆]DMSO): δ = 159.7 (CO), 158.9 (C(NH₂)₂), 63.1 (CH₂), 41.7 (C) ppm. ¹⁴N NMR ([D₆]DMSO): δ = -2 (NO₂) ppm. EA: C₁₃H₃₆N₂₄O₁₆ (784.58):

calc. C 19.90, H 4.62, N 42.85 %; found C 20.03, H 4.51, N 42.61 %. **IS:** 40 J (grain size <100 μm). **FS:** 360 N (grain size <100 μm). **ESD:** 1.50 J (grain size <100 μm). **DSC** (5 $^{\circ}\text{C min}^{-1}$): 149 $^{\circ}\text{C}$ (dec.).

Tetralithium PETNC · 2.5 hydrate (4)

$^1\text{H NMR}$ ($[\text{D}_6]$ DMSO): $\delta = 3.81$ (s, 8H, CH_2) ppm. **$^{13}\text{C NMR}$** ($[\text{D}_6]$ DMSO): $\delta = 159.8$ (CO), 62.0 (CH_2), 42.0 (C) ppm. **$^{14}\text{N NMR}$** ($[\text{D}_6]$ DMSO): $\delta = -7$ (NO_2) ppm. **EA:** $\text{Li}_4\text{C}_9\text{H}_8\text{N}_8\text{O}_{16} \cdot 2.5 \text{H}_2\text{O}$ (557.0): calc. C 19.41, H 2.35, N 20.12 %; found C 19.56, H 2.39, N 19.98 %. **IS:** >20 J (grain size <100 μm). **FS:** 360 N (grain size <100 μm). **ESD:** 1.50 J (grain size <100 μm). **DSC** (5 $^{\circ}\text{C min}^{-1}$): 186 $^{\circ}\text{C}$ (dec.).

Tetrasodium PETNC · x hydrate (5)

$^1\text{H NMR}$ ($[\text{D}_6]$ DMSO): $\delta = 3.88$ (s, 8H, CH_2) ppm. **$^{13}\text{C NMR}$** ($[\text{D}_6]$ DMSO): $\delta = 159.8$ (CO), 62.2 (CH_2), 42.1 (C) ppm. **$^{14}\text{N NMR}$** ($[\text{D}_6]$ DMSO): $\delta = -13$ (NO_2) ppm. **DSC** (5 $^{\circ}\text{C min}^{-1}$): 156 $^{\circ}\text{C}$ (dec.).

Tetrapotassium PETNC · 2 hydrate (6)

$^1\text{H NMR}$ ($[\text{D}_6]$ DMSO): $\delta = 3.88$ (s, 8H, CH_2) ppm. **$^{13}\text{C NMR}$** ($[\text{D}_6]$ DMSO): $\delta = 158.8$ (CO), 62.3 (CH_2), 42.1 (C) ppm. **$^{14}\text{N NMR}$** ($[\text{D}_6]$ DMSO): $\delta = -12$ (NO_2) ppm. **EA:** $\text{K}_4\text{C}_9\text{H}_8\text{N}_8\text{O}_{16} \cdot 2 \text{H}_2\text{O}$ (676.6): calc. C 15.98, H 1.79, N 16.56 %; found C 16.51, H 2.15, N 16.77 %. **IS:** 7 J (grain size 100–250 μm). **FS:** 360 N (grain size 100–250 μm). **DSC** (5 $^{\circ}\text{C min}^{-1}$): 177 $^{\circ}\text{C}$ (dec.).

Dicalcium PETNC · 7 hydrate (7)

$^1\text{H NMR}$ ($[\text{D}_6]$ DMSO): $\delta = 3.86$ (s, 8H, CH_2) ppm. **$^{13}\text{C NMR}$** ($[\text{D}_6]$ DMSO): $\delta = 160.4$ (CO), 62.3 (CH_2), 42.1 (C) ppm. **$^{14}\text{N NMR}$** ($[\text{D}_6]$ DMSO): $\delta = -8$ (NO_2) ppm. **EA:** $\text{Ca}_2\text{C}_9\text{H}_8\text{N}_8\text{O}_{16} \cdot 7 \text{H}_2\text{O}$ (690.5): calc. C 15.66, H 3.21, N 16.23 %; found C 15.88, H 3.24, N 16.16 %. **IS:** 40 J (grain size <100 μm). **FS:** 360 N (grain size <100 μm). **ESD:** 1.50 J (grain size <100 μm). **DSC** (5 $^{\circ}\text{C min}^{-1}$): 167 $^{\circ}\text{C}$ (dec.).

Distrontium PETNC · 7 hydrate (8)

$^1\text{H NMR}$ ($[\text{D}_6]$ DMSO): $\delta = 3.91$ (s, 8H, CH_2) ppm. **$^{13}\text{C NMR}$** ($[\text{D}_6]$ DMSO): $\delta = 160.5$ (CO), 62.5 (CH_2), 42.1 (C) ppm. **$^{14}\text{N NMR}$** ($[\text{D}_6]$ DMSO): $\delta = -7$ (NO_2) ppm. **EA:** $\text{Sr}_2\text{C}_9\text{H}_8\text{N}_8\text{O}_{16} \cdot 7 \text{H}_2\text{O}$ (785.6): calc. C 13.76, H 2.82, N 14.26 %; found C 13.29, H 2.41, N 12.43 %. **IS:** 40 J (grain size <100 μm). **FS:** 360 N (grain size <100 μm). **ESD:** 1.50 J (grain size <100 μm). **DSC** (5 $^{\circ}\text{C min}^{-1}$): 152 $^{\circ}\text{C}$ (dec.).

Dibarium PETNC · 4 hydrate (9)

$^1\text{H NMR}$ ($[\text{D}_6]$ DMSO): $\delta = 3.91$ (s, 8H, CH_2) ppm. **$^{13}\text{C NMR}$** ($[\text{D}_6]$ DMSO): $\delta = 160.3$ (CO), 62.5 (CH_2), 42.0 (C) ppm. **$^{14}\text{N NMR}$** (not visible due to low solubility). **EA:** $\text{Ba}_2\text{C}_9\text{H}_8\text{N}_8\text{O}_{16} \cdot 4 \text{H}_2\text{O}$ (830.9): calc. C 13.01, H 1.94, N 13.49 %; found C 13.03, H 1.82, N 13.38 %. **IS:** 35 J (grain

size <100 μm). **FS**: 360 N (grain size <100 μm). **ESD**: 0.80 J (grain size <100 μm). **DSC** (5 $^{\circ}\text{C min}^{-1}$): 156 $^{\circ}\text{C}$ (dec.)

Silver PETNC (10)

Pentaerythritol tetranitrocarbamate (143 mg, 0.3 mmol) was suspended in dry acetonitrile (10 mL) and silver carbonate (163 mg, 0.6 mmol) was added at 0 $^{\circ}\text{C}$ under exclusion of light. Immediately within 10 minutes, the PETNC dissolved, impurities were filtered, and the solution was evaporated in the dark at ambient temperature. Silver pentaerythritol tetranitrocarbamate (**10**) was obtained as a colorless solid in 86% yield.

$^1\text{H NMR}$ ($[\text{D}_6]$ DMSO): δ = 4.03 (s, 8H, CH_2), 2.07 (s, 6H, CH_3) ppm. $^{13}\text{C NMR}$ ($[\text{D}_6]$ DMSO): δ = 157.2 (CO), 118.1 (CN), 64.2 (CH_2), 41.6 (C), 1.16 (CH_3) ppm. $^{14}\text{N NMR}$ ($[\text{D}_6]$ DMSO): δ = -13 (NO_2) -134 (CN) ppm. ^{109}Ag ($[\text{D}_6]$ DMSO) δ = 255 ppm. **EA**: $\text{Ag}_4\text{C}_{13}\text{H}_{14}\text{N}_{10}\text{O}_{16}$ (997.78): calc. C 15.65, H 1.41, N 14.04 %; found C 12.78, H 1.54, N 12.58 %.

6.6 References

1. Akhavan, J. *The Chemistry of Explosives*. 2nd Ed.; The Royal Society of Chemistry: Cambridge, 2004.
2. Klapötke, T. M. *Chemistry of High-Energy Materials*. 4th ed.; de Gruyter: Berlin, 2017.
3. Klapötke, T. M.; Krumm, B.; Ilg, R.; Troegel, D.; Tacke, R. The Sila-Explosives $\text{Si}(\text{CH}_2\text{N}_3)_4$ and $\text{Si}(\text{CH}_2\text{ONO}_2)_4$: Silicon Analogues of the Common Explosives Pentaerythrityl Tetraazide, $\text{C}(\text{CH}_2\text{N}_3)_4$, and Pentaerythritol Tetranitrate, $\text{C}(\text{CH}_2\text{ONO}_2)_4$. *J. Am. Chem. Soc.* **2007**, *129*, 6908–6915.
4. Axthammer, Q. J.; Klapötke, T. M.; Krumm, B.; Reith, T. Energetic Sila-Nitrocarbamates: Silicon Analogues of Neo-Pentane Derivatives. *Inorg. Chem.* **2016**, *55*, 4683–4692.
5. Frankel, M. B. N-Nitrocarbamates. US2978485A, 1961.
6. Aas, B.; Kettner, M. A.; Klapötke, T. M.; Sućeska, M.; Zoller, C. Asymmetric Carbamate Derivatives Containing Secondary Nitramine, 2,2,2-Trinitroethyl, and 2-Fluoro-2,2-dinitroethyl Moieties. *Eur. J. Inorg. Chem.* **2013**, 6028–6036.
7. Axthammer, Q. J.; Klapötke, T. M.; Krumm, B.; Moll, R.; Rest, S. F. The Energetic Nitrocarbamate $\text{O}_2\text{NN}(\text{H})\text{CO}[\text{OCH}_2\text{C}(\text{NO}_2)_3]$ Derived from Phosgene. *Z. Anorg. Allg. Chem.* **2014**, *640*, 76–83.
8. Axthammer, Q. J.; Klapötke, T. M.; Krumm, B. Synthesis of Energetic Nitrocarbamates from Polynitro Alcohols and Their Potential as High Energetic Oxidizers. *J. Org. Chem.* **2015**, *80*, 6329–6335.

9. Klapötke, T. M.; Krumm, B.; Reith, T. Polynitrocarbamates Derived from Nitromethane. *Z. Anorg. Allg. Chem.* **2017**, *643*, 1474–1481.
10. Gattow, G.; Knoth, W. K. Über Chalkogenolate. 119. Untersuchungen über N-Nitrocarbamate, N-Nitrocarbaminsäure-O-ethylester und Salze dieses Esters. Versuche zur Darstellung von N-Nitrodithiocarbamaten. *Z. Anorg. Allg. Chem.* **1983**, *499*, 194–204.
11. Axthammer, Q. J.; Krumm, B.; Klapötke, T. M. Pentaerythritol-Based Energetic Materials Related to PETN. *Eur. J. Org. Chem.* **2015**, 723–729.
12. Li, Y.; Huang, H., Lin, X.; Pan, R., Yang, J. Oxygen-rich Anion Based Energetic Salts with High Detonation Performances. *RSC Adv.* **2016**, *6*, 54310–54317.
13. Li, Y.; Huang, H., Yang, J. N-Nitrotrinitroethyl Carbamate Energetic Ionic Salts and Preparation Method and Application thereof. CN105777587 (A), 2016.
14. Klapötke, T. M.; Witkowski, T. G., Wilk, Z.; Hadzik, J. Determination of the Initiating Capability of Detonators Containing TKX-50, MAD-X1, PETNC, DAAF, RDX, HMX or PETN as a Base Charge, by Underwater Explosion Test. *Propellants, Explos., Pyrotech.* **2016**, *41*, 92–97.
15. Cotarca, L.; Eckert, H. *Phosgenations – A Handbook*. Wiley-VCH: Weinheim, 2005.
16. Rasmussen, J. K.; Hassner, A. Recent Developments in the Synthetic Uses of Chlorosulfonyl Isocyanate. *Chem. Rev.* **1976**, *76*, 389–408.
17. Graf, R. Über die Umsetzung von Chlorcyan mit Schwefeltrioxyd. *Chem. Ber.* **1956**, *89*, 1071–1079.
18. Dhar, D. N.; Dhar, P. *The Chemistry of Chlorosulfonyl Isocyanate*. World Scientific: Singapore, 2002.
19. Cox, B. G.; Natarajan, R.; Waghorne, W. E. Thermodynamic Properties for Transfer of Electrolytes from Water to Acetonitrile and to Acetonitrile + Water Mixtures. *J. Chem. Soc., Faraday Trans. 1* **1979**, *75*, 86–95.
20. Guinand, L., Hobt, K. L., Mittermaier, E., Rößler, E., Schwenk, A., Schneider, H. ¹⁰⁹Ag NMR-Study of the Selective Solvation of the Ag⁺ Ion in Solvent Mixtures of Water and the Organic Solvents: Pyridine, Acetonitrile, Dimethyl Sulfoxide. *Z. Naturforsch.* **1984**, *39A*, 83–94.
21. Klapötke, T. M.; Krumm, B.; Moll, R.; Penger, A.; Sproll, S. M.; Berger, R. J. F.; Hayes, S. A., Mitzel, N. W. Structures of Energetic Acetylene Derivatives HC≡CCH₂ONO₂, (NO₂)₃CCH₂C≡CCH₂C(NO₂)₃ and Trinitroethane, (NO₂)₃CCH₃. *Z. Naturforsch.* **2013**, *68B*, 719.
22. Sućeska, M., *EXPLO5 V6.03*. Zagreb (Croatia), 2015.

23. Frisch, M. J.; Trucks, G. W.; Schlegel, H. B.; Scuseria, G. E.; Robb, M. A.; Cheeseman, J. R.; Scalmani, V. B.; Mennucci, B.; Petersson, G. A.; Nakatsuji, H.; Caricato, M.; Li, X.; Hratchian, H. P.; Izmaylov, A. F.; Bloino, J.; Zheng, G.; Sonnenberg, J. L.; Hada, M.; Ehara, M.; Toyota, K.; Fukuda, R.; Hasegawa, J.; Ishida, M.; Nakajima, T.; Honda, Y.; Kitao, O.; Nakai, H.; Vreven, T.; J. A. Montgomery, J.; Peralta, J. E.; Ogliaro, F.; Bearpark, M.; Heyd, J. J.; Brothers, E.; Kudin, K. N.; Staroverov, V. N.; Kobayashi, R.; Normand, J.; Raghavachari, K.; Rendell, A.; Burant, J. C.; Iyengar, S. S.; Tomasi, J.; Cossi, M.; Rega, N.; Millam, J. M.; Klene, M.; Knox, J. E.; Cross, J. B.; Bakken, V.; Adamo, C.; Jaramillo, J.; Gomperts, R.; Stratmann, R. E.; Yazyev, O.; Austin, A. J.; Cammi, R.; Pomelli, C.; Ochterski, J. W.; Martin, R. L.; Morokuma, K.; Zakrzewski, V. G.; Voth, G. A.; Salvador, P.; Dannenberg, J. J.; Dapprich, S.; Daniels, A. D.; Farkas, Ö.; Foresman, J. B.; Ortiz, J. V.; Cioslowski, J.; Fox, D. J. *Gaussian 09*. Rev. A.02 ed.; Gaussian, Inc.: Wallingford CT (US), 2009.
24. NATO *Standardization Agreement 4489 (STANAG 4489), Explosives, Impact Sensitivity Tests*; Brussels, Belgium, 1999.
25. NATO *Standardization Agreement 4487 (STANAG 4487), Explosives, Friction Sensitivity Tests*; Brussels, Belgium, 2002.
26. *Laying down test methods pursuant to Regulation (EC) No 1907/2006 of the European Parliament and of the Council on the Evaluation, Authorisation and Restriction of Chemicals (REACH)*. 2008; Vol. Abl. L 142, p 93–103.
27. Cao, C. J.; Johnson, M. S.; Hurley, M. M.; Klapötke, T. M. In Vitro Approach to Rapid Toxicity Assessment of Novel High-Nitrogen Energetics. *JANNAF J. Propuls. Energet.* **2012**, *5*, 41–51.
28. Fischer, D.; Klapötke, T. M.; Reymann, M.; Stierstorfer, J. Dense Energetic Nitraminofurazanes. *Chem. – Eur. J.* **2014**, *20*, 6401–6411.
29. Wasserbeschaffenheit – Bestimmung der Hemmwirkung von Wasserproben auf die Lichtemission von *Vibrio Fischeri* (Leuchtbakterientest). In *Wasserbeschaffenheit – Bestimmung der Hemmwirkung von Wasserproben auf die Lichtemission von Vibrio Fischeri (Leuchtbakterientest)*, 2009; Vol. DIN EN ISO 11348-2.
30. Altomare, A.; Cascarano, G.; Giacobazzo, C.; Guagliardi, A.; Moliterni, A. G. G.; Burla, M. C.; Polidori, G.; Camalli, M.; Spagna, R. *SIR97*, 1997.
31. Altomare, A.; Burla, M. C.; Camalli, M.; Cascarano, G. L.; Giacobazzo, C.; Guagliardi, A.; Moliterni, A. G. G.; Polidori, G.; Spagna, R. *SIR97: a New Tool for Crystal Structure Determination and Refinement*. *J. Appl. Crystallogr.* **1999**, *32*, 115–119.

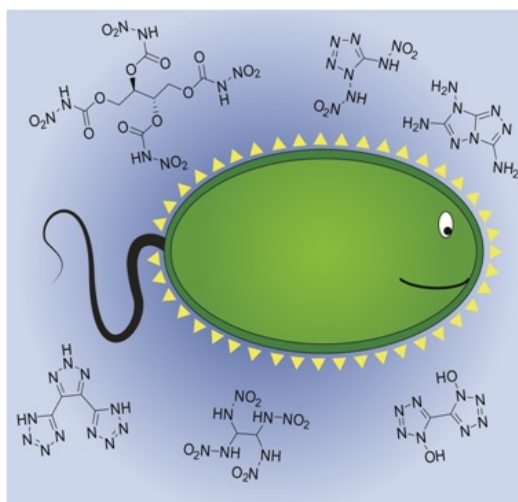
32. Sheldrick, G. M. *SHELX-97, Programs for Crystal Structure Determination*, University of Göttingen, Göttingen (Germany), 1997.
33. Sheldrick, G. M. A. Short History of SHELX. *Acta Crystallogr.* **2008**, *64A*, 112–122.
34. Farrugia, L. J. WinGX Suite for Small-molecule Single-crystal Crystallography. *J. Appl. Crystallogr.* **1999**, *32*, 837–838.
35. Spek, A. Structure Validation in Chemical Crystallography. *Acta Crystallogr.* **2009**, *65D*, 148–155.
36. Dennington II, R. D.; Keith, T. A.; Millam, J. M. *GaussView*. Ver. 5.08 ed.; Semichem, Inc.: Wallingford CT (US), 2009.
37. Byrd, E. F. C.; Rice, B. M. Improved Prediction of Heats of Formation of Energetic Materials Using Quantum Mechanical Calculations. *J. Phys. Chem.* **2005**, *110*, 1005–1013.
38. Jenkins, H. D. B.; Roobottom, H. K., Passmore, J., Glasser, L. Relationships among Ionic Lattice Energies, Molecular (Formula Unit) Volumes, and Thermochemical Radii. *Inorg. Chem.* **1999**, *38*, 3609–3620.
39. Jenkins, H. D. B.; Tudela, D., Glasser, L. Lattice Potential Energy Estimation for Complex Ionic Salts from Density Measurements. *Inorg. Chem.* **2002**, *41*, 2364–2367.
40. Jenkins, H. D. B.; Glasser, L. Ionic Hydrates, $M_pX_q \cdot H_2O$: Lattice Energy and Standard Enthalpy of Formation Estimation. *Inorg. Chem.* **2002**, *41*, 4378–4388.
41. Jenkins, H. D. B. *Chemical Thermodynamics at a Glance*. 1st ed.; Blackwell: Oxford, 2007

7 Aquatic Toxicity Measurements

Toxicity Assessment of Energetic Materials by Using the Luminescent Bacteria Inhibition Test Toxicity Assessment of Energetic Materials by Using the Luminescent Bacteria Inhibition Test

T. M. Klapötke, R. Scharf, J. Stierstorfer and C. C. Unger

Propellants, Explos. Pyrotech. **2020**, in press.



7.1 Abstract

The luminescent bacteria inhibition test using *Aliivibrio fischeri* is a well-established method to determine the aquatic toxicity of soluble chemicals. More precisely, the effective concentration (EC_{50}) after 15 and 30 min is determined in this test. The inhibition of natural bioluminescence of these bacteria gives a first idea of the toxicity of compounds towards some aquatic organisms. It is a cost and time efficient experimental method, which does not involve animals. In this contribution the experimental set up, comparability with other measurements and results of recently described compounds is presented. Different types of energetic materials such as coordination (*e. g.* $[Cu(dtp)_3](ClO_4)_2$ and $[Fe(MTZ)_6](ClO_4)_2$), neutral (*e. g.* azidoethanol, 1 and 2 aminotetrazole) and ionic (*e. g.* polynitropyrazolates and PETNC salts) compounds were investigated and compared to commonly used materials, like RDX, ammonium perchlorate (AP) and azide salts. Furthermore, different substitution patterns and energetic functionalities such as azido-, nitro- and nitramino-groups were investigated.

7.2 Introduction

Strong research efforts are ongoing to find new energetic materials with superior energetic properties like higher performance, lower sensitivities and better stabilities during the last decades.^[1] However, not only physicochemical properties are important but also environmentally friendly substances are requested. Unfortunately some commonly used explosives, such as hexogen (RDX) and 2,4,6-trinitrotoluene (TNT) have shown to be toxic depending on dose and organism.^[2] Furthermore, waste streams of TNT, are a possible source for pollution of drinking water with TNT, dinitrotoluene, nitrotoluene and acids.^[3] Another example how the ecosystem could be affected, is that munitions manufacturing led to contamination of soils, sediments, and water with explosives such as TNT, RDX and PETN.^[4] Furthermore, lead is a highly poisonous metal whether it is inhaled or swallowed affecting the whole body and may even cause death in high concentrations.^[5] Studies showed that at shooting ranges and military training grounds the maximum accepted concentration of lead (0.15 mg m^{-3})^[6] is often exceeded by far.^[1c, 7] One possible reason is that lead is the main element of lead shots, which also contain variable amounts of tin, arsenic and antimony.^[8] The latter and also lead are replaced in the SINTOX primer composition, developed at the Dynamit Nobel AG.^[9] Amongst others, this development provoked the research towards 'greener' primer compositions and pyrotechnics. Still, ammonium perchlorate is the commonly used oxidizer in solid rocket propellants. Furthermore, many pyrotechnical formulations contain perchlorates, since there is a lack of suitable alternatives. It is known that the

perchlorate anion interferes with the thyroid function.^[10] Therefore, there is need for new environmentally friendlier energetic materials.

Several tests have been implemented to determine the toxicity of compounds or ground waters utilizing plants, algae, fishes, mice or water fleas.^[11] However most of these tests show disadvantages like huge test volume, long exposure periods, difficulties with the standardizations of the organisms and subsequent low reproducibilities.^[12] Comparing the toxicity levels of TNT and PETN in *Aliivibrio fischeri*, *Daphnia magna* and *Pimephales promales*, as well as the LD₅₀ value in rats, TNT is more toxic than PETN in every organism. Comparing the exposure periods, *Aliivibrio fischeri* (30 min) is superior to *Daphnia magna* (48 h) as well as *Pimephales promales* (96 h) and amongst them the only animal free test. Therefore, Luminescent Bacteria Inhibition Test provides a quick, simple and reproducible possibility to test new energetic materials towards their environmental acceptability for aquatic organisms. Since the bioluminescent bacterium *Aliivibrio fischeri* is an excellent representative for aquatic life, it is used as indicator for groundwater pollution^[13] and gained more attention in different research areas over the last years.^[14] Bioluminescence is a form of chemiluminescence where light is released by a chemical reaction. The complex biochemical mechanism of the bioluminescent marine bacteria *Aliivibrio fischeri* is shown in Figure 7.1.^[15] In the system three enzymatic complexes are involved: the Flavin Reductase (FMN Reductase), the Luciferase and the Fatty Acid Reductase. In the first step flavin mononucleotide (FMN) is metabolized to its reduced form (FMNH₂) catalyzed by the FMN Reductase. The reduced flavin molecule is able to bind to the Luciferase and in combination with an aliphatic aldehyde and under consumption of oxygen the peroxihemiacetal complex L--FMNH-O-O-CHOH-R is formed. In the following step aliphatic acid is released and a singlet excited hydroxide complex (L--FMNH-OH)* is generated, which directly reacts to the hydroxide complex L--FMNHOH in the ground state under liberation of light in a chemically initiated electron exchange luminescence (CIEEL) mechanism (see Appendix A7). The emitted light with a wavelength of 490 nm can be observed and measured by a photomultiplier.^[15-16]

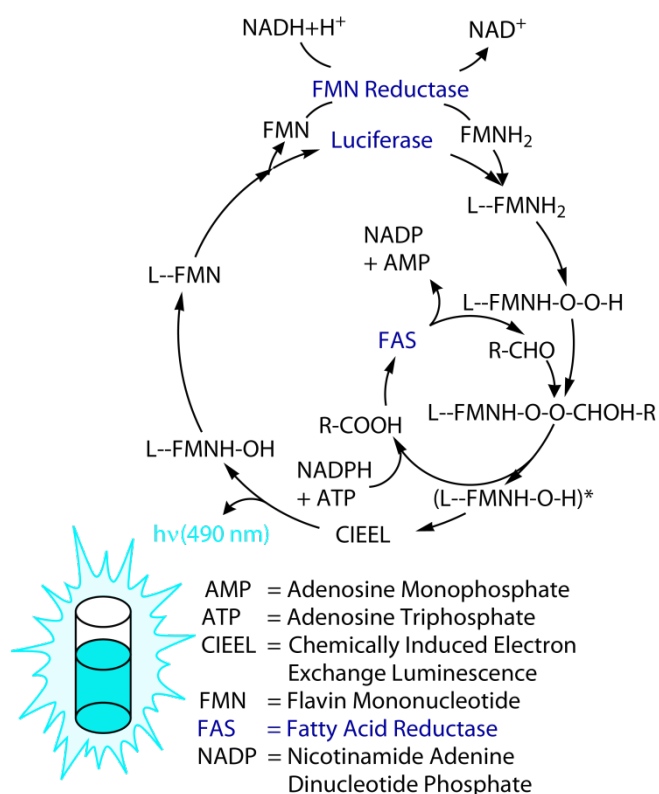


Figure 7.1 Schematic overview of the biochemical light emitting pathway of the bioluminescent bacteria *Aliivibrio fischeri* and *Photobacterium*.

The metabolic activity of the bacteria is directly proportional to the light production and any inhibition of enzymatic activity due to toxicant causes a corresponding decrease in bioluminescence. The value at which the luminescence of *Aliivibrio fischeri* is reduced by 50% at its specific concentration is determined and is defined as EC₅₀ (effective concentration). This concentration is determined after 15 min and 30 min, respectively, for various energetic materials such as RDX, ammonium perchlorate and several more recently synthesized neutral and ionic compounds, as well as complexes

7.3 Experimental Section

7.3.1 Test Compounds

Commercially available compounds were used as supplied without further purification. The purity of in-house synthesized materials was determined using elemental analysis.

7.3.2 Measurement

Liquid dried luminescent bacteria of the strain *Aliivibrio fischeri* NRRL-B-11177 obtained by HACH LANGE GmbH (Düsseldorf, Germany) were used for the luminescent bacteria inhibition test.

Prior to the measurements a 2% NaCl stock solution was prepared using HPLC-grade water to ensure optimal salt conditions for the bacteria. The tested compounds of known weight are diluted in this stock solution and after complete solvation, as well as setting the pH value to 6–8, were adjusted to a final volume. A dilution series was prepared out of this test solution referring to DIN 38412 L34, L341. The dilutions range from 1:2 to 1:32. Due to the low solubility of RDX in water RDX was first dissolved in acetone and then diluted in 2% NaCl stock solution to obtain a 1% (vol%) acetone concentration for each dilution. A 1% acetone concentration in the control of the measurement showed a negligible effect on the bacteria.^[17] Our resulting values for RDX are consistent with literature values.^[18]

The measurements were performed on a *LUMIStox 300* spectrometer obtained by HACH LANGE GmbH (Düsseldorf, Germany), were DIN EN ISO 11348-2, which is similar to ASTM method D5660, was used as a guideline.^[19] The samples were incubated at 15 °C and the luminescence was tested in the beginning of each experiment and after 15 min and 30 min. During the whole measurement the temperature must be kept at this temperature within a range of ± 0.3 °C. Each dilution step was measured twice. To calculate the correction factor of a non-toxic control two bacteria suspensions with 1% NaCl were measured at the beginning of each measurement. The toxicity data with the inhibition were used to fit a straight line, and therefore to calculate the EC₅₀ value. For details of the calculation see Appendix A7. When the inhibition of a compound did not reach the 10% limit, the EC₅₀ reported ">>" for the highest measured.

7.4 Results and Discussion

Table 7.1–Table 7.8 summarize the toxicity data of several neutral and ionic compounds like ammonium, hydroxylammonium, sodium and potassium salts. Most of the compiled compounds are useful energetic materials or potential precursors. An important factor when measuring the toxicities of energetic materials is the water solubility of the substances. To increase the water solubility RDX was first dissolved in acetone and then diluted to get a 1% acetone solution. The EC₅₀ value of RDX after 15 min incubation (EC₅₀ = 0.327 g L⁻¹) fits well with the value of EC₅₀ = 0.322 g L⁻¹ given in the literature.^[18] Nevertheless, it was not possible to obtain a concentration high enough to determine the EC₅₀ values of pentaerythritol tetranitrate (PETN), cyclotetramethylene tetranitramine (HMX), 2,4,6,8,10,12-hexanitro-2,4,6,8,10,12-hexanitrohexaazaisowurtzitane (CL-20) and 2,2-dinitroethene-1,1-diamine (FOX-7). For classification of the toxicity the compounds with EC₅₀ values lower than 0.10 g L⁻¹ are categorized as very toxic (++) while compounds with EC₅₀ values between 0.10 g L⁻¹ and 1.00 g L⁻¹ are rated as toxic (+) and above 1.00 g L⁻¹ as less toxic (–) to the marine bacteria *Aliivibrio fischeri* after 30 min incubation time.^[18] Therefore mainly the EC₅₀ value after 30 min

incubation will be discussed. The concentration of the compounds was mainly chosen to be over 3 g L^{-1} in the stock, in order to have the series of dilution be in the range of the above-mentioned categorization. Still the toxicity according to EC_{50} values is relative and can be more or less toxic at higher or lower concentrations. To get a detailed impression on the toxicity, the EC_{50} values should be measured in various concentrations and compared to other organisms in the further development. This categorization is also common amongst other scientific fields, such as antibiotics research, furthermore, labelling following the globally harmonized system (GHS) is possible.^[20] The GHS refers to three acute toxicity classification categories. Therefore, they recommend determining a fish 96 hour LC_{50} , a crustacea species 48 hour EC_{50} and/or an algal species 72 or 96 hour EC_{50} . Substances classified according to the criteria are categorized as 'hazardous to the aquatic environment' as it follows:

- $\leq 1 \text{ mg L}^{-1}$ → Acute 1
- $>1 - \leq 10 \text{ mg L}^{-1}$ → Acute 2
- $>10 - \leq 100 \text{ mg L}^{-1}$ → Acute 3

The toxicity measurements of commercially available salts like potassium chlorate, bromate and iodate as well as ammonium nitrate and perchlorate showed almost no toxicity of the salts towards the bacteria, because no inhibition of luminescence was observed with concentrations of 2.5 g L^{-1} and an incubation time of 30 min. Besides, the highest toxicity is observed for the azide anion followed by the periodate anion, whereas ammonium nitrate and dinitramide led to higher EC_{50} values as seen in Table 7.1 and Figure 7.2. Similar toxicity trends against *Aliivibrio fischeri* were observed for the azide, nitrate and dinitramide salts of 1,4-dimethyl-5-aminotetrazole in the literature.^[18] The perchlorate anion showed no effect on the luminescence of the bacteria. Studies showed a toxicity of the perchlorate anion towards vertebrates, which probably only results from the interaction with the sodium/iodide symporter.^[21]

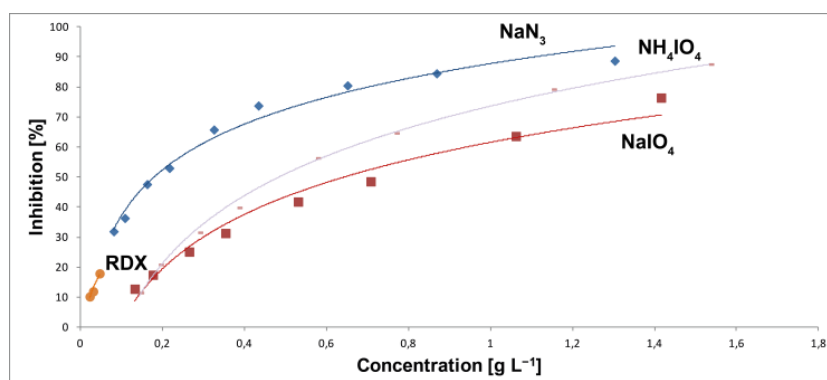


Figure 7.2 Diagram of the inhibition of some common energetic salts and RDX after 30 min of incubation.

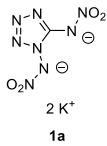
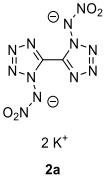
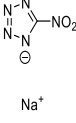
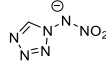
Nonetheless, also for the hydroxylammonium cation a negative effect on the toxicity was observed. The primary explosives dipotassium 1,5-di(nitramino)tetrazolate (**1a**)^[22] and dipotassium 1,1'-di(nitramino)-5,5'-bitetrazolate (**2a**)^[22] as well as copper(I) 5-nitrotetrazolate (DBX-1)^[23] are potential lead-free replacements for lead azide (Table 7.2).

Table 7.1 Toxicity data of common energetic materials and ionic compounds after 15 min and 30 min of incubation and their considered toxicity level after 30 minutes [less toxic (-), toxic (+), very toxic (++)^[18]].

	EC ₅₀ (15 min) [g L ⁻¹]	EC ₅₀ (30 min) [g L ⁻¹]	Toxicity level
NaN ₃	0.25	0.18	+
NaIO ₄	0.77	0.65	+
KIO ₄	0.89	0.68	+
KClO ₃	>>2.49	>>2.49	-
KBrO ₃	>>2.49	>>2.49	-
KIO ₃	>>2.53	>>2.53	-
NH ₃ OHCl	0.59	0.22	+
NH ₄ N ₃	0.26	0.15	+
NH ₄ NO ₃	10.49	6.39	-
NH ₄ ClO ₄	14.58	11.13	-
NH ₄ IO ₄	0.58	0.48	+
NH ₄ N(NO ₂) ₂	7.25	4.50	-
RDX	0.33	0.24	+

Since DBX-1 is nearly insoluble in water no EC₅₀ value could be determined. Therefore, the precursor of DBX-1 sodium 5-nitrotetrazolate (**3a**)^[23b] was measured. With EC₅₀ values higher than 3.9 g L⁻¹ all of these compounds are classified as not toxic towards the marine bacteria *Aliivibrio fischeri*.^[18] Further salts of 5-nitrotetrazole were mentioned so far, e. g. the guanazinium (EC₅₀ (30 min) = 0.10 g L⁻¹), the guanidinium (EC₅₀ (30 min) = 0.78 g L⁻¹), the aminoguanidinium (EC₅₀ (30 min) = 2.65 g L⁻¹) and the 1,4-dimethyl-5-aminotetrazolium (EC₅₀ (30 min) = 3.61 g L⁻¹) salts.^[18]

Table 7.2 Toxicity data of neutral and ionic energetic materials **1a–7a** after 15 min and 30 min of incubation and their considered toxicity level after 30 minutes [less toxic (–), toxic (+), very toxic (++)]^[18]

							
	1a	2a	3a	4	5	6a	7a
EC₅₀ (15 min) [g L⁻¹]	>1.63	>5.93	14.08	7.23	6.69	>>1.60	>>1.61
EC₅₀ (30 min) [g L⁻¹]	3.92	11.63	4.35	4.58	3.87	>>1.60	>>1.61
Toxicity level	–	–	–	–	–	–	–

Another evaluated variation affecting the tetrazole scaffold, listed in Table 7.2 as well, are the 1- and 2-amino as well as the nitramino substituted derivatives **4–7a**. These show EC₅₀ values much higher than 1.00 g L⁻¹, therefore are classified as non-toxic against *Aliivibrio fischeri*.^[24]

The toxicities of different hydroxyl ammonium (Figure 7.3) and ammonium bitetrazolates were determined (Table 7.3). Bis(hydroxylammonium) 5,5'-bitetrazole-1,1'-dioxide (**8a**, TKX-50)^[25], bis(hydroxylammonium) and bis(ammonium) 5-(1-oxidotetrazolyl)-tetrazolate (**9a** and **9b**)^[26], bis(hydroxylammonium) and bis(ammonium) 5-(2-oxidotetrazolyl)-tetrazolate (**10a** and **10b**)^[27] and bis(hydroxylammonium) 5,5'-bitetrazole 1,2'-dioxide (**11a**)^[28] are potential replacements for the secondary explosive RDX. All of these salts as well as the neutral compound 5-(1*H*-tetrazolyl)-2-hydroxytetrazole monohydrate (**10**)^[27] were tested by the luminescent bacteria inhibition test. The ammonium salts **9b** and **10b** showed with EC₅₀ values of 3.68 g L⁻¹ and 1.03 g L⁻¹, respectively, low toxicities towards the marine bacteria. However, the exchange of the non-toxic ammonium cation with the hydroxylammonium cation significantly increases the toxicity of the bitetrazolate salts. With EC₅₀ values in the range of 0.10–0.58 g L⁻¹ after 30 min incubation, the compounds are classified as toxic. Nevertheless, for **8a** (EC₅₀ (30 min) = 0.58 g L⁻¹) and **9a** (EC₅₀ (30 min) = 0.33 g L⁻¹) lower toxicities than for RDX (EC₅₀ (30 min) = 0.24 g L⁻¹) were observed. The EC₅₀ value for the neutral bitetrazole **10** (EC₅₀ (30 min) = 0.33 g L⁻¹) is in between the hydroxylammonium salt **10a** and the ammonium salt **10b**. As **10a** is more toxic than **9a** and **11a** is more toxic than **8a**, it seems that a substitution at 2-position results in higher toxicity values compared to toxicity values of the derivatives with substitution at 1-position. Still they are less toxic compared to the divalent hydroxylammonium (**12a**) and ammonium (**12b**) salts of the unsubstituted bitetrazole. The monovalent ammonium 1,5-bistetrazole was described to have an EC₅₀ value of 0.84 g L⁻¹ after 30 minutes of incubation

against *Aliivibrio fischeri*, which is in a comparable range as the divalent **12b** ($EC_{50} = 0.89 \text{ g L}^{-1}$).^[18]

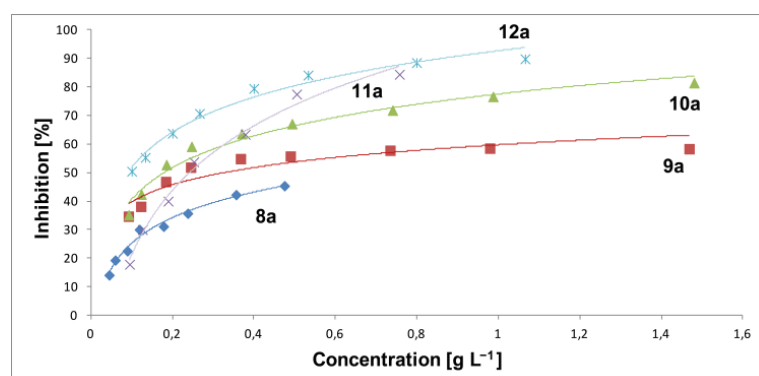


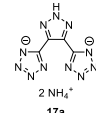
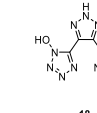
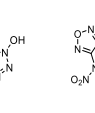
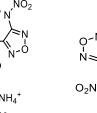
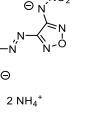
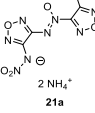
Figure 7.3 Diagram of the inhibition of the hydroxylammonium salts of bitetrazoles **8a–12a** after 30 min of incubation.

Table 7.3 Toxicity data of neutral and ionic energetic materials **8a–15a** after 15 min and 30 min of incubation and their considered toxicity level after 30 minutes [less toxic (-), toxic (+), very toxic (++)]^[18].

EC₅₀	1.17	1.63	4.21	0.60	0.39	1.73	0.32
(15 min)		a	b		a	b	
[g L⁻¹]							
EC₅₀	0.58	0.33	3.68	0.49	0.18	1.03	0.24
(30 min)		a	b		a	b	
[g L⁻¹]							
Toxicity level	+	+	-	+	+	-	+
EC₅₀	0.25	2.03	0.33	0.13	0.75	>>1.58	>1.04
(15 min)	a	b			a	b	
[g L⁻¹]							
EC₅₀	0.10	0.89	0.19	0.07	0.35	>>1.58	3.78
(30 min)	a	b			a	b	
[g L⁻¹]							
Toxicity level	+	-	+	++	+	-	-

Also the toxicities of the hydroxylammonium salts of 3,3'-dinitro-5,5'-bi-1,2,4-triazole-1,1'-diol (**13a**, MAD-X1)^[29] and 5,5'-diamino-4,4'-dinitramino-3,3'-bi-1,2,4-triazole (**14a**)^[30] have been investigated. Both compounds are toxic to aquatic life with EC₅₀ values of 0.19 g L⁻¹ (**13a**) and 0.35 g L⁻¹ (**14a**). The neutral compound 5,5'-diamino-4,4'-dinitramino-3,3'-bi-1,2,4-triazole^[30] is classified as very toxic (EC₅₀ (30 min) = 0.07 g L⁻¹). The thermally stable nitrogen-rich aromatic cations have been investigated, too. Toxicity measurements for 4,4',5,5'-tetramino-3,3'-bi-1,2,4-triazolium dinitramide (**15a**)^[31] as well as 3,6,7-triamino-7*H*-[1,2,4]triazolo[4,3-*b*][1,2,4]triazolium nitrate (**16a**)^[32] and its neutral analogue 3,6,7-triamino-7*H*-[1,2,4]triazolo[4,3-*b*][1,2,4]triazole (**16**)^[33] showed EC₅₀ values higher than 3.36 g L⁻¹ and are therefore low toxic for marine organisms.

Table 7.4 Toxicity data of neutral and ionic energetic materials **16–22a** after 15 min and 30 min of incubation and their considered toxicity level after 30 minutes [less toxic (-), toxic (+), very toxic (++)^[18]].

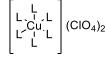
								
	16	16a = NO ₃ ⁻	17a = 2 NH ₄ ⁺	18	19a = 2 NH ₄ ⁺	20a = 2 NH ₄ ⁺	21a = 2 NH ₄ ⁺	22a = 2 NH ₄ ⁺
EC ₅₀ (15 min) [g L ⁻¹]	5.01	3.56	2.97	0.59	2.88	0.09	1.19	5.73
EC ₅₀ (30 min) [g L ⁻¹]	4.84	3.36	1.82	0.55	2.80	0.07	0.71	5.42
Toxicity level	-	-	-	+	-	++	+	-

The compounds 4,5-bi-(1*H*-tetrazol-5-yl)-2*H*-1,2,3-triazole (**17**) and 4,5-bi-(1-hydroxytetrazol-5-yl)-2*H*-1,2,3-triazole (**18**) combine the advantages of the triazole and tetrazole heterocycles by forming energetic and thermally stable molecules.^[34] For toxicity measurements the ammonium salt of **17** as well as the neutral compound **18** were investigated. While bis(ammonium) 4,5-bi-(1*H*-tetrazol-5-yl)-2*H*-1,2,3-triazolate (**17a**) is less toxic to *Aliivibrio fischeri* (EC₅₀ (30 min) = 1.82 g L⁻¹) a decrease of luminescence is observed for **18** (EC₅₀ (30 min) = 0.55 g L⁻¹) (Table 7.4).

The energetic nitrofurazans 3,3'-dinitramino-4,4'-bifurazan (**19**), 3,3'-dinitramino-4,4'-azobifurazan (**20**), 3,3'-dinitramino-4,4'-azoxybifurazan (**21**) and bi(1-oxidotetrazolyl)-furazan (**22**) as well as their salts are also possible RDX replacements.^[35] For toxicity assessment the ammonium salts of these compounds (**19a**, **20a**, **21a** and **22a**) were tested. The bifurazan salt **19a** and the bi(tetrazolyl)-furazan salt **22a** show both low toxicities, while the azo-bridged compounds

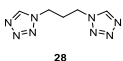
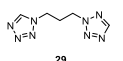
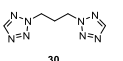
possess moderate (**21a**) to high toxicities (**20a**) towards aquatic life. Unfortunately, also the thermal stabilities and sensitivities of most of the furazan compounds are worse than of RDX.

Table 7.5 Toxicity data of energetic ligands and complexes **23–27** after 15 min and 30 min of incubation and their considered toxicity level after 30 minutes [less toxic (–), toxic (+), very toxic (++)^[18]].

					
	23	24 L = 23	25 L ₁ = 23 L ₂ = ClO ₃ [–]	26 L = 23	27 L ₁ = 23 L ₂ = BrO ₃ [–]
EC₅₀ (15 min) [g L^{–1}]	31.51	2.62	0.19	0.53	0.29
EC₅₀ (30 min) [g L^{–1}]	5.45	1.66	0.19	0.13	0.21
Toxicity level	–	–	+	+	+

The 1-methyl-substituted tetrazole **23** is as comparably non-toxic as the salts of amino-, nitro- and nitramino-substituted tetrazoles **1a**, **3a**, **4**, **5**, **6a** and **7a**. Also the iron(II)complex **24** of **23** remains non-toxic according to this test.^[36] Its toxicity drops towards the classification of toxic compounds upon complex formation using copper(II)metal, regardless if the used anion was chlorate (**25**), perchlorate (**26**) or bromate (**27**), as listed in Table 7.5.^[36–37] Due to the toxicity of the copper(II)metal towards microorganisms,^[38] similar results were observed for the copper(II)complexes **31–33**, which were more toxic compared to their used ligands only (Table 7.6). Those propyl-linked bitetrazoles (**28–30**) have a little variation in their substitution pattern, but the EC₅₀ values are in the range of 0.36 g L^{–1} (**30**) to 10.30 g L^{–1} (**28**).^[39] Whereby, the 2,2-substituted is the most toxic, followed by 1,2-substituted and the 1,1-substituted is the non-toxic tetrazole. This trend was also observed for the bitetrazoles around TKX-50 (**8a–11a**).

Table 7.6 Toxicity data of energetic ligands and complexes **28–33** after 15 min and 30 min of incubation and their considered toxicity level after 30 minutes [less toxic (–), toxic (+), very toxic (++)]^[18].

				$\left[\begin{array}{c} L_1 \\ \\ L_2-Cu-L_1 \\ \\ L_2 \end{array} \right] (ClO_4)_2$	$\left[\begin{array}{c} L_1 \\ \\ L_2-Cu-L_1 \\ \\ L_2 \end{array} \right] (ClO_4)_2$	$\left[\begin{array}{c} L_2-L_1-L_1 \\ \\ L_2-Cu-L_1 \\ \\ L_2-L_1-L_1 \end{array} \right] (ClO_4)_2$
	28	29	30	31 L = 28	32 L = 29	33 L ₁ = 30 L ₂ = H ₂ O
EC₅₀ (15 min) [g L⁻¹]	13.90	0.81	0.36	0.44	0.64	0.34
EC₅₀ (30 min) [g L⁻¹]	10.30	0.79	0.36	0.35	0.44	0.28
Toxicity level	–	+	+	+	+	+

Pyrazoles are depicted in Table 7.7 and form a class of substances, which gained more attention in the energetic community recently. Their concentration depending inhibition is shown in Figure 7.4. According to former studies, pyrazoles in general are biologically active, whereby they inhibit several enzymes and led to centrilobular necrosis of the liver as well as the thyroid and adrenals in both rats and mice.^[40] There were also investigations on 3-nitropyrazoles, which showed an effect on bacterial infections, but the acute toxicity against mice, rats, or dogs was relatively low.^[41] In addition, we recently published a study on high performing dinitropyrazoles including the aquatic toxicities.^[42] They also include a comparative study of aquatic toxicity and the mutagenic potential of BDNAPM.^[1c, 43] Further effort is part of our ongoing research.

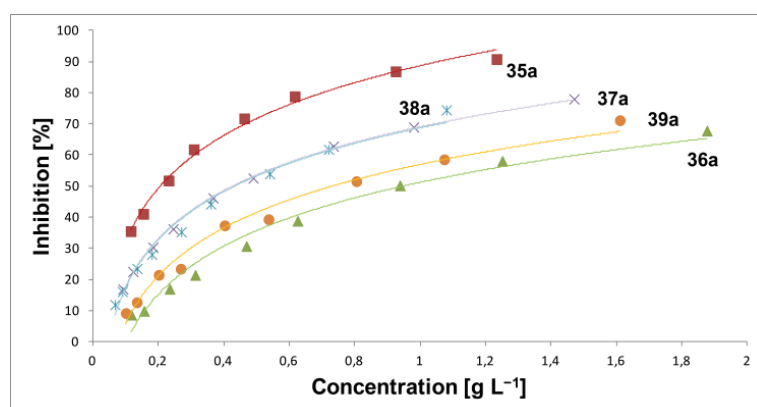


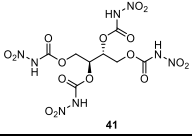
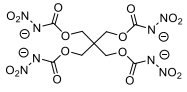
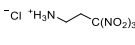
Figure 7.4 Diagram of the inhibition of the potassium salts of pyrazoles **35a–39a** after 30 min of incubation.

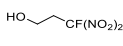
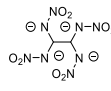
Table 7.7 Toxicity data of neutral and ionic energetic materials **34a–40a** after 15 min and 30 min of incubation and their considered toxicity level after 30 minutes [less toxic (-), toxic (+), very toxic (++)^[18]].

	 K ⁺ , H ₂ O 34a	 K ⁺ 35a	 36	 K ⁺ 36a	 K ⁺ , 0.5 H ₂ O 37a	 K ⁺ 38a	 K ⁺ 39a	 Na ⁺ , H ₂ O 39b	 K ⁺ , H ₂ O 40a
EC₅₀ (15 min) [g L⁻¹]	<0.10	0.27	0.27	1.21 a	0.70	0.61	0.75 a	0.60 b	2.86
EC₅₀ (30 min) [g L⁻¹]	<0.08	0.20	0.19	0.95 a	0.43	0.30	0.74 a	0.58 b	1.42
Toxicity level	++	+	+	+	+	+	+	+	-

The synthesis of meso-erythritol tetranitrocarbamate (**41**) started from corresponding sugar alcohol by an economically benign two-step synthesis.^[44] Primary nitrocarbamates form a new class of energetic materials with good detonation performances and lower sensitivities than the commonly used nitrate ester explosive PETN. During the toxicity measurements a moderate inhibition of luminescence was observed for compound **41** (EC₅₀ = 0.87 g L⁻¹) which is in comparison to RDX still less toxic. The PETN analogous PETNC (**42**), which is synthesized from the same starting material as PETN, is not water soluble itself.^[45] Therefore the aquatic toxicity of its ammonium (**42a**) and guanidinium (**42b**) salts were determined. Both showed no toxic effect towards *Aliivibrio fischeri* (Table 7.8).^[46]

Table 7.8 Toxicity data of neutral and ionic energetic materials **41–49a** after 15 min and 30 min of incubation and their considered toxicity level after 30 minutes [less toxic (-), toxic (+), very toxic (++)]^[18]

					
	41	42a = 4 NH₄⁺ 42b = 4 C(NH₂)₃⁺	43	44	
EC₅₀ (15 min) [g L⁻¹]	0.87	>>2.02 a	2.86 b	0.29	<0.10
EC₅₀ (30 min) [g L⁻¹]	0.87	>>2.02 a	1.42 b	0.22	<0.10
Toxicity level	+	-	-	+	++

					
	45	46	47	48	49a
EC₅₀ (15 min) [g L⁻¹]	0.002	8.70	6.00	0.01	>15.07
EC₅₀ (30 min) [g L⁻¹]	0.001	8.55	5.89	0.01	>15.07
Toxicity level	++	-	-	++	-

An important building block for the synthesis of oxygen-rich energetic compounds is the 2,2,2-trinitroethanol (**43**). It is formed by a simple Henry reaction starting from trinitromethane and formaldehyde.^[1c, 47] In contact with nucleophiles and bases it decomposes into its starting materials. When measuring the toxicity of the alcohol **43** and its decomposition products by the luminescent bacteria inhibition test an EC₅₀ value of 0.22 g L⁻¹ was determined. Therefore, **43** has to be classified as toxic. The toxicity of another water-soluble trinitroalkyl compound, trinitropropylammonium chloride (**44**), is lower and in the range of very toxic compounds (EC₅₀ < 0.10 g L⁻¹).^[48] A further trinitroalkyl substituted compound, (bis(2,2,2-trinitroethyl)-hydrazodicarboxylate), was reported to show high aquatic toxicity against *Aliivibrio fischeri* (EC₅₀ (30 min) = 0.02 mg L⁻¹).^[18] With a fluorodinitroethyl moiety attached to an ethanol backbone, as in **45**, the toxicity drops further to 0.001 g L⁻¹.^[49] This high toxicity value is consistent with former measurements using gram positive bacteria such as *Staphylococcus aureus* and *Intestinal bacillus*.^[50] Adding 2-azidoethanol (**46**) to the row of aliphatic alcohols, which are

important in the field of energetic materials, especially for propellants, it's the least toxic compound towards *Aliivibrio fischeri*. It is also relatively low in toxicity compared to ionic azide compounds NaN_3 and NH_4N_3 and also to monomethylhydrazine (**47**).^[51] The trend of covalent azides being less toxic compared to their ionic representatives continues according to our ongoing research.

6-Diazonium-3-hydroxy-2,4-dinitrophenolate (**48**) is a derivative of the commercially used primary explosive 2-diazonium-4,6-dinitrophenolate (DDNP). Chemical and physical studies as well as detonation calculations showed similar or even better properties than DDNP.^[52] However toxicity measurements of the benzene derivative **48** revealed a high toxic effect on the marine bacteria (EC_{50} (30 min) = 0.01 g L^{-1}).

1,1,2,2-Tetranitraminoethane (**49**) was first synthesized in 1988 as an intermediate for the synthesis of CL-20.^[53] However, **48** itself and the salts thereof are already energetic materials with a high oxygen content, high density and high thermal stability. Toxicity measurements of the potassium salt of **49** (**49a**)^[54] showed even at high concentrations negligible effects on the luminescence of the bacteria ($\text{EC}_{50} > 15.07 \text{ g L}^{-1}$). Therefore, compound **49a** is more than 50 times less toxic to the bacteria *Aliivibrio fischeri* than RDX.

7.5 Conclusion

The toxicities of several energetic neutral and ionic compounds as well as complexes have been tested using the luminescence bacteria inhibition test. Some trends according the EC_{50} values are discussed. Even though the median effective concentration just shows a point estimate from a dose response curve and the toxicity might vary in higher or lower concentrations. Even to an order of magnitude. During the measurements of salts, a minor toxic effect of the ammonium, potassium and sodium cations was found, whereas the hydroxylammonium cation showed a considerable toxicity. For the azide and periodate anion on the one hand high aquatic toxicities were observed, where on the other hand the perchlorate anion led to low toxicity values against *Aliivibrio fischeri*.

For the primary explosives measured (**1a** and **2a**) and the sodium salt **3a**, a precursor for the synthesis of DBX-1, hardly no toxicities towards the marine bacteria were observed. Also, most of the secondary explosives revealed good to excellent properties regarding the toxicity to aquatic life. For the intensively investigated secondary explosives **8a** (TKX-50, $\text{EC}_{50} = 0.58 \text{ g L}^{-1}$) and **13a** (MAD-X1, $\text{EC}_{50} = 0.19 \text{ g L}^{-1}$) EC_{50} values similar to RDX ($\text{EC}_{50} = 0.24 \text{ g L}^{-1}$) were observed (for EC_{20} and EC_{80} values see Appendix A7).

Furthermore, trends which were observed and are under constant investigation:

- The tetrazole moiety revealed to have a low toxic effect on the marine bacteria *Aliivibrio fischeri*. Thereby, the 2-substitution showed the higher impact on the toxicity than 1-substitution.
- Adding an azo-coupling increases the aquatic toxicity dramatically at least for furazans **19–22**.
- The nitramino functionality mainly has no toxic effect, especially for the potassium salt **49a**, which possesses four of those functionalities. It exhibits with a value higher than 15.07 g L^{-1} a very low toxicity.
- There is a trend that covalent azides are less toxic compared to their ionic representatives.
- The pyrazole scaffold represents a relatively toxic unit, no matter how many nitro-groups they carry. This is also indicated by the effect that C–C connected dipyrazoles drop in their toxicity towards the marine bacteria.
- For the trinitroalkyl and the fluorodinitroethyl moiety very toxic effects were observed. Second one is significantly more toxic
- The aquatic toxicity of complexes is mainly dominated by the chosen metal, as the toxicity of the free ligands often differ more.

Further attempts towards the comparability of the aquatic toxicity of energetic materials using *Aliivibrio fischeri* and other biological assays is ongoing research within our group.

7.6 References

- [1] a) P. F. Pagoria, G. S. Lee, A. R. Mitchell, R. D. Schmidt, A Review of Energetic Materials Synthesis, *Thermochim. Acta* **2002**, *384*, 187–204; b) S. Zeman, M. Jungová, Sensitivity and Performance of Energetic Materials, *Propellants, Explos., Pyrotech.* **2016**, *41*, 426–451; c) T. M. Klapötke, *Chemistry of High-Energy Materials*, 5th ed., De Gruyter, Berlin, **2019**.
- [2] a) B. S. Levine, E. M. Furedi, D. E. Gordon, J. M. Burns, P. M. Lish, Thirteen Week Toxicity Study of Hexahydro-1,3,5-trinitro-1,3,5-triazine (RDX) in Fischer 344 Rats, *Toxicol. Lett.* **1981**, *8*, 241–245; b) J. K. Haseman, J. Huff, G. A. Boorman, Use of Historical Control Data in Carcinogenicity Studies in Rodents, *Toxicol. Pathol.* **1984**, *12*, 126–135; c) P. Richter-Torres, A. Dorsey, C. S. Hodes, *Toxicological Profile for 2,4,6-Trinitrotoluene*, U.S. Department of Health and Human Services, Agency for Toxic Substances and Disease Registry, Atlanta,

Georgia, **1995**; d) E. L. Etnier, W. R. Hartley, Comparison of Water Quality Criterion and Lifetime Health Advisory for Hexahydro-1,3,5-trinitro-1,3,5-triazine (RDX), *Regul. Toxicol. Pharmacol.* **1990**, *11*, 118–122; e) Y. P. Robidoux, J. Hawari, G. Bardai, L. Paquet, G. Ampleman, S. Thiboutot, I. G. Sunahara, TNT, RDX, and HMX Decrease Earthworm (*Eisenia Andrei*) Life-Cycle Responses in a Spiked Natural Forest Soil, *Arch. Environ. Contam. Toxicol.*, **2002**, *43*, 379–388.

[3] a) L. R. Johnson, R. Davenport, H. Balbach, D. J. Schaeffer, Phototoxicology: 2. Near-ultraviolet Light Enhancement of Microtox Assays of Trinitrotoluene and Aminodinitrotoluenes, *Ecotoxicol. Environ. Saf.* **1994**, *27*, 23–33; b) O. Drzyzga, T. Gorontzy, A. Schmidt, K. H. Blotevogel, Toxicity of Explosives and Related Compounds to the Luminescent Bacterium *Vibrio fischeri* NRRL-B-11177, *Arch. Environ. Contam. Toxicol.* **1995**, *28*, 229–235.

[4] D. H. Rosenblatt, E. P. Burrows, W. R. Mitchell, D. L. Parmer, *Organic Explosives and Related Compounds*, Springer, Berlin/Heidelberg, **1991**.

[5] H. Abadin, A. Ashizawa, Y.-W. Stevens, F. Lladós, G. Diamond, G. Sage, M. Citra, A. Qinoes, S. Bosch, S. Swarts, *Toxicological Profile for Lead*, Agency for Toxic Substances and Disease Registry, Atlanta, Georgia, **2007**.

[6] Institut Für Arbeitsschutz Der Deutschen Gesetzlichen Unfallversicherung, <http://www.dguv.de/ifa/index.jsp> (accessed March 05, 2019)

[7] P. Mühle, Ludwig-Maximilians-Universität München (Munich), *Untersuchung der Bleiaufnahme bei kurzzeitigen Aufenthalten in Schießständen*, **2010**.

[8] M.-J. Mann, E. O. Espinoza, R. M. Ralston, R. K. Stroud, M. D. Scanlan, S. J. Strauss, Shot Pellets: An Overview, *AFTE J.* **1994**, *26*, 222–241.

[9] R. Hagel, K. Redecker, Sintox - a New, Non-toxic Primer Composition by Dynamit Nobel AG, *Propellants, Explos., Pyrotech.* **1986**, *11*, 184–187.

[10] E. D. McLanahan, J. L. Campbell, Jr., D. C. Ferguson, B. Harmon, J. M. Hedge, K. M. Crofton, D. R. Mattie, L. Braverman, D. A. Keys, M. Mumtaz, J. W. Fisher, Low-dose Effects of Ammonium Perchlorate on the Hypothalamic-Pituitary-Thyroid Axis of Adult Male Rats Pretreated with PCB126, *Toxicol. Sci.* **2007**, *97*, 308–317.

[11] M. Farré, D. Barceló, Toxicity Testing of Wastewater and Sewage Sludge by Biosensors, Bioassays and Chemical Analysis, *TrAC, Trends Anal. Chem.* **2003**, *22*, 299–310.

[12] S. Parvez, C. Venkataraman, S. Mukherji, A Review on Advantages of Implementing Luminescence Inhibition Test (*Vibrio Fischeri*) for Acute Toxicity Prediction of Chemicals, *Environ. Int.* **2006**, *32*, 265–268.

[13] K. L. Kaiser, Correlations of *Vibrio Fischeri* Bacteria Test Data with Bioassay Data for Other Organisms, *Environ. Health Perspect.* **1998**, *106*, 583–591.

- [14] a) M. Reichel, J. Martens, C. C. Unger, K. Karaghiosoff, Reactivity of Phosphines with Iodomethane Analog Fluoroiodomethane, *Phosphorus, Sulfur Silicon Relat. Elem.* **2019**, *194*, 467–468; b) M. A. Althoff, C. C. Unger, P. Bützer, M. Metzulat, T. M. Klapötke, K. L. Karaghiosoff, Bioactivity and Toxicological Study of Amiton and Related Isomers, *Phosphorus, Sulfur Silicon Relat. Elem.* **2019**, *194*, 333–334.
- [15] J.-J. Bourgois, F. E. Sluse, F. Baguet, J. Mallefet, Kinetics of Light Emission and Oxygen Consumption by Bioluminescent Bacteria, *J. Bioenerg. Biomembr.*, **2001**, *33*, 353–363.
- [16] S. Inouye, NAD(P)H-flavin Oxidoreductase from the Bioluminescent Bacterium, *Vibrio Fischeri* Atcc 7744, is a Flavoprotein, *FEBS Lett.* **1994**, *347*, 163–168.
- [17] a) G. I. Sunahara, S. Dodard, M. Sarrazin, L. Paquet, G. Ampleman, S. Thiboutot, J. Hawari, A. Y. Renoux, Development of a Soil Extraction Procedure for Ecotoxicity Characterization of Energetic Compounds, *Ecotoxicol. Environ. Saf.* **1998**, *39*, 185–194; b) P. Gong, G. I. Sunahara, S. Rocheleau, S. G. Dodard, P. Y. Robidoux, J. Hawari, Preliminary Ecotoxicological Characterization of a New Energetic Substance, CL-20, *Chemosphere* **2004**, *56*, 653–658; c) K. L. E. Kaiser, V. S. Palabrica, *Photobacterium Phosphoreum* Toxicity Data Index, *Water Qual. Res. J.* **1991**, *26*, 361–431.
- [18] C. J. Cao, M. S. Johnson, M. M. Hurley, T. M. Klapötke, In Vitro Approach to Rapid Toxicity Assessment of Novel High-Nitrogen Energetics, *JANNAF J. Propuls. Energet.* **2012**, *5*, 41–51.
- [19] a) *Wasserbeschaffenheit - Bestimmung der Hemmwirkung von Wasserproben auf die Lichtemission von Vibrio Fischeri (Leuchtbakterientest)*, Vol. DIN EN ISO 11348-2, **2009**; b) *Standard Test Method for Assessing the Microbial Detoxification of Chemically Contaminated Water and Soil Using a Toxicity Test With a Luminescent Marine Bacterium*, ASTM D5660-96, **1996**.
- [20] a) T. Backhaus, L. H. Grimme, The Toxicity of Antibiotic Agents to the Luminescent Bacterium *Vibrio Fischeri*, *Chemosphere* **1999**, *38*, 3291–3301; b) United Nations, *Globally Harmonized System of Classification and Labeling of Chemicals (GHS)*, 8th ed., UN, New York, **2019**.
- [21] a) A. Srinivasan, T. Viraraghavan, Perchlorate: Health Effects and Technologies for Its Removal from Water Resources, *Int. J. Environ. Res. Public Health* **2009**, *6*, 1418–1442; b) J. Wolff, Perchlorate and the Thyroid Gland, *Pharmacol. Rev.* **1998**, *50*, 89–105; c) O. Dohnán, A. de la Vieja, V. Paroder, C. Riedel, M. Artani, M. Reed, C. S. Ginter, N. Carrasco, The Sodium/Iodide Symporter (NIS): Characterization, Regulation, and Medical Significance, *Endocr. Rev.* **2003**, *24*, 46–77.

- [22] D. Fischer, T. M. Klapötke, J. Stierstorfer, 1,5-Di(nitramino)tetrazole: High Sensitivity and Superior Explosive Performance, *Angew. Chem., Int. Ed.* **2015**, *54*, 10299–10302.
- [23] a) J. W. Fronabarger, M. D. Williams, W. B. Sanborn, J. G. Bragg, D. A. Parrish, M. Bichay, DBX-1 – a Lead Free Replacement for Lead Azide, *Propellants, Explos., Pyrotech.* **2011**, *36*, 541–550; b) T. M. Klapötke, D. G. Piercey, N. Mehta, K. D. Oyler, M. Jorgensen, S. Lenahan, J. S. Salan, J. W. Fronabarger, M. D. Williams, Preparation of High Purity Sodium 5-nitrotetrazolate (NANT): An Essential Precursor to the Environmentally Acceptable Primary Explosive, DBX-1, *Z. Anorg. Allg. Chem.* **2013**, *639*, 681–688.
- [24] a) N. Szimhardt, M. H. H. Wurzenberger, L. Zeisel, M. S. Gruhne, M. Lommel, J. Stierstorfer, Maximization of the Energy Capability Level in Transition Metal Complexes through Application of 1-Amino- and 2-Amino-5H-tetrazole Ligands, *J. Mater. Chem. A* **2018**, *6*, 16257–16272; b) N. Szimhardt, M. Wurzenberger, P. Spieß, T. Klapötke, J. Stierstorfer, Potassium *N*-nitramino-5*H*-tetrazolates - Powerful Green Primary Explosives with High Initiation Capabilities, *Propellants, Explos. Pyrotech.* **2018**, *43*, 1–8.
- [25] N. Fischer, D. Fischer, T. M. Klapötke, D. G. Piercey, J. Stierstorfer, Pushing the Limits of Energetic Materials - the Synthesis and Characterization of Dihydroxylammonium 5,5'-bistetrazole-1,1'-diolate, *J. Mater. Chem.* **2012**, *22*, 20418–20422.
- [26] D. Fischer, T. M. Klapötke, M. Reymann, P. C. Schmid, J. Stierstorfer, M. Sućeska, Synthesis of 5-(1*H*-tetrazolyl)-1-hydroxy-tetrazole and Energetically Relevant Nitrogen-Rich Ionic Derivatives, *Propellants, Explos., Pyrotech.* **2014**, *39*, 550–557.
- [27] T. M. Klapötke, M. Q. Kurz, R. Scharf, P. C. Schmid, J. Stierstorfer, M. Sućeska, 5-(1*H*-Tetrazolyl)-2-hydroxy-tetrazole: A Selective 2*N*-monoxidation of Bis(1*H*-tetrazole), *ChemPlusChem* **2015**, *80*, 97–106.
- [28] K. Hafner, T. M. Klapötke, P. C. Schmid, J. Stierstorfer, Synthesis and Characterization of Asymmetric 1,2-Dihydroxy-5,5'-bitetrazole and Selected Nitrogen-Rich Derivatives, *Eur. J. Inorg. Chem.* **2015**, 2794–2803.
- [29] T. M. Klapötke, A. Dippold, *Preparation of 3,3'-dinitro-5,5'-bistriazole-1,1'-diol and Salts Thereof as Energetic Materials*, WO2014086599A1 Ludwig-Maximilians-Universität, München, Germany., **2014**.
- [30] T. M. Klapötke, M. Leroux, P. C. Schmid, J. Stierstorfer, Energetic Materials Based on 5,5'-Diamino-4,4'-dinitramino-3,3'-bi-1,2,4-triazole, *Chem. – Asian J.* **2016**, *11*, 844–851.
- [31] T. M. Klapötke, P. C. Schmid, S. Schnell, J. Stierstorfer, Thermal Stabilization of Energetic Materials by the Aromatic Nitrogen-rich 4,4',5,5'-tetraamino-3,3'-bi-1,2,4-triazolium Cation, *J. Mater. Chem.* **2015**, *3A*, 2658–2668.

- [32] T. M. Klapötke, P. C. Schmid, S. Schnell, J. Stierstorfer, 3,6,7-Triamino-[1,2,4]triazolo[4,3-B][1,2,4]triazole: A Non-Toxic, High-Performance Energetic Building Block with Excellent Stability, *Chem. – Eur. J.* **2015**, *21*, 9219–92228.
- [33] K. T. Potts, H. R. Burton, J. Bhattacharyya, 1,2,4-Triazoles. XIII. Derivatives of the S-triazolo[1,5-a]pyridine ring System, *J. Org. Chem.* **1966**, *31*, 260–265.
- [34] A. A. Dippold, D. Izsak, T. M. Klapötke, C. Pflüger, Combining the Advantages of Tetrazoles and 1,2,3-Triazoles: 4,5-Bis(tetrazol-5-yl)-1,2,3-triazole, 4,5-Bis(1-hydroxytetrazol-5-yl)-1,2,3-Triazole, and Their Energetic Derivatives, *Chem. - Eur. J.* **2016**, *22*, 1768–1778.
- [35] D. Fischer, T. M. Klapötke, M. Reymann, J. Stierstorfer, Dense Energetic Nitraminofurazanes, *Chem. - Eur. J.* **2014**, *20*, 6401–6411.
- [36] N. Szimhardt, M. H. H. Wurzenberger, A. Beringer, L. J. Daumann, J. Stierstorfer, Coordination Chemistry with 1-Methyl-5H-tetrazole: Cocrystallization, Laser-Ignition, Lead-Free Primary Explosives – One Ligand, Three Goals, *J. Mater. Chem. A* **2017**, *5*, 23753–23765.
- [37] a) M. H. H. Wurzenberger, N. Szimhardt, J. Stierstorfer, Nitrogen-Rich Copper(II) Bromate Complexes: An Exotic Class of Primary Explosives, *Inorg. Chem.* **2018**, *57*, 7940–7949; b) M. H. H. Wurzenberger, N. Szimhardt, J. Stierstorfer, Copper(II) Chlorate Complexes: The Renaissance of a Forgotten and Misjudged Energetic Anion, *J. Am. Chem. Soc.* **2018**, *140*, 3206–3209.
- [38] V. Ochoa-Herrera, G. León, Q. Banihani, J. A. Field, R. Sierra-Alvarez, Toxicity of Copper(II) Ions to Microorganisms in Biological Wastewater Treatment Systems, *Sci. Total Environ.* **2011**, *412–413*, 380–385.
- [39] N. Szimhardt, M. H. H. Wurzenberger, T. M. Klapötke, J. T. Lechner, H. Reichherzer, C. C. Unger, J. Stierstorfer, Highly Functional Energetic Complexes: Stability Tuning Through Coordination Diversity of Isomeric Propyl-linked Ditetrazoles, *J. Mater. Chem. A* **2018**, *6*, 6565–6577.
- [40] A. R. Katritzky, C. W. Rees, *Comprehensive Heterocyclic Chemistry*, Pergamon, Oxford, **1984**.
- [41] W. E. Wick, D. A. Preston, N. H. Terando, J. S. Welles, R. S. Gordee, New Synthetic Antibacterial Compound, 1-(2-Hydroxyethyl)-3-nitro-4-pyrazolecarboxamide, *Antimicrob. Agents Chemother.* **1973**, *4*, 343–345.
- [42] a) M. F. Bölter, A. Harter, T. M. Klapötke, J. Stierstorfer, Isomers of Dinitropyrazoles: Synthesis, Comparison and Tuning of Their Physicochemical Properties, *ChemPlusChem* **2018**, *83*, 804–811; b) M. F. Bölter, T. M. Klapötke, T. Kustermann, T. Lenz, J. Stierstorfer, Improving the Energetic Properties of Dinitropyrazoles by Utilization of Current Concepts, *Eur. J. Inorg. Chem.* **2018**, 4125–4132.

- [43] T. M. Klapötke, J. Stierstorfer, R. Terreux, C. C. Unger, Recent Results in Toxicity Measurements of Energetic Materials, *Int. Annu. Conf. ICT* **2019**, 50th, 85/81–85/89.
- [44] Q. J. Axthammer, T. M. Klapötke, B. Krumm, Efficient Synthesis of Primary Nitrocarbmates of Sugar Alcohols: From Food to Energetic Materials, *Chem. – Asian J.* **2016**, 11, 568–575.
- [45] Q. J. Axthammer, B. Krumm, T. M. Klapötke, Pentaerythritol-Based Energetic Materials Related to PETN, *Eur. J. Org. Chem.* **2015**, 723–729.
- [46] T. M. Klapötke, B. Krumm, C. C. Unger, Energetic Metal and Nitrogen-Rich Salts of the Pentaerythritol Tetranitrate Analogue Pentaerythritol Tetranitrocarbmate, *Inorg. Chem.* **2019**, 58, 2881–2887.
- [47] Q. Zhang, J. Zhang, D. A. Parrish, J. M. Shreeve, Energetic N-trinitroethyl-substituted Mono-, Di-, and Triaminotetrazoles, *Chem. – Eur. J.* **2013**, 19, 11000–11006.
- [48] Q. J. Axthammer, T. M. Klapötke, B. Krumm, R. Scharf, C. C. Unger, Convenient Synthesis of Energetic Polynitro Materials Including (NO₂)₃CCH₂CH₂NH₃-Salts Via Michael Addition of Trinitromethane, *Dalton Trans.* **2016**, 45, 18909–18920.
- [49] T. M. Klapötke, B. Krumm, R. Moll, Polynitroethyl- and Fluorodinitroethyl Substituted Boron Esters, *Chem. – Eur. J.* **2013**, 19, 12113–12123.
- [50] A. L. Fridman, O. B. Kremleva, V. S. Zalesov, Z. V. Platonova, F. A. Gabitov, L. A. Rubinshtein, A. N. Plaksina, Synthesis and Physiological Activity of Aliphatic Nitro Compounds, *Pharm. Chem. J.* **1977**, 11, 64–67.
- [51] S. Heimsch, T. M. Klapötke, Hypergolicity and Ignition Delay Study of 2-Azidoethanol and Hydrogen Peroxide, *Int. J. Energ. Mater. Chem. Propul.* **2019**, 18, 1–8.
- [52] T. M. Klapötke, *Energetic Materials Encyclopedia*, De Gruyter, Berlin, **2018**.
- [53] a) Y. Zheng, J. Zhou, D. Zhou, M. Zhang, Synthesis of 1,1,2,2-Tetrakis(difluoroaminomethylenenitroamino)ethane and Its Related Compounds, *Binggong Xuebao* **1988**, 59–63; b) D. Wan, Reactions of 1,1,2,2-Tetranitroaminoethane and Properties of Its Tetrasodium Salt, *Proc. Int. Pyrotech. Semin.* **1991**, 17th, 231–234.
- [54] Y. Lee, P. Goede, N. Latypov, H. Oestmark, Synthesis and Analysis of N,N',N'',N'''-Tetranitro-1,1,2,2-ethanetetramine and Energetic Salts Thereof, *Int. Annu. Conf. ICT* **2005**, 36th, 124/121–124/129.

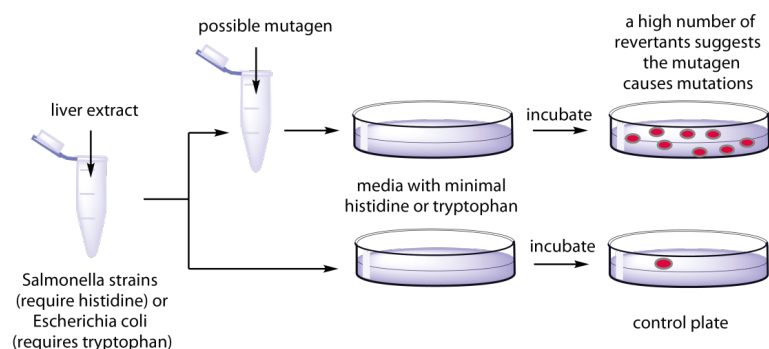
8 Comparative Toxicological Study

Recent Results in Toxicity Measurements of Energetic Materials

T. M. Klapötke, J. Stierstorfer, R. Terreux and C. C. Unger

Proceedings of the 50th Int. Annual Conference of the Fraunhofer ICT,

Karlsruhe, Germany, **2019**, 18909–18920.



8.1 Abstract

The luminescent bacteria inhibition test using *Vibrio fischeri* is a well-established method to determine the aquatic toxicity. The determined parameter is the effective concentration (EC₅₀) after 15 and 30 min. The inhibition of natural bioluminescence of these bacteria gives a first idea of the toxicity of compounds towards different ecosystems. It is a cost and time efficient experimental method, which does not involve animals. Different types of energetic materials such as coordination (*e. g.* [Cu(dtp)₃](ClO₄)₂), neutral (*e. g.* azidoethanol and propyl-linked ditetrazoles) and ionic (*e. g.* polynitropyrazoles, -triazoles and tetrazoles) compounds were investigated and compared to commonly used materials, like RDX, ammonium perchlorate (AP) and azide salts. Furthermore, different substitution patterns and energetic functionalities such as azido-, nitro-, fluorodinitro- and nitramino-groups were investigated.

Another well-established method for evaluating the harmful potential of a certain substance is the AMES test. This OECD accepted method uses bacteria to test if mutations can be caused in the DNA of the organism and is the minimum test carried out in the course of REACH. The herein provided study includes first comprehensive results of time economic aquatic toxicity measurements and well approved AMES test for energetic materials. The experimental results were further compared to *in silicio* studies based on a highly developed algorithm.

8.2 Introduction

Research efforts in the field of energetic materials are constantly driven towards finding new energetic ingredients or materials with maximum performance and acceptable insensitivity characteristics, which are affordable, due to an efficient up-scalable synthesis.¹⁻³ Since the 70 s and early 90 s, first reports show that munitions manufacturing and ancillary operations led to concerns of the environmental impact, too.⁴⁻⁵ In the specific cases, the loss of entire biological communities has been associated with dispersal of trinitrotoluene (TNT) waste streams into surface waters and onto soil, ranging from plants up to fishes.⁶⁻⁹ Further toxicological evaluation of TNT wastewaters towards mammals (dogs, rats and mice) confirmed former findings¹⁰ and demonstrated, that damaging the ecosystem could also have a direct impact for humans, especially once drinking water is contaminated.¹¹ This further influenced the development of new explosives, propellants and pyrotechnics, and therefore, the requirement for fast, cost-effective and reliable toxicity tests. Despite different toxicity mechanisms for various organisms of different species, a substance that is toxic for an organism often demonstrates similar toxic effects on another organism. Comparing the toxicity values of pentaerythritol tetranitrate (PETN) and

TNT in *Vibrio fischeri* (a bioluminescent bacteria), *Daphnia magna* (a planktonic crustacean), *Pimephales promelas* (fathead minnow) and rats, the effective concentration (EC), lethal concentration (LC) respectively the lethal dose (LD) of TNT is lower than those of PETN (Table 8.1).^{4, 12-13} In summary, TNT is more toxic than PETN in every organism, but the incubation time varies dramatically.

Table 8.1 Half maximal concentration (EC₅₀), median lethal concentration (LC₅₀) and median lethal dose (LD₅₀) of PETN and TNT in *Vibrio fischeri*, *Daphnia magna*, *Pimephales promelas* and rats.

Compound	<i>Vibrio fischeri</i> EC ₅₀ (30 min) [mg L ⁻¹]	<i>Daphnia magna</i> EC ₅₀ (48 h) [mg L ⁻¹]	<i>Pimephales promelas</i> LC ₅₀ (96 h) [mg L ⁻¹]	Rat LD ₅₀ (oral) [mg kg ⁻¹]
TNT	3.59	11.9	3.1	607
PETN	14.54	8500	2700	1660

Regarding Table 8.1 the gram-negative bacteria *Vibrio fischeri* is the organism of choice to get a first impression how a new energetic material once entered the environment could affect the groundwater. In the continuing development of an explosive, further tests are needed especially when the progress is on an industrial scale. In 2007 REACH (Registration, Evaluation and Authorization of Chemicals) became law in the European Union, aiming to evaluate the risk of chemical substances produced, used or imported in quantities of 1–100 tons per year. The first test, which should be performed for registration under REACH is the OECD-accepted AMES test. The so called bacterial reverse mutation test is a straightforward, relatively cheap and fast (incubation period of 48–72 hours) test to recognize the mutagenic potential of a certain compound.¹⁴ Even faster and way cheaper is to predict the test results using Quantitative Structure-Activity Relationship (QSAR), which the European Chemicals Agency (ECHA) directly encourages to apply.¹⁵ In this contribution a comprehensive study of experimental and *in silico* AMES test results as well as experimental EC₅₀ values obtained from *Vibrio fischeri* are presented.

8.3 Materials and Methods

8.3.1 Test Compounds

Commercially available compounds were used as supplied without further purification. In house synthesized materials were at least analyzed with NMR and vibrational spectroscopy and purity was determined using elemental analysis.

8.3.2 Microtox Assay

The EC_{50} (effective concentration) values were determined with a LUMI-Stox 300 spectrometer obtained by HACH LANGE GmbH, as described by the provider. The measurement is based on the bioluminescence of *Vibrio fischeri* NRRL-B-11177 bacteria strains, whereby the EC_{50} is the concentration level where the bioluminescence is decreased by 50%. Prior to the measurement, a ten-point dilution series was prepared according to DIN/EN/ISO 11348 (without G1 level) with a known weight of the compounds and a 2% NaCl stock solution.¹⁶ The measurements, which strictly have to be carried out at 15 °C, than started by determination of the bioluminescence of untreated reactivated bacteria. After 15 and 30 minutes exposure time with a specific amount of component, the bioluminescence was determined again. The compounds toxicity was afterwards classified according to their EC_{50} values (non-toxic $> 1.00 \text{ g L}^{-1}$; toxic $0.10\text{--}1.00 \text{ g L}^{-1}$; very toxic $< 0.10 \text{ g L}^{-1}$).¹⁷

8.3.3 Experimental Ames test

The Ames test is used to detect point mutations, which involves substitution, addition or deletion of one or a few DNA base pairs. OECD Guidelines for Testing of Chemicals (No. 471) form the basis for the test, which employs auxotrophic strains of *Salmonella typhimurium* (TA98, TA100, TA1535, TA1537) and *Escheria coli* (wp2[pKM101]+wp2 uvrA mixed 1:2).¹⁴ The biosynthesis of the corresponding amino acids is blocked by point mutations, made in the histidine (*Salmonella typhimurium*) or the tryptophan (*Escheria coli*) operon. The mutagenic potential is evaluated by detecting the appearance of the reverse mutants of the auxotrophic strains, making them prototrophs, able to grow in corresponding deficient media. In addition, rat liver S9 was chemically introduced to simulate the effect of metabolism, since certain compounds, like benzopyren, become mutagenic only after their metabolic conversion. The tests were carried out by the company Enamine Ltd.

8.3.4 QSAR Ames test

QSAR Ames Test provides predicted values of the experimental Ames test. Values are determined for one molecule. Quantitative structure activity relationship (QSAR) methods used require a linear model made of molecular descriptors. This model is set by fitting descriptors of the training set molecule with their experimental values. In our system, experimental AMES tests values come from five different AMES databases experimentally validated; the final database is composed of more than 7.700 molecules with experimental values of the AMES test.

The AMES test is a macroscopic test which is the result of thousands of biochemical mechanisms. One limitation of QSAR methods is that they are only able to model one single mechanism. This is why, one QSAR model which could provide predicted AMES values for one

kind of molecules is not possible. The idea is to create an ad-hoc QSAR model devoted to predicting only one molecule using similar molecules. The assumption that we made is that similar molecules should have the same mechanism as the molecule to predict. We used On-the-flight QSAR methods to develop such one-shot model. To select similar compounds, we developed a Recursive Molecular Search (R.Mo.S) algorithm which selects similar compounds based on MACCS fingerprint and computes a virtual fingerprint signature. This signature is then used in the next round to select more molecules. The algorithm stops when a sufficient number of molecules is selected or when there is no more similar compound to select. The algorithm is patented by ArianeGroup (AGS) and French National Center for Scientific Research (CNRS). Using the training set with experimental value of the AMES test, 2D descriptors are computed and machine learning algorithm, extra trees from scikit learn package, are used to predict the AMES test values. The predicted value is comprised between 0 and 1. If the predicted AMES value is between 0 and 0.4 the result is non mutagenic, between 0.4 and 0.6 the molecule should be mutagenic and if the value is comprised between 0.6 and 1 the result is doubtful.

8.4 Results and Discussion

To show a trend in the aquatic toxicity towards *Vibrio fischeri*, different types of energetic materials were tested. The herein presented compounds are a small selection of possible primary- and secondary explosives, oxidizers and pyrotechnical materials with different chemical constitution. There are coordination (*e. g.* $[\text{Cu}(\text{dtp})_3](\text{ClO}_4)_2$), neutral (*e. g.* azidoethanol and propyl-linked ditetrazoles) and ionic (*e. g.* polynitropyrazoles, -triazoles and tetrazoles) compounds, also different substitution patterns and energetic functionalities such as azido-, nitro-, fluorodinitro- and nitramino-groups were investigated. Finally, they were compared to commonly used materials, like RDX, ammonium perchlorate (AP) and azide salts.

Comparative Toxicological Study

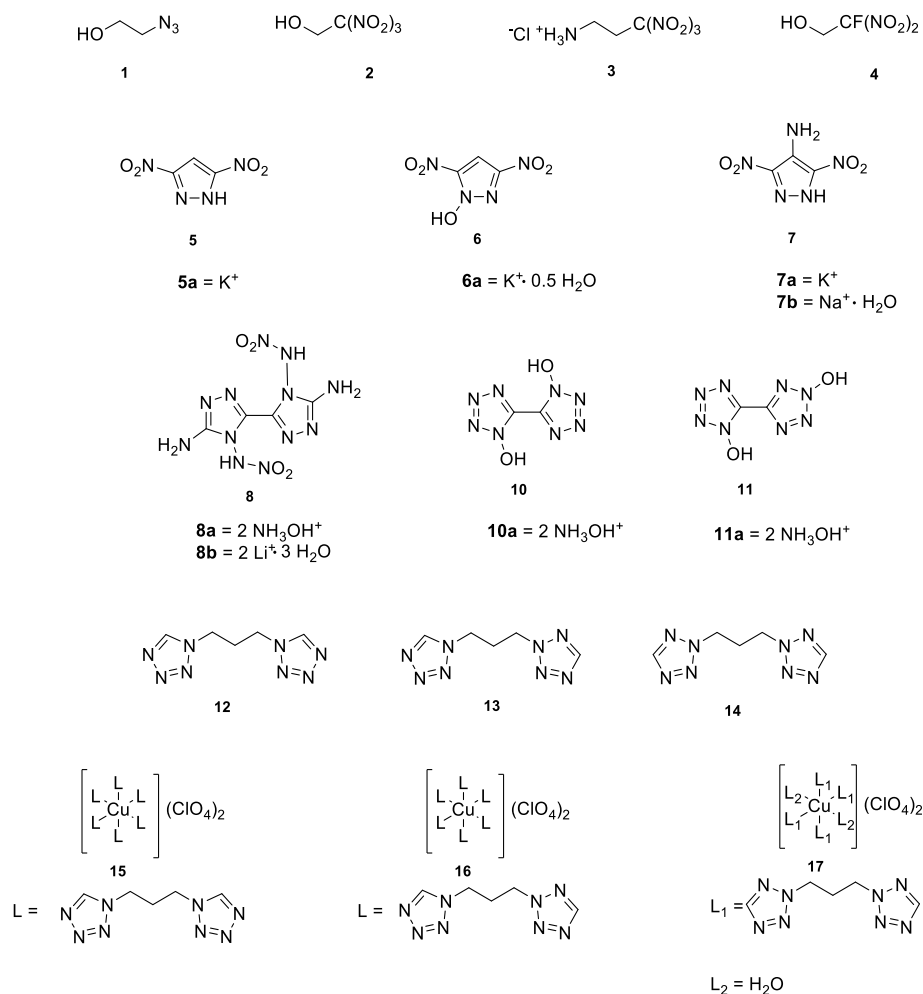


Figure 8.1 Overview of measured compounds 1–17.

Comparing 2-azidoethanol (**1**), 2,2,2-trinitroethanol (**2**), 3,3,3-trinitropropylammonium chloride (**3**) and 2-fluoro-2,2-dinitroethanol (**4**), **1** is the least toxic compound towards *Vibrio fischeri*.¹⁸⁻²¹ It is also relatively low in toxicity compared to ionic azide compounds NaN_3 and NH_4N_3 . Once adding a trinitroalkyl moiety the toxicity drops dramatically and is even worse with a fluorodinitroethyl moiety. This is consistent with former toxicity measurements using gram positive bacteria such as *Staphylococcus aureus* and *Intestinal bacillus*.²² 2,4-Dinitropyrozoles show toxicity towards the aquatic bacteria, though it is considered as moderate toxic. The findings were comparable, no matter if they were measured as neutral compound as 1-oxid or 3-amin, or measured as salts.²³⁻²⁵ The neutral nitraminotriazole **8** is very toxic towards *Vibrio fischeri*, whereas the hydroxylammonium salt **8a** is moderately toxic and the lithium salt **8b** is considered not toxic in this test. The substitution pattern can have a varying effect on the toxicity of tetrazoles. Tetrazoles **10a** and **11a** are both moderately toxic, whereby TKX-50 (salt **10a**) still is less toxic.²⁶ Furthermore, it is even less toxic than the common used secondary explosive RDX.²⁷ For tetrazoles **12–14**, which also have varying substitution patterns, the toxicity ranges from EC_{50} values of 0.36 g L^{-1} (**14**) to 10.30 g L^{-1} (**12**). Once adding the copper(II) metal, which is known

for being toxic to microorganisms,²⁸ the toxicities of the complexes of tetrazoles **12–14** increases partially dramatically. Nonetheless, complexes **15–17**, which could be used as potential primary explosives are less toxic compared to the measured azide salts.²⁹

Table 8.2 EC₅₀ values of measured compounds after 15 and 30 minutes in g L⁻¹ and their considered toxicity level after 30 minutes (-/+/>++).

Compound	EC50 (15 min) [g L ⁻¹]	EC50 (30 min) [g L ⁻¹]	Toxicity level	Compound	EC50 (15 min) [g L ⁻¹]	EC50 (30 min) [g L ⁻¹]	Toxicity level
NaN ₃	0.25	0.18	+	7a	0.75	0.74	+
NH ₄ N ₃	0.26	0.15	+	7b	0.60	0.58	+
NH ₄ NO ₃	10.49	6.39	-	8	0.13	0.07	++
NH ₄ N(NO ₂) ₂	7.25	4.50	-	8a	0.75	0.35	+
NH ₄ ClO ₄	14.58	11.13	-	8b	>1.58	>1.58	-
RDX	0.33	0.24	+	10a	1.17	0.58	+
1	8.70	8.55	-	11a	0.32	0.24	+
2	0.29	0.22	+	12	13.90	10.30	-
3	<0.10	<0.10	++	13	0.81	0.79	+
4	0.002	0.001	++	14	0.36	0.36	+
5	0.27	0.19	++	15	0.44	0.35	+
5a	1.21	0.95	-	16	0.64	0.44	+
6a	0.70	0.43	+	17	0.34	0.28	+

The mutagenic potential of salts **8b** (Li₂ANAT) and **10a** (TKX-50) were evaluated using the AMES test with S9 mixture.¹⁴ The toxicological potential of salt **7a** was evaluated using *Vibrio fischeri*, due to its high water-solubility and because it is the water-soluble monomer of BDNAPM, a highly potential secondary explosive. BDNAPM (Figure 8.1) was also experimentally tested with the AMES test, but cannot be evaluated using *Vibrio fischeri* itself, because of its low water-solubility. All experimental findings were calculated using a smart algorithm and are listed in Table 8.3.³⁰ The toxicity respectively mutagenic potential of the compounds in Table 8.2 and Table 8.3 are rated as non-toxic/mutagenic (-), moderately toxic/mutagenic (+) and toxic/mutagenic (++).

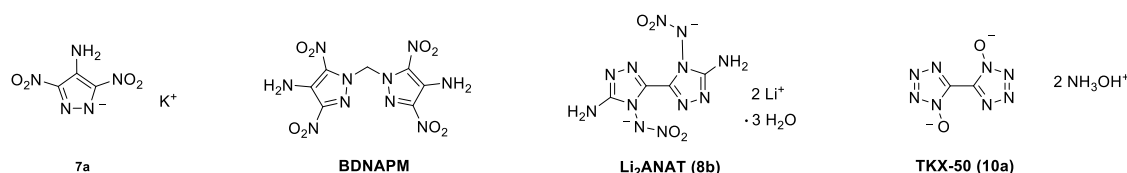


Figure 8.2 Compounds evaluated using AMES test and *Vibrio fischeri*.

The R.Mo.S QSAR offers good predictions for the values of the AMES test. The selection made by R.Mo.S probably chose few similar molecules to have the right prediction. Other software, such as ACD percepta, predict all three molecules to be mutagenic. Aromatic nitro moiety is also well known to be more mutagenic than the nitro chemical function. These moieties are probably involved in the positive mutagenic prediction of ACD Percepta software. The absence of this moiety could explain the non-mutagenic properties of TKX-50. This indeed was confirmed by the experimental AMES test. It was no mutagenic potential in all tested strains of *S. typhimurium* and *E. coli* observed. For Li₂ANAT there was mutagenic activity in some strains of *S. typhimurium* (TA1535 and TA100) as well as for *E. coli*. The same compound showed in the metabolic activation assay a weak mutagenic activity for TA98, TA1535 and for *E. coli*. These results correlate well with the calculations of the *in silicio* AMES test, pointing out that there is no result which indicates clearly if the compound is mutagenic or not. In contrast, BDNAPM shows mutagenic activity in all tested strains with and without metabolic activation, as well as the QSAR AMES test. Also, its water-soluble precursor **7a** has a mutagenic activity by calculating its AMES test results. Comparing the AMES test results with the aquatic toxicity using *Vibrio fischeri*, the correspondence is not perfect but up to now, a slight trend can be drawn. The mutagenic compounds **7a** and BDNAPM also show a moderate aquatic toxicity for the water-soluble **7a**, in consequence these findings could further emphasize the impact of pyrazoles towards humans and the environment. The somehow mutagenic Li₂ANAT is not toxic towards *Vibrio fischeri*, whereas TKX-50 is not mutagenic, but TKX-50 has a slight impact on the economy. This could also result from the hydroxylammonium cation, which is known for having a more negative effect on the toxicity against *Vibrio fischeri* than other cations.¹⁹

Table 8.3 Results of experimental and *in silicio* AMES test and the considered mutagenicity/toxicity level (-/+/>+).

Compound	QSAR AMES test	Experimental AMES test	<i>Vibrio fischeri</i>
7a	++	n.a.	+
BDNAPM	++	++	n.a.
Li₂ANAT	Doubtful	+	-
TKX-50	-	-	+

8.5 Conclusion

The aquatic toxicity of 20 energetic compounds of different types, such as coordination, ionic and neutral with varying substitution pattern were investigated and some trends are discussed. Furthermore, they were compared to commonly used materials, like RDX, ammonium perchlorate (AP) and azide salts. Three compounds were further investigated according their mutagenic potential using the AMES test. The experimental AMES test values range from not mutagenic (TKX-50), to somehow mutagenic (Li₂ANAT) and to mutagenic (BDNAPM). The R.MoS QSAR offers good predictions for the values of the AMES test, all calculated results are consistent with the experimental values. *Vibrio fischeri* seems to show comparable trends, but further research effort is ongoing to underline these results.

8.6 References

1. Office of Naval Research Home Page. <http://www.onr.navy.mil> (accessed April 02, 2019).
2. Klapötke, T. M., *Chemistry of High-Energy Materials*. 4th ed., De Gruyter, Berlin, **2017**.
3. Pagoria, P. F.; Lee, G. S.; Mitchell, A. R.; Schmidt, R. D., A review of energetic materials synthesis. *Thermochim. Acta* **2002**, *384*, 187–204.
4. Drzyzga, O.; Gorontzy, T.; Schmidt, A.; Blotevogel, K. H., Toxicity of Explosives and Related Compounds to the Luminescent Bacterium *Vibrio fischeri* NRRL-B-11177. *Arch. Environ. Contam. Toxicol.* **1995**, *28*, 229–235.
5. Rosenblatt, D. H.; Burrows, E. P.; Mitchell, W. R.; Parmer, D. L., *Organic Explosives and Related Compounds*. Springer, Berlin/Heidelberg, **1991**.
6. Johnson, L. R.; Davenport, R.; Balbach, H.; Schaeffer, D. J., Phototoxicology.: 2. Near-Ultraviolet Light Enhancement of Microtox Assays of Trinitrotoluene and Aminodinitrotoluenes. *Ecotoxicol. Environ. Saf.* **1994**, *27*, 23–33.
7. Cairns, J.; Dickson, K. L. *The Effects of Waste Discharges from Radford Army Ammunition Plant on the biota of the New River, Virginia*, 1973.
8. Palazzo, A. J.; Leggett, D. C. *Effect and Disposition of TNT in a Terrestrial Plant and Validation of Analytical Methods*; Maryland, 1986.
9. Sanocki, S. L.; Simon, P. B.; Weitzel, R. L.; Jerger, D. E.; Schenk, J. E. *Aquatic Field Surveys at Iowa, Radford and Joliet Army Ammunition Plants*; Washington, D. C., 1976.
10. Dilley, J. V.; Tyson, C. A.; Newell, G. W. *Mammalian Toxicological Evaluation of TNT Wastewaters*; Washington, D. C., 1978.

11. United States Environmental Protection Agency (EPA) Home Page. <https://www.epa.gov/> (accessed April 03, 2019).
12. Reddy, G.; Chandra, S. A. M.; Lish, J. W.; Charles W. Quails, J., Toxicity of 2,4,6-Trinitrotoluene (TNT) in Hispid Cotton Rats (*Sigmodon hispidus*): Hematological, Biochemical, and Pathological Effects. *Int. J. Toxicol.* **2000**, *19*, 169–177.
13. TOXNET Toxicology Data Network. <https://chem.nlm.nih.gov/chemidplus/> (accessed April 03, 2019).
14. OECD, *Test No. 471: Bacterial Reverse Mutation Test*. **1997**.
15. ECHA, *Guidance on Information Requirements and Chemical Safety Assessment. Chapter R.6: QSARs and Grouping of Chemicals*. **2008**.
16. Wasserbeschaffenheit - Bestimmung der Hemmwirkung von Wasserproben auf die Lichtemission von *Vibrio Fischeri* (Leuchtbakterientest). In *Wasserbeschaffenheit - Bestimmung der Hemmwirkung von Wasserproben auf die Lichtemission von Vibrio Fischeri (Leuchtbakterientest)*, 2009; Vol. DIN EN ISO 11348-2.
17. Cao, C. J.; Johnson, M. S.; Hurley, M. M.; Klapötke, T. M., In Vitro Approach to Rapid Toxicity Assessment of Novel High-Nitrogen Energetics. *JANNAF J. Propuls. Energet.* **2012**, *5*, 41–51.
18. Heimsch, S.; Klapötke, T. M., Hypergolicity and Ignition Delay Study of 2-azidoethanol and Hydrogen Peroxide. *Int. J. Energ. Mater. Chem. Propul.* **2019**, *18*, 1–8.
19. Klapötke, T. M.; Scharf, R.; Stierstorfer, J. In *Aquatic toxicity determination of energetic materials using the luminescent bacteria inhibition test*, University of Pardubice, Institute of Energetic Materials, **2014**; 769–773.
20. Göbel, M.; Klapötke, T. M., 2,2,2-Trinitroethanol. *Acta Crystallogr., Sect. C: Cryst. Struct. Commun.* **2007**, *63*, 562–o564.
21. Klapötke, T. M.; Krumm, B.; Moll, R., Polynitroethyl- and Fluorodinitroethyl Substituted Boron Esters. *Chem. – Eur. J.* **2013**, *19*, 12113–12123.
22. Fridman, A. L.; Kremleva, O. B.; Zalesov, V. S.; Platonova, Z. V.; Gabitov, F. A.; Rubinshtein, L. A.; Plaksina, A. N., Synthesis and Physiological Activity of Aliphatic Nitro Compounds. *Pharm. Chem. J.* **1977**, *11*, 64–67.
23. Bölter, M. F.; Harter, A.; Klapötke, T. M.; Stierstorfer, J., Isomers of Dinitropyrazoles: Synthesis, Comparison and Tuning of their Physicochemical Properties. *ChemPlusChem* **2018**, *83*, 804–811.
24. Bölter, M. F.; Klapötke, T. M.; Kustermann, T.; Lenz, T.; Stierstorfer, J., Improving the Energetic Properties of Dinitropyrazoles by Utilization of Current Concepts. *Eur. J. Inorg. Chem.* **2018**, 4125–4132.

25. Fischer, D.; Gottfried, J. L.; Klapötke, T. M.; Karaghiosoff, K.; Stierstorfer, J.; Witkowski, T. G., Synthesis and Investigation of Advanced Energetic Materials Based on Bispyrazolylmethanes. *Angew. Chem.* **2016**, *128*, 16366–16369.
26. Fischer, D.; Klapötke, T. M.; Reymann, M.; Schmid, P. C.; Stierstorfer, J.; Sućeska, M., Synthesis of 5-(1*H*-Tetrazolyl)-1-hydroxy-tetrazole and Energetically Relevant Nitrogen-Rich Ionic Derivatives. *Propellants, Explos., Pyrotech.* **2014**, *39*, 550–557.
27. Fischer, D.; Klapötke, T. M.; Reymann, M.; Stierstorfer, J., Dense Energetic Nitraminofurazanes. *Chem. - Eur. J.* **2014**, *20*, 6401–6411.
28. Ochoa-Herrera, V.; León, G.; Banihani, Q.; Field, J. A.; Sierra-Alvarez, R., Toxicity of Copper(II) Ions to Microorganisms in Biological Wastewater Treatment Systems. *Sci. Total Environ.* **2011**, *412–413*, 380-385.
29. Szimhardt, N.; Wurzenberger, M. H. H.; Beringer, A.; Daumann, L. J.; Stierstorfer, J., Coordination chemistry with 1-methyl-5*H*-tetrazole: cocrystallization, laser-ignition, lead-free primary explosives - one ligand, tree goals. *J. Mater. Chem. A* **2017**, *5*, 23753–23765.
30. Alliod, C.; Chemelle, J.-A.; Jacob, G.; Terreux, R., Ames Test Prediction on High Energy Molecules by On-The-Fly QSAR (OTF-QSAR). *Propellants, Explos., Pyrotech.* **2017**, *42*, 24–35.

III Summary and Conclusion

With the aim to develop an alternative to the commonly used oxidizer ammonium perchlorate (AP), various oxygen-rich molecules were synthesized and thoroughly characterized. In order to find use as high-energy dense oxidizers (HEDOs) in composite propellants, these molecules were designed to meet further requirements besides an excellent oxygen content. A high thermal stability ($T_{\text{melt}} > 150\text{ }^{\circ}\text{C}$), moderate sensitivity ($\text{IS} > 4\text{ J}$, $\text{FS} > 80\text{ N}$) and sufficient specific impulse ($I_s > 250\text{ s}$) was achieved by some of the perchlorate-free molecules.

Synthetic strategies in chapters 1–6 of this thesis are based on the insertion of trinitroethyl moieties, salt formation and/or the combination with oxygen- and nitrogen-rich heterocycles. The most promising candidates of each chapter are depicted in Figure S1. Chapters 7 and 8 address the toxicity of energetic materials by the determination of the aquatic toxicity with the luminescent bacteria inhibition test as well as the AMES test. Each chapter is a research project including its own abstract, introduction, results and discussion, experimental section and conclusion.

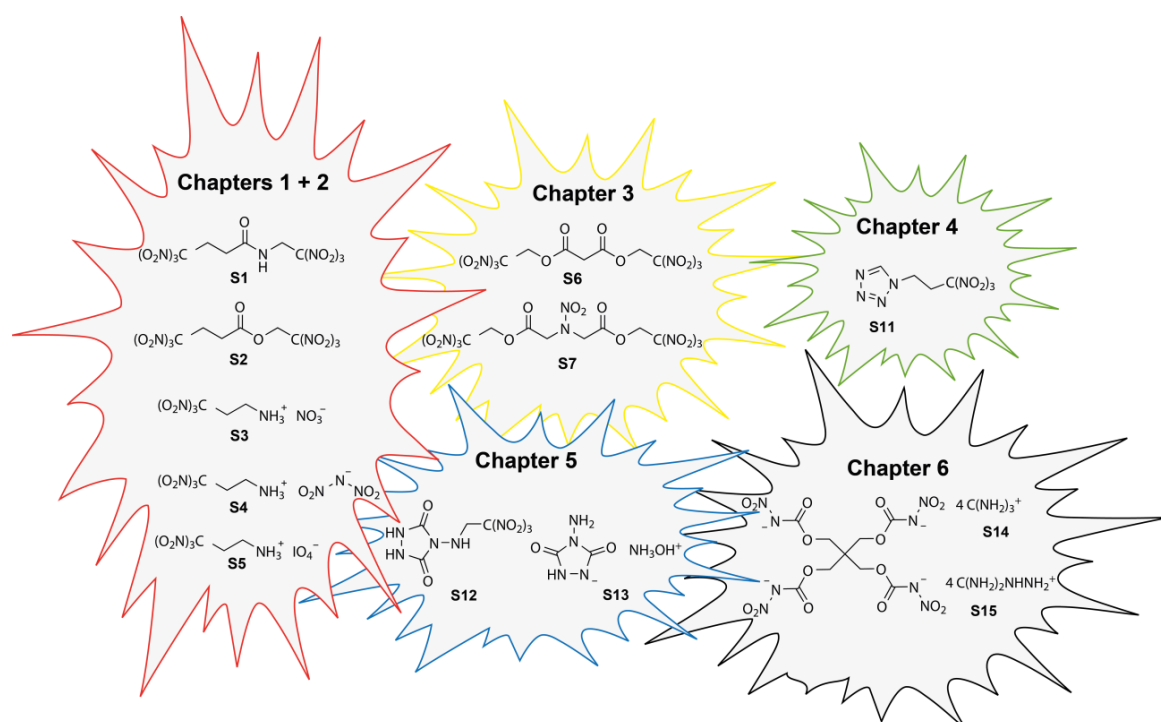


Figure S1. Overview of the most promising molecules.

Chapter 1 and **Chapter 2** start with the Michael addition of trinitromethane to acrylamide, which is a straightforward synthesis. The first two promising candidates of **Chapter 1** are the 4,4,4-trinitro-*N*-(2,2,2-trinitroethyl)butanamide (**S1**) and 2,2,2-trinitroethyl-4,4,4-trinitrobutanoate (**S2**), which already have oxygen balances of 20.7% (**S1**) and 14.5% (**S2**) assuming the formation

of CO. Furthermore, they are relatively easily accessible, in contrast to the trinitropropylammonium cation-based nitrate (**S3**) and dinitramide salts (**S4**), which synthesis needs more effort. Nonetheless, the salts show extraordinary detonation and combustion parameters, especially **S4**. With a detonation velocity of 9401 m s^{-1} and a detonation pressure of 375 kbar according to EXPLO5, it even exceeds common secondary explosives like TNT, PETN, and RDX by far. Furthermore, the specific impulse ($I_s = 270 \text{ s}$) is superior to AP ($I_s = 261 \text{ s}$) in comparable mixtures.

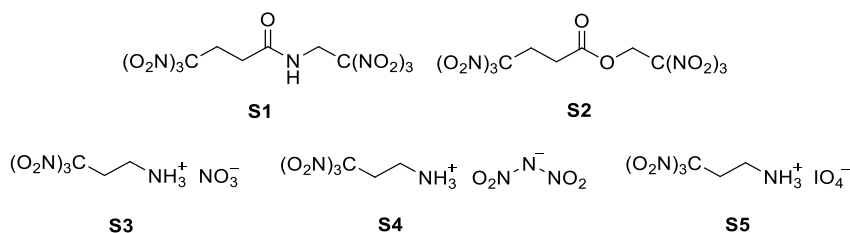
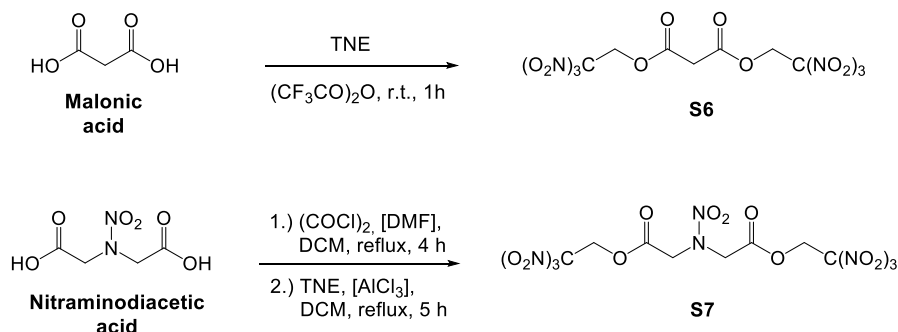


Figure S2. Molecular structures of 4,4,4-trinitro-*N*-(2,2,2-trinitroethyl)butanamide (**S1**), 2,2,2-trinitroethyl-4,4,4-trinitrobutanoate (**S2**) and the nitrate (**S3**), dinitramide (**S4**) and periodate (**S5**) salt of the trinitropropylammonium cation.

More unusual anions were introduced to the trinitropropylammonium cation in **Chapter 2**. Thereby, the periodate anion was evaluated as alternative to perchlorates. Even though the performance of the trinitropropylammonium periodate (**S5**) was not comparable to the nitrate and dinitramide salt, the high density of $\delta = 2.12 \text{ g cm}^{-3}$ and relatively high thermal stability of $T_{\text{dec}} = 138 \text{ }^\circ\text{C}$ (cf. **S3** ($138 \text{ }^\circ\text{C}$) and **S4** ($112 \text{ }^\circ\text{C}$)) is remarkable.

Chapter 3 is based on the economic starting materials, malonic acid and iminodiacetic acid. After nitration of iminodiacetic acid, the nitraminodiacetic acid and malonic acid were converted into the corresponding bis(2,2,2-trinitroethyl) ester in a one-step procedure (Scheme S1).



Scheme S1. Synthesis of the malonic acid bis(2,2,2-trinitroethyl ester) (MaBTNE, **S6**) and nitraminodiacetic acid bis(2,2,2-trinitroethyl ester) (NABTNE, **S7**).

Due to the promising thermal stability of **S7** ($T_{melt} = 151\text{ °C}$), sensitivity ($IS = 6\text{ J}$; $FS = 252\text{ N}$) and oxygen balance ($\Omega_{CO} = 19.1\%$), the specific impulse was calculated with EXPLO5 V6.03 in various binder systems for a potential application. In a mixture with 14% bis(azidomethyl)oxetane (BAMO) and 16% aluminum, the specific impulse ($I_s = 261\text{ s}$) slightly exceeded the values of AP in a common composite propellant mixture with HTPB ($I_s = 259\text{ s}$). The aging behavior, which is crucial for long-time storage, was estimated using the AKTS software package based on TGA measurements (Figure S3).

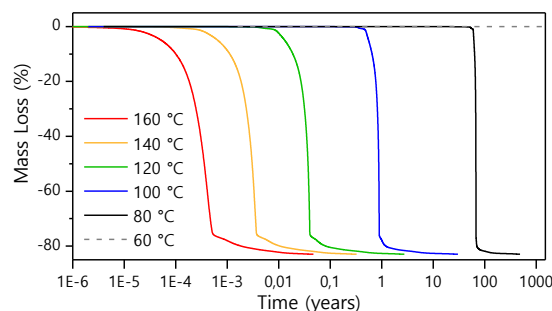
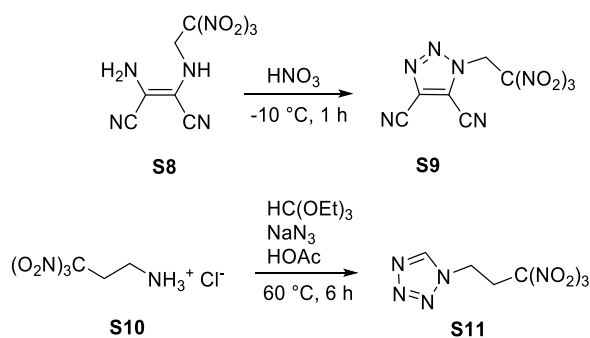


Figure S3. Simulation of the decomposition of **S7** at different temperatures under isothermal conditions.

The simulations are based on different models and revealed, *e. g.* constant storing of **S7** at 80 °C for 1000 d would not lead to significant decomposition reactions. Further results showed, that **S7** could be a promising candidate according to its storability.

In **Chapter 4** two heterocycles equipped with the trinitroethyl moiety, which were accessed *via* different synthetic approaches, are compared (Scheme S2). The ring closure from amino-(trinitroethylamino)maleonitrile (**S8**) to 4,5-dicyano-1*N*-(trinitroethyl)-1,2,3-triazole (**S9**) occurred unexpectedly by nitrosation through treatment with HNO_3 . It was assumed, that in the nitric acid sufficient amounts of the nitrosonium cation NO^+ prevail and reacts with the maleonitrile, as control experiments with nitrite in HCl and H_2SO_4 resulted in **S9** as well. Whereas, the 1*N*-trinitropropyl tetrazole (**S11**) was obtained by the classical cyclization of trinitropropylammonium chloride (**S10**) with sodium azide and triethyl orthoformate, leading to the first isolated *N*-substituted trinitroalkyl tetrazole (**S11**).



Scheme S2. Reaction sequence to triazole **S9** and tetrazole **S11**.

Suitable single crystals for X-ray diffraction measurements were obtained for compounds **S9** and **S11** as shown in Figure S4. The trinitro moiety in both structures is arranged in the classical propeller-like motif, furthermore they crystallize in the related monoclinic space groups $P2_1/n$ and $P2_1/c$.

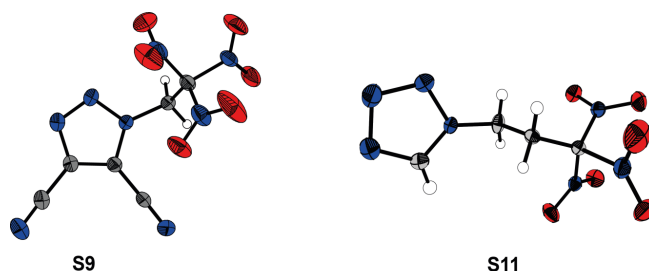


Figure S4. Molecular structures of **S9** and **S11** determined by X-ray diffraction.

The energetic parameters of **S11** ($V_{\text{Det}} = 8388 \text{ m s}^{-1}$, $p_{\text{CJ}} = 293 \text{ kbar}$) are almost in the range of PETN (pentaerythritol tetranitrate; $V_{\text{Det}} = 8405 \text{ m s}^{-1}$ and $p_{\text{CJ}} = 319 \text{ kbar}$), which is a commonly used secondary explosive. Moreover, the specific impulse I_{sp} in mixtures with 15% aluminium and 14% binder is 252 s, compared to the AP ($I_{\text{sp}} = 256 \text{ s}$) this still is in an appropriate range.

In **Chapter 5** the heterocycle urazine was used as starting material, which can be obtained from the low-cost starting materials carbonylhydrazide and HCl. Based on the amphoteric character of urazine, cationic and anionic salts were synthesized. The molecule was also incorporated in a copper(II) complex as neutral ligand. Furthermore, the formation of 4-[(2,2,2-trinitroethyl)amino]-urazole (**S12**) was achieved by the reaction of urazine with nitroform and formaldehyde. Apart from **S12** the hydroxylammonium salt (**S13**) revealed to be an oxygen-rich molecule with good energetic performance parameters but suffered from thermal stability problems.

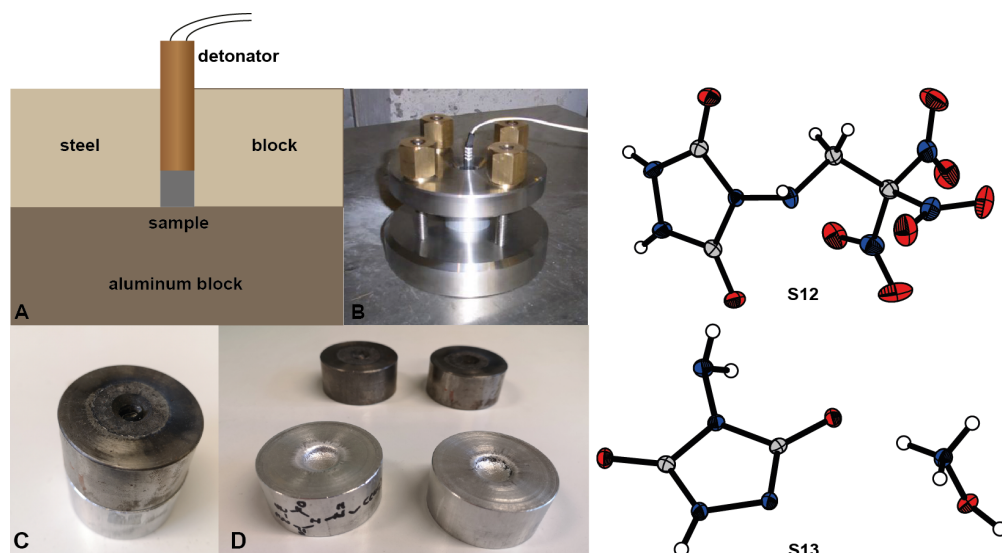
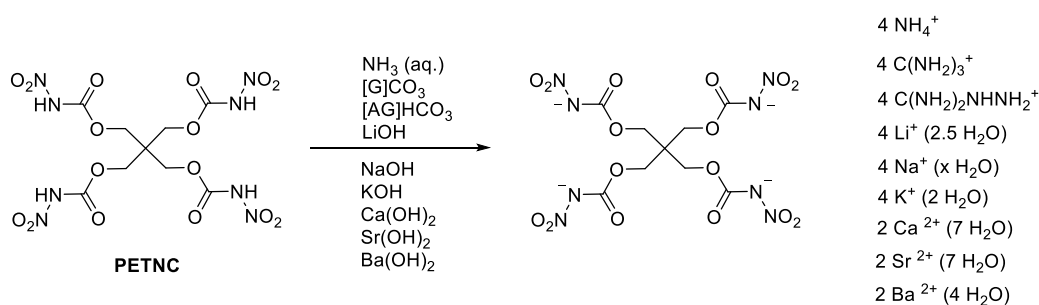


Figure S5. Small-scale shock reactivity test (SSRT) of 4-[(2,2,2-trinitroethyl)amino]-urazole (**S12**). Right: Molecular structure of **S12** and **S13** determined by X-ray diffraction.

In order to get a deeper insight of the detonation performance a small-scale shock reactivity test (SSRT) was performed (Figure S5). After the initiation a dent in the aluminum block is produced, which can be compared to other energetic materials. According to this test, the performance of **S12** ($m_{\text{SiO}_2} = 661 \text{ mg}$) is comparable to classical secondary explosives, such as RDX ($m_{\text{SiO}_2} = 589 \text{ mg}$).

In **Chapter 6** the tetravalent pentaerythritol tetranitrocarbamate (PETNC) is deprotonated by several bases. The resulting salts of the relatively oxygen-rich organic anion were thoroughly characterized. Including multinuclear NMR, vibrational spectroscopy, elemental analysis, thermoanalytical techniques, single crystal X-ray diffraction measurements and the aquatic toxicity against *Aliivibrio fischeri*.



Scheme S3. Salt formation of PETNC resulting in its tetravalent anion.

Though the thermal stability of the resulting salts was lower compared to PETNC itself, the resulting salts showed the tendency of having a low sensitivity and a low toxicity towards the luminescent marine bacteria *Aliivibrio fischeri*.

Chapter 7 is about aquatic toxicity measurements against the luminescent bacteria *Aliivibrio fischeri*. In this cost- and time-efficient experimental test the inhibition of the natural bioluminescence of the bacteria was determined, depending on the concentration (Figure S6). More specifically, after 15 and 30 min the half maximal effective concentration (EC₅₀) was investigated. Therefore, some water-soluble energetic materials, with different functionalities and substitution patterns were compared to commonly used materials, like RDX, AP and azide salts.

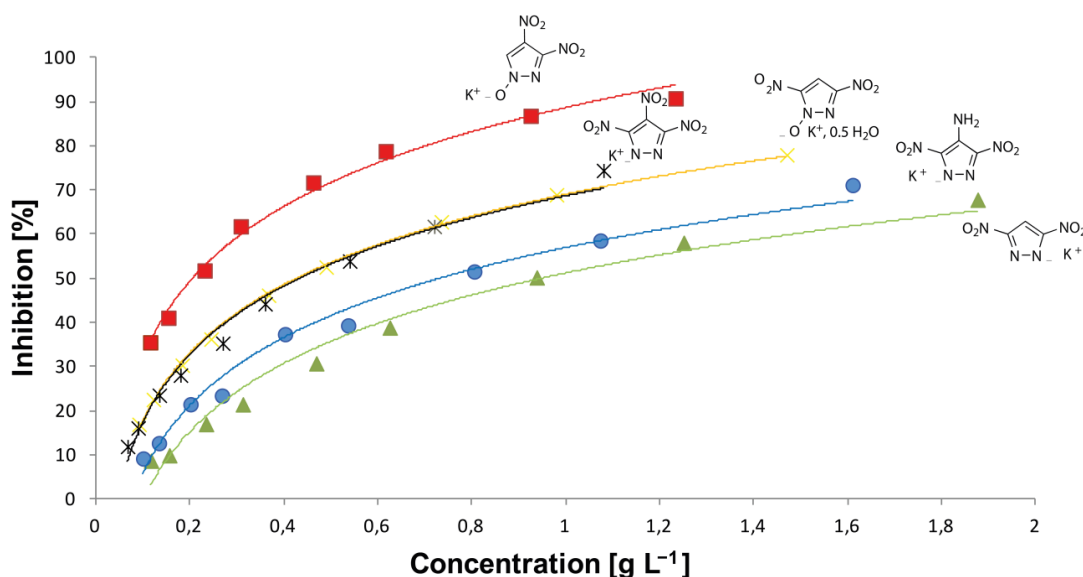


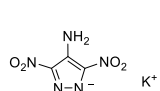
Figure S6. Concentration depending inhibition plot of several measured potassium salts of pyrazoles.

Just to name a few trends: The ammonium, potassium and sodium cations showed a minor toxic effect, while the hydroxylammonium cation was more toxic against *Aliivibrio fischeri*. Rather toxic anions for example were azide and periodate. On the other hand, the perchlorate anion had a negligible toxic effect on this aquatic bacterium. Another observation was concerning the secondary explosives TKX-50 and MAD-X1, which EC₅₀ values were similar to RDX.

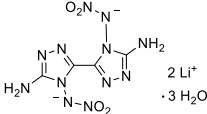
In **Chapter 8** the median effective concentrations from the aquatic toxicity measurements were presented along with results from the AMES test. The AMES test or bacterial reverse mutation test gives an idea about the mutagenic potential of a compound and is the first test, which should be performed in the course of REACH. Therefore, three promising energetic molecules were analyzed *in vitro* and *in silicio*. For the experimental determination of point mutations, the auxotrophic strains of *Salmonella typhimurium* and *Escheria coli* were employed. Moreover, to simulate the effect of metabolic conversion rat liver S9 was chemically introduced. For predicting values of the AMES test, quantitative structure activity relationships (QSAR) methods were used, which are based on five different validated AMES databases. The employed algorithm selects similar compounds, as similar molecules should have a similar effect.

Table S1. Results of experimental and *in silico* AMES test and the considered mutagenicity/toxicity [less toxic/mutagenic (-), moderately toxic/mutagenic (+), toxic/mutagenic (++)].

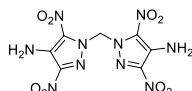
Compound	QSAR AMES test	Experimental AMES test	<i>Vibrio fischeri</i>
KDNAP	++	n.a.	+
BDNAPM	++	++	n.a.
Li ₂ ANAT	doubtful	+	-
TKX-50	-	-	+



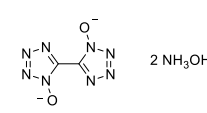
KDNAP



Li₂ANAT



BDNAPM

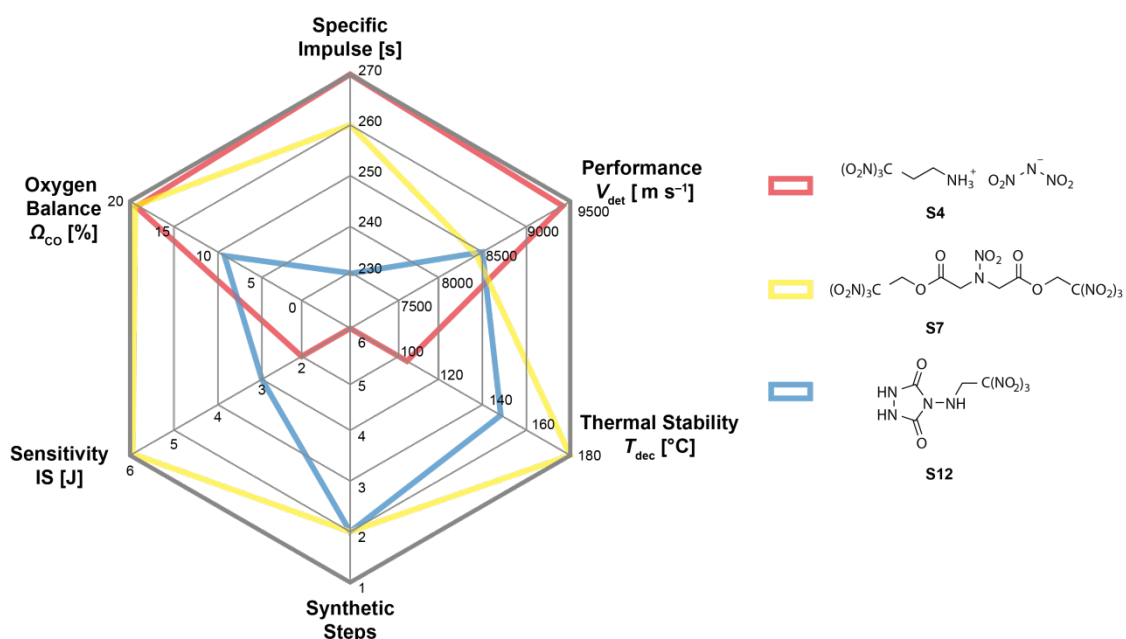


TKX-50

The experimental AMES test revealed that TKX-50 had no mutagenic effect, whereas Li₂ANAT had a mutagenic effect in some bacteria strains and BDNAPM had a mutagenic effect in all selected bacteria strains. All values calculated by R.Mo.S. QSAR were consistent with the experimental values.

General Conclusion and Outlook on Oxygen-rich Molecules:

In this thesis several interesting compounds with good oxygen balances are presented. The thorough characterization revealed sufficient thermal stabilities, moderate sensitivities towards external stimuli and favorable densities for a number of molecules. Moreover, some showed great energetic performance data and were accessed through facile synthesis. Different strategies, like introducing trinitroalkyl moieties, oxygen rich ions or/and nitrogen- and oxygen-rich heterocycles were applied. The three most promising molecules out of each strategy are highlighted in Figure S7.



With regard as a possible alternative to the common high energy dense oxidizer AP **S7** would be the most suitable candidate. In addition to the depicted properties, it is long-term storable and was comparable to AP in different binder systems. Still, the dinitramide salt **S3** has outstanding performance data and the heterocycle urazine **S12** meets most of the requirements of a promising oxygen-rich molecule. Future trends on the research of HEDOs are driven towards oxygen-rich heterocycles such as furoxans, moreover further small naturally occurring molecules, which already possess a high amount of oxygen are favorable.

IV Appendix

1 Supporting Information to Michael Addition of Trinitromethane

1.1 Single Crystal X-ray Diffraction

1.1.1 4,4,4-Trinitrobutanamide (1)

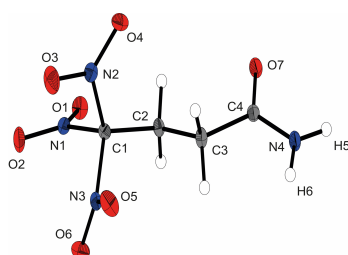


Figure A1.1 Molecular structure of 4,4,4-trinitrobutanamide (1).

Table A1.1 Hydrogen bonds of 4,4,4-trinitrobutanamide (1).

D–H···A			sym. of A	H···A	D–H	D···A	angle, DHA
C3	H3	O5	1–x, 1–y, –z	2.702	0.96	3.600	155.6
C2	H2	O4	1–x, 1–y, 1–z	2.434	0.95	3.276	145.7
N4	H6	O7	2–x, –y, 1–z	2.073	0.89	2.933	170.9
N4	H5	O6	2–x, 1–y, –z	2.440	0.86	3.314	168.3
C2	H1	O7	2–x, 1–y, 1–z	2.640	0.95	3.531	156.2

1.1.2 4,4,4-Trinitrobutanoic acid (2)

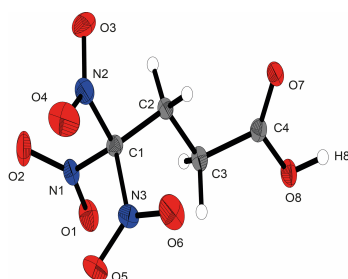
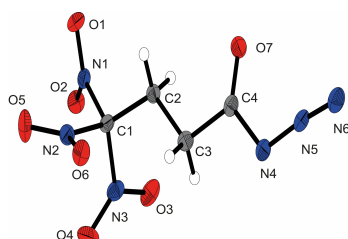


Figure A1.2 Molecular structure of 4,4,4-trinitrobutanoic acid (2).

Table A1.2 Hydrogen bonds of 4,4,4-trinitrobutanoic acid (**2**).

D–H···A			sym. of A	H···A	D–H	D···A	angle, DHA
C2	H1	O1	$-1+x, y, z$	2.628	0.96	3.565	166.3
O8	H5	O7	$1-x, -y, -z$	1.769	0.86	2.632	176.5
C2	H2	O4	$-0.5+x, 0.5-y, -\frac{1}{2}+z$	2.547	0.94	3.253	136.1
C2	H2	O2	$-0.5+x, 0.5-y, 0.5+z$	2.653	0.94	3.389	132.5

1.1.3 4,4,4-Trinitrobutanoyl azide (**4**).

**Figure A1.3** Molecular structure of 4,4,4-trinitrobutanoyl azide (**4**)**Table A1.3** Hydrogen bonds of 4,4,4-trinitrobutanoyl azide (**4**).

D–H···A			sym. of A	H···A	D–H	D···A	angle, DHA
C2	H2	O1	$-x, 1-y, -z$	2.535	0.96	3.373	144.7
C2	H1	O7	$1-x, 1-y, -z$	2.386	1.00	3.221	141.3

1.1.4 3,3,3-Trinitropropyl-1-ammonium chloride (**6a**)

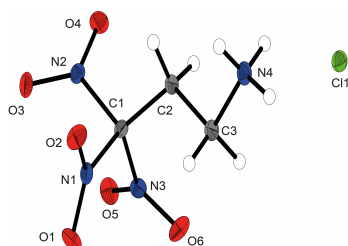
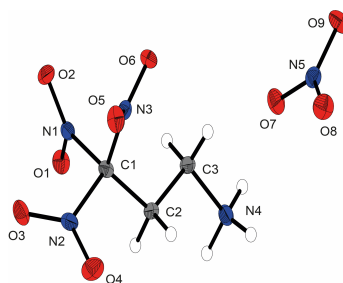
**Figure A1.4** Molecular structure of 3,3,3-trinitropropyl-1-ammonium chloride (**6a**).

Table A1.4 Hydrogen bonds of 3,3,3-trinitropropyl-1-ammonium chloride (**6a**).

D–H···A			sym. of A	H···A	D–H	D···A	angle, DHA
N4	H6	O7		1.909	0.88	2.779	168.7
N4	H7	C11	$-x+1, -y+2, -z+1$	2.549	0.88	3.254	137.6
N4	H7	O5	$x+1, y+1, z$	2.574	0.88	3.206	129.3
N4	H8	C11		2.273	0.88	3.146	169.6
O7	H9	C11	$x+1, y, z$	2.469	0.82	3.235	155.2
O7	H10	C11	$-x+1, -y+1, -z+1$	2.380	0.82	3.184	169.0

1.1.5 3,3,3-Trinitropropyl-1-ammonium nitrate (**6b**)

**Figure A1.5** Molecular structure of 3,3,3-trinitropropyl-1-ammonium nitrate (**6b**)**Table A1.5** Hydrogen bonds of 3,3,3-trinitropropyl-1-ammonium nitrate (**6b**)

D–H···A			sym. of A	H···A	D–H	D···A	angle, DHA
N4	H5	O9	$-x+1, y-0.5, -z+\frac{1}{2}$	1.948	0.91	2.859	173.6
N4	H6	O7		1.957	0.90	2.818	160.0
N4	H6	N5		2.667	0.90	3.391	138.3
N4	H7	O7	$-x+2, y-0.5, -z+0.5$	2.080	0.92	2.954	158.0
N4	H7	O9	$-x+2, y-0.5, -z+0.5$	2.361	0.92	3.094	136.5
N4	H7	N5	$-x+2, y-0.5, -z+0.5$	2.570	0.92	3.465	164.4
C2	H2	O7	$-x+2, y-0.5, -z+0.5$	2.546	0.91	3.286	138.4

1.1.6 3,3,3-Trinitropropyl-1-ammonium dinitramide (6d)

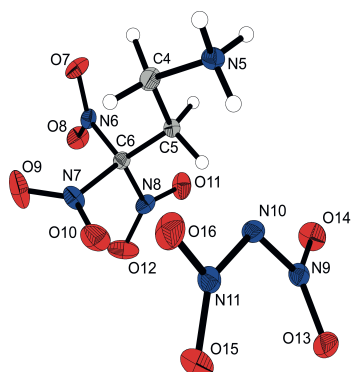


Figure A1.6 Molecular structure of 3,3,3-trinitropropyl-1-ammonium dinitramide (6d).

Table A1.6 Hydrogen bonds of 3,3,3-trinitropropyl-1-ammonium dinitramide (6d).

	D–H	⋯A		H⋯A	D–H	D⋯A	angle, DHA
C1	H4	O3		2.398	0.990	3.027	120.79
C1	H5	O4		2.828	0.990	3.446	121.23
C2	H7	O4		2.930	0.990	3.608	126.54
C1	H5	O2	$-x, -y, 1-z$	2.485	0.990	3.439	161.87
N1	H1	O7	$-1+x, -1+y, z$	2.425	0.892	3.281	161.01
C4	H12	O6		2.935	0.990	3.887	161.55
C2	H7	O10	$-1+x, y, z$	2.709	0.990	3.673	164.62
C1	H4	O11	$x, -1+y, z$	2.487	0.990	3.146	123.74
N1	H2	O15	$-1+x, y, z$	2.056	0.904	2.960	178.00
N1	H2	O16	$-1+x, y, z$	2.600	0.904	3.221	126.51
C2	H6	O13		2.574	0.990	3.460	148.97
N1	H3	O19		2.000	0.898	2.845	156.46
C2	H6	O19		2.579	0.990	3.460	134.42
N5	H9	O16		2.790	0.893	3.422	128.91
C5	H14	O14		2.641	0.990	3.605	164.55
N5	H10	O14	$1+x, y, z$	2.256	0.921	2.966	133.51
N5	H10	O16	$2-x, 1-y, -z$	2.356	0.921	3.089	136.31
C5	H13	O20	$x, 1+y, z$	2.508	0.990	3.334	140.81
N5	H8	O19	$1-x, 1-y, -z$	2.147	0.875	2.990	161.70
C4	H11	O17	$2-x, 1-y, -z$	2.408	0.990	3.335	155.71

1.1.7 2,2,2-Trinitroethyl-4,4,4-trinitrobutanoate (8)

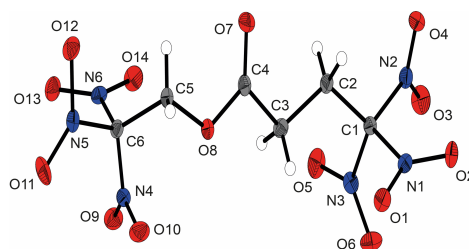


Figure A1.7 Molecular structure of 2,2,2-trinitroethyl-4,4,4-trinitrobutanoate (8).

Table A1.7 Hydrogen bonds of 2,2,2-trinitroethyl-4,4,4-trinitrobutanoate (8).

D–H···A			sym. of A	H···A	D–H	D···A	∠, DHA
C2	H3	O6	$-1+x, y, z$	2.673	0.95	3.556	155.5
C5	H6	O10	$-1+x, y, z$	2.612	0.94	3.388	140.4
C2	H4	O7	$-x, 1-y, 1-z$	2.509	0.96	3.391	152.1
C3	H1	O12	$-0.5+x, 0.5-y, 0.5+z$	2.618	0.95	3.419	142.1

1.1.8 Crystallographic Data and Structure Refinements

Table A1.8 Crystallographic data and structure refinements of **1**, **2**, **4**, and **6a**.

	1	2	4	6a
formula	C ₄ H ₆ N ₄ O ₇	C ₄ H ₅ N ₃ O ₈	C ₄ H ₄ N ₆ O ₇	C ₃ H ₇ N ₄ O ₆ Cl × H ₂ O
formula weight [g mol ⁻¹]	222.11	223.11	248.13	248.58
temperature [K]	100(2)	100(2)	100(2)	100(2)
crystal system	triclinic	monoclinic	triclinic	triclinic
space group (No.)	<i>P</i> − <i>I</i> (2)	<i>P</i> 2 ₁ / <i>n</i> (14)	<i>P</i> − <i>I</i> (2)	<i>P</i> − <i>I</i> (2)
<i>a</i> [Å]	6.1081(5)	6.1307(7)	7.4160(5)	6.7434(6)
<i>b</i> [Å]	7.5366(6)	16.7082(6)	7.5385(6)	7.8045(8)
<i>c</i> [Å]	8.8543(7)	8.5025(4)	9.0347(8)	10.0663(10)
α [°]	80.728(7)	90	70.713(8)	90.393(8)
β [°]	87.505(7)	98.296(4)	80.100(7)	98.800(8)
γ [°]	88.355(6)	90	81.601(7)	114.135(9)
<i>V</i> [Å ³]	401.80(6)	861.82(7)	467.47(6)	476.36(8)
<i>Z</i>	2	4	2	2
$\rho_{\text{calc.}}$ [g cm ⁻³]	1.836	1.720	1.763	1.733
μ [mm ⁻¹]	0.177	0.171	0.168	0.430
<i>F</i> (000)	228	456	252	256
crystal habit	colorless plate	colorless block	colorless block	colorless plate
crystal size [mm]	0.35 × 0.21 × 0.05	0.25 × 0.22 × 0.18	0.35 × 0.27 × 0.25	0.32 × 0.27 × 0.08
<i>q</i> range [°]	4.27 – 28.27	4.15 – 26.37	4.20 – 26.36	4.23 – 28.28
index ranges	−8 ≤ <i>h</i> ≤ 8 −10 ≤ <i>k</i> ≤ 10 −11 ≤ <i>l</i> ≤ 11	−7 ≤ <i>h</i> ≤ 5 −18 ≤ <i>k</i> ≤ 20 −8 ≤ <i>l</i> ≤ 10	−9 ≤ <i>h</i> ≤ 9 −9 ≤ <i>k</i> ≤ 9 −11 ≤ <i>l</i> ≤ 11	−7 ≤ <i>h</i> ≤ 8 −10 ≤ <i>k</i> ≤ 8 −13 ≤ <i>l</i> ≤ 13
reflections measured	3448	3513	4352	4182
reflections independent	1971	1750	1909	2345
reflections unique	1685	1484	1653	2050
<i>R</i> _{int}	0.019	0.019	0.021	0.021
<i>R</i> ₁ , <i>wR</i> ₂ (2σ data)	0.0308, 0.0735	0.0306, 0.0708	0.0309, 0.0726	0.0287, 0.0641
<i>R</i> ₁ , <i>wR</i> ₂ (all data)	0.0380, 0.0794	0.0384, 0.0764	0.0384, 0.0782	0.0355, 0.0680
data/restraints/parameters	1971/0/154	1750/0/156	1909/0/170	2345/0/172
GOOF on <i>F</i> ²	1.060	1.040	1.040	1.083
residual el. density [e Å ⁻³]	−0.228/0.388	−0.198/0.228	−0.215/0.302	−0.292/0.336
CCDC	1506284	1506285	1506286	1506287

Table A1.9 Crystallographic data and structure refinements of **6b**, **6d**, and **8**.

	6b	6d	8
formula	C ₃ H ₇ N ₄ O ₆ ·NO ₃	C ₃ H ₇ N ₄ O ₆ ·N ₃ O ₄	C ₆ H ₆ N ₆ O ₁₄
formula weight [g mol ⁻¹]	257.14	301.16	386.14
temperature [K]	173(2)	123(2)	173(2)
crystal system	orthorhombic	triclinic	monoclinic
space group (No.)	<i>P</i> 2 ₁ 2 ₁ 2 ₁ (14)	<i>P</i> -1 (2)	<i>P</i> 2 ₁ / <i>n</i> (14)
<i>a</i> [Å]	5.6622(4)	6.7087(5)	5.7264(3)
<i>b</i> [Å]	10.2826(7)	11.2547(7)	21.6530(11)
<i>c</i> [Å]	16.2582(18)	15.2144(9)	11.0910(6)
α [°]	90	75.527(5)	90
β [°]	90	79.280(5)	93.555(4)
γ [°]	90	75.733(6)	90
<i>V</i> [Å ³]	946.59(14)	1068.48(13)	1372.57(12)
<i>Z</i>	4	4	4
ρ_{calc} [g cm ⁻³]	1.804	1.872	1.869
μ [mm ⁻¹]	0.181	0.188	0.188
<i>F</i> (000)	528	616	784
crystal habit	colorless plate	colorless block	colorless plate
crystal size [mm]	0.32 × 0.28 × 0.08	0.36 × 0.13 × 0.04	0.12 × 0.11 × 0.04
<i>q</i> range [°]	4.11 – 31.44	4.19 – 26.00	4.14 – 27.09
index ranges	-8 ≤ <i>h</i> ≤ 7 -15 ≤ <i>k</i> ≤ 7 -11 ≤ <i>l</i> ≤ 23	-8 ≤ <i>h</i> ≤ 6 -13 ≤ <i>k</i> ≤ 13 -18 ≤ <i>l</i> ≤ 18	-3 ≤ <i>h</i> ≤ 7 -21 ≤ <i>k</i> ≤ 27 -14 ≤ <i>l</i> ≤ 14
reflections measured	5194	8204	6223
reflections independent	3069	4176	3023
reflections unique	2567	3456	2572
<i>R</i> _{int}	0.029	0.021	0.021
<i>R</i> ₁ , <i>wR</i> ₂ (2 σ data)	0.0424, 0.0793	0.0336, 0.0436	0.0301, 0.0652
<i>R</i> ₁ , <i>wR</i> ₂ (all data)	0.0584, 0.0883	0.1020, 0.1144	0.0390, 0.0700
data/restraints/parameters	3069/0/175	4176/0/361	3023/0/259
GOOF on <i>F</i> ²	1.058	0.826	1.025
residual el. density [e Å ⁻³]	-0.229/0.418	-0.288/0.278	-0.240/0.379
CCDC	1506288	1506289	1506290

1.2 Theoretical Studies

The energy of all the compounds were calculated with the quantum chemical composite method CBS- 4M. The *ab initio* calculations were carried out using the program package Gaussian 09 (Revision A.03). The geometric structure optimizations and the frequency analyses were performed with Becke's B3 parameter hybrid functional using the B3LYP correlation functional with 6-31G** basis set. All of the optimized structures were verified to be a local energy minimum on the potential energy surface without imaginary frequencies. The structures were optimized with symmetry constraints and the energy is corrected with the zero point vibrational energy (ZPEV). The enthalpies (H) and free energies (G) were calculated using the complete basis set (CBS) method in order to obtain accurate values

The CBS-4M method starts with a HF/3-21G(d) geometry optimization, which is the initial guess for the following SCF calculation as a base energy and a final MP2/6-31+G calculation with a CBS extrapolation to correct the energy in second order. The used reparametrized CBS-4M method additionally implements a MP4(SDQ)/6-31+(d,p) calculation to approximate higher order contributions and also includes some additional empirical corrections.

The quantum chemical calculation results in an absolute value for H_{QC}° of the compound. The gas phase enthalpies of formation $\Delta_f H_{(g)}^{\circ}$ can be determined using the atomization method (Equation 1) with the number n_i of atoms A_i in the calculated substance. The values for $\Delta_f H^{\circ}(A_i)$ are taken from the NIST database.

$$\Delta_f H_{(g)}^{\circ}(M) = H_{QC}^{\circ} - \sum_i^{atoms A} n_i H_{QC}^{\circ}(A_i) + \sum_i^{atoms A} n_i \Delta_f H^{\circ}(A_i) \quad (1)$$

Using the approximation of the Trouton's rule the enthalpy of sublimation $\Delta_{sub} H^{\circ}$ or enthalpy of vaporization $\Delta_{vap} H^{\circ}$ can be determined (Equations 2 and 3):

$$\Delta_{sub} H = C_{sub} \cdot T_{melt} \approx 188 \frac{J}{mol \cdot K} \cdot T_{melt}, \quad (2)$$

$$\Delta_{vap} H = \Delta S_{vap} \cdot T_{boil} \approx 90 \frac{J}{mol \cdot K} T_{boil}. \quad (3)$$

The enthalpy of formation $\Delta_f H^{\circ}(s,l)$ for the solid (*s*) or liquid (*l*) state can be calculated by Equation 4:

$$\Delta_f H_{(s,l)}^{\circ} = \Delta_f H_{(g)}^{\circ} - \Delta_{sub/vap} H. \quad (4)$$

The molar standard enthalpies of formation $\Delta_f H^\circ$ were used to calculate the molar solid state energies of formation $\Delta_f U^\circ_{(s,l)}$ according to Equation 5, where Δn is the change of moles of gaseous components:

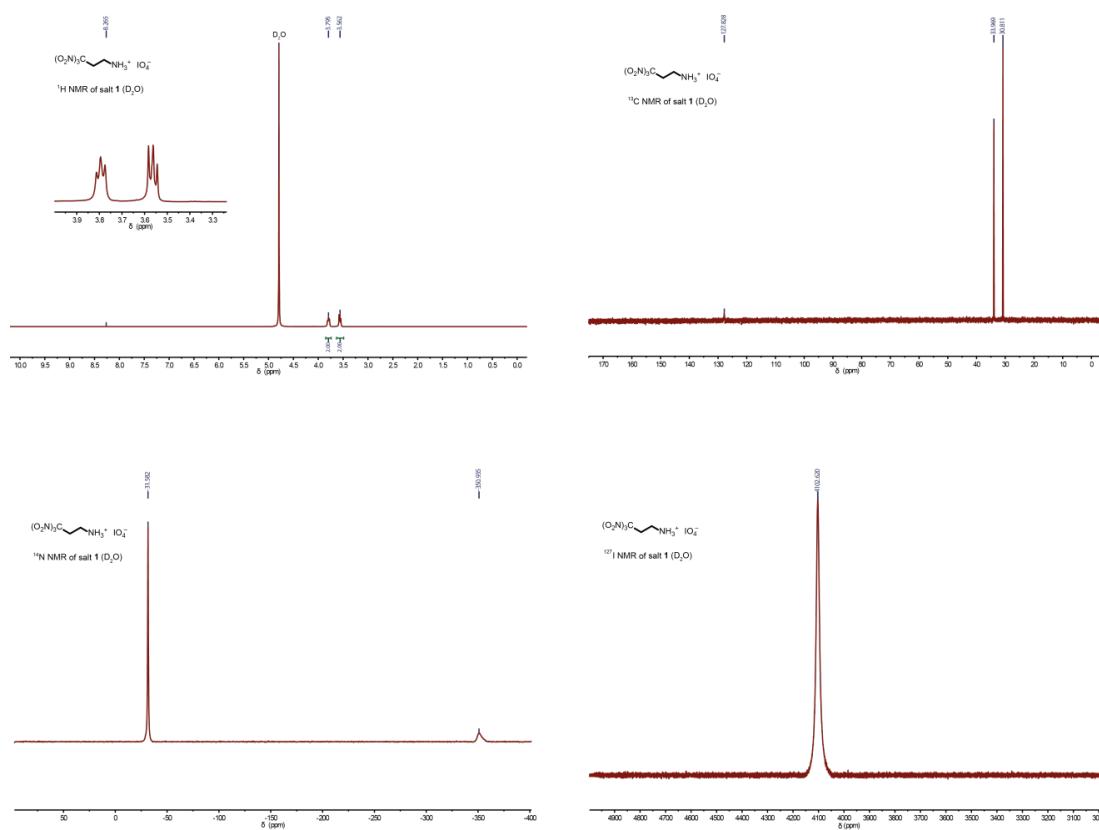
$$\Delta_f U^\circ_{(s,l)} = \Delta_f H^\circ_{s,l} - \Delta n_g RT \quad (5)$$

2 Supporting Information to Trinitropropylammonium Salts

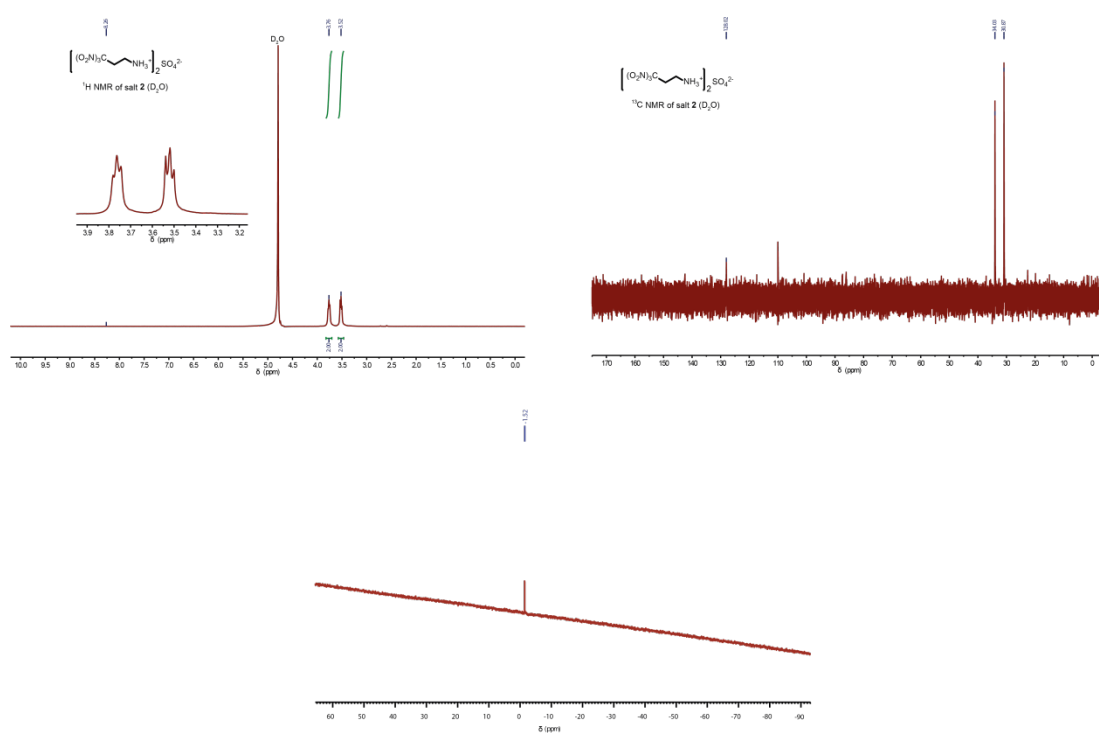
2.1 General Experimental Details

Solvents, deuterated solvents for NMR experiments and all further chemicals were used as received from the suppliers, without further purification. The salts were analyzed using NMR spectroscopy (Bruker 400 TR) at ambient temperature, whereby the chemical shifts were determined with respect to external standards, Me₄Si (¹H 399.8 MHz; ¹³C 100.5 MHz), MeNO₂ (¹⁴N 28.9 MHz), KI (¹²⁷I 80.2 MHz) and Cs₂SO₄ (³³S 30.7 MHz). Furthermore, IR and Raman spectra were recorded using a PerkinElmer Spectrum BX-FTIR spectrometer equipped with a Smiths DuraSampIR ATR device or a Bruker MultIRAM FT Raman spectrometer with ND:YAG laser with excitation up to 1000 mW at 1064 nm respectively. All spectra were recorded at ambient temperature, for the Raman spectra additionally glass tubes were used. The purity was then checked by elemental analysis using an Elementar vario EL or Elementar Vario micro cube. A Lineis DSC-PT10 apparatus with a linear heating range of 5 °C min⁻¹ was used to determine melting and decomposition points. For testing the sensitivities towards impact and friction a BAM drophammer¹ and BAM friction tester² were applied. Single crystal X-ray diffraction studies of salt **2** were performed on an Oxford Diffraction XCalibur3 diffractometer with a generator (voltage 50 kV, current 40 mA) and a Kappa CCDarea detector operating with Mo-K α radiation ($\lambda = 0.7107 \text{ \AA}$). For solving the structure direct methods were used (SIR97)³⁻⁴ and refined by full-matrix least-squares on F2 (ShelXL)⁵⁻⁶ implemented in the WinGX software package.⁷ All non-hydrogen atoms were refined anisotropically and the Diamond plots are shown with thermal ellipsoids at the 50% probability level.

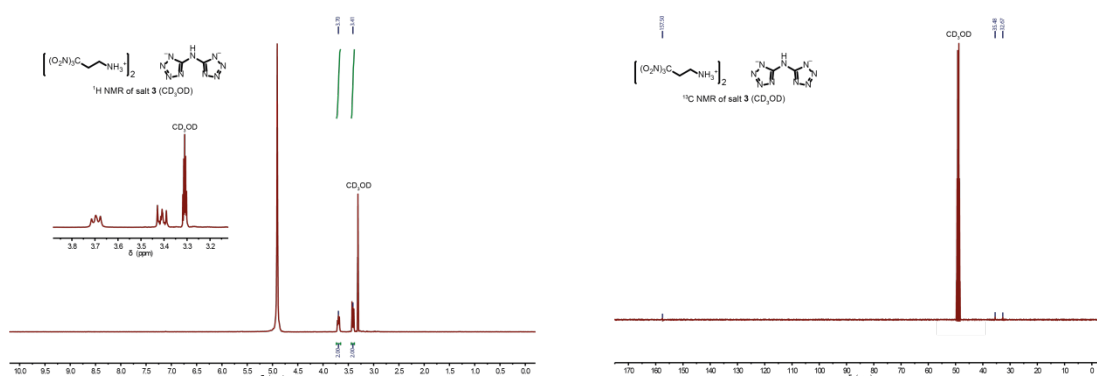
2.2 ^1H , ^{13}C , ^{14}N and ^{127}I NMR Data of 1



2.3 ^1H , ^{13}C and ^{33}S NMR Data of 2



2.4 ^1H and ^{13}C NMR Data of **3**



2.5 Vibrational Spectroscopy

IR and Raman spectra of salts **1–3** were recorded and the most characteristic vibrations are listed in Table A2.1. The NH-stretching modes can be found in the range $\tilde{\nu} = 3213\text{--}3007\text{ cm}^{-1}$ the asymmetric ($\nu_{\text{as}}(\text{NO}_2)$) and symmetric ($\nu_{\text{s}}(\text{NO}_2)$) stretching vibrations of the trinitromethyl group are found in the range $\tilde{\nu} = 1618\text{--}1586\text{ cm}^{-1}$ (asymmetric) and $\tilde{\nu} = 1302\text{--}1295\text{ cm}^{-1}$ (symmetric) respectively. For the periodate anion of salt **1** additional stretching vibrations $\nu_{\text{s}}(\text{IO})$ are observed in the IR spectra at $\tilde{\nu} = 832\text{ cm}^{-1}$ and in the Raman spectra at $\tilde{\nu} = 852\text{ cm}^{-1}$. For the anion of **2**, there are asymmetric stretching vibrations $\nu_{\text{as}}(\text{SO})$ at $\tilde{\nu} = 1030\text{ cm}^{-1}$ (Raman) and at $\tilde{\nu} = 1051\text{ cm}^{-1}$ (IR) observed.⁸

Table A2.1 Selected IR and Raman bands of salts **1–3** in cm^{-1} and the corresponding assignments.

	1		2		3	
	IR	Raman	IR	Raman	IR	Raman
$\nu(\text{NH})$	3208–3103	3007	—	3100–3042	3213–3023	3080–3039
$\nu_{\text{as}}(\text{NO}_2)$	1586	1618	1602	1589	1586	1606
$\nu_{\text{s}}(\text{NO}_2)$	1297	1298	1297	1300	1295	1302

2.6 Crystallographic Data of 2

2	
formula	$C_6H_{14}N_8O_{16}S \cdot H_2O$
<i>FW</i> [g mol ⁻¹]	504.33
<i>T</i> [K]	173 (2)
λ [Å]	0.71073
crystal system	monoclinic
space group	<i>I</i> 2/a
crystal size [mm]	0.40 x 0.06 x 0.02
crystal habit	colorless needle
<i>a</i> [Å]	28.502 (2)
<i>b</i> [Å]	5.8411 (4)
<i>c</i> [Å]	24.249 (2)
α, γ [deg]	90
β [deg]	108.424 (9)
<i>V</i> [Å ³]	3830.1 (6)
<i>Z</i>	8
ρ_{calc} [g cm ⁻³]	1.749
μ	0.276
<i>F</i> (000)	2080
2 θ range [deg]	4.41 – 31.55
index ranges	$-35 \leq h \leq 35$ $-7 \leq k \leq 7$ $-30 \leq l \leq 18$
reflections collected	15176
reflections independent	3902
reflections unique	3058
data/restraints/ parameters	3902/0/379
GooF	1.033
<i>R</i> ₁ / <i>wR</i> ₂ [<i>I</i> > 2 σ (<i>I</i>)]	0.0358 / 0.0521
<i>R</i> ₁ / <i>wR</i> ₂ (all data)	0.0861 / 0.0955
max / min residual electron density [Å ⁻³]	0.270 / -0.349

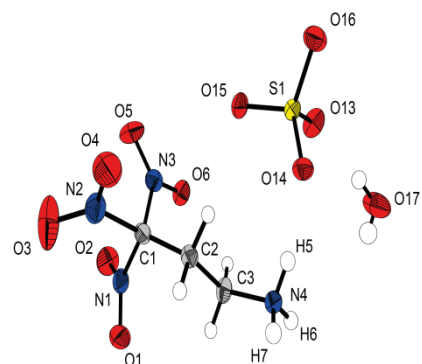


Figure A2.1 X-ray molecular structure of bis(trinitropropyl)-ammonium sulfate hydrate (**2**). Thermal ellipsoids represent the 50% probability level.

CCDC: 1941571

2.7 Theoretical Calculations

In order to calculate the solid state enthalpies, the sublimation enthalpy calculated using Trouton's rule⁹ were subtracted from the calculated gas phase enthalpies. For the gas phase enthalpies of formation itself the modified CBS-4M method, which is a re-parameterized version of the original CBS-4 method and includes some additional empirical corrections.¹⁰⁻¹¹ All *ab initio* calculations were carried out by using the program package Gaussian 09¹² and were visualized by GaussView 5.08.¹³

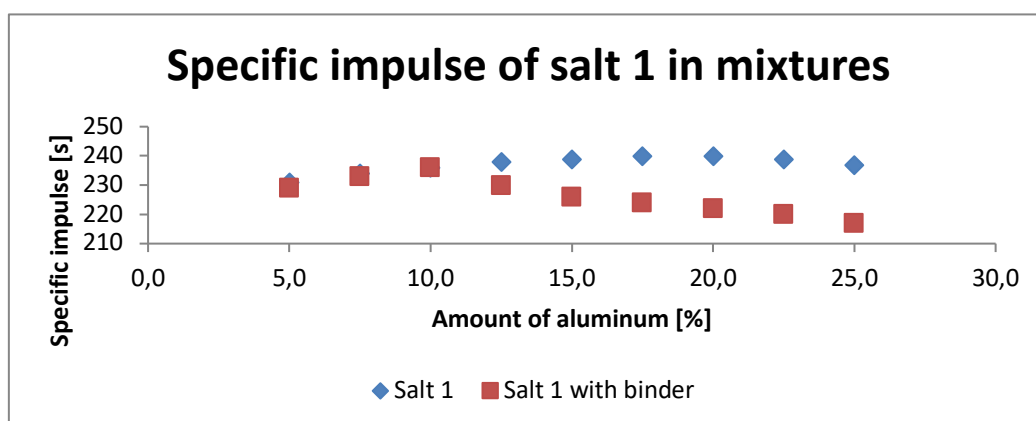
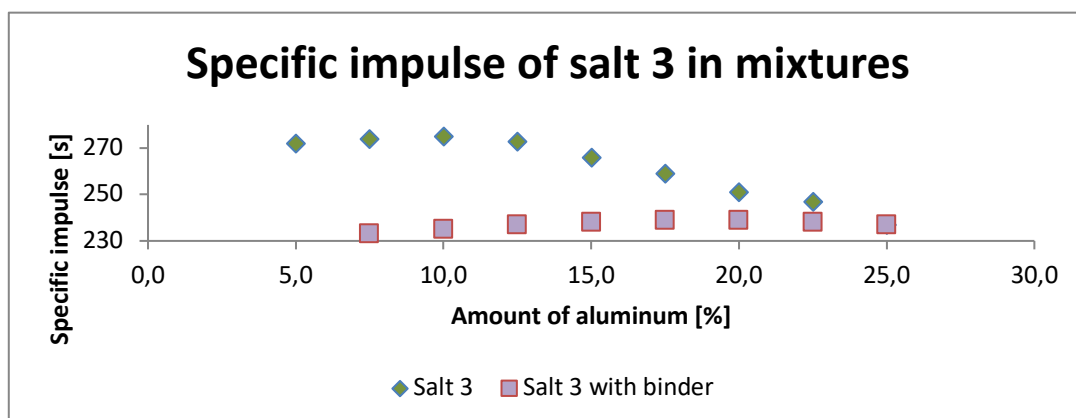
Based on this calculations, the detonation parameters were calculated using the program package EXPLO5(V6.03).¹⁴ The detonation parameters were calculated at the Chapman–Jouget (C–J) point, which was found from the Hugoniot curve of the system by its first derivative. The program is based on the steady-state model of equilibrium using a modified Becker-Kistiakowski-Wilson equation of state for modeling the system. For the calculations the maximum densities at room temperature was used (298 K), which were either obtained by pycnometer measurement or calculated from the corresponding crystal densities. Therefore, the following equation and the α_v coefficient of volume expansion from the nitramine HMX ($\alpha_v = 1.6 \cdot 10^{-4}$ K) was used:

$$\rho_{298K} = \rho_T / (1 + \alpha_v(298 - T)).$$

The specific impulses (I_{sp}) were calculated as well at 70.0 bar chamber pressure, isobaric combustion conditions (1 bar) and equilibrium to throat and frozen to exit. I_{sp} was calculated for the neat compound, for optimized mixtures with aluminum and for a three component composition with oxidizer, aluminum and 14% binder consisting of 6% polybutadiene acrylic acid, 6% polybutadiene acrylonitrile and 2% bisphenol A ether. In order to find the optimal composition the amount of aluminum was varied from 5% to 25% and plotted against the specific impulses as shown in Graph A2.1 and Graph A2.2.

Table A2.2 Specific impulses of salts **1** and **3** with varying amounts of aluminum, calculated without and with binder.

	1	1 (14% binder)	3	3 (14% binder)
I_s / s (5.0% Al)	231	229	272	229
I_s / s (7.5% Al)	234	233	274	233
I_s / s (10.0% Al)	236	236	275	235
I_s / s (12.5% Al)	238	230	273	237
I_s / s (15.0% Al)	239	226	266	238
I_s / s (17.5% Al)	240	224	259	239
I_s / s (20.0% Al)	240	222	251	239
I_s / s (22.5% Al)	239	220	247	238
I_s / s (25.0% Al)	237	217	237	237

Graph A2.1 Specific impulse of periodate **1** in aluminum mixtures without and with binder.**Graph A2.2** Specific impulse of amino-bis(5-tetrazolate) **3** in aluminum mixtures without and with binder.

3 Supporting Information to Trinitroethyl esters Based on Divalent Acids

3.1 General Experimental Details

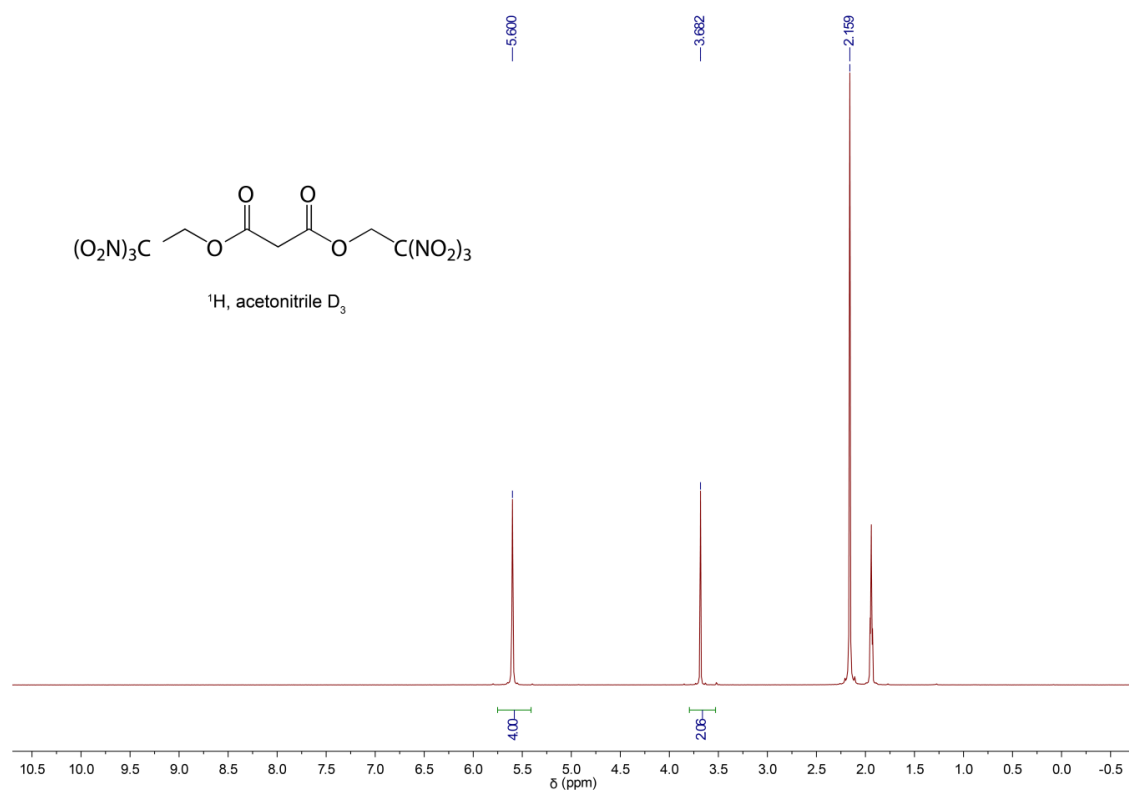
^1H , ^{13}C and ^{14}N NMR spectra were recorded on a 400 MHz (Bruker 400 TR) spectrometer at ambient temperature, whereby the chemical shifts were determined with respect to external standards, Me_4Si (^1H 399.8 MHz; ^{13}C 100.5 MHz) and MeNO_2 (^{14}N 28.9 MHz). IR and spectra were measured with a PerkinElmer Spectrum One FTIR equipped an ATR device. Furthermore, Raman spectra were recorded using a Bruker MultiRAM FT Raman spectrometer with ND:YAG laser with excitation up to 1000 mW at 1064 nm respectively at ambient temperature. For the Raman spectra additionally glass tubes were used. Elemental analyses were obtained on an Elementar vario EL or Elementar Vario micro cube. Simple melting und decomposition points were measured with an OZM Research DTA 552-Ex apparatus with a linear heating rate of $5\text{ }^\circ\text{C min}^{-1}$ in a temperature range of 15 to $400\text{ }^\circ\text{C}$ and checked by a Büchi Melting Point B-430 apparatus (not corrected). For the stability evaluation; DSC measurements were carried out on a DSC 2+ from Mettler Toledo in sealed high pressure crucibles. Furthermore, a TGA/DSC 3+ was used for the TGA measurements, whereby aluminum oxide crucibles were used. The sensitivity data towards impact and friction were obtained using a BAM drophammer¹ and BAM friction tester². The low temperature single-crystal X-ray diffraction studies were performed on an Oxford XCalibur3 diffractometer with a generator (voltage 50 kV, current 40 mA) and a Kappa CCDarea detector operating with Mo- $K\alpha$ radiation ($\lambda = 0.7107\text{ \AA}$). For solving the structure direct methods were used (*e. g.* SIR97)³⁻⁴ and refined by full-matrix least-squares on F^2 (SHELXL)⁵⁻⁶ implemented in the WINGX software package.⁷ All non-hydrogen atoms were refined anisotropically and the DIAMOND plots are shown with thermal ellipsoids at the 50% probability level. CCDC 2009758 (nitraminodiacetic acid) and CCDC 2009759 (NABTNE) contains the supplementary crystallographic data for this paper. These data can be obtained free of charge from The Cambridge Crystallographic Data Centre via www.ccdc.cam.ac.uk/data_request/cif.

3.2 NMR Data of MaBTNE

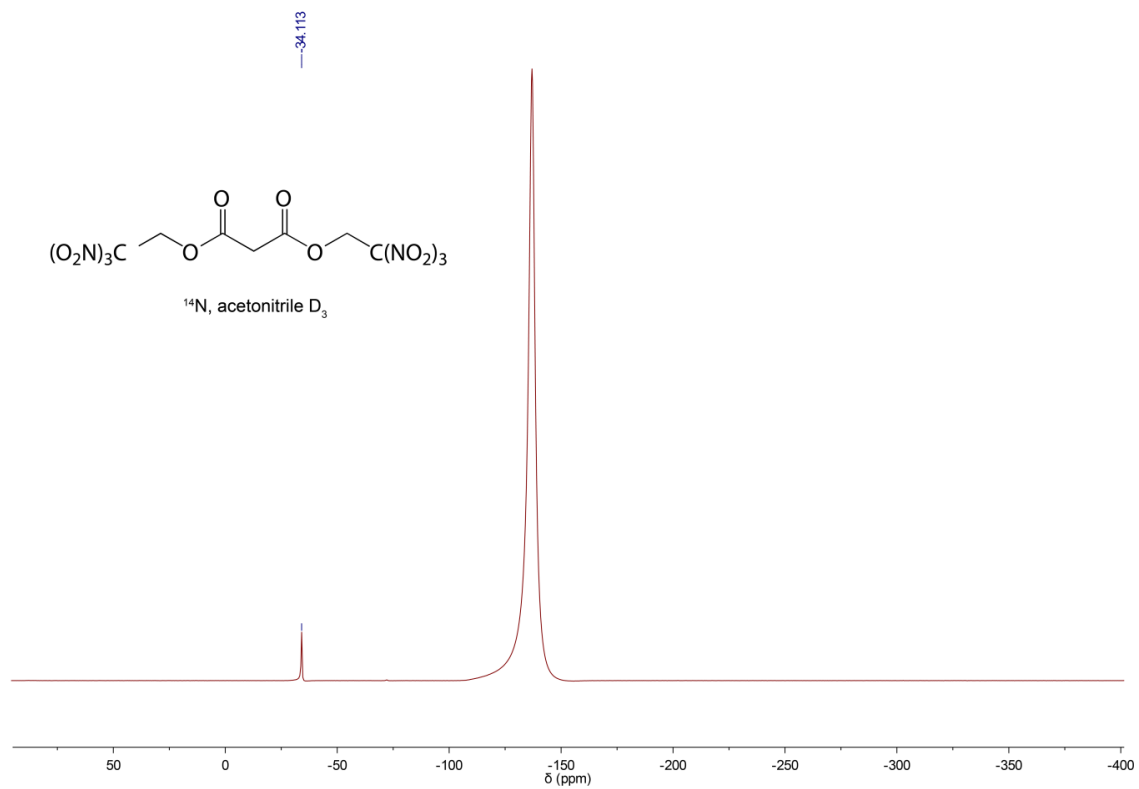
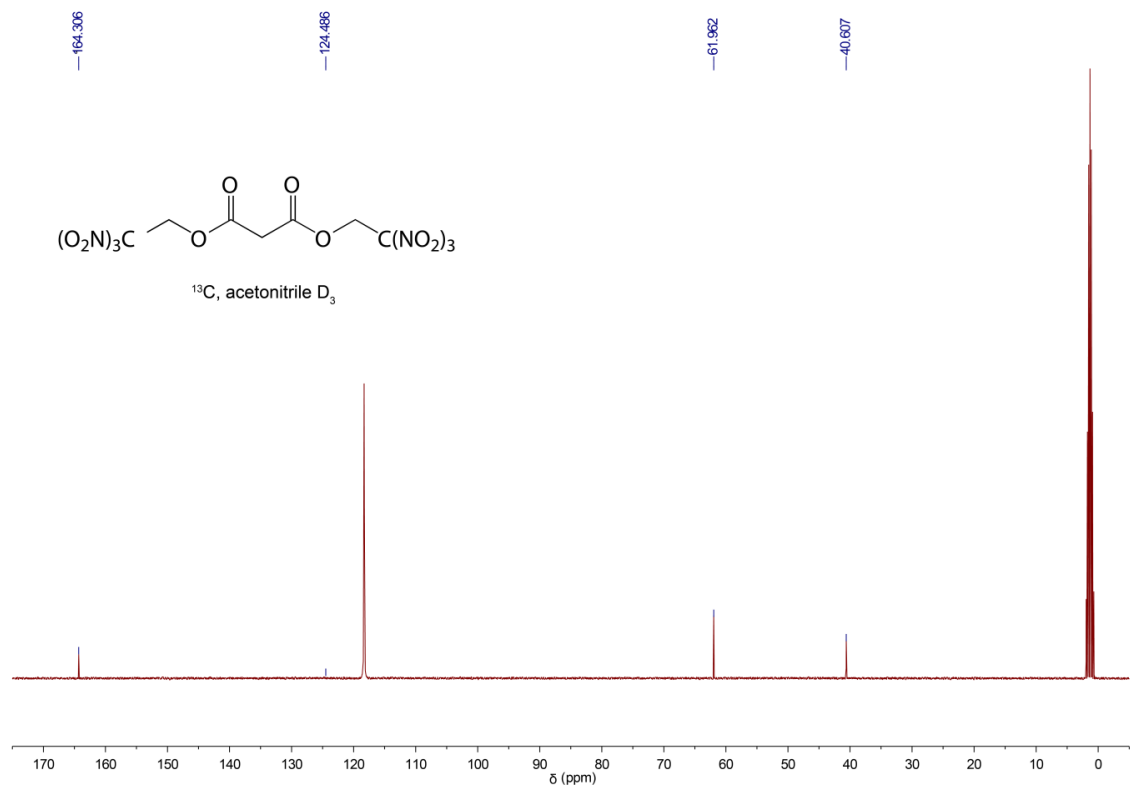
The ^1H and ^{13}C NMR shifts of malonic acid bis(2,2,2-trinitroethyl ester) were measured in various solvents and are listed in Table A3.1. Since MaBTNE is not stable in acetone, no shifts are listed for this solvent. As an example, the spectra including the ^{14}N NMR spectra in CD_3CN are depicted.

Table A3.1 MaBTNE in various deuterated solvents. Values in ppm.

Spectra/Solvent	DMSO	MeOD	CD_3CN	CDCl_3
^1H CH_2	5.97	5.79	5.60	5.45
CH_2	3.96	3.72	3.68	3.63
^{13}C CO	163.6	164.6	164.3	162.4
$\text{C}(\text{NO}_2)_3$	124.3	125.24	124.5	122.7
CH_2	61.1	62.5	62.0	61.5
CH_2	39.4	48.8	40.6	39.8



Appendix

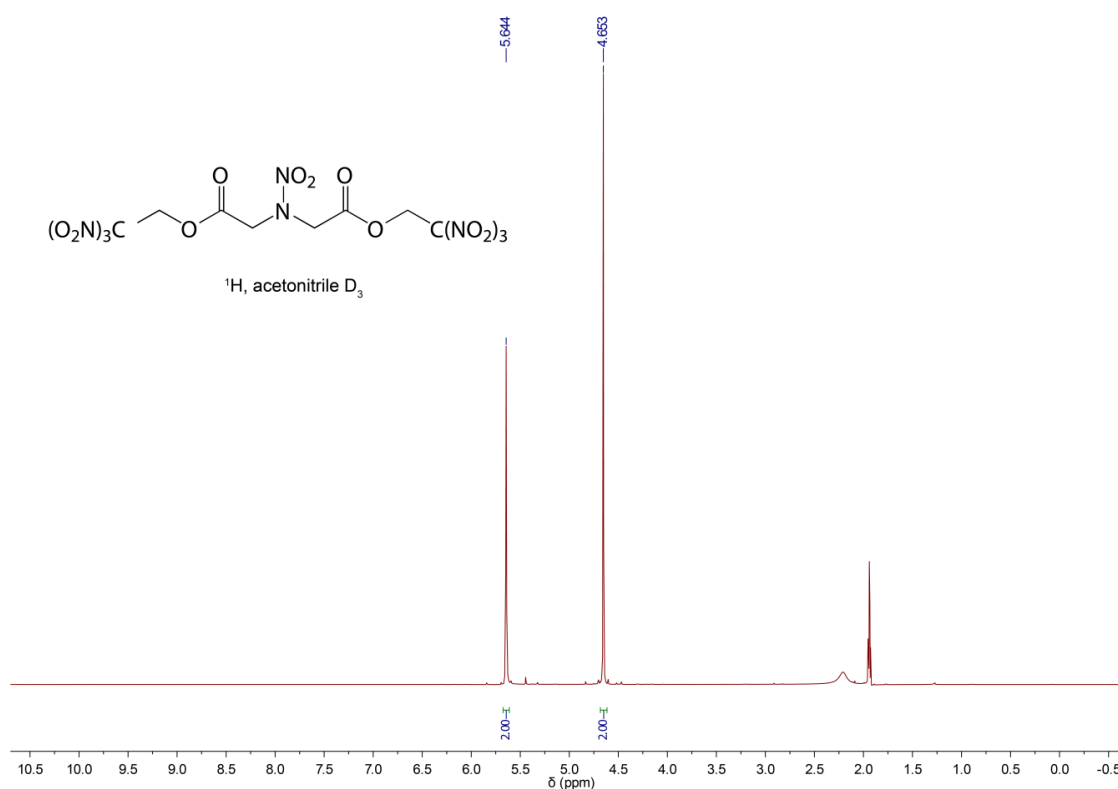


3.3 NMR Data of NABTNE

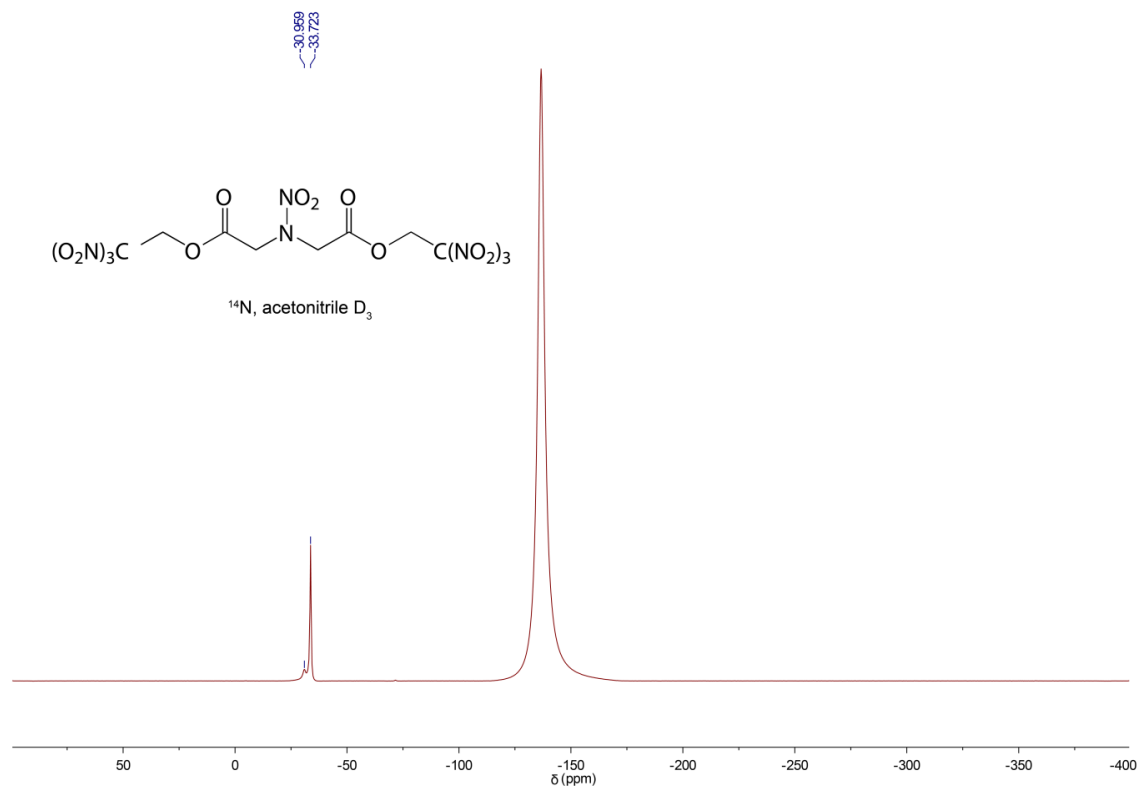
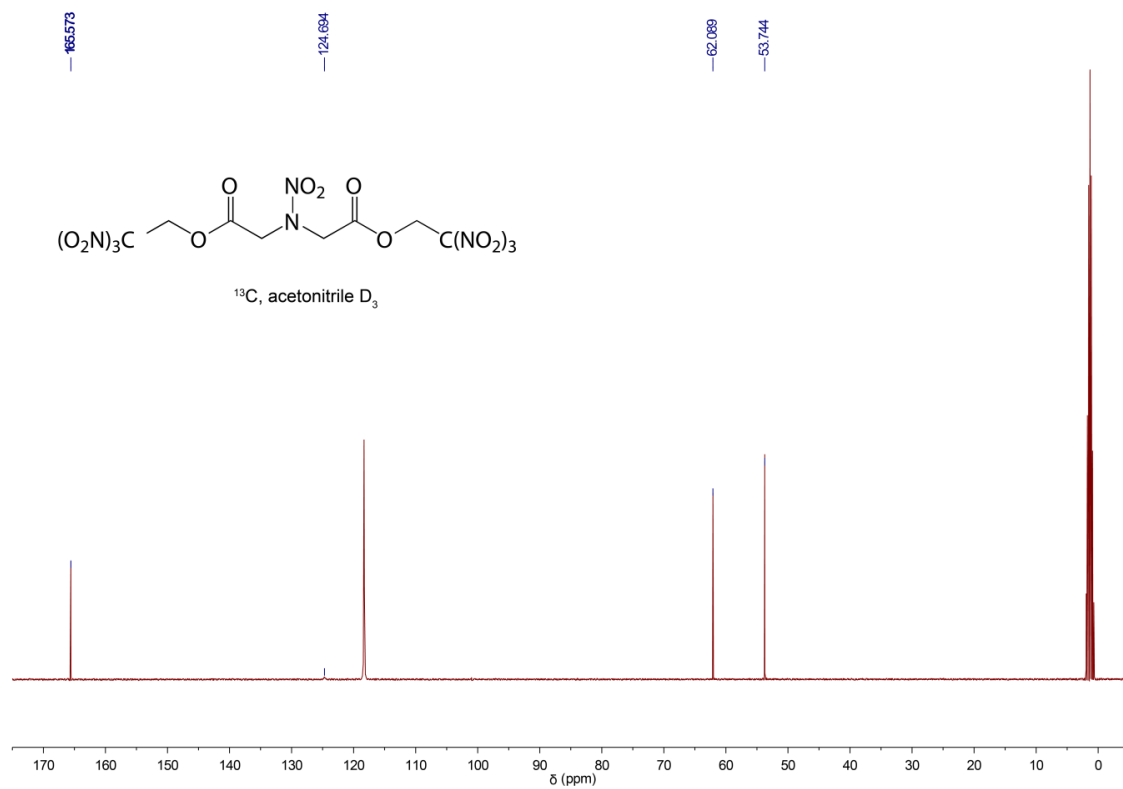
The ^1H and ^{13}C NMR shifts of nitramino diacetic acid bis(2,2,2-trinitroethyl ester) were measured in various solvents and are listed in Table A3.2. NABTNE is barely soluble in CDCl_3 , therefore only ^1H NMR resonances are listed. As an example, the spectra including the ^{14}N NMR spectra in CD_3CN are depicted.

Table A3.2 NABTNE in various deuterated solvents, shifts in ppm.

Spectra/Solvent	DMSO	MeOD	CD_3CN	CDCl_3	$(\text{CD}_3)_2\text{CO}$
^1H CH_2	6.03	5.84	5.64	5.50	5.96
CH_2	4.85	4.76	4.65	4.64	4.96
^{13}C CO	164.7	166.1	165.6	—	165.7
$\text{C}(\text{NO}_2)_3$	124.3	129.1	124.7	—	131.8
CH_2	61.2	62.6	62.1	—	62.3
CH_2	52.6	53.6	53.7	—	53.5



Appendix



3.4 Vibrational Spectroscopy

The most characteristic vibration frequencies in the IR and Raman spectra are the carbonyl and nitro groups, which are along with $\nu(\text{CH})$, summarized in Table A3.3. Thereby, the CH-stretching modes can be found in the range $\tilde{\nu} = 2998\text{--}2960\text{ cm}^{-1}$ and the $\nu(\text{C=O})$ stretching vibrations are located in the large range $\tilde{\nu} = 1785\text{--}1683\text{ cm}^{-1}$. Regarding the nitro groups, vibrational analysis showed the characteristic asymmetric ($\nu_{\text{as}}(\text{NO}_2)$) stretching vibrations in the range from 1618 cm^{-1} to 1561 cm^{-1} . Furthermore, the symmetric ($\nu_{\text{s}}(\text{NO}_2)$) stretching are found in the range $\tilde{\nu} = 1305\text{--}1279\text{ cm}^{-1}$.

Table A3.3 Selected IR and Raman bands of MaBTNE, nitraminodiactic acid and NABTNE in cm^{-1} .

	MaBTNE		Nitraminodiactic acid		NABTNE	
	IR	Raman	IR	Raman	IR	Raman
$\nu(\text{CH})$	2973	2960	2967	2964	2998–2960	2996–2960
$\nu(\text{C=O})$	1764	1785	1719	1683	1785	1781
$\nu_{\text{as}}(\text{NO}_2)$	1582	1611	1561	1568	1590	1618
$\nu_{\text{s}}(\text{NO}_2)$	1297	1305	1279	1287	1290	1293

3.5 Microscope Images

Images of the crystals of MaBTNE and NABTNE were taken on a Leica S9i stereo microscope in magnifications from $500\text{ }\mu\text{m}$ to 2 mm , using a polarization filter.



Figure A3.1 Microscope images of MaBTNE (left) and NABTNE (center and right).

3.6 Crystallographic Data

3.6.1 Nitraminodiacetic Acid

Nitraminodiacetic acid	
formula	C ₄ H ₆ N ₂ O ₆
<i>FW</i> [g mol ⁻¹]	178.11
<i>T</i> [K]	123 (2)
λ [Å]	0.71073
crystal system	orthorhombic
space group	<i>Pnma</i>
crystal size [mm]	0.40 x 0.06 x 0.15
crystal habit	colorless plate
<i>a</i> [Å]	8.8051 (4)
<i>b</i> [Å]	14.4941 (7)
<i>c</i> [Å]	5.2206 (2)
α, β, γ [deg]	90
<i>V</i> [Å ³]	666.26 (5)
<i>Z</i>	4
ρ_{calc} [g cm ⁻³]	1.776
μ	0.170
<i>F</i> (000)	368
2 θ range [deg]	4.15 – 26.37
index ranges	-10 ≤ <i>h</i> ≤ 11 -18 ≤ <i>k</i> ≤ 18 -6 ≤ <i>l</i> ≤ 6
reflections collected	4692
reflections independent	709
<i>R</i> _{int}	0.0329
Observed reflections	603
Parameters	70
<i>R</i> ₁ (obs)	0.029
w <i>R</i> ₂ (all data)	0.0709
GooF	1.076
Resd. Dens. [e Å ⁻³]	-0.230; 0.248

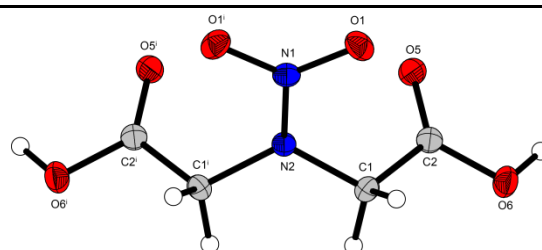


Figure A3.2 X-ray molecular structure of nitraminodiacetic acid. Thermal ellipsoids represent the 50% probability level.

CCDC: 2009758

3.6.2 NABTNE

NABTNE	
formula	C ₈ H ₈ N ₈ O ₁₈
<i>FW</i> [g mol ⁻¹]	504.22
<i>T</i> [K]	153 (2)
λ [Å]	0.71073
crystal system	triclinic
space group	<i>P</i> -1
crystal size [mm]	0.20 x 0.18 x 0.14
crystal habit	colorless needle
<i>a</i> [Å]	5.8695 (7)
<i>b</i> [Å]	17.401 (2)
<i>c</i> [Å]	18.116 (2)
α [deg]	88.360 (9)
β [deg]	86.992 (10)
γ [deg]	84.906 (10)
<i>V</i> [Å ³]	1839.9 (4)
<i>Z</i>	4
ρ_{calc} [g cm ⁻³]	1.82016
μ	0.182
<i>F</i> (000)	1024
2 θ range [deg]	3.38 – 26.37
index ranges	$-7 \leq h \leq 6$ $-21 \leq k \leq 20$ $-16 \leq l \leq 22$
reflections collected	7532
reflections independent	7532
<i>R</i> _{int}	0.0975
Observed reflections	2872
Parameters	614
<i>R</i> 1 (obs)	0.0715
w <i>R</i> ₂ (all data)	0.1466
GooF	0.926
Resd. Dens. [e Å ⁻³]	-0.341; 0.326

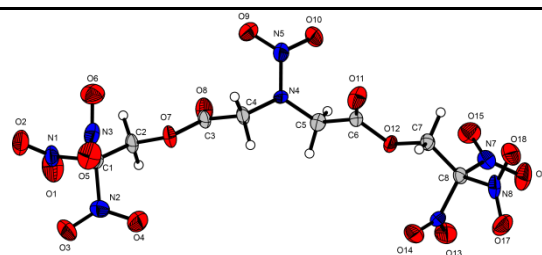


Figure A3.3 X-ray molecular structure of nitramino diacetic acid bis(trinitroethyl ester) (NABTNE). Thermal ellipsoids represent the 50% probability level.

CCDC: 2009759

3.7 Plots of DSC Measurements of NABTNE (2)

The DSC Measurements were carried out on a DSC 2+ from Mettler Toledo in heating rates of 0.5 °C min^{-1} , 1 °C min^{-1} , 2 °C min^{-1} , 4 °C min^{-1} and 8 °C min^{-1} .

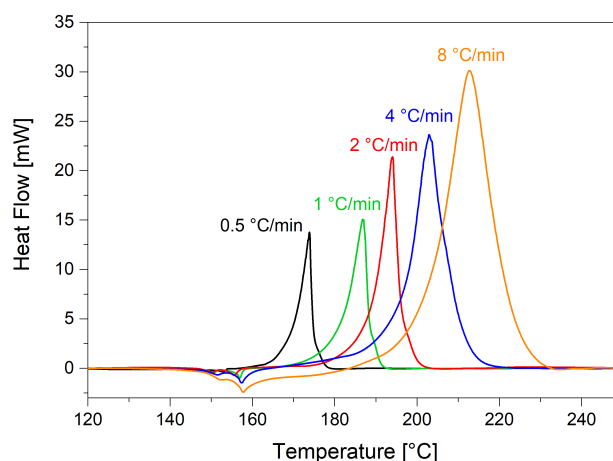


Figure A3.4 DSC measurements in various heating rates plotted against the resulting heat flow.

3.8 Theoretical Calculations

In order to calculate the enthalpies and energies of formation, CBS4-M level calculations were used as implemented in GAUSSIAN 09.^[6] Gas phase enthalpies were transformed to solid state enthalpies by using Trouton's rule for neutral compounds.^[7] All *ab initio* calculations were carried out by using the program package Gaussian 09 and were visualized by GaussView 5.08.^[8]

Based on these calculations, the detonation parameters were calculated using the EXPLO5(V6.03) program package.^[9] The program is based on the steady-state model of equilibrium and uses the Becker-Kistiakowski-Wilson equation of state (BKW EOS) for gaseous detonation products. EXPLO5 is designed to enable the calculation of detonation parameters at the Chapman–Jouget (C–J) point, which was found from the Hugoniot curve of the system by its first derivative. For the calculations the maximum densities at room temperature were used (298 K), which were calculated from the corresponding crystal densities. Therefore, the following equation and the α_v coefficient of volume expansion from the nitramine HMX ($\alpha_v = 1.6 \cdot 10^{-4}\text{ K}^{-1}$) was used.

$$\rho_{298\text{K}} = \rho_T / (1 + \alpha_v(298 - T))$$

The specific impulses (I_{sp}) were calculated as well at 70.0 bar chamber pressure, isobaric combustion conditions (1 bar) and equilibrium to throat and frozen to exit. I_{sp} was calculated for the neat compound, for optimized mixtures with aluminum and for a three-component composition with oxidizer, aluminum and 14% binder. In order to find the most suitable binder,

HTPB, PBAN (6% polybutadiene acrylic acid, 6% polybutadiene acrylonitrile and 2% bisphenol A ether) and the more energetic binder GAP and BAMO, were taken into account. The amount of aluminum was varied from 5% to 25% and plotted against the specific impulses as shown in Graph A3.1 and Graph A3.2.

Table A3.4 Specific impulses of MaBTNE with varying amounts of aluminum, calculated with 14% HTPB, PBAN, GAP and BAMO as binder.

	HTPB	PBAN	GAP	BAMO
I_s /s (5.0% Al)	232	231	251	251
I_s /s (7.5% Al)	235	235	253	253
I_s /s (10.0% Al)	240	240	255	255
I_s /s (12.5% Al)	239	243	256	257
I_s /s (15.0% Al)	238	240	258	258
I_s /s (17.5% Al)	236	238	258	259
I_s /s (20.0% Al)	234	235	256	256
I_s /s (22.5% Al)	232	233	251	249
I_s /s (25.0% Al)	229	230	243	241

Graph A3.1 Specific impulse of MaBTNE in aluminum mixtures with different binders.

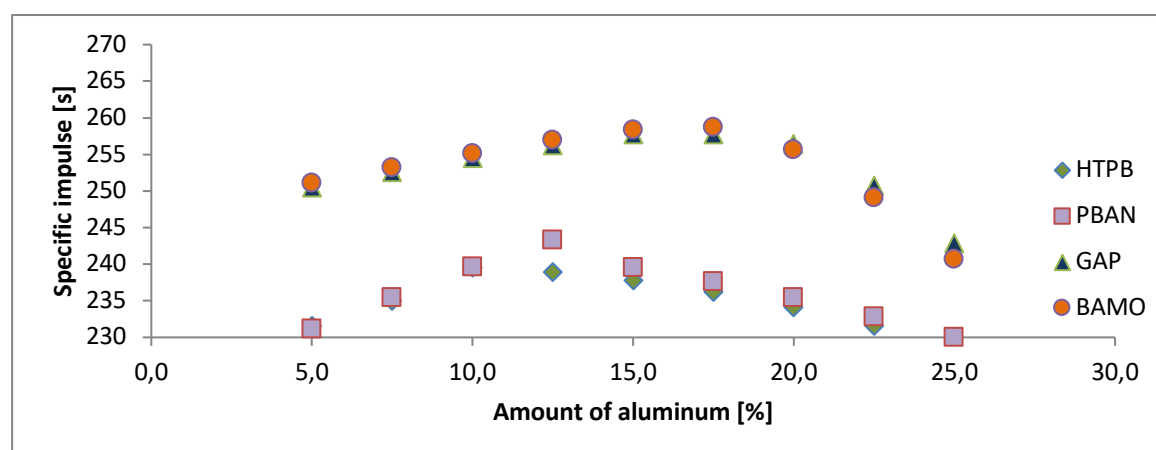
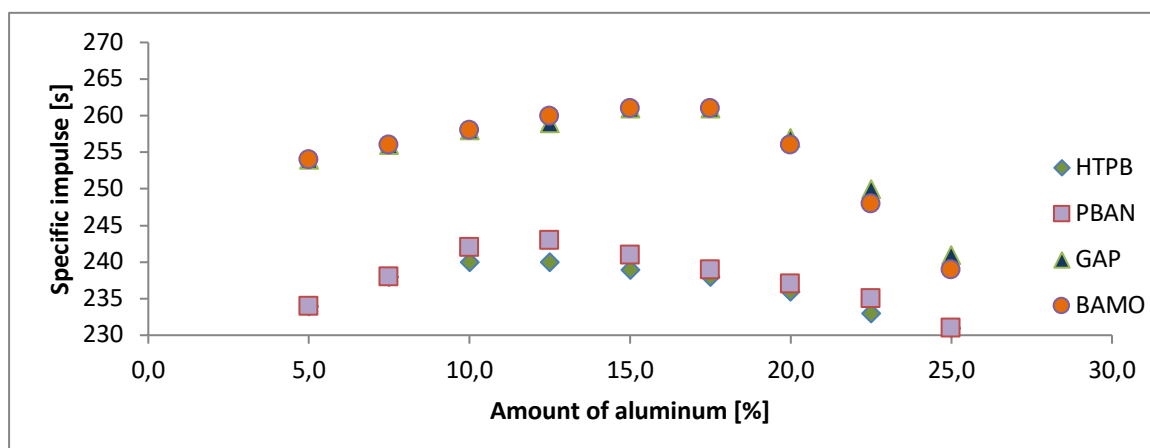


Table A3.5 Specific impulses of NABTNE with varying amounts of aluminum, calculated with 14% HTPB, PBAN, GAP and BAMO as binder.

	HTPB	PBAN	GAP	BAMO
I_s /s (5.0% Al)	234	234	254	254
I_s /s (7.5% Al)	238	238	256	256
I_s /s (10.0% Al)	240	242	258	258
I_s /s (12.5% Al)	240	243	259	260
I_s /s (15.0% Al)	239	241	261	261
I_s /s (17.5% Al)	238	239	261	261
I_s /s (20.0% Al)	236	237	257	256
I_s /s (22.5% Al)	233	235	250	248
I_s /s (25.0% Al)	231	231	241	239

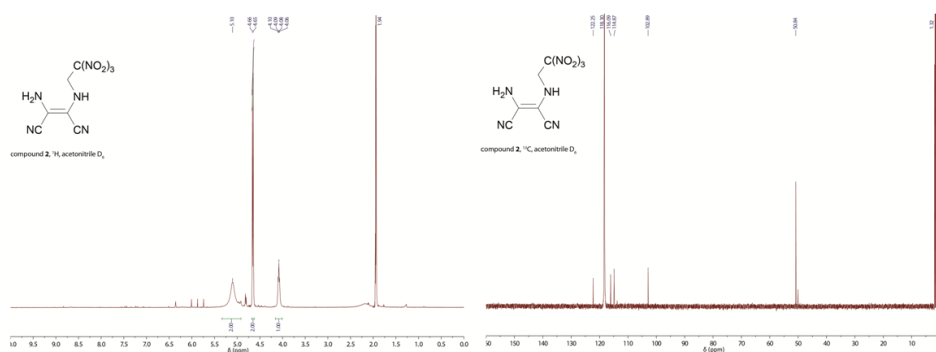
Graph A3.2 Specific impulse of NABTNE in aluminum mixtures with different binders.

3.9 References

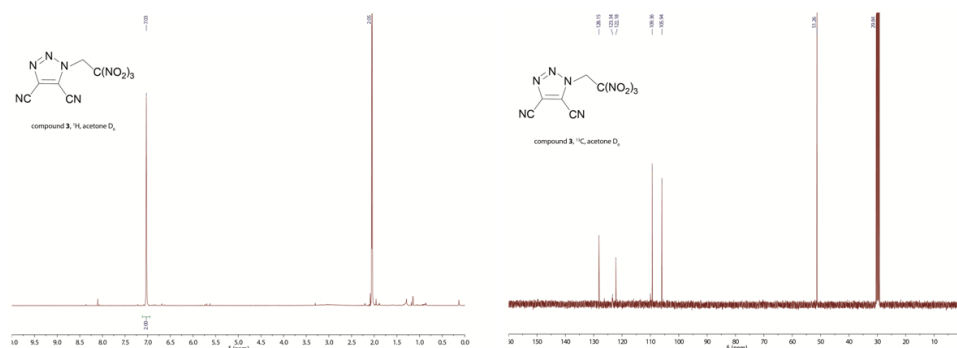
1. NATO. *Explosives, Impact Sensitivity Tests*; Standardization Agreement 4489 (STANAG 4489), Brussels, Belgium, 1999.
2. NATO. *Explosives, Friction Sensitivity Tests*; Standardization Agreement 4487 (STANAG 4487), Brussels, Belgium, 2002.
3. Altomare, A.; Cascarano, G.; Giacovazzo, C.; Guagliardi, A.; Moliterni, A. G. G.; Burla, M. C.; Polidori, G.; Camalli, M.; Spagna, R. *SIR97*, Univeristy of Bari (Italy), 1997.
4. Altomare, A.; Burla, M. C.; Camalli, M.; Cascarano, G. L.; Giacovazzo, C.; Guagliardi, A.; Moliterni, A. G. G.; Polidori, G.; Spagna, R., *SIR97: a New Tool for Crystal Structure Determination and Refinement. J. Appl. Crystallogr.* **1999**, *32*, 115–119.
5. Sheldrick, G. M., A Short History of SHELX. *Acta Crystallogr.* **2008**, *64A*, 112–122.
6. Sheldrick, G. M. *SHELX-97, Programs for Crystal Structure Determination*, University of Göttingen: University of Göttingen, Göttingen (Germany), 1997.
7. Farrugia, L. J., WinGX Suite for Small-molecule Single-crystal Crystallography. *J. Appl. Crystallogr.* **1999**, *32*, 837–838.
8. Frisch, M. J.; Trucks, G. W.; Schlegel, H. B.; Scuseria, G. E.; Robb, M. A.; Cheeseman, J. R.; G. Scalmani, V. B.; Mennucci, B.; Petersson, G. A.; Nakatsuji, H.; Caricato, M.; Li, X.; Hratchian, H. P.; Izmaylov, A. F.; Bloino, J.; Zheng, G.; Sonnenberg, J. L.; Hada, M.; Ehara, M.; Toyota, K.; Fukuda, R.; Hasegawa, J.; Ishida, M.; Nakajima, T.; Honda, Y.; Kitao, O.; Nakai, H.; Vreven, T.; J. A. Montgomery, J.; Peralta, J. E.; Ogliaro, F.; Bearpark, M.; Heyd, J. J.; Brothers, E.; Kudin, K. N.; Staroverov, V. N.; Kobayashi, R.; Normand, J.; Raghavachari, K.; Rendell, A.; Burant, J. C.; Iyengar, S. S.; Tomasi, J.; Cossi, M.; Rega, N.; Millam, J. M.; Klene, M.; Knox, J. E.; Cross, J. B.; Bakken, V.; Adamo, C.; Jaramillo, J.; Gomperts, R.; Stratmann, R. E.; Yazyev, O.; Austin, A. J.; Cammi, R.; Pomelli, C.; Ochterski, J. W.; Martin, R. L.; Morokuma, K.; Zakrzewski, V. G.; Voth, G. A.; Salvador, P.; Dannenberg, J. J.; Dapprich, S.; Daniels, A. D.; Farkas, Ö.; Foresman, J. B.; Ortiz, J. V.; Cioslowski, J.; Fox, D. J., *Gaussian 09*. Rev. A.02 ed., Gaussian, Inc., Wallingford CT (US), **2009**.
9. Ochterski, J. W.; Petersson, G. A.; Montgomery, J. A., A Complete Basis Set Model Chemistry. V. Extensions to Six or More Heavy Atoms. *J. Chem. Phys.* **1996**, *104*, 2598–2619.
10. J. A. Montgomery; Frisch, M. J.; Ochterski, J. W.; Petersson, G. A., A Complete Basis Set Model Chemistry. VII. Use of the Minimum Population Localization Method. *J. Chem. Phys.* **2000**, *112*, 6532–6542.
11. Trouton, F., On Molecular Latent Heat. *Philos. Mag.* **1884**, *18*, 54–57.
12. Dennington II, R. D.; Keith, T. A.; Millam, J. M., *GaussView*. Ver. 5.08 ed., Semichem, Inc., Wallingford CT (US), **2009**.
13. Sućeska, M., *EXPLO5 V6.03*. Zagreb (Croatia), **2015**.

4 Supporting Information to Azoles with Trinitroethyl Substitution

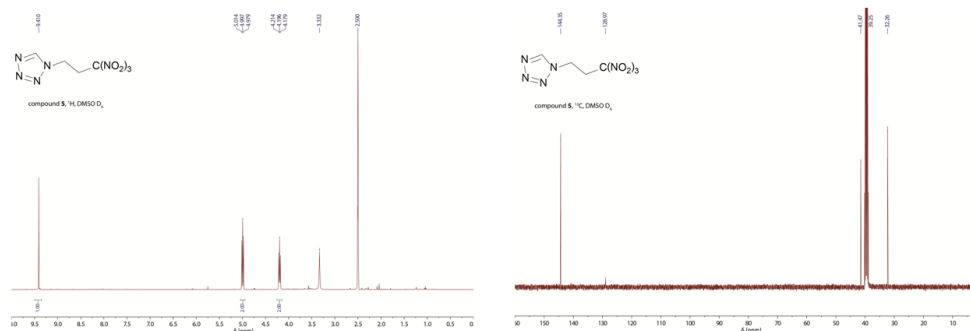
4.1 ^1H and ^{13}C NMR Data of 2



4.2 ^1H and ^{13}C NMR Data of Triazole 3



4.3 ^1H and ^{13}C NMR Data of Tetrazole 5



4.4 Crystallographic Data of Triazole 3

3	
formula	C ₆ H ₂ N ₈ O ₆
<i>FW</i> [g mol ⁻¹]	282.13
<i>T</i> [K]	173
λ [Å]	0.71073
crystal system	monoclinic
space group	<i>P</i> 2 ₁ / <i>n</i>
crystal size [mm]	0.37 x 0.04 x 0.04
crystal habit	colorless needle
<i>a</i> [Å]	10.933 (7)
<i>b</i> [Å]	9.353 (5)
<i>c</i> [Å]	11.274 (9)
α, γ [deg]	90
β [deg]	108.6 (8)
<i>V</i> [Å ³]	1092.3 (9)
<i>Z</i>	4
ρ_{calc} [g cm ⁻³]	1.72
μ	0.155
<i>F</i> (000)	568
2 θ range [deg]	4.50 – 27.47
index ranges	-12 ≤ <i>h</i> ≤ 13 -11 ≤ <i>k</i> ≤ 11 -14 ≤ <i>l</i> ≤ 14
reflections collected	8407
reflections unique	2221
parameters	189
GooF	1.023
<i>R</i> ₁ / <i>wR</i> ₂ [<i>I</i> > 2 σ (<i>I</i>)]	0.0453 / 0.0773
<i>R</i> ₁ / <i>wR</i> ₂ (all data)	0.0923 / 0.1064
max / min residual electron density [Å ⁻³]	0.367 / -0.321

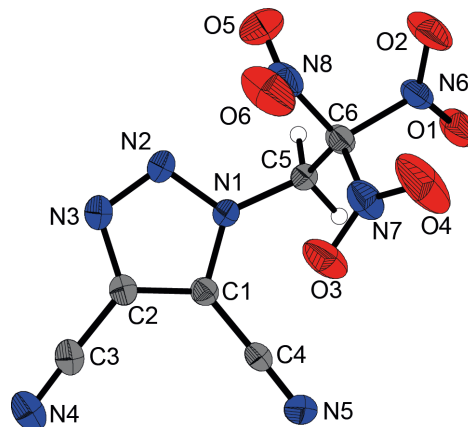


Figure A4.1 X-ray molecular structure of 4,5-dicyano-1*N*-(trinitroethyl)-1,2,3-triazole (**3**). Thermal ellipsoids represent the 50% probability level.

CCDC: 1587493

4.5 Crystallographic Data of Tetrazole 5

5	
formula	C ₄ H ₅ N ₇ O ₆
<i>FW</i> [g mol ⁻¹]	247.13
<i>T</i> [K]	143
λ [Å]	0.71073
crystal system	monoclinic
space group	<i>P</i> 2 ₁ / <i>c</i>
crystal size [mm]	0.35 x 0.15 x 0.03
crystal habit	yellow platelet
<i>a</i> [Å]	11.0691 (16)
<i>b</i> [Å]	7.7257 (9)
<i>c</i> [Å]	12.030 (2)
α, γ [deg]	90
β [deg]	114.457 (19)
<i>V</i> [Å ³]	936.5 (3)
<i>Z</i>	4
$\rho_{\text{calc.}}$ [g cm ⁻³]	1.75
μ	0.163
<i>F</i> (000)	504
2 θ range [deg]	4.20 – 29.34
index ranges	-14 ≤ <i>h</i> ≤ 14 -10 ≤ <i>k</i> ≤ 10 -13 ≤ <i>l</i> ≤ 16
reflections collected	2197
reflections unique	1463
parameters	174
Goof	0.977
<i>R</i> ₁ / <i>wR</i> ₂ [<i>I</i> > 2 σ (<i>I</i>)]	0.0449 / 0.0795
<i>R</i> ₁ / <i>wR</i> ₂ (all data)	0.0769 / 0.0911
max / min residual electron density [Å ⁻³]	0.285 / -0.308

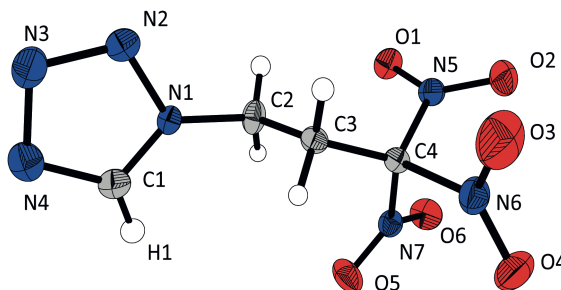


Figure A4.2 X-ray molecular structure of 1*N*-trinitropropyl tetrazole (**5**). Thermal ellipsoids represent the 50% probability level

CCDC: 1822024

4.6 Theoretical Calculations

Enthalpies of formation of all presented compounds were calculated using the CBS-4M quantum chemical method¹⁻² with Gaussian09 A.02³. The CBS (complete basis set) models use the known asymptotic convergence of pair natural orbital expressions to extrapolate from calculations using a finite basis set to the estimated complete basis set limit. In this study we applied the modified CBS-4M method (M referring to the use of Minimal Population localization) which is a re-parametrized version of the original CBS-4 method and also includes some additional empirical corrections. The calculated gas phase enthalpies were transformed to solid state enthalpies by subtraction of sublimation enthalpy calculated by using Trouton's rule.⁴

Detonation parameters were calculated using the EXPLO5 6.03 computer code⁵ with the CBS-4M calculated enthalpies of formation. The program is based on the steady-state model of equilibrium and uses the Becker-Kistiakowsky-Wilson equation of state (BKW EOS.) for gaseous detonation products and the Murnaghan EOS for both solid and liquid products. It is designed to enable the calculation of detonation parameters at the Chapman–Jouguet point (C–J point). The C–J point was found from the Hugoniot curve of the system by its first derivative.⁶ The calculations were performed using the maximum densities at room temperature. The densities at 298 K were either obtained by pycnometer measurement or calculated from the corresponding crystal densities by following equation and the α_v coefficient of volume expansion from the nitramine HMX ($\alpha_v = 1.6 \cdot 10^{-4} \text{ K}^{-1}$):

$$\rho_{298\text{K}} = \rho_T / (1 + \alpha_v(298 - T)).$$

4.7 Calculation Details of Triazole 3

3			
Minimum energy of optimized structure, MP4(SDQ)/6-31 G	-1114.2693144 a.u.		
CBS-4M enthalpy, basis for EXPLO5 6.03 calculations	-1117.430133 a.u.		
CSB-4M energy	-1117.431077 a.u.		
CSB-4M free energy	-1117.495594 a.u.		
Number of imaginary frequencies	0		
Cartesian coordinates			
Atom	x	y	z
O	2.68780900	1.54869300	-1.32770500
N	2.80273600	0.51135300	-0.64590100
O	3.81387700	-0.10310200	-0.35292900
C	1.49748900	0.03367500	-0.07749500
N	1.65442700	-1.40693400	0.27369100
C	0.40985900	0.22857200	-1.13125300
N	1.29480100	0.83850400	1.16643700
O	1.95589800	-2.10324800	-0.70163500
O	1.43550400	-1.73519900	1.43298300
N	-0.87095000	-0.27747900	-0.69285200
H	0.33443000	1.27775700	-1.35037800
H	0.71964300	-0.31809400	-2.00608100
O	0.19042500	1.37593400	1.30163800
O	2.26561200	0.88598200	1.91565200
C	-2.00656400	0.37975900	-0.37081100
N	-1.09395900	-1.64310600	-0.62222900
C	-2.15450400	1.77638000	-0.37966500
C	-2.92135800	-0.59094000	-0.09648800
N	-2.31383000	-1.81270600	-0.25850200
N	-2.29004900	2.90633600	-0.39936900
C	-4.26637300	-0.43593000	0.28205700
N	-5.35436900	-0.29614400	0.58649000

4.8 Calculation Details of Tetrazole 5

5			
Minimum energy of optimized structure, MP4(SDQ)/6-31 G	−985.6322218 a.u.		
CBS-4M enthalpy, basis for EXPLO5 6.03 calculations	−988.475794 a.u.		
CSB-4M energy	−988.476738 a.u.		
CSB-4M free energy	−988.537654 a.u.		
Number of imaginary frequencies	0		
Cartesian coordinates			
Atom	x	y	z
N	1.72577700	−0.62568700	1.21272700
O	0.84589700	2.10968400	−0.78089200
N	2.01293300	−0.69509600	−1.18667300
O	1.14065600	−0.17592000	2.21227900
O	2.54166700	1.71967200	0.59715500
N	−2.56799000	0.15800200	0.24925700
N	−3.11557300	−1.11304100	0.26856500
N	1.56761900	1.39347400	−0.06949200
O	2.63820900	−1.43702800	1.16565900
N	−4.31106300	−1.00814700	−0.17538600
O	1.66047900	−1.84169700	−1.47462500
O	2.91589500	−0.02100500	−1.67807600
N	−4.59573900	0.33463100	−0.49957400
C	−1.20438700	0.37416400	0.70529600
C	−0.26171000	−0.31395200	−0.30365800
C	−3.51002300	0.99472800	−0.22567000
C	1.21689200	−0.06475200	−0.07730200
H	−0.48318300	0.06365200	−1.29057900
H	−0.42272000	−1.38049600	−0.29774600
H	−1.02484900	1.43624100	0.72735000
H	−1.09773400	−0.03909300	1.68977400
H	−3.37030600	2.03995800	−0.34875800

4.9 References

1. Montgomery, J. J. A.; Frisch, M. J.; Ochterski, J. W.; Petersson, G. A. A Complete Basis Set Model Chemistry. VII. Use of the Minimum Population Method. *J. Chem. Phys.* **2000**, *112*, 6532–6542.
2. Ochterski, J. W.; Petersson, G. A.; Montgomery, J. J. A. A Complete Basis Set Model Chemistry. V. Extensions to Six or More Heavy Atoms. *J. Chem. Phys.* **1996**, *104*, 2598–2619.
3. Frisch, M. J.; Trucks, G. W.; Schlegel, H. B.; Scuseria, G. E.; Robb, M. A.; Cheeseman, J. R.; Scalmani, G.; Barone, V.; Mennucci, B.; Petersson, G. A.; Nakatsuji, H.; Caricato, M.; Li, X.; Hratchian, H. P.; Izmaylov, A. F.; Bloino, J.; Zheng, G.; Sonnenberg, J. L.; Hada, M.; Ehara, M.; Toyota, K.; Fukuda, R.; Hasegawa, J.; Ishida, M.; Nakajima, T.; Honda, Y.; Kitao, O.; Nakai, H.; Vreven, T.; Montgomery Jr., J. A.; Peralta, J. E.; Ogliaro, F.; Bearpark, M. J.; Heyd, J.; Brothers, E. N.; Kudin, K. N.; Staroverov, V. N.; Kobayashi, R.; Normand, J.; Raghavachari, K.; Rendell, A. P.; Burant, J. C.; Iyengar, S. S.; Tomasi, J.; Cossi, M.; Rega, N.; Millam, N. J.; Klene, M.; Knox, J. E.; Cross, J. B.; Bakken, V.; Adamo, C.; Jaramillo, J.; Gomperts, R.; Stratmann, R. E.; Yazyev, O.; Austin, A. J.; Cammi, R.; Pomelli, C.; Ochterski, J. W.; Martin, R. L.; Morokuma, K.; Zakrzewski, V. G.; Voth, G. A.; Salvador, P.; Dannenberg, J. J.; Dapprich, S.; Daniels, A. D.; Farkas, Ö.; Foresman, J. B.; Ortiz, J. V.; Cioslowski, J.; Fox, D. J. *Gaussian 09*, Gaussian, Inc.: Wallingford, **2009**.
4. Trouton, F. IV. On Molecular Latent Heat. *Philos. Mag.* **1884**, *18*, 54–57.
5. Sućeska, M. EXPLO5 program, 6.03 ed., Zagreb, Croatia, **2015**.
6. Sućeska, M. Calculation of the Detonation Properties of CHNO Explosives. *Propellants, Explos., Pyrotech.* **1991**, *16*, 197–202.
7. Xue, C.; Sun, J.; Kang, B.; Liu, Y.; Liu, X.; Song, G.; Xue, Q. The β - δ -Phase Transition and Thermal Expansion of Octahydro-1,3,5,7-tetranitro-1,3,5,7-tetrazocine. *Propellants, Explos., Pyrotech.* **2010**, *35*, 333–338.

5 Supporting Information to Urazine Derivatives

5.1 General Information

Raman spectra were recorded in glass tubes with a Bruker MultiRAM FT-Raman spectrometer with a Klaastech DENICAFC LC-3/40 laser (Nd:YAG, 1064 nm, up to 1000 mW). The measurement range is from 4000 to 400 cm^{-1} . IR spectra were recorded on an ATR device using the Perkin-Elmer One spectrometer. All Raman and IR spectra were recorded at ambient temperature. NMR spectra were recorded with the 400 MHz spectrometers JOEL Eclipse and Bruker TR at 25 °C. Me_4Si (^1H , 399.8 MHz, ^{13}C , 100.5 MHz) and MeNO_2 (^{14}N , 28.9 MHz) were used as external standards to determine the chemical shifts relative to. Analysis of C/H/N were performed on an Elementar vario EL, C/H/N/S on an Elementar vario micro cube and Cl with a Metrohm 888 Titrand. Melting and decomposition points were determined by differential thermal analysis (DTA) using an OZM Research DTA 552-Ex instrument at a heating rate of 5 °C min^{-1} and checked by a BÜCHI melting- point apparatus B-540. Temperature-dependent weight loss was detected using Thermal Gravimetry Analysis with a Perkin Elmer, TGA4000 in the temperature range from 30 °C–400 °C. Measurements were performed in a temperature range of 15 to 400 °C against a reference material. The sensitivity data were acquired by using a BAM drop hammer and BAM friction tester.^[1]

5.2 X-ray Crystallography

Suitable crystals for X-ray crystallography were selected by means of a polarization microscope, mounted on the tip of a glass fiber. All measurements were investigated with an Oxford Xcalibur CCD diffractometer at low temperatures. Mo- K_α radiation ($\lambda = 0.7107 \text{ \AA}$) was delivered by a Spellman generator (voltage 50 kV, current 40 mA) The solution of the structures was performed by direct methods (*e. g.* SIR97)^[2] and refined by full-matrix least-squares on F^2 (SHELXL),^[3] both implemented in the program package WINGX.^[4] At the end, all structures were checked using the PLATON software.^[5] All non-hydrogen atoms were refined anisotropically and structures displayed with ORTEP plots are drawn with thermal ellipsoids at 50% probability level.

Crystallographic data (excluding structure factors) for the structures in this paper have been deposited with the Cambridge Crystallographic Data Centre, CCDC, 12 Union Road, Cambridge CB21EZ, UK. Copies of the data can be obtained free of charge on quoting the CCDC numbers 2000061 (**2**), 1992639 (**3**), 1992643 (**4**), 1992641 (**6**) 1992642 (**7**), 1992644 (**8**), 1992640 (**9**), 1992645 (**10**) and 1993031 (**12**) (<http://www.ccdc.cam.ac.uk>)

Table A5.1 Crystallographic data of **2–4**

	2	3	4
Formula	C ₄ H ₅ N ₇ O ₈	C ₂ H ₉ N ₅ O ₃	C ₂ H ₇ N ₅ O ₃
FW [g mol ⁻¹]	279.15	151.14	149.13
Crystal system	orthorhombic	triclinic	triclinic
Space Group	<i>Pbca</i>	<i>P</i> -1	<i>P</i> -1
Color / Habit	colorless block	colorless plate	colorless plate
Size [mm]	0.16 x 0.27 x 0.55	0.20 x 0.40 x 0.40	0.20 x 0.40 x 0.40
<i>a</i> [Å]	11.3543(6)	5.8479(6)	5.8801(5)
<i>b</i> [Å]	11.5615(5)	6.5506(6)	6.6460(7)
<i>c</i> [Å]	15.3582(7)	8.5116(8)	8.3699(8)
α [°]	90	69.929(9)	69.586(9)
β [°]	90	74.878(9)	75.035(8)
γ [°]	90	87.356(8)	65.149(9)
<i>V</i> [Å ³]	2016.11(17)	295.31(5)	275.75(5)
<i>Z</i>	8	2	2
$\rho_{\text{calc.}}$ [g cm ⁻³]	1.839	1.700	1.796
μ [mm ⁻¹]	0.177	0.152	0.162
<i>F</i> (000)	1136	160	156
$\lambda_{\text{MoK}\alpha}$ [Å]	0.71073	0.71073	0.71073
<i>T</i> [K]	115	114	127
θ Min–Max [°]	2.7, 28.7	2.6, 32.2	2.6, 28.3
Index ranges	-13 ≤ <i>h</i> ≤ 15 -15 ≤ <i>k</i> ≤ 14 -20 ≤ <i>l</i> ≤ 20	-8 ≤ <i>h</i> ≤ 5 -9 ≤ <i>k</i> ≤ 6 -12 ≤ <i>l</i> ≤ 8	-7 ≤ <i>h</i> ≤ 7 -8 ≤ <i>k</i> ≤ 8 -11 ≤ <i>l</i> ≤ 11
Reflections collected	24181	2871	2376
Independent refl.	2607	1910	1360
<i>R</i> _{int}	0.045	0.020	0.019
Observed reflections	2049	1619	1172
Parameters	192	127	119
<i>R</i> ₁ (obs) ^a	0.0478	0.0380	0.0356
<i>wR</i> ₂ (all data) ^b	0.1424	0.1004	0.0961
Goof ^c	1.06	1.09	1.05
Resd. Dens. [e Å ⁻³]	-0.23, 0.66	-0.31, 0.33	-0.30, 0.29
Absorption correction	multi-scan	multi-scan	multi-scan
CCDC	2000061	1992639	1992643

a) $R_1 = \frac{\sum ||F_o| - |F_c||}{\sum |F_o|}$; b) $wR_2 = \frac{[\sum [w(F_o^2 - F_c^2)^2] / \sum [w(F_o^2)]]^{1/2}}$; $w = [\sigma^2(F_o^2) + (xP)^2 + yP]^{-1}$ and $P = (F_o^2 + 2F_c^2) / 3$; c) $\text{Goof} = \frac{\sum [w(F_o^2 - F_c^2)] / (n-p)}{(n-p)^{1/2}}$ (*n* = number of reflections; *p* = total number of parameters)

Table A 5.2 Crystallographic data of **6–8**.

	6	7	8
Formula	C ₃ H ₁₂ N ₈ O ₃	C ₄ H ₁₄ Li ₂ N ₈ O ₈	C ₂ H ₅ N ₄ NaO ₃
FW [g mol ⁻¹]	208.21	316.11	156.09
Crystal system	triclinic	triclinic	triclinic
Space Group	<i>P</i> -1	<i>P</i> -1	<i>P</i> -1
Color / Habit	colorless plate	colorless block	colorless block
Size [mm]	0.10 x 0.40 x 0.50	0.30 x 0.35 x 0.40	0.35 x 0.40 x 0.40
<i>a</i> [Å]	5.8393(5)	5.7310(8)	5.8666(5)
<i>b</i> [Å]	7.1775(5)	7.0776(7)	6.5673(5)
<i>c</i> [Å]	11.0273(9)	8.7697(11)	7.7285(7)
α [°]	82.779(6)	108.08(1)	77.932(7)
β [°]	77.775(7)	96.899(11)	81.768(7)
γ [°]	76.647(7)	106.053(11)	67.305(7)
<i>V</i> [Å ³]	438.05(6)	316.60(8)	267.99(4)
<i>Z</i>	2	1	2
$\rho_{\text{calc.}}$ [g cm ⁻³]	1.579	1.658	1.934
μ [mm ⁻¹]	0.135	0.150	0.237
<i>F</i> (000)	220	164	160
$\lambda_{\text{MoK}\alpha}$ [Å]	0.71073	0.71073	0.71073
<i>T</i> [K]	110	123	123
θ Min–Max [°]	2.9, 26.4	2.5, 26.4	2.7, 32.1
Index ranges	$-7 \leq h \leq 4$ $-8 \leq k \leq 8$ $-13 \leq l \leq 11$	$-7 \leq h \leq 7$ $-8 \leq k \leq 8$ $-10 \leq l \leq 10$	$-8 \leq h \leq 8$ $-9 \leq k \leq 9$ $-11 \leq l \leq 11$
Reflections collected	3102	4661	5460
Independent refl.	1789	1297	1769
<i>R</i> _{int}	0.022	0.034	0.029
Observed reflections	1446	1074	1509
Parameters	175	128	112
<i>R</i> ₁ (obs) ^a	0.0375	0.0356	0.0348
<i>wR</i> ₂ (all data) ^b	0.0938	0.0866	0.0861
GooF ^c	1.05	1.08	1.06
Resd. Dens. [e Å ⁻³]	-0.23, 0.23	-0.30, 0.20	-0.30, 0.46
Absorption correction	multi-scan	multi-scan	multi-scan
CCDC	1992641	1992642	1992644

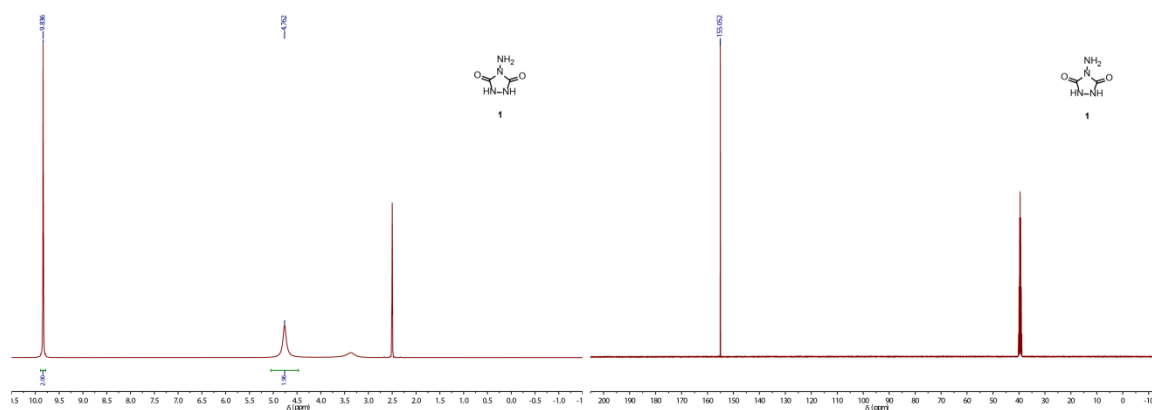
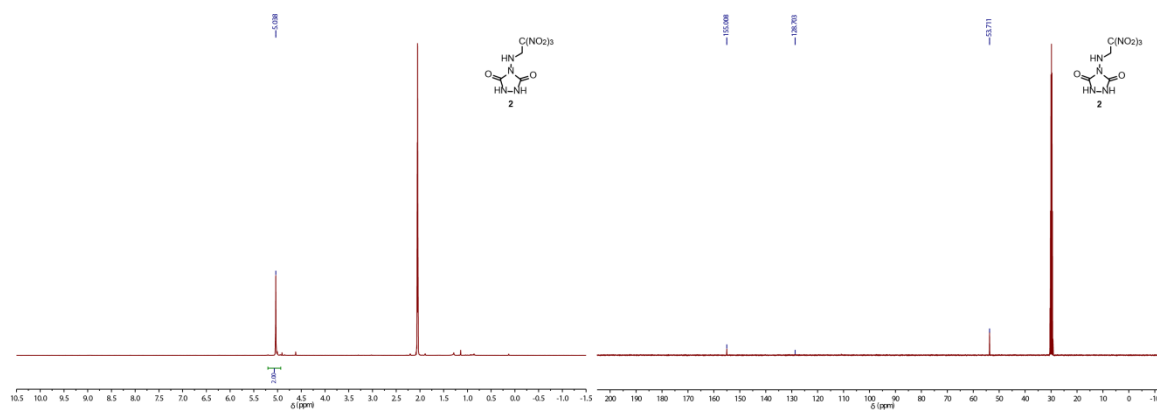
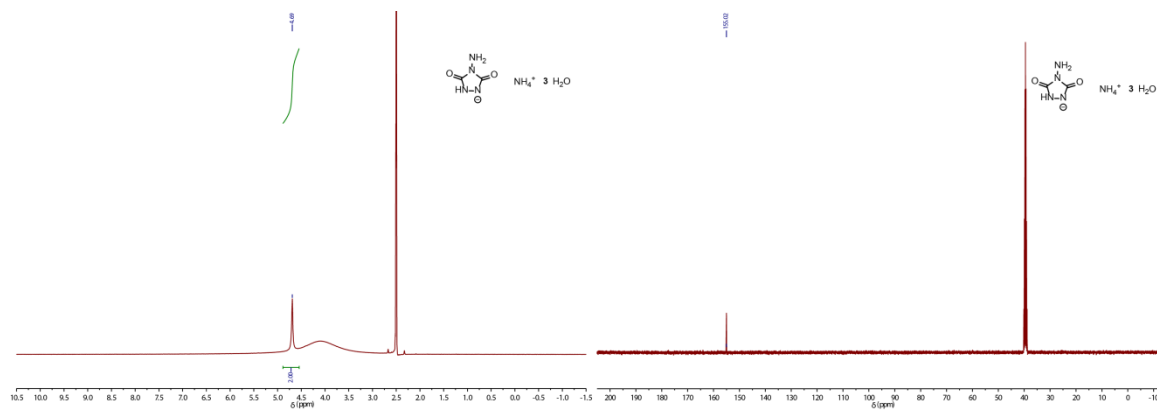
a) $R_1 = \frac{\sum |F_o| - |F_c|}{\sum |F_o|}$; b) $wR_2 = \frac{[\sum [w(F_o^2 - F_c^2)^2] / \sum [w(F_o^2)]]^{1/2}}$; $w = [\sigma^2(F_o^2) + (xP)^2 + yP]^{-1}$ and $P = (F_o^2 + 2F_c^2) / 3$; c) GooF = $\{\sum [w(F_o^2 - F_c^2)^2] / (n-p)\}^{1/2}$ (n = number of reflections; p = total number of parameters).

Table A 5.3 Crystallographic data of **9**, **10** and **12**.

	9	10	12
Formula	C ₂ H ₃ KN ₄ O ₃	C ₂ H ₅ ClN ₄ O ₆	C ₄ H ₈ Cl ₂ CuN ₈ O ₈
FW [g mol ⁻¹]	172.20	216.55	494.62
Crystal system	triclinic	orthorhombic	monoclinic
Space Group	<i>P</i> -1	<i>Pbca</i>	<i>P2₁/n</i>
Color / Habit	colorless block	colorless block	green rod
Size [mm]	0.05 x 0.10 x 0.20	0.10 x 0.15 x 0.30	0.17 x 0.24 x 0.34
<i>a</i> [Å]	5.8036(8)	8.8439(3)	5.8880(1)
<i>b</i> [Å]	6.5418(8)	9.3739(4)	7.7225(1)
<i>c</i> [Å]	8.3032(13)	16.1673(6)	15.5139(3)
α [°]	69.940(13)	90	90
β [°]	74.677(13)	90	100.622(2)
γ [°]	84.165(10)	90	90
<i>V</i> [Å ³]	285.57(7)	1340.30(9)	693.33(2)
<i>Z</i>	2	8	2
$\rho_{\text{calc.}}$ [g cm ⁻³]	2.003	2.146	2.369
μ [mm ⁻¹]	0.877	0.583	2.058
<i>F</i> (000)	176	880	494
$\lambda_{\text{MoK}\alpha}$ [Å]	0.71073	0.71073	0.71073
<i>T</i> [K]	122	200	293
θ Min–Max [°]	2.7, 26.4	4.3, 27.0	4.4, 26.5
Index ranges	$-7 \leq h \leq 6$ $-8 \leq k \leq 6$ $-10 \leq l \leq 8$	$-11 \leq h \leq 11$ $-11 \leq k \leq 11$ $-12 \leq l \leq 20$	$-7 \leq h \leq 7$ $-9 \leq k \leq 9$ $-19 \leq l \leq 19$
Reflections collected	1538	6933	6996
Independent refl.	1143	1462	1440
<i>R</i> _{int}	0.020	0.036	0.018
Observed reflections	984	1168	1399
Parameters	111	138	140
<i>R</i> ₁ (obs) ^a	0.0336	0.0308	0.0199
<i>wR</i> ₂ (all data) ^b	0.0754	0.0835	0.0529
Goof ^c	1.05	1.03	1.07
Resd. Dens. [e Å ⁻³]	-0.33, 0.32	-0.62, 0.27	-0.38, 0.32
Absorption correction	multi-scan	multi-scan	multi-scan
CCDC	1992640	1992645	1993031

a) $R_1 = \sum ||F_0| - |F_c|| / \sum |F_0|$; b) $wR_2 = [\sum [w(F_0^2 - F_c^2)^2] / \sum [w(F_0^2)]]^{1/2}$; $w = [\sigma^2(F_0^2) + (xP)^2 + yP]^{-1}$ and $P = (F_0^2 + 2F_c^2) / 3$; c) $\text{Goof} = \{\sum [w(F_0^2 - F_c^2)^2] / (n-p)\}^{1/2}$ (*n* = number of reflections; *p* = total number of parameters).

5.3 Plots of NMR Spectra

Figure A5.1 ^1H and ^{13}C NMR spectra of compound 1.Figure A5.2 ^1H and ^{13}C NMR spectra of compound 2.Figure A5.3 ^1H and ^{13}C NMR spectra of salt 3

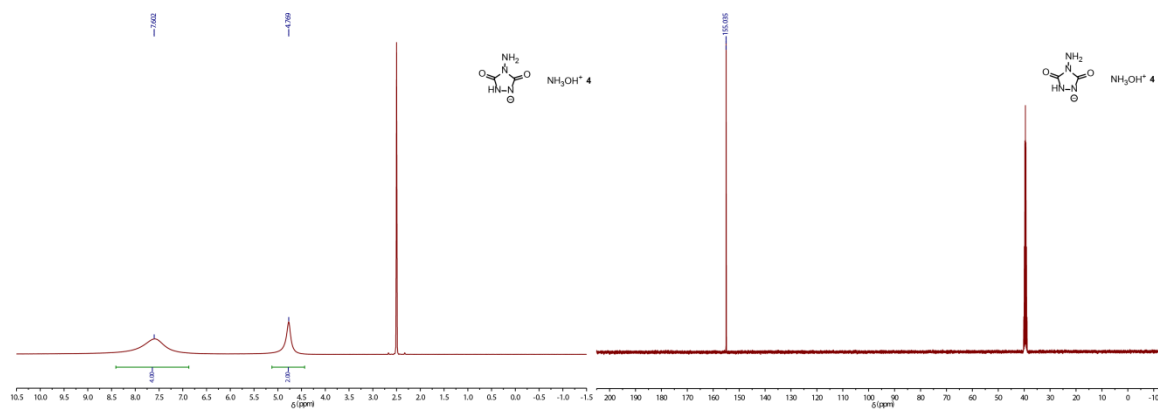


Figure A5.4 ^1H and ^{13}C NMR spectra of salt 4.

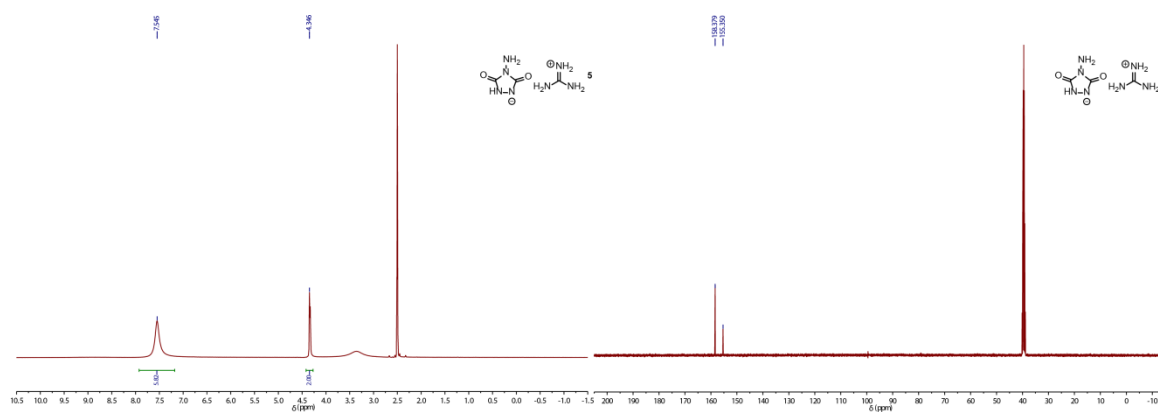


Figure A5.5 ^1H and ^{13}C NMR spectra of salt 5.

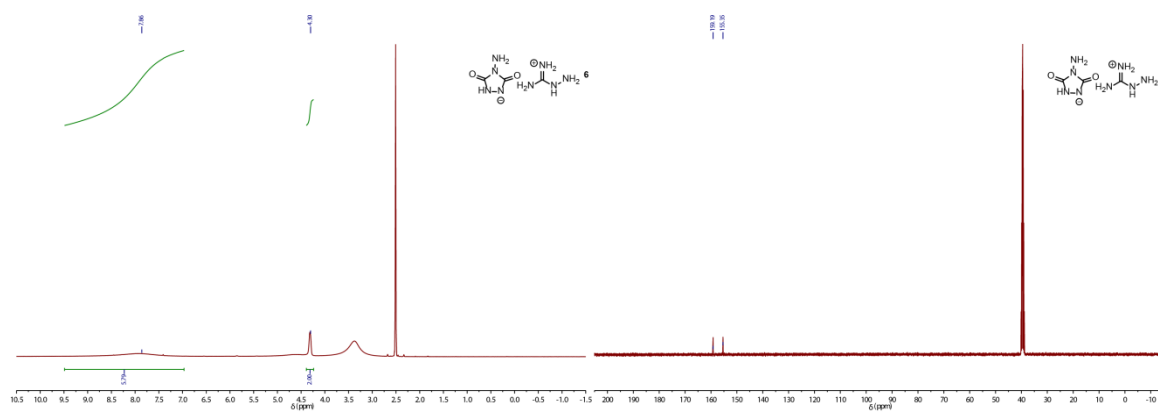


Figure A5.6 ^1H and ^{13}C NMR spectra of salt 6.

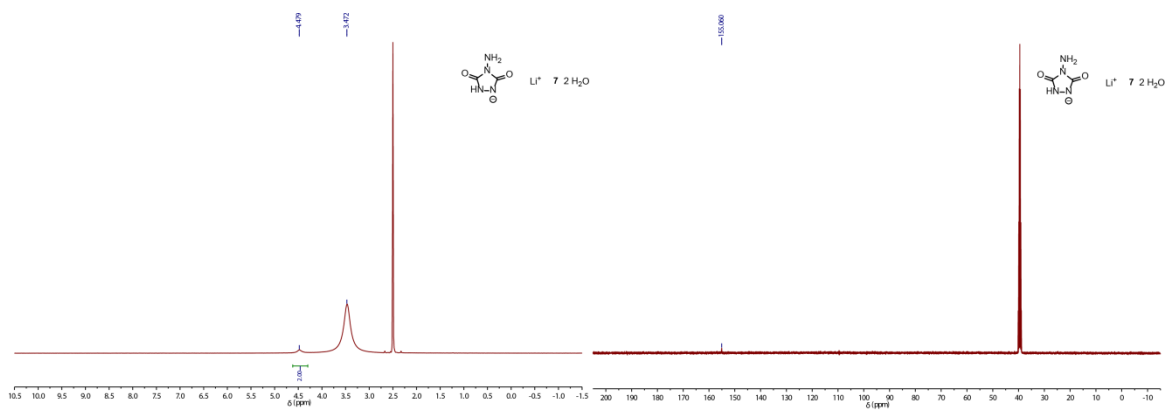


Figure A5.7 ^1H and ^{13}C NMR spectra of salt 7.

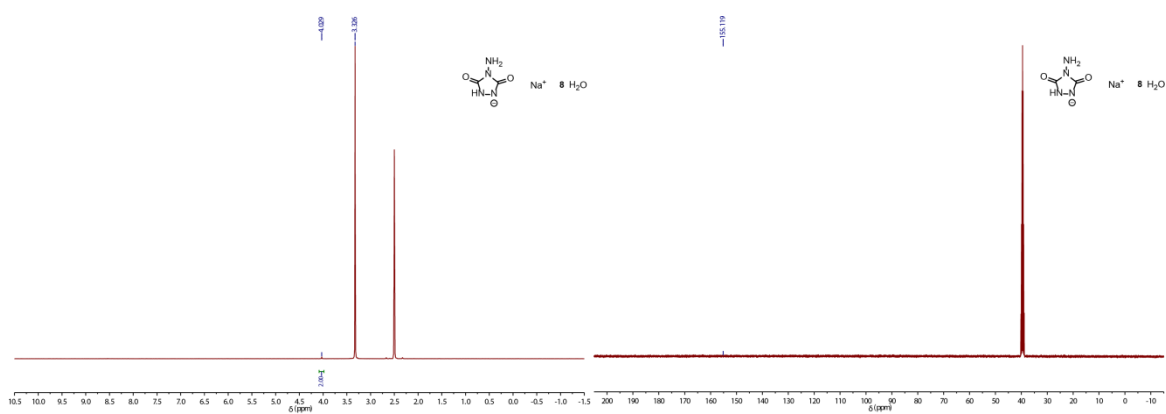


Figure A5.8 ^1H and ^{13}C NMR spectra of salt 8.

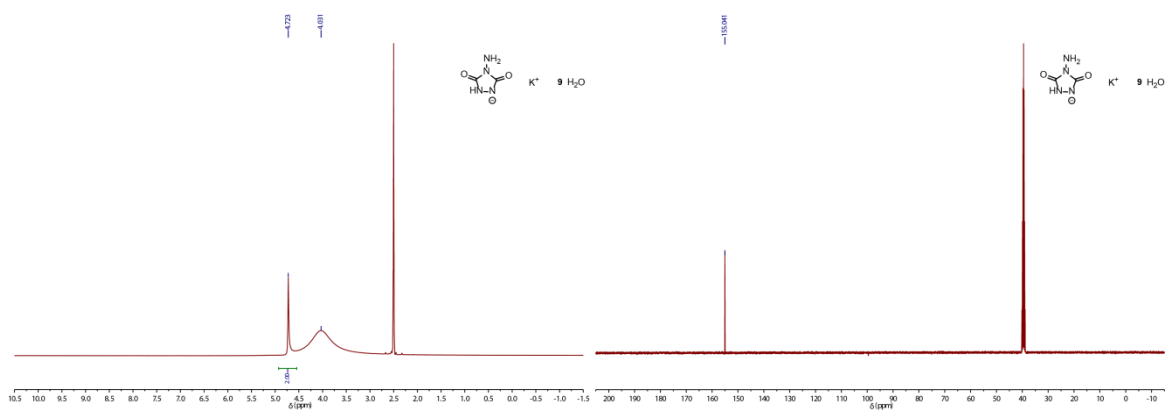


Figure A5.9 ^1H and ^{13}C NMR spectra of salt 9.

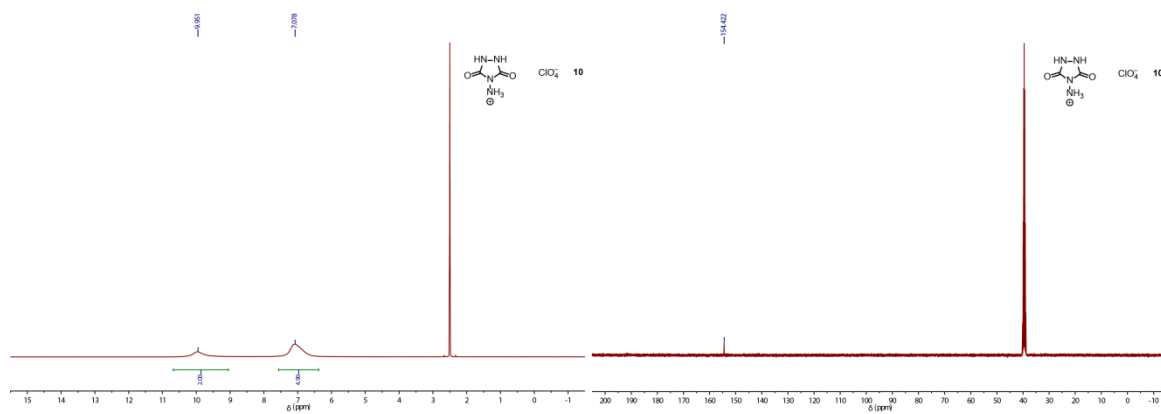


Figure A5.10 ^1H and ^{13}C NMR spectra of salt 10.

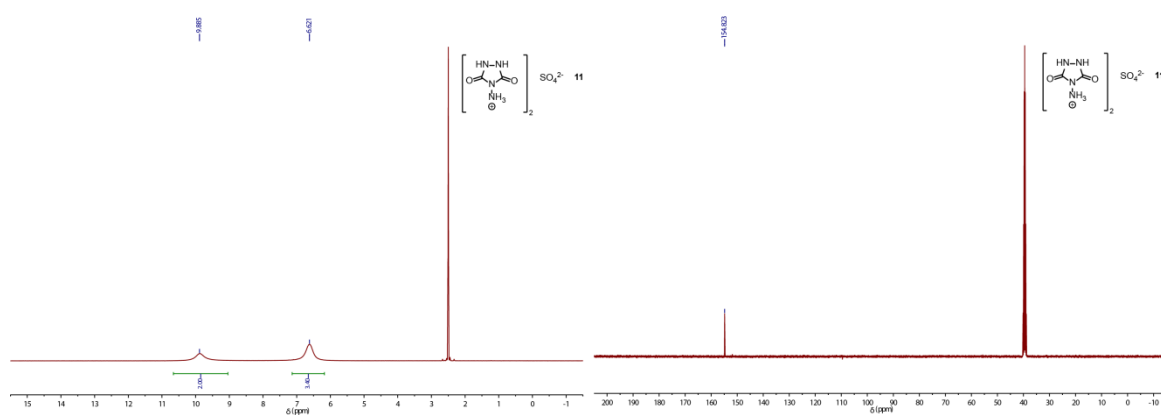


Figure A5.11 ^1H and ^{13}C NMR spectra of salt 11.

5.4 Plots of IR Spectra

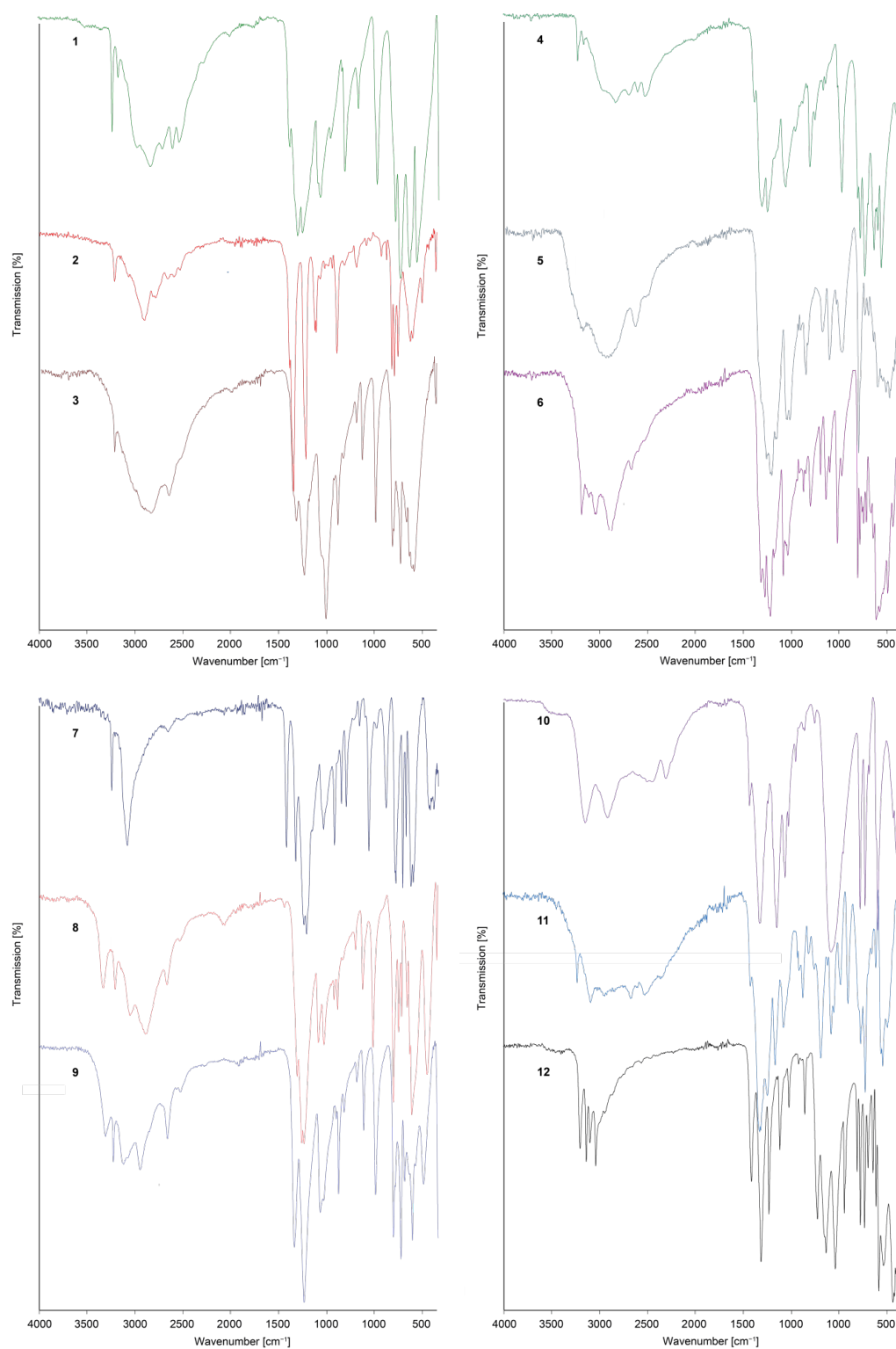


Figure A5.12 Infrared spectra of compounds 1–12.

5.5 DTA Plots

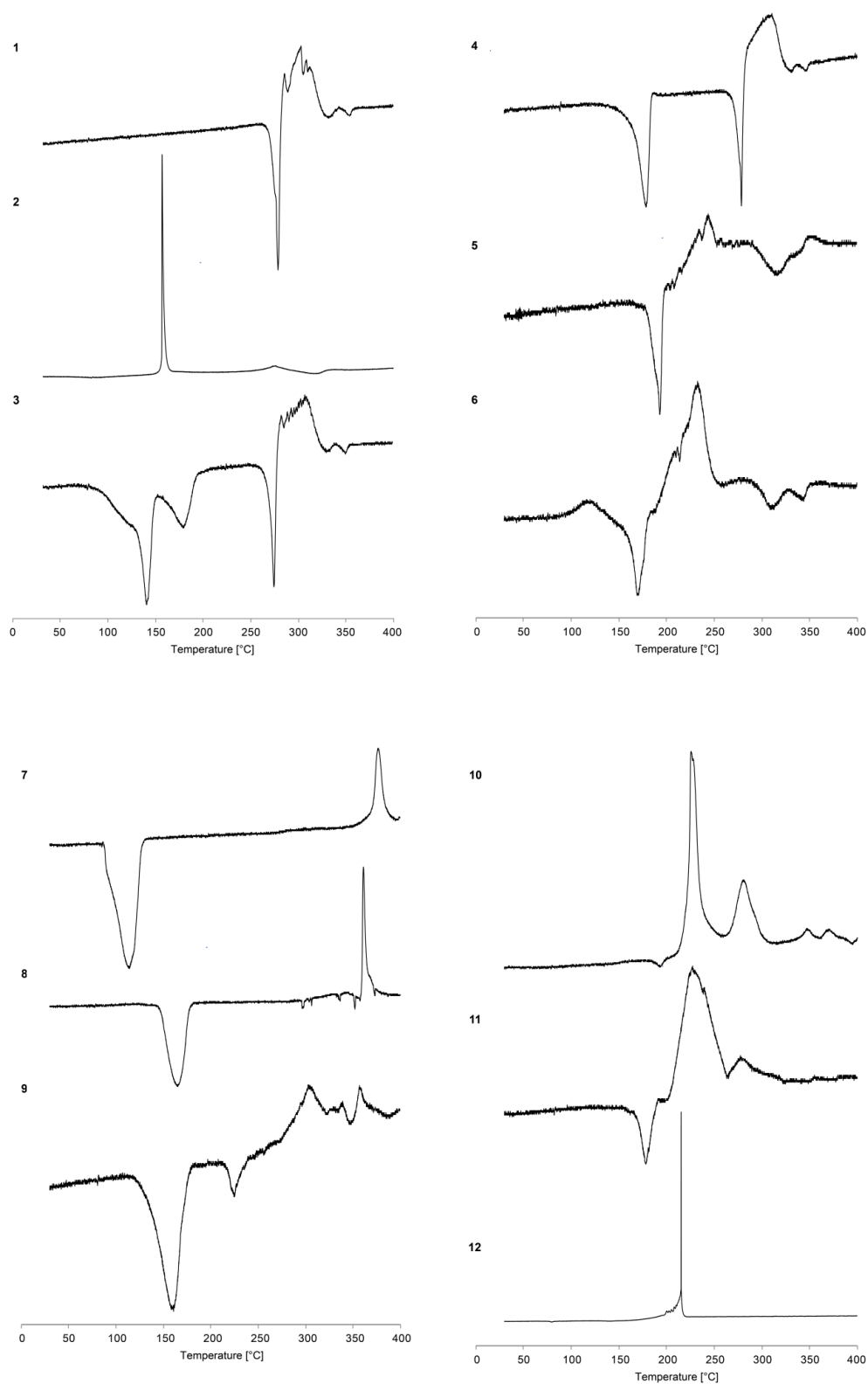
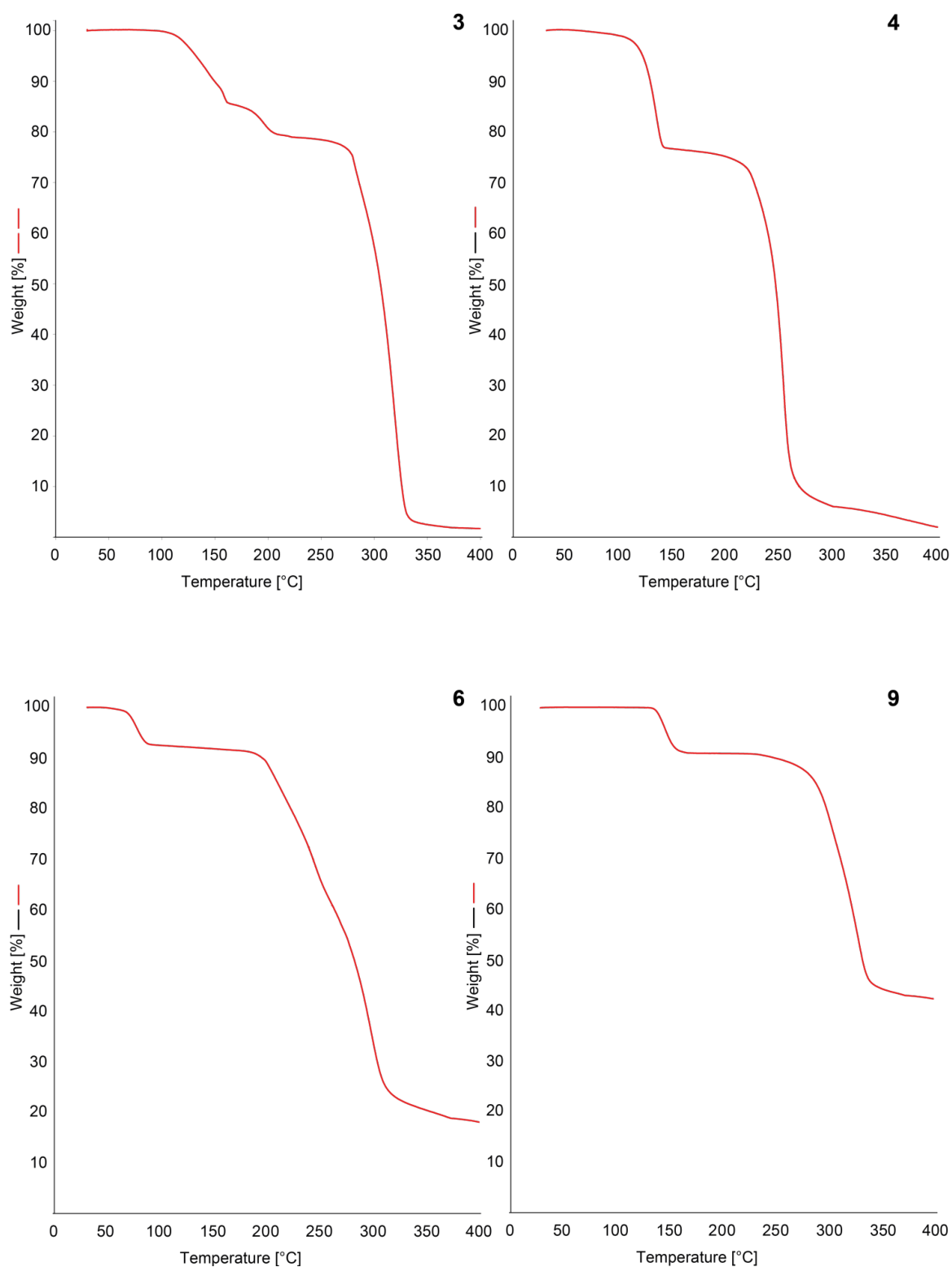


Figure A5.13 DTA plots of compounds 1–12.

5.6 TGA Plots

**Figure A5.14** TGA plots of salts **3**, **4**, **6** and **9**.

5.7 Calculation of Energetic Performance

The detonation parameters of trinitroethyl compound **2** and the water-free salts **4–6** as well as **10** and **11** were calculated with the EXPLO5 (version 6.03) computer code.^[6] The program is based on the steady-state model of equilibrium and uses the Becker–Kistiakowski–Wilson equation of state.^[7] It is designed to enable the calculation of detonation parameters at the Chapman–Jouguet (CJ) point, which itself is found from the Hugoniot curve of the system by its first derivative. These calculations are based on the theoretical maximum density (TMD) and on the calculated enthalpies of formation. If a water-free crystal structure was available, the densities were calculated from the corresponding crystal densities by Equation 1. To obtain the densities of **5**, dehydrated **6** and **12** a He pycnometer from Linseis was used.

$$\rho_{298\text{K}} = \frac{\rho_{\text{T}}}{1 + \alpha_v(298 - T)} \quad (1)$$

α_v is the coefficient of volume expansion of the nitramine HMX (octogen, $\alpha_v = 1.6 \times 10^{-4} \text{ K}$).^[8]

The CBS-4M quantum chemical method^[9] with GAUSSIAN 09^[10] was used to calculate the enthalpies of formation. Furthermore, based on Trouton's rule the gas-phase enthalpies were converted to solid-state enthalpies.^[11]

5.8 Hot plate and Hot Needle

The hot-plate (HP, Figure A5.15) and hot-needle (HN, Figure A5.16) were used to estimate if complex **12** shows a fast detonation to deflagration transition (DDT).



Figure A5.15 HP of complex **12**. Moment of deflagration shown as a sequence.

The decomposition of the urazine complex in the hot plate test proceeded with deflagration. As expected for a cooper(II) halide containing compound the flame color was blue. Also, in the hot needle test, a deflagration was observed.



Figure A5.16 HN of complex **12**. Moment of deflagration shown as a sequence.

5.9 Laser Initiation Test

For testing compound **12** towards its laser-ignitability, 15 mg of the complex was carefully filled into a transparent plastic cup, pressed with a pressure force of 1 kN and sealed with a UV-curing adhesive. The ECC was irradiated with a 45 W InGaAs laser diode working in the single-pulsed mode. The diode is attached to an optical fiber with a core diameter of 400 μm and a cladding diameter of 480 μm . The optical fiber is linked via a SMA type connector to the laser and to a collimator. This collimator is plugged to an optical lens, which is positioned in its focal distance ($f = 29.9 \text{ mm}$) to the sample. The lens is protected from the explosive using a sapphire glass. The laser diode is working at a wavelength of 915 nm, a voltage of 4 V, a current of 7 A and a pulse length of 1 ms yielding a total energy output of 1.7 mJ, which revealed a very strong detonation of compound **12** (Figure A5.17)



Figure A5.17 Moment of detonation during the positive laser initiation test of complex **12**.

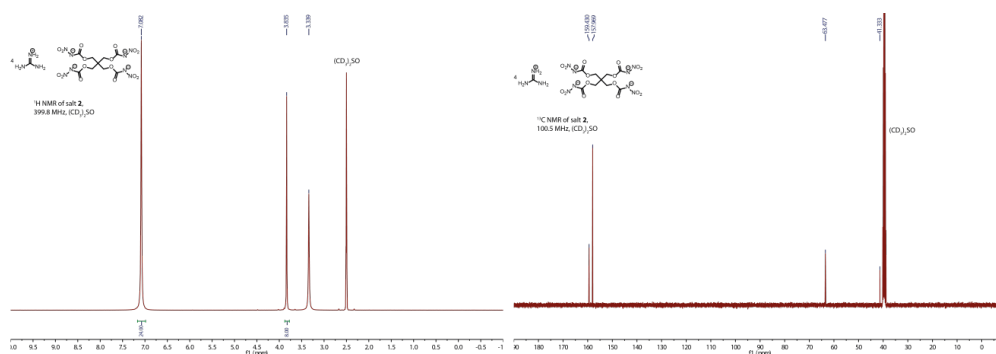
5.10 References

- [1] a) NATO Standardization Agreement 4489 (STANAG 4489), Explosives, Impact Sensitivity Tests, **1999**; b) NATO, Standardization Agreement 4487 (STANAG 4487), Explosives, Friction Sensitivity Tests, **2002**.
- [2] a) A. Altomare, M. C. Burla, M. Camalli, G. L. Cascarano, C. Giacovazzo, A. Guagliardi, A. G. G. Moliterni, G. Polidori, R. Spagna, *J. Appl. Crystallogr.* **1999**, *32*, 115–119; b) A. Altomare, G. Cascarano, C. Giacovazzo, A. Guagliardi, A. G. G. Moliterni, M. C. Burla, G. Polidori, M. Camalli, R. Spagna, SIR97, University of Bari (Italy) **1997**.
- [3] G. M. Sheldrick, SHELX-97, Programs for Crystal Structure Determination, University of Göttingen, Göttingen (Germany), **1997**.
- [4] L. Farrugia, *J. Appl. Crystallogr.* **1999**, *32*, 837–838.

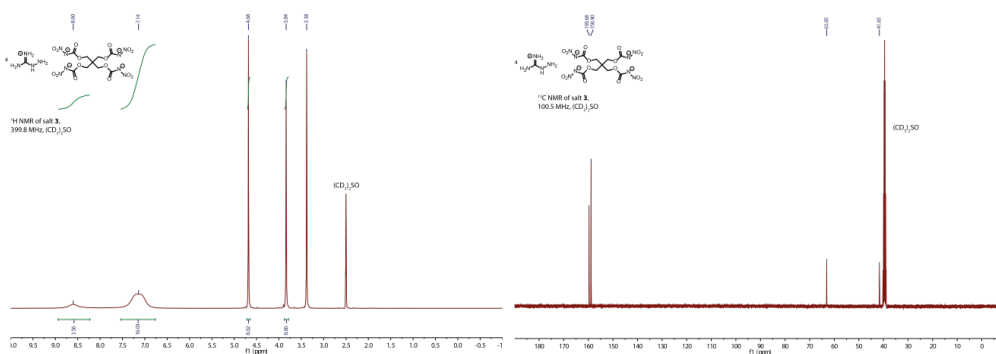
- [5] A. Spek, *Acta Crystallogr.* **2009**, *65D*, 148–155.
- [6] M. Sućeska, *Explo5 V6.03*, Zagreb (Croatia), **2015**.
- [7] M. Sućeska, *Propellants, Explos., Pyrotech.* **1991**, *16*, 197–202.
- [8] C. Xue, J. Sun, B. Kang, Y. Liu, X. Liu, G. Song, Q. Xue, *Propellants, Explos., Pyrotech.* **2010**, *35*, 333–338.
- [9] a) J. W. Ochterski, G. A. Petersson, J. A. Montgomery, *J. Chem. Phys.* **1996**, *104*, 2598–2619; b) J. A. Montgomery, M. J. Frisch, J. W. Ochterski, G. A. Petersson *J. Chem. Phys.* **2000**, *112*, 6532–6542.
- [10] M. J. Frisch, G. W. Trucks, H. B. Schlegel, G. E. Scuseria, M. A. Robb, J. R. Cheeseman, V. B. G. Scalmani, B. Mennucci, G. A. Petersson, H. Nakatsuji, M. Caricato, X. Li, H. P. Hratchian, A. F. Izmaylov, J. Bloino, G. Zheng, J. L. Sonnenberg, M. Hada, M. Ehara, K. Toyota, R. Fukuda, J. Hasegawa, M. Ishida, T. Nakajima, Y. Honda, O. Kitao, H. Nakai, T. Vreven, J. J. A. Montgomery, J. E. Peralta, F. Ogliaro, M. Bearpark, J. J. Heyd, E. Brothers, K. N. Kudin, V. N. Staroverov, R. Kobayashi, J. Normand, K. Raghavachari, A. Rendell, J. C. Burant, S. S. Iyengar, J. Tomasi, M. Cossi, N. Rega, J. M. Millam, M. Klene, J. E. Knox, J. B. Cross, V. Bakken, C. Adamo, J. Jaramillo, R. Gomperts, R. E. Stratmann, O. Yazyev, A. J. Austin, R. Cammi, C. Pomelli, J. W. Ochterski, R. L. Martin, K. Morokuma, V. G. Zakrzewski, G. A. Voth, P. Salvador, J. J. Dannenberg, S. Dapprich, A. D. Daniels, Ö. Farkas, J. B. Foresman, J. V. Ortiz, J. Cioslowski, D. J. Fox, *Gaussian 09*, Wallingford CT (US), **2009**.
- [11] F. Trouton, *Philos. Mag.* **1884**, *18*, 54–57.

6 Supporting Information to Salts of Pentaerythritol Tetranitrocarbamate

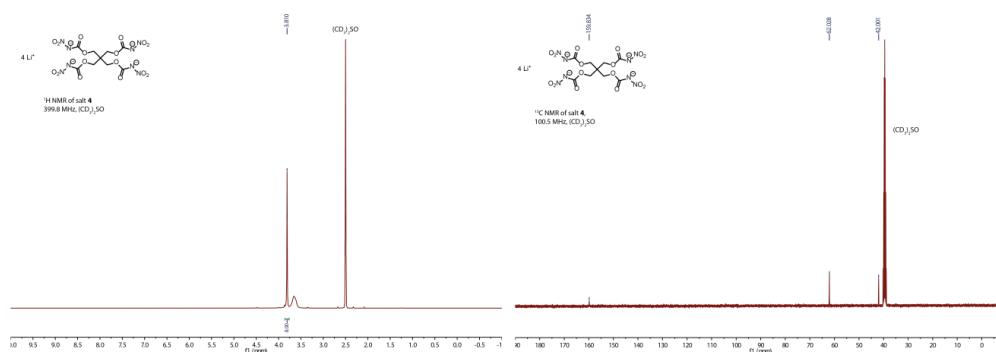
6.1 ^1H and ^{13}C NMR Data of Salt 2

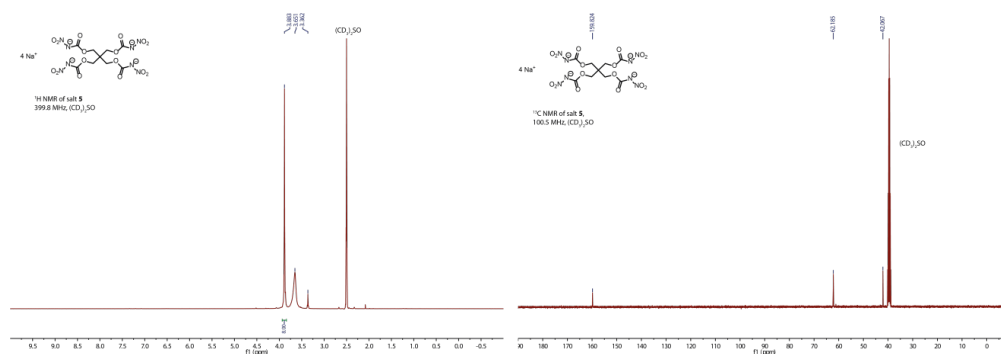
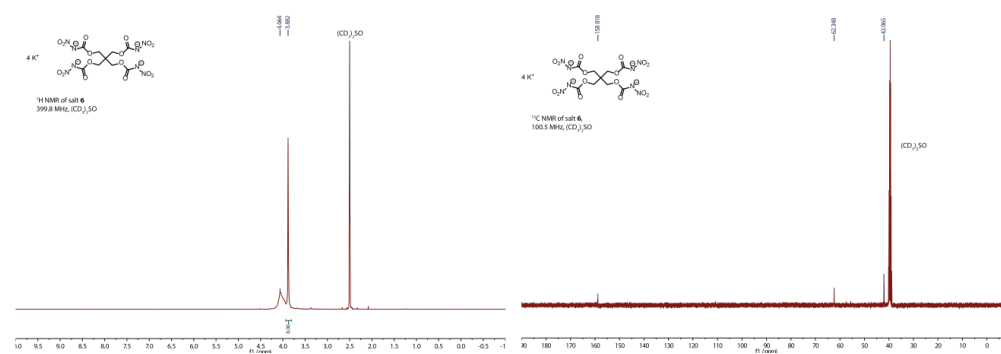
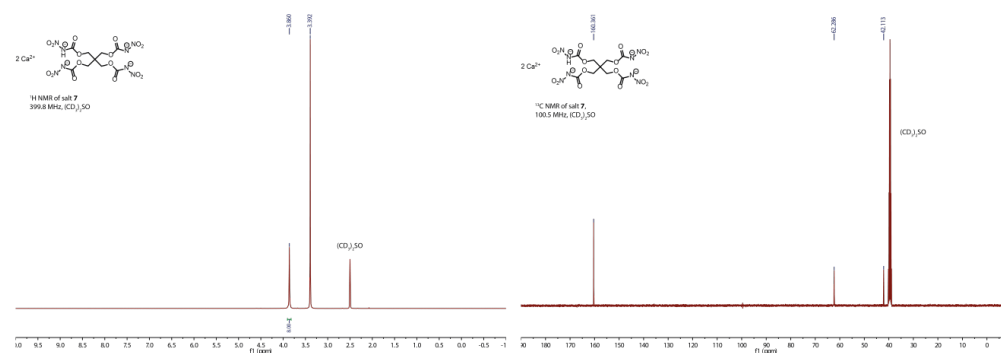


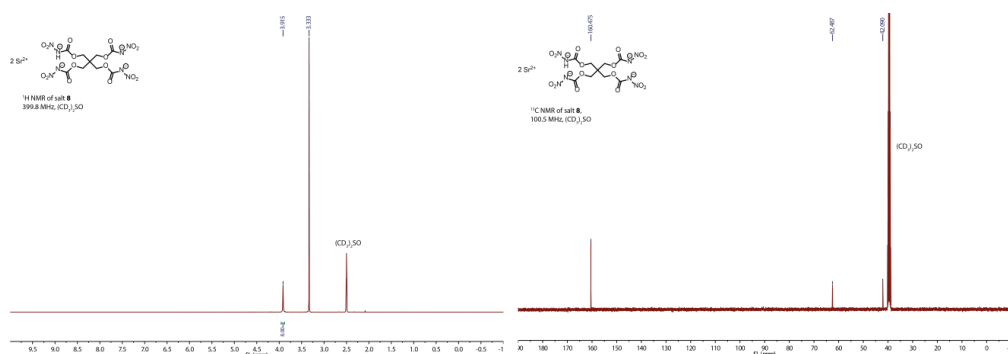
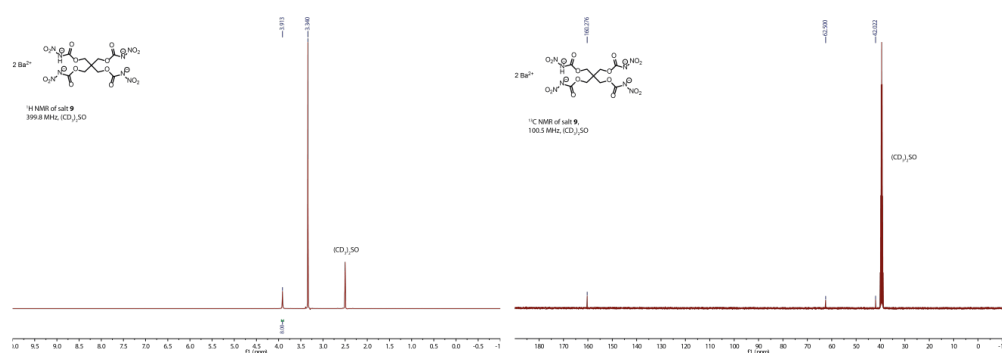
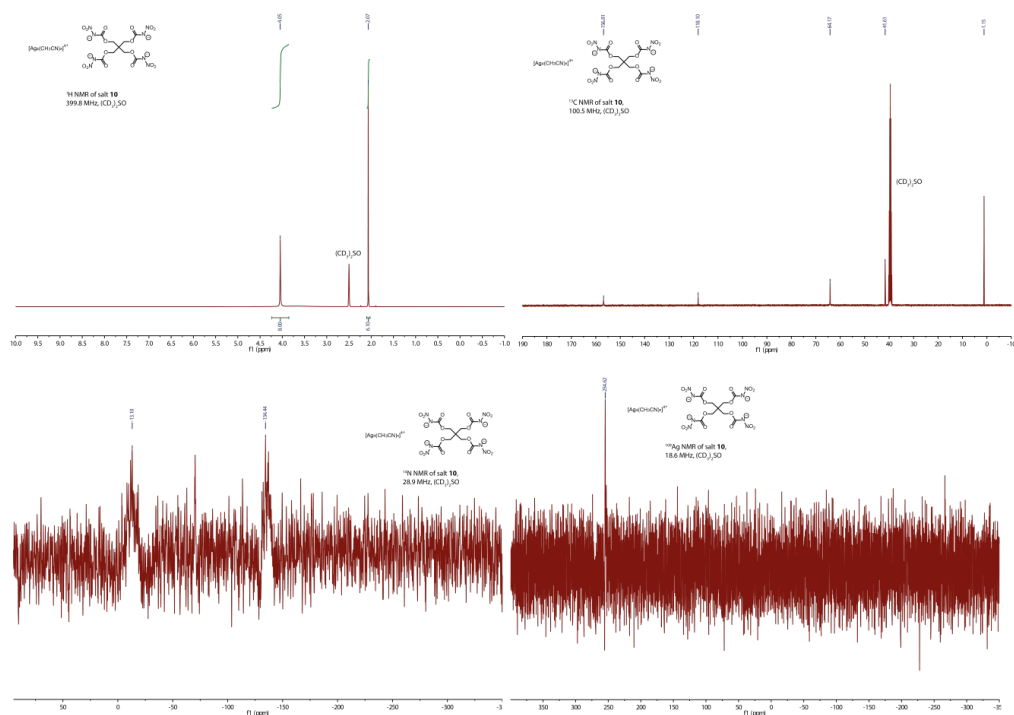
6.2 ^1H and ^{13}C NMR Data of Salt 3



6.3 ^1H and ^{13}C NMR Data of Salt 4



6.4 ^1H and ^{13}C NMR Data of Salt 56.5 ^1H and ^{13}C NMR Data of Salt 66.6 ^1H and ^{13}C NMR Data of Salt 7

6.7 ^1H and ^{13}C NMR Data of Salt 86.8 ^1H and ^{13}C NMR Data of Salt 96.9 ^1H , ^{13}C , ^{14}N and ^{109}Ag Data of Salt 10

6.10 IR and Raman Data of Salts 2–10

Tetrakis(guanidinium) PETNC (2)

IR (ATR): $\tilde{\nu} = 3338$ (m), 3124 (m), 3000 (m), 2980 (m), 2839 (m), 2750 (m), 1651 (s), 1568 (m), 1382 (s), 1231 (m), 1182 (m), 1168 (m), 1117 (m), 1086 (m), 1009 (w), 971 (w), 881 (w), 825 (m), 785 (w), 708 (w), 669 (w), 589 (w), 552 (w), 548 (m), 534 (m) cm^{-1} . **Raman (500 mW):** $\tilde{\nu} = 3277$ (5), 2964 (9), 2906 (5), 1694 (14), 1579 (6), 1467 (10), 1415 (8), 1314 (9), 1225 (6), 1125 (12), 1092 (6), 1060 (26), 1041 (13), 1014 (100), 976 (20), 850 (5), 819 (4), 787 (11), 540 (20), 496 (14), 317 (7) cm^{-1} .

Tetrakis(aminoguanidinium) PETNC (3)

IR (ATR): $\tilde{\nu} = 3415$ (w), 3299 (m), 1790 (w), 1760 (w) 1660 (s), 1597 (m), 1452 (w), 1416 (m), 1327 (w), 1295 (w), 1206 (s), 1187 (s), 1082 (s), 980 (m), 957 (m), 935 (m), 782 (m), 748 (w), 587 (w), cm^{-1} . **Raman (500 mW):** $\tilde{\nu} = 3351$ (11), 3332 (10), 3292 (15), 3267 (15), 3244 (12), 3229 (12), 3208 (9), 2977 (21), 2944 (9), 1684 (37), 1466 (25), 1434 (16), 1325 (26), 1309 (30), 1251 (10), 1200 (14), 1127 (31), 1095 (15), 1040 (56), 980 (100), 852 (15), 797 (22), 759 (10), 621 (14), 504 (29), 493 (29), 402 (11), 308 (22) cm^{-1} .

Tetralithium PETNC · 2.5 hydrate (4)

IR (ATR): $\tilde{\nu} = 3452$ (w), 2967 (w), 1773 (w), 1680 (m), 1620 (w), 1464 (w), 1407 (m), 1322 (m), 1206 (s), 1082 (s), 968 (m), 913 (w), 826 (w), 783 (m) cm^{-1} . **Raman (1000 mW):** $\tilde{\nu} = 3011$ (29), 3000 (24), 2972 (40), 2934 (16), 2915 (29), 1692 (81), 1480 (40), 1465 (14), 1426 (41), 1380 (22), 1347 (21), 1264 (39), 1247 (21), 1144 (26), 1111 (22), 1061 (22), 1035 (29), 1019 (17), 988 (100), 895 (14), 830 (13), 799 (17), 751 (15), 456 (11), 375 (12), 345 (18) cm^{-1} .

Tetrasodium PETNC · x hydrate (5)

IR (ATR): $\tilde{\nu} = 3457$ (w), 2960 (w), 1778 (w), 1679 (m), 1617 (w), 1467 (w), 1409 (m), 1322 (w), 1210 (s), 1082 (s), 966 (m), 905 (w), 824 (w), 784 (m) cm^{-1} . **Raman (500 mW):** $\tilde{\nu} = 3119$ (10), 3109 (9), 2974 (55), 2913 (29), 2820 (9), 2807 (10), 2708 (8), 2685 (8), 1755 (8), 1748 (8), 1702 (38), 1691 (39), 1645 (12), 1621 (8), 1583 (9), 1466 (33), 1451 (34), 1441 (30), 1430 (30), 1395 (18), 1376 (11), 1333 (33), 1294 (22), 1271 (23), 1262 (22), 1250 (20), 1232 (25), 1221 (24), 1182 (7), 1175 (7), 1153 (6), 1129 (34), 1112 (23), 982 (100), 916 (7), 857 (14), 845 (16), 830 (15), 799 (28), 764 (11), 751 (9), 739 (8), 701 (7), 571 (16), 563 (6), 516 (11), 502 (21), 444 (7), 434 (7), 424 (8), 415 (8), 391 (8), 346 (7), 331 (9), 318 (10), 288 (8) cm^{-1} .

Tetrapotassium PETNC · 2 hydrate (6).

IR (ATR): $\tilde{\nu} = 3459$ (w), 2967 (w), 1778 (w), 1679 (m), 1615 (w), 1464 (w), 1407 (m), 1321 (m), 1205 (s), 1079 (s), 968 (m), 913 (w), 826 (w), 784 (m) cm^{-1} . **Raman (1000 mW):** $\tilde{\nu} = 3043$

(11), 2972 (76), 2912 (38), 2905 (38), 1787 (10), 1772 (14), 1743 (10), 1697 (41), 1689 (40), 1608 (8), 1467 (43), 1447 (36), 1339 (36), 1311 (38), 1258 (26), 1217 (21), 1182 (9), 1123 (30), 1050 (23), 983 (100), 928 (9), 847 (19), 835 (19), 801 (30), 760 (13), 740 (11), 620 (8), 493 (24), 466 (18), 318 (10) cm^{-1} .

Dicalcium PETNC · 7 hydrate (7)

IR (ATR): $\tilde{\nu} = 3454$ (w), 2907(w), 1775 (w), 1679 (m), 1622 (w), 1467 (w), 1407 (m), 1321 (m), 1205 (s), 1079 (vs), 968 (m), 908 (w), 826 (w), 784 (m) cm^{-1} . **Raman** (1000 mW): $\tilde{\nu} = 2999$ (28), 2979 (41), 2918 (22), 1712 (10), 1679 (51), 1580 (5), 1471 (13), 1448 (24), 1409 (9), 1392 (14), 1349 (39), 1254 (13), 1234 (10), 1206 (4), 1145 (21), 1126 (11), 1086 (7), 999 (100), 978 (31), 934 (4), 874 (10), 855 (6), 833 (10), 804 (14), 753 (10), 739 (5), 550 (4), 507 (21), 486 (16), 355 (8), 314 (6), 229 (19) cm^{-1} .

Distrontium PETNC · 7 hydrate (8)

IR (ATR): $\tilde{\nu} = 3437$ (w), 1682 (s), 1478 (w), 1423 (m), 1391 (m), 1315 (w), 1230 (s), 1176 (w), 1116 (s), 981 (m), 922 (w), 882 (w), 856 (w), 789 (m), 775 (w), 747 (w), 624 (m), 504 (w) cm^{-1} . **Raman** (500 mW): $\tilde{\nu} = 3284$ (5), 2996 (32), 2980 (43), 2918 (29), 1713 (12), 1682 (63), 1582 (5), 1472 (13), 1440 (21), 1392 (14), 1345 (39), 1254 (17), 1239 (13), 1206 (5), 1142 (26), 1122 (14), 1072 (15), 1030 (10), 996 (100), 977 (37), 934 (5), 872 (16), 853 (8), 833 (13), 803 (16), 770 (5), 748 (9), 735 (6), 505 (26), 485 (21), 343 (10), 306 (7), 215 (24) cm^{-1} .

Dibarium PETNC · 4 hydrate (9)

IR (ATR): $\tilde{\nu} = 3458$ (w), 2968 (w), 2902 (w), 1770 (w), 1679 (m), 1617 (w), 1470 (w), 1407 (m), 1321 (m), 1205 (s), 1079 (vs), 968 (m), 916 (w), 826 (w), 784 (m) cm^{-1} . **Raman** (1000 mW): $\tilde{\nu} = 2956$ (7), 2905 (4), 2886 (4), 1685 (7), 1568 (2), 1507 (3), 1471 (3), 1421 (6), 1285 (5), 1228 (5), 1132 (5), 1060 (100), 985 (16), 875 (2), 799 (4), 691 (14), 497 (3), 335 (3), 225 (7) cm^{-1} .

Silver PETNC (10)

IR (ATR): $\tilde{\nu} = 3503$ (w), 3234 (w), 3182 (w), 2358 (w), 2263 (m), 1786 (w), 1688 (m), 1680 (m), 1612 (w), 1446 (w), 1397 (w), 1372 (w), 1211 (vs), 1195 (vs), 1114 (s), 1024 (w), 951 (m), 823 (w), 766 (m), 679 (w) cm^{-1} . **Raman** (500 mW): $\tilde{\nu} = 2979$ (61), 2939 (29), 2913 (27), 2308 (5), 2273 (10), 1714 (11), 1673 (46), 1649 (18), 1627 (24), 1558 (11), 1471 (33), 1426 (25), 1412 (25), 1381 (13), 1364 (8), 1322 (37), 1287 (16), 1246 (37), 1222 (32), 1202 (38), 1134 (36), 1030 (100), 982 (65), 892 (34), 828 (20), 796 (42), 769 (11), 734 (9), 527 (11), 511 (16), 485 (35), 387 (11), 336 (16), 284 (8) cm^{-1} .

6.11 Crystallographic data of salt 3

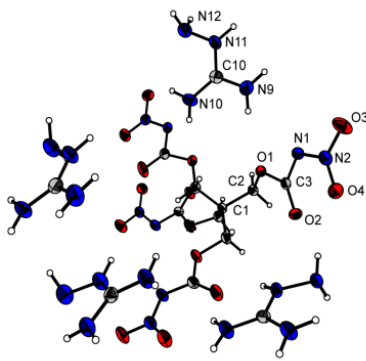
3			
formula	C ₁₃ H ₄₄ N ₂₄ O ₁₆		
formula weight [g mol ⁻¹]	792.65		
temperature [K]	173(2)		
crystal system	triclinic		
space group (No.)	<i>P</i> -1 (2)		
<i>a</i> [Å]	7.4041(4)		
<i>b</i> [Å]	12.2568(6)		
<i>c</i> [Å]	18.2301(8)		
α [°]	83.478(4)		
β [°]	80.963(4)		
γ [°]	75.422(4)		
<i>V</i> [Å ³]	1576.51(13)		
<i>Z</i>	2		
ρ_{calc} [g cm ⁻³]	1.653		
μ [mm ⁻¹]	0.147		
<i>F</i> (000)	820		
crystal habit	colorless block		
crystal size [mm]	0.40 × 0.32 × 0.12		
<i>q</i> range [°]	4.20 – 32.39		
index ranges	-10 ≤ <i>h</i> ≤ 11 -17 ≤ <i>k</i> ≤ 17 -25 ≤ <i>l</i> ≤ 26		
reflections measured	17568	GOOF on <i>F</i> ²	1.030
reflections independent	10133	residual el. density [e Å ⁻³]	-0.294/0.371
reflections unique	7202	CCDC	1850912
<i>R</i> _{int}	0.022	data/restraints/parameters	10133/0/622
<i>R</i> ₁ , <i>wR</i> ₂ (2 σ data)	0.0453, 0.0729	<i>R</i> ₁ , <i>wR</i> ₂ (all data)	0.1003, 0.1186

Figure A6.1 X-ray molecular structure of tetrakis(aminoguanidinium) PETNC (**3**). Thermal ellipsoids represent the 50% probability level.

6.12 Room Temperature Densities

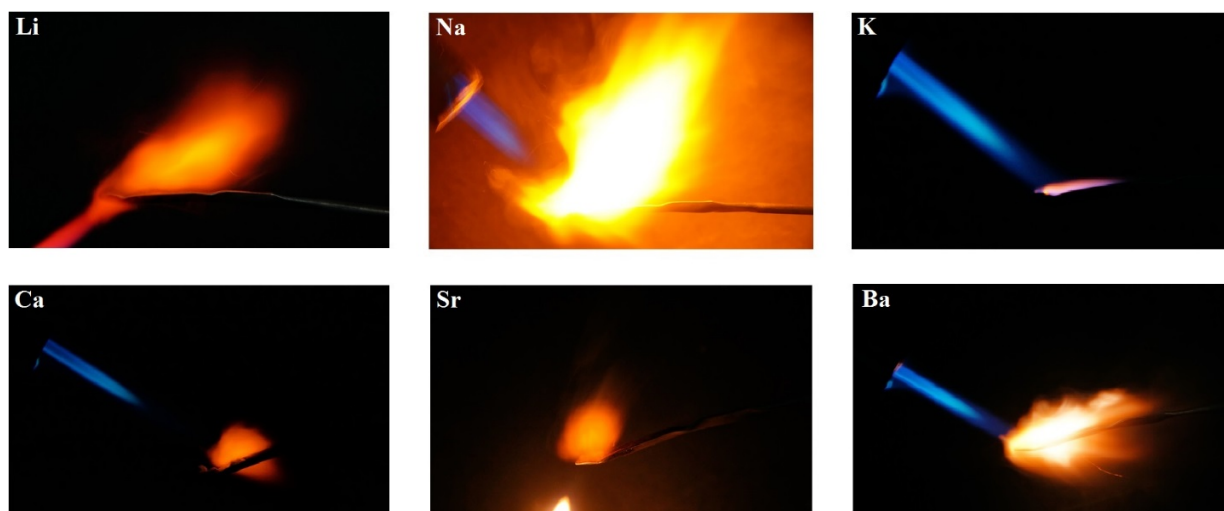
The densities at 298 K were either obtained by calculation from the corresponding crystal densities according the following equation using α_v coefficient of volume expansion from the nitramine HMX ($\alpha_v = 1.6 \cdot 10^{-4} \text{ K}^{-1}$)

$$\rho_{298\text{K}} = \rho_T / (1 + \alpha_v(298 - T))$$

or were obtained by gas pycnometer measurement.

6.13 Burning Behavior

Combustion test of lithium (4), sodium (5), potassium (6), calcium (7), strontium (8) and barium (9) salts.



6.14 Reference

- [1] Xue, C.; Sun, J.; Kang, B.; Liu, Y.; Liu, X.; Song, G.; Xue, Q. *Propellants, Explos., Pyrotech.* **2010**, *35*, 333–338.

7 Supporting Information to Aquatic Toxicity Measurements

7.1 Light Emitting Pathway

In the system three enzymatic complexes are involved: the Flavin Reductase (FMN Reductase), the Luciferase and the Fatty Acid Reductase. In the first step flavin mononucleotide (FMN) is reacted to its reduced form (FMNH₂) catalyzed by the FMN Reductase. The reduced flavin molecule is able to bind to the Luciferase and in combination with an aliphatic aldehyde and under consumption of oxygen the peroxihemiacetal complex L--FMNH-O-O-CHOH-R is formed (Figure A7.1).^[1]

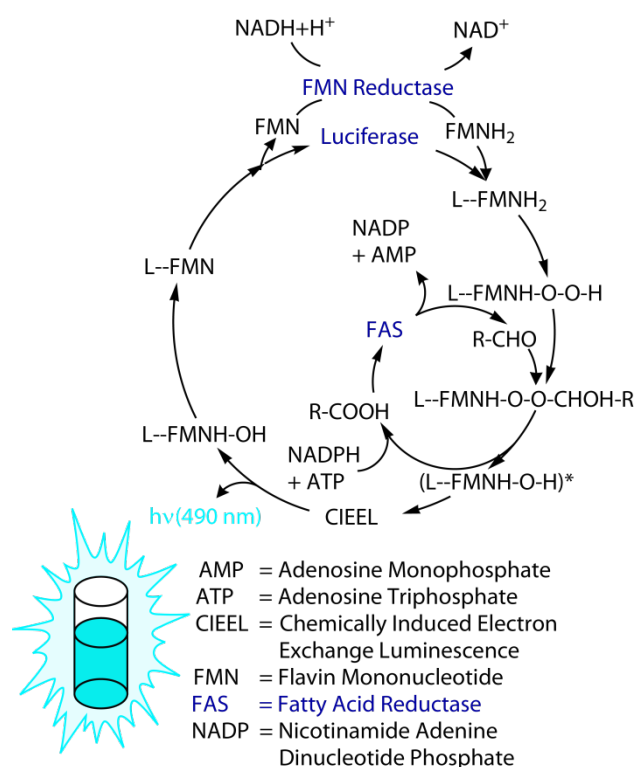


Figure A7.1 Schematic overview of the biochemical light emitting pathway of the bioluminescent bacteria *Vibrio fischeri* and *Photobacterium*.

In the following step aliphatic acid is released and a singlet excited hydroxide complex (L--FMNH-OH)* is generated which directly reacts to the hydroxide complex L--FMNH-OH in the ground state under liberation of light in a chemically initiated electron exchange luminescence (CIEEL) mechanism (Figure A7.2).^[2] The emitted light with a wavelength of 490 nm can be observed and measured by a photomultiplier.

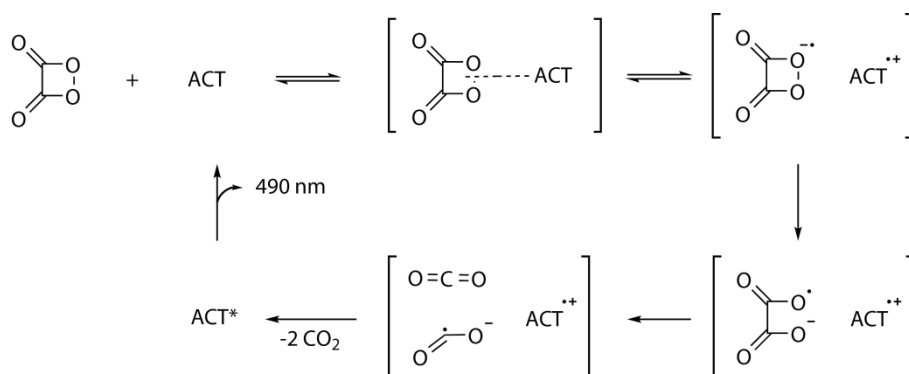


Figure A7.2 Schematic overview of the chemically initiated electron exchange luminescence (CIEEL) mechanism.

7.2 Calculation

The correction factor (fK) is calculated with the following equation (1)

$$fK = I_t / I_0 \quad (1)$$

where I_t is the luminescence of the control at a specific time and I_0 is the luminescence of the control at the beginning. The corrected luminescence I_{ct} is obtained by multiplying I_0 of all concentrations with fK (2)

$$I_{ct} = fK * I_0 \quad (2)$$

And the inhibition is calculated as follows:

$$inhibition (\%) = (I_{ct} - I_t) * 100 / I_{ct} \quad (3)$$

For calculating the EC_{50} value of a substance Γ was plotted against the concentration c in a diagram with a logarithmic scale:

$$\Gamma = inhibition (\%) / (100 - inhibition (\%)) \quad (4)$$

The toxicity data with the inhibition were used to fit a straight line and therefore to calculate the EC_{50} value. The EC_{50} value is identical with the point where the line crosses the X-axis at $\Gamma = 1$.

When the inhibition of a compound did not reach the 10% limit, the EC_{50} reported ">>>" for the highest measured.

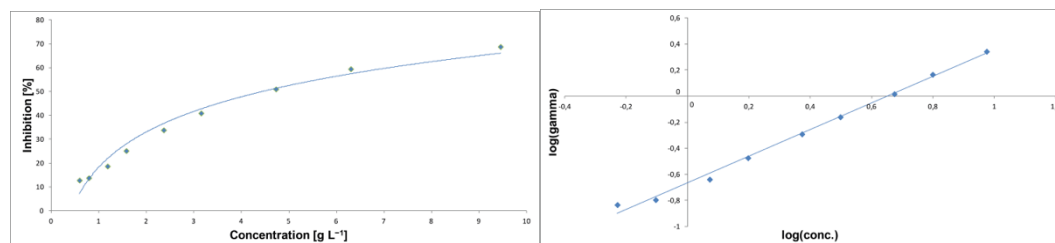


Figure A7.3 Concentration against Inhibition plot of ammonium dinitramide (left) and plot of the logarithmic concentration against the logarithm of gamma of ammonium dinitramide (right).

As EC_{50} values are point estimates it is important to clarify, that the concentration directly interferes with the inhibition and can vary in an order of magnitude in other concentrations. To show the dose specific response some graphs of 30 minutes incubation time are provided:

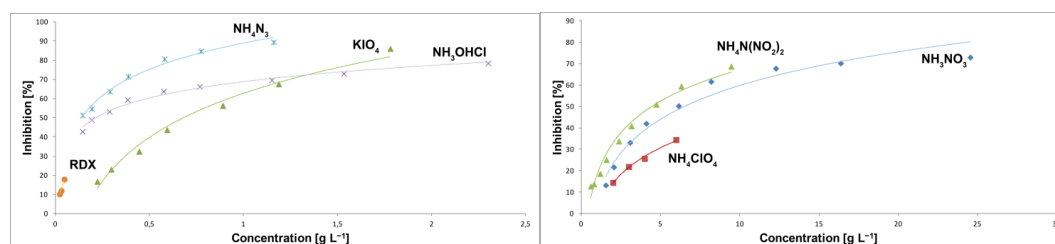


Figure A7.4 Diagram of the inhibition of some common energetic salts and RDX (left) and of some common energetic salts (right).

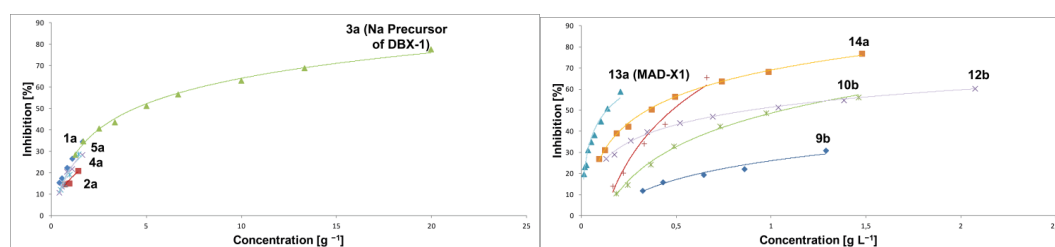


Figure A7.5 Diagram of the inhibition of energetic materials with tetrazole scaffold (left) and of ammonium salts of bitetrazoles and MAD-X1 (right).

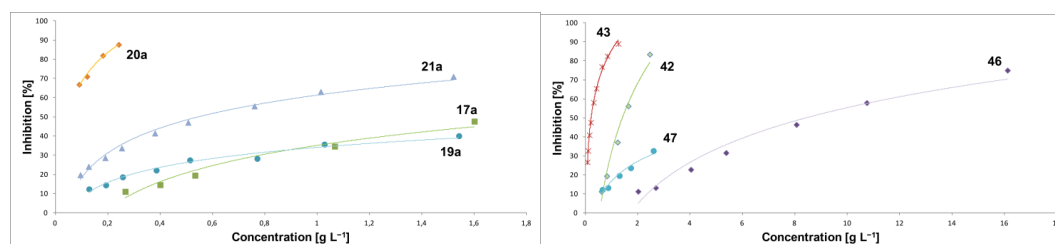


Figure A7.6 Diagram of the inhibition of ammonium salts of fused heterocycles (left) and of some some aliphatic energetic materials (right).

To point out the importance of the slope of the dose response curve EC_{20} and EC_{80} values of prominent energetic materials after 30 minutes of incubation are presented in Table A7.1. *e. g.* some secondary explosives revealed EC_{50} values in comparable ranges, such as TKX-50 ($EC_{50} = 0.58 \text{ g L}^{-1}$), MAD-X1 ($EC_{50} = 0.19 \text{ g L}^{-1}$) and RDX ($EC_{50} = 0.24 \text{ g L}^{-1}$), but especially the EC_{80} values drift further apart.

Table A7.1 EC_{20} and EC_{80} values of some energetic materials after 30 minutes of incubation.

Compound	EC_{20} (30 min) [g L ⁻¹]	EC_{80} (30 min) [g L ⁻¹]	Compound	EC_{20} (30 min) [g L ⁻¹]	EC_{80} (30 min) [g L ⁻¹]
NaN ₃	0.05	0.66	NH ₄ N(NO ₂) ₂	1.16	17.44
NaIO ₄	0.21	1.99	RDX	0.06	1.02
KIO ₄	0.28	1.63	3a (DBX-1 Precursor)	0.66	28.59
NH ₃ OHCl	0.02	2.91	8a (TKX-50)	0.05	5.59
NH ₄ N ₃	0.04	0.58	13a (MAD-X1)	0.02	1.81
NH ₄ NO ₃	1.76	25.66	43 (2,2,2-trinitroethanol)	0.06	0.74
NH ₄ ClO ₄	2.84	43.71	46 (Azidoethanol)	3.49	20.98
NH ₄ IO ₄	0.20	1.15	47 (Monomethylhydrazine)	1.34	26.01

7.3 References

- [1] a) J.-J. Bourgois, F. E. Sluse, F. Baguet, J. Mallefet, Kinetics of Light Emission and Oxygen Consumption by Bioluminescent Bacteria, *J. Bioenerg. Biomembr.*, **2001**, *33*, 353–363;
 b) S. Inouye, NAD(P)H-Flavin Oxidoreductase from the Bioluminescent Bacterium, *Vibrio Fischeri* ATCC 7744, is a Flavoprotein, *FEBS Lett.* **1994**, *347*, 163–168.
- [2] S. P. Schmidt, G. B. Schuster, Dioxetanone Chemiluminescence by the Chemically Initiated Electron Exchange Pathway. Efficient Generation of Excited Singlet States, *J. Am. Chem. Soc.* **1978**, *100*, 1966–1968.

8 Credits

Reprinted (adapted) with permission from (C. C. Unger, M. Holler, T. M. Klapötke and B. Krumm, Oxygen-rich Bis(trinitroethyl esters): Suitable Oxidizers as Potential Ammonium Perchlorate Replacement, *Energy Fuels* **2020**, in press). Copyright (2020) American Chemical Society.

Reprinted (adapted) with permission from (T. M. Klapötke, B. Krumm, C. C. Unger, Energetic Metal and Nitrogen-Rich Salts of Pentaerythritol Tetranitrate Analogue Pentaerythritol Tetranitrocarbamate, *Inorg. Chem.*, **2019**, 58, 2881–2887.). Copyright (2019) American Chemical Society.

Reprinted (adapted) with permission from (T. M. Klapötke, B. Krumm, T. Reith, C. C. Unger, Synthetic Routes to a Triazole and Tetrazole with Trinitroalkyl Substitution at Nitrogen, *J. Org. Chem.*, **2018**, 83, 10505–10509.). Copyright (2018) American Chemical Society.

Q. J. Axthammer, T. M. Klapötke, B. Krumm, R. Scharf, C. C. Unger, Convenient Synthesis of Energetic Polynitro Materials including $(\text{NO}_2)_3\text{CCH}_2\text{CH}_2\text{NH}_3$ -Salts *via* Michael Addition of Trinitromethane, *Dalton Trans.* **2016**, 45, 18909–18920. DOI: 10.1039/C6DT03779H - Published by The Royal Society of Chemistry.